Beyond Cost-risk Analysis: Combining Climate Targets with Climate Damage Information

Dissertation

with the aim of obtaining a degree of

Doktor der Naturwissenschaften (Dr. rer. nat.)

at the Faculty of Mathematics, Informatics, and Natural Sciences
Department of Earth System Sciences
at the University of Hamburg

Submitted in total fulfillment of the requirements of the degree of

Doctor of Philosophy (Ph.D.)

at the Faculty of Science
School of Agriculture, Food and Ecosystem Sciences
at the University of Melbourne

submitted by

Vito Avakumović

Hamburg, 2025

ORCID: 0000-0002-0339-7870

Examination Information

Date of Oral Defense:	17.12.2025
Reviewers:	Prof. Dr. Hermann Held Prof. Dr. Tom Kompas Prof. Dr. Phillip D. Adams Prof. Dr. Wilfried Rickels
Members of the examination commission:	Prof. Dr. Hermann Held Prof. Dr. Jürgen Böhner Prof. Dr. Tom Kompas Prof. Dr. Victor Brovkin Prof. Dr. Phillip D. Adams Prof. Dr. Wilfried Rickels

Chair of the Subject Doctoral Committee

Earth System Sciences:	Prof. Dr. Dirk Notz
Dean of Faculty MIN:	Prof. Dr.-Ing. Norbert Ritter

Nigdar ni tak bilo	Never was it so
da ni nekak bilo,	that it wasn't somehow,
pak ni vezda nebu	and it won't ever be
da nam nekak nebu.	that somehow it won't be (for us).

— Krleža, M. (1936). *Khevenhiller. Balade Petrice Kerempuha.*

I dedicate this thesis to my grandmother,

Prof. Dipl. Ing. Zorka Treusch,

born Babović

(1933–2023)

Beyond Cost-risk Analysis: Combining Climate targets with Climate Damage Information

Vito Avakumović
Principal Supervisor: Prof. Hermann Held (Universität Hamburg)
Principal Supervisor: Prof. Tom Kompas (University of Melbourne)
Co-supervisor: Prof. Andreas Lange (Universität Hamburg)
Co-supervisor: Dr. James Camac (University of Melbourne)

Abstract

Anthropogenic climate change creates a decision-making problem between near-term mitigation costs and long-term risks of severe impacts. Traditional frameworks such as cost-benefit analysis (CBA) and cost-effectiveness analysis (CEA) represent two ends of a spectrum: the former trades off mitigation costs against expected damages, while the latter seeks the least-cost path to meet climate targets, assuming damages cannot be reliably quantified. Cost-risk analysis (CRA) emerged to reconcile CEA's temperature objectives with utility-based flexibility; however, improved damage quantification calls for a more integrated approach. This thesis develops Cost-Benefit-Risk Analysis (CBRA)—a novel framework that integrates explicit (partial) damage estimates into a reduced-weight risk function for temperature targets, bridging target-based and trade-off-based methods. The thesis first examines the carbon budget concept, which posits a near-linear relationship between cumulative CO_2 emissions and global temperature rise (TCRE)—a key condition for CRA–CEA equivalence. Scenario-dependent deviations are analyzed using an optimization program, demonstrating maximal deviations of less than 10% of total temperature rise, which rapidly diminish thereafter. Using FaIRv2 and a one-box model, it is shown that scenario dependence can be explained by the shape of the pulse response, interpreted as Green's function. This approach generalizes to models of any complexity and helps characterize nonlinearity in the carbon budget. Combined with projections for agriculture and mortality, and implemented in the CGE model GTAP-INT 2, the results reveal substantial regional disparities and significant global damages, particularly in poorer, populous regions—with long-term GDP reductions of up to 50% for certain countries, while a few specific regions may experience marginal GDP gains (less than 1%) under high-emission scenarios. Finally, CBRA is implemented within the MIND-L integrated assessment model, incorporating hereby modified FaIR climate module with probabilistic climate sensitivity and a partial damage function derived from CGE-informed economic damages. It confirms that, under a carbon budget-consistent module, CRA and CEA yield equivalent outcomes. Moreover, we show that, by calibrating the CBRA framework to meet the predefined temperature target, one can assess how much of the unknown

risks embodied in the climate target are explicitly quantified by the implemented damage function. These findings position CBRA as a consistent, flexible tool for climate policy design.

Zusammenfassung

Der anthropogene Klimawandel erzeugt ein Entscheidungsproblem zwischen kurzfristigen Kosten für Klimaschutz und langfristigen Risiken schwerer Schäden. Traditionelle Entscheidungswerkzeuge wie die Kosten-Nutzen-Analyse (KNA/CBA) und die Kosteneffektivitätsanalyse (KEA/CEA) bilden dabei zwei Enden eines Spektrums: Erstere wägt Kosten gegen erwartete Schäden ab, während Letztere, unter der Annahme, dass Schäden nicht verlässlich zu quantifizieren sind, den kostengünstigsten Pfad zur Erreichung vorgegebener Klimaziele sucht. Die Kosten-Risiko-Analyse (KRA/CRA) entstand, um die temperaturbasierten Zielvorgaben der KEA mit der Zeitkonsistenz unter Unsicherheit des Nutzenmaximierungskonzepts zu verbinden; verbesserte Schadensquantifizierungen erfordern jedoch einen stärker integrierten Ansatz. Diese Dissertation entwickelt daher die Kosten-Nutzen-Risiko-Analyse (KNRA/CBRA) – ein neuartiges Entscheidungswerkzeug, das explizite (partielle) Schadensschätzungen in eine abgeschwächt gewichtete Risikofunktion für Temperaturziele integriert und damit zielbasierte und abwägende Methoden vereint.

Zunächst wird das Kohlenstoff-Budget-Konzept untersucht, das eine nahezu lineare Beziehung zwischen kumulativen CO_2-Emissionen und dem globalen Temperaturanstieg (TCRE) postuliert – eine Schlüsselbedingung für die Äquivalenz von KRA und KEA. Szenarioabhängige Abweichungen werden mittels eines Optimierungsprogramms analysiert; sie betragen maximal weniger als 10% des gesamten Temperaturanstiegs und klingen danach rasch ab. Mit FaIRv2 und einem Ein-Box-Modell wird gezeigt, dass die Szenarioabhängigkeit durch die Form der Impulsantwort (als Greensfunktion interpretierbar) erklärt werden kann. Dieser Zugang lässt sich auf Modelle beliebiger Komplexität verallgemeinern und hilft, Nichtlinearitäten in der Kohlenstoff-Budget-Temperatur-Beziehung zu charakterisieren.

Projektionen von Auswirkungen des Klimawandels für Landwirtschaft und Mortalität, implementiert im CGE-Modell GTAP-INT 2, zeigen die Ergebnisse erhebliche regionale Ungleichheiten und bedeutende globale Schäden, insbesondere in ärmeren und bevölkerungsreichen Regionen – mit langfristigen BIP-Rückgängen von bis zu 50% für einzelne Länder (bei einer langfristigen Erwärmung um 4 °C), während wenige spezifische Regionen unter hohen Emissionsszenarien BIP-Zuwächse unter 1% verzeichnen können.

Zuletzt wird KNRA im integrierten Bewertungsmodell MIND-L implementiert. Hierzu wird eine angepasste Version des FaIR-Klimamodells mit probabilistischer Klimaunsicherheit und partieller Schadensfunktion eingesetzt. Letztere basiert auf den Ergebnissen der im CGE-Modell bestimmten ökonomischen Schäden. Ergebnisse mit diesem Modellaufbau bestätigen, dass KEA und KRA sich äquivalent verhalten. Darüber hinaus wird gezeigt, dass es möglich ist abzuschätzen, wie viel der in den Temperaturzielen impliziten unbekannten Risiken durch die partielle Schadensfunktion quantifiziert werden. Damit wird KNRA als transparentes und anpassungsfähiges Entscheidungswerkzeug für die Klimapolitik demonstriert.

Declaration

Eidesstattliche Versicherung — Declaration on Oath

I hereby declare and affirm that this doctoral dissertation is my own work and that I have not used any aids and sources other than those indicated.

If electronic resources based on generative artificial intelligence (gAI) were used in the course of writing this dissertation, I confirm that my own work was the main and value-adding contribution and that complete documentation of all resources used is available in accordance with good scientific practice. I am responsible for any erroneous or distorted content, incorrect references, violations of data protection and copyright law or plagiarism that may have been generated by the gAI.

Additional declarations (University of Melbourne):

- the thesis comprises only my original work towards the joint doctoral degree (Doctor of Philosophy);
- due acknowledgement has been made in the text to all other material used;
- the thesis is less than 100,000 words in length, exclusive of tables, maps, bibliographies and appendices; and
- the thesis comprises 100% dissertation as agreed by the advisory committee.

Hamburg, 14. 10. 2025

Preface

This joint thesis research was conducted at the Faculty of Mathematics, Informatics and Natural Sciences, University of Hamburg, Germany, and the Faculty of Science, University of Melbourne, Australia. The work was carried out under the supervision of Prof. Hermann Held, Prof. Tom Kompas, Prof. Andreas Lange, and Dr. James Camac. While the work presented in this thesis is largely my own, the use of "we" throughout the chapters reflects standard academic writing conventions.

This thesis is presented in the form of a cumulative dissertation, comprising three papers—both published and unpublished—which constitute Chapters 2, 3, and 4. The Introduction, along with the Discussion and Conclusion, does not only provide general context and summarize the main findings, but also serve to establish the coherence between the individual papers—guiding the reader through the overarching narrative of the thesis.

- Paper 1 (Published in *Earth System Dynamics*, 18. 04. 2024)
- Paper 2 (Submitted — currently under editorial consideration)
- Paper 3 (Invited to revise and resubmit — currently under revision)

All three articles included in this thesis were entirely written by me. Paper 1 is a single-author publication, and both the research and the writing are solely my own (100 %). For Paper 2, I contributed approximately 80 % of the research work, with the remaining contributions made by Pham Van Ha and Tom Kompas. For Paper 3, my contribution amounts to approximately 75 %, with the remainder contributed by Benjamin Blanz. In all cases, the complete drafting and writing of the manuscripts were carried out exclusively by me. Digital editorial assistance was used solely for language editing.

Funding.

This research was funded by the Deutsche Forschungsgemeinschaft (DFG, German Research Foundation) under Germany's Excellence Strategy – EXC 2037 "CLICCS – Climate, Climatic Change, and Society" – project number 390683824. Additional institutional support was provided by the University of Hamburg (President's Office and Faculty of Mathematics, Informatics and Natural Sciences (MIN)), including the Research Unit Sustainability and Climate Risk. Further support came from the Centre for Environmental and Economic Research (CEER) at the University of Melbourne.

Acknowledgements

I would like to express my deepest gratitude to my Doktorvater, Prof. Hermann Held. From the beginning of our interaction during my master's studies until the end of this thesis—developed around topics he generously proposed— he showed infinite patience and provided guidance throughout my academic journey. With academic and non-academic matters alike, he never hesitated to go the extra mile to offer support. For this and many other things, thank you Hermann.

To Prof. Tom Kompas, for welcoming me into his group on the other side of the planet with open arms; for teaching me how to be concise, to appreciate the value of shorter meetings, and for showing me a different perspective on academia. Most importantly, for ensuring that I always felt at home, even while being so far from home. Cheers, Tom!

This thesis also owes a great deal of gratitude to my panel chairs, Dr. David Grawe and Prof. Brendan Cullen. David has been involved since the beginning of my PhD, consistently ensuring that meetings were held regularly, while generously offering his time whenever I needed support or simply someone to talk to. Brendan assumed the role of my panel chair in Melbourne and ensured that everything proceeded smoothly and effortlessly, helping me navigate the formal aspects of a joint PhD with clarity and ease.

To Benjamin, for discussions of many kinds, invaluable practical and theoretical help, and continuous support in most difficult times. To Ha, for his patience, positive outlook, and support throughout the writing and revisions.

Next, my family. To my mother, Tihana — thank you for always being just one phone call away when things became overwhelming, and for your unwavering understanding even when I wasn't always available, caught up in thesis stress or other challenges. I promise to do better. To my sister, Maša — thank you for your constant presence and support during our time in Hamburg, and for offering me a second home here. This gratitude extends to Lennard, and of course, to Lola.

Lastly — but most certainly not least — thank you to all the friends out there. There are too many of you, and I have only one page. I love you all. Special thanks to Alex for the final proofreading, and to Jihye and Nicole for checking in on me during the final weeks of writing. Finally, heartfelt thanks to Benjamin for being full-time support throughout the time of working on this thesis.

Vito Avakumović
Sternschanze, Freie und Hansestadt Hamburg, Germany, April 2025

Contents

List of Figures

List of Tables

Nomenclature

CBRA	Cost-Benefit-Risk Analysis — a decision-making framework integrating CBA and CRA principles.
CBA	Cost-Benefit Analysis — a trade-off-based decision-making framework based on expected utility maximization.
CEA	Cost-Effectiveness Analysis — a target-based decision-making framework for finding least-cost mitigation pathways.
CGE	Computable General Equilibrium — an economic modeling approach used in IAMs.
CS	Climate sensitivity — the equilibrium temperature response to a doubling of atmospheric CO_2 concentration.
CRA	Cost-Risk Analysis — a decision-making framework that embeds targets within a utility-maximizing framework.
ESM	Earth System Model — complex climate models representing coupled physical, chemical, and biological systems.
FaIR	Finite Amplitude Impulse Response — a climate model of reduced complexity.
GDP	Gross Domestic Product — a measure of economic output.
GHG	Greenhouse Gases — gases that trap heat in the atmosphere, driving global warming.
GTAP	Global Trade Analysis Project — a multiregion, multisector CGE model, with perfect competition and constant returns to scale.

IAM Integrated Assessment Model — tools that combine knowledge from multiple disciplines to analyze climate policy.

IPCC Intergovernmental Panel on Climate Change — the UN body for assessing climate science.

MIND-L Model of Investment and Technological Development including Learning — a globally aggregated IAM.

TCR Transient Climate Response — global temperature increase at the time of CO_2 doubling under a 1%/year increase scenario.

TCRE Transient Climate Response to Cumulative Emissions — the ratio of global warming to cumulative carbon emissions.

Chapter 1

Introduction

Anthropogenic climate change demands societal trade-offs between near-term mitigation costs and longer-term, uncertain but potentially severe costs from damages associated with rising temperatures, changing precipitation patterns and increased frequency of extreme events, to name a few. Numerous lines of evidence, including observed warming trends, sea-level rise, and ocean acidification, point to the urgency of reducing greenhouse gas (GHG) emissions if we are to meet internationally agreed temperature targets, which were set to minimize uncertain adverse socio-economic future impacts [5, 6]. Yet, turning mitigation needs into practical economic policies is an exceedingly difficult challenge. Climate economics tackles this complexity by assessing the costs of climate change and offering frameworks that aim for optimal, intergenerationally fair policy solutions, ensuring that while the current generation bears a portion of mitigation costs, future generations are safeguarded from the most severe climate damages.

Various tools of climate economics can be used to strive toward designing an optimal climate policy. However, at least three building blocks are essential: (1) understanding the relationship between emissions and temperature rise, (2) quantifying the economic damages associated with increasing temperatures, and (3) designing rational decision-making frameworks under uncertainty—where uncertainty, as defined by the IPCC, is "a state of incomplete knowledge that can result from a lack of information or from disagreement about what is known or even knowable" [7]. Building on these interconnected blocks, this thesis presents three distinct yet complementary studies. The first paper refines our understanding of the emissions-temperature relationship by providing new perspectives on

the carbon budget concept and its potential deviations. The second paper advances climate impact quantification by developing and integrating sector-specific damage functions into a globally disaggregated economic model, translating them into regional and global economic losses. Finally, drawing on the insights gained from the first two papers, the third paper applies a unified decision-making framework that synthesizes trade-off-based and target-based approaches to inform optimal climate policy design.

Taken together, these three contributions reinforce a central theme of this thesis: as our understanding of climate modeling (Paper 1) and economic impacts improves (Paper 2), the rationale behind climate policy recommendations becomes more refined (Paper 3).

1.1 Thesis context: decision-making between trade-offs and targets

Designing an optimal climate policy consists of deriving an optimal mitigation pathway that aims to achieve an intergenerationally fair balance. This balance lies between the economic sacrifices borne by the present-day generation in the form of mitigation costs and the anticipated losses that future generations may face due to climate change. Given the inherent uncertainties and the interdisciplinary nature of this challenge, an appropriate tool and a well-founded decision-making framework to guide the mitigation choices under uncertainty is paramount.

A standard tool of climate economics for deriving policy recommendations is the Integrated Assessment Model (IAM). Broadly defined, IAMs are modeling frameworks that integrate knowledge from multiple disciplines to simulate the complex interactions between human and natural systems [8, 9]. In climate economic analyses, IAMs consist of two main structural elements: the climate system and the economic system. The climate system is represented by a simplified climate model that translates GHG emissions into global temperature rise. This condenses complex Earth System Model (ESM) behavior into just a handful of equations (e.g. [1, 10]). Thus, the reduced climate complexity enables computationally feasible coupling with the economic module [11]. The economic models then simulate economic activities that generate GHG emissions, which feed back into the climate module. In turn, the resultant temperature increases further affect economic processes, creating a feedback loop between the two coupled systems, internalizing

the economic externality of climate change, and thus allowing analysis of different mitigation scenarios.

The level of detail and degree of aggregation in IAMs shapes not only their structure but also the range and feasibility of their applications, as highlighted by [12]. He differentiates between two categories of IAMs in the field of climate economics: those focusing on policy evaluation (e.g. [13–15]), and those designed for policy optimization (e.g. [16–19]). In this thesis, we refer to IAMs as policy optimizers characterized by a high level of sectoral and regional aggregation, often representing the whole climate and economic system in one homogeneous unit.

Decision-making frameworks underpin the outputs of policy-optimizing IAMs, as they define how normative pathways are generated and how optimality is evaluated. Following a neoclassical economic approach, climate policy analysis typically assumes a rational decision-maker [20]. Within this framework, intertemporal welfare optimization serves as a central mechanism for generating policy scenarios. However, this approach does not, by itself, unequivocally prescribe how to address climate change. Two complementary schools of thought illustrate the range of decision-making approaches: (1) the trade-off-based approach and (2) the target-based approach, which differ primarily in how they account for climate externality. In addition to these approaches, the IPCC also recognizes other decision-making tools, such as multi-criteria analysis, robust decision-making, and real option analysis, which are not in the focus of this thesis [21, 22].

The trade-off based approach and a traditional economist's first choice is cost-benefit analysis (CBA). This is a well-established, axiomatically grounded method based on expected utility maximization [22–24]. In climate economics, CBA seeks to determine an optimal trade-off between contemporary emission reduction costs and future economic damages avoided by mitigation efforts [25]. However, the policy prescriptions arising from CBA-based IAMs can differ significantly, depending on underlying model assumptions. For example, Nordhaus demonstrates, using the IAM he developed, DICE, a preferred policy of only modest mitigation later in the twenty-first century, with 'optimal' global warming reaching around 3°C by 2100 [19, 26, 27]. Yet, using the same model with modified damage quantification and an improved climate model, Hänsel et al. found that the optimal mitigation strategy was more likely to align with Paris Agreement targets of limiting warming to 2°C [28]. In compelling contrast, Weitzman highlighted the fat-tailed

nature of climate sensitivity estimates and the structural uncertainty of climate-economy feedbacks to justify immediate, total emissions cuts, because the potential for catastrophic consequences far outweighs even the enormous mitigation costs [29].

These wildly divergent policy recommendations highlight the limitations of CBA, especially relating to damage function quantification. By design, CBA assumes a precise knowledge of the functional representation of climate damages, an assumption widely criticized as untenable [30, 31]. Moreover, critics like Pindyck argue that IAMs give a false sense of precision and that "current methods and models are not fit for purpose", urging for better damage representation [32]. As repeatedly emphasized in IPCC [33, 34], more research into impact models is required to address the issue of the damages on a sectoral level and in individual regions, let alone for aggregate damage functions used in CBA.

In contrast to CBA, cost-effectiveness analysis (CEA) is a target-based approach that does not attempt to explicitly quantify climate damages. Rather, it considers climate externalities in terms of temperature guardrails [35][1]. CEA rests on the idea, that if the policy-makers can agree on a climate target, then a tolerable window of emission pathways adhering to the target can be established, from which the least costly option can be selected [16, 37, 38]. If the costs are "sufficiently small", the thinking goes, then this should be enough of an argument for societal action to avoid uncertain future consequences [39]. More broadly, the normative rationale of CEA can be seen through the lens of one of the interpretations of precautionary principle as a justifiable response to deep uncertainty about possible future climate impacts [40, 41].

While CEA can be considered to be a viable alternative to CBA until climate impact quantification improves, Schmidt et al. highlight a critical flaw in how CEA handles learning events [42]. That is, if the anticipation of future learning is introduced, CEA can lead to infeasible solutions, or even result in negative expected values of information, incentivizing decision-makers to reject learning [43, 44]. To address this conceptual issue, Schmidt et al. introduced cost-risk analysis (CRA).

CRA is a hybrid decision-making framework that translates the target-based principles and underlying rationale of CEA into the trade-off based structural logic of CBA.

[1]Strictly defined, CEA branches into Chance-Constrained Programming (CCP) in its probabilistic form [36]. It was invented to deal with decision-making under long probability distribution tails of climate response, in case when traditional optimization tends to recommend extreme mitigation [37]. In this thesis, however, we put it under the umbrella of CEA to keep the focus on the conceptual issues of target-based approaches rather than on definitional distinctions

As such, it salvages the precautionary approach from CEA, but it avoids its dynamical inconsistencies by reinstating the utility maximization framework that underpins CBA [23]. It achieves this by introducing a risk function that reduces utility when the target is breached, calibrated such that it reflects the preferences of the target formulation. Risk function can be straightforwardly interpreted as a penalty for crossing the target, representing the decision-maker's aversion towards crossing the target.

While CRA's mathematical structure makes it appear to be just another version of CBA, in reality, CRA addresses the problem from a fundamentally opposite standpoint: given the insufficiency of damage estimates for a valid assessment, the precautionary principle should serve as the guiding rationale. For an in-depth discussion of CRA, see [45], and for its applications, see [46–49].

As climate impacts research advances, the justification for strict target-based approaches is bound to be called into question. A growing body of literature attempts to integrate the two approaches: incorporating damage quantifications, while still observing the guardrail [50, 51]. Held proposed an analytical framework that serves as a foundation for the gradual, systematic integration of well-known impacts into the current form of CRA [52]. Building on such integration efforts, this thesis set out to explore and implement this new framework that we call Cost-Benefit-Risk Analysis (CBRA), which explicitly integrates CRA and CBA. The mathematical formulation and more detailed descriptions of each decision-making framework discussed above, including CBRA, are formally introduced in Paper 3. This paper presents the first-ever operationalization of CBRA and demonstrates its capability to bridge trade-off-based and target-based approaches. As such, Paper 3 builds on the findings from Paper 1 and Paper 2 and represents a culmination of recent integration efforts, while also providing a springboard for future research using the integrated CBRA approach.

The incorporation of well-known impacts into cost-risk analysis was the initial motivation for the thesis. However, the research ultimately evolved into a work on three disjoint but decisive features underpinning climate economics. This thesis addresses: 1) climate modeling (contributing new insights on one of the two modules in IAMs used for mitigation analyses); 2) impact quantification and translation into the damage function necessary for trade-off-based approaches, and 3) the integration of tools and insights from these two domains into a novel CBRA decision-making framework.

Paper 1 explores the domain of climate modeling by examining the functional relationship between cumulative emissions and the global mean temperature. We refer to this as the carbon budget approach. In Paper 1, we investigate potential deviations from the carbon budget approach, and from the approximately linear observed relationship between these two variables. We develop a method for deriving the deviations and include potential non-linearities in a modified carbon budget equation. Besides being a relevant concept in simplified climate economic models, the carbon budget approach provides a crucial link in CRA. Held (2019) provides a theorem suggesting that under the condition that the carbon budget approach holds true, CEA and the dynamically consistent target-based alternative, CRA, would yield equivalent policy recommendations. Paper 3 numerically proves this hypothesis.

Paper 2 addresses the overarching challenge of translating physical climate changes into quantified monetary impacts and economic damages on the global and regional levels, structured in two stages. In the first stage, the impact function on the labor sector is calculated at a country-level resolution. These newly calculated functions, along with two others from the recent literature, replace the older impact functions in a regionally and sectorally disaggregated economic model, which then translates the revised sectoral impacts into updated assessments of globally disaggregated GDP-related economic effects. The results highlight regional disparities in losses while also providing globally aggregated estimates.

Paper 3 synthesizes insights from Papers 1 and 2, and contributes to broader efforts at integrating decision criteria in the field of climate economics. Firstly, Paper 3 augments the climate model investigated in Paper 1 by including a tailored, reduced uncertainty scheme for climate sensitivity that allows the user to conduct a probabilistic analysis, for which both CRA and CBRA are designed to account. Meanwhile, Paper 3 also integrates partial global economic losses from climate change, derived in Paper 2, as a global production damage function within a globally aggregated IAM. This is interpreted as an incomplete damage function, which includes both the partial damage aspect while keeping the target in the risk function of reduced weight. Thus, Paper 3 contributes by formulating the first-ever operationalization of CBRA.

The subsequent section offers more detailed introductions to each of the papers discussed, and the issues that they tackle. While the titles of the subsections do not directly

replicate those of the papers, they have been modified to more precisely reflect the relevant subtopics within climate economics and the specific issues each paper addresses.

The next section introduces each of the papers in more detail.

1.2 Mapping the thesis: topics across three papers

1.2.1 Climate modeling: Exploring the carbon budget equation and its deviations

In 2009, several climate modeling studies independently pointed toward a surprisingly simple relationship with profound consequences for the behavior of the climate system: the increase in global mean temperature appears to be roughly linearly dependent on the cumulative emissions of CO_2 [53–56]. This finding quickly received wider recognition, initially included in IPCC AR5 as a natural science finding [57]. By IPCC AR6, this relationship was a central tool for shaping mitigation policies because it could be used to determine 'carbon budgets'. These budgets represent the permissible carbon emissions in order to stay below a corresponding temperature target [58]. Hence, this link between temperature increase and cumulative emissions is referred to as the 'carbon budget approach' or, when referring to the mathematical formula describing this relationship, the 'carbon budget equation'. The key parameter in this equation—the proportionality factor that relates cumulative CO_2 emissions to global temperature rise—is known as the transient climate response to cumulative carbon emissions (TCRE).

The ability to directly quantify carbon budgets rests on a key assumption: cumulative emissions uniquely determine temperature increase, implying that this relationship holds regardless of the emission pathway (i.e., it is scenario independent). Studies using highly complex climate models (ESMs) supports the notion of scenario independence [59, 60]. However, due to their high computational demands, ESMs can only be used to examine a limited set of stylized emission scenarios, thereby providing incomplete evidence. This issue was partially addressed in other studies using simpler models with a range of emission scenarios [61, 62], but a comprehensive test across a full range of possible scenarios remains lacking. When describing the functional relationship between global temperature and cumulative emissions, relevant literature often vaguely represents it as "nearly

linear". Notably, natural science detected two non-linear mechanisms that counteract each other to form this "near linearity": the concave temperature dependency on the atmospheric carbon content, stemming from the radiance efficiency saturation, and the convex atmospheric carbon content dependency on cumulative emissions, stemming from declining natural carbon sinks [54, 63, 64]. Moreover, more recent evidence suggests that either of these two mechanisms could outweigh the other, leading to nonlinearities in the carbon budget approach [65, 66].

The first paper of this thesis tests both the scenario-independency and the (non)linearity assumptions, by introducing the concept of pulse response representation that reinterprets the carbon budget equation through the lens of Green's function. This novel approach demonstrates that by examining the shape of the temperature response to emission pulse, it is possible to quantify the maximum possible scenario-dependent carbon budget deviations that the model can produce. Using an optimization program that explores the entire range of possible emission scenarios within given constraints, the results confirm scenario dependency and indicate that these deviations diminish over time, if they appear at all. In addition, this study demonstrates that by observing the evolution of pulse response dynamics as the system undergoes climatic changes, one can directly derive the carbon budget equation in its non-linear form. In essence, this paper illustrates that by examining how the model's temperature responds to an emission pulse (pulse response), one can derive all of the information on the carbon budget equation – including its degree of (non)linearity and the potential for scenario (in)dependency. Moreover, the results indicate that different parameterizations of the same climate emulator can exhibit varying degrees of carbon budget deviations, thereby paving the way for future research. Since the study explores the whole range of maximum possible deviations, the results are constrained by the use of simple climate emulators, where we use FaIR 2.0.0 model [1].

While this paper arguably belongs to the domain of natural sciences, its methods and findings offer significant insights for the discipline of climate economics. In the analytic climate economy (ACE) models that combine general production systems with climate dynamics in an analytically tractable way, the carbon budget approach proves to be a convenient tool that simplifies the analytical approach [67]. Since ACE models have a similar structure as to their numerical counterparts, IAMs, this paper supports the notion that if only carbon dioxide emissions are being considered in the economic analyses, one could potentially bypass coupling the climate module with the economic module by

simply introducing the carbon budget equation, directly linking the emissions to the temperature increase. Moreover, Dietz et al. provide an overview of the climate emulators used in various IAMs and compare their pulse response behavior [68]. When interpreted through the pulse response representation, it is clear that most of the up-to-date IAMs implement climate emulators that do not adhere to the carbon budget approach. This finding therefore questions the validity of the conclusions stemming from many of these analyses. For instance, examining the pulse response shape of the climate module developed by Geoffroy et al. [10], as incorporated into the DICE IAM model by Nordhaus [69], reveals that this model does not adhere to the carbon budget approach. Similarly, the one-box climate module [70], implemented in other IAMs such as PAGE [71], FUND [17], and MIND [72], is explicitly calculated in the paper to show non-adherence as well, as both of those climate emulators show scenario-dependency of carbon budget approach.

Recall from section 1.1 how Held analytically proved that if the climate system adheres to the carbon budget approach, the different approaches of CEA and CRA should nevertheless arrive at equivalent results [73]. This provided a bridge between the target-based and trade-off-based approaches. The findings from the first paper directly address Held's proof and thus serve as a further crucial step toward this theoretical synthesis. This point will be conclusively demonstrated in the third and final paper of this thesis.

1.2.2 Economic damages: Impact quantification and GDP losses in the general equilibrium (CGE) framework

The following subsection serves two purposes. First, it provides a condensed overview of the challenges in quantifying economic damages and highlights why the debate on total climate damages remains unresolved. This overview underscores the need for a more robust decision-making framework for climate policy, as outlined in 1.1. Second, this subsection explains the rationale behind the climate damage quantification approach adopted in this thesis and how this was applied in the second paper. Quantitative projections of future economic impacts from climate change show considerable variation, reflecting differing methodologies and impacts studied [74–76]. Curiously, advances in empirical and interdisciplinary research on climate and socioeconomic systems have further extended this range of estimates [77, 78]. As a prominent example, the latest IPCC 6AR estimated potential global changes in GDP for 3 °C global temperature change ranging from about -55%

to modest GDP gains of 3%, depending on modeling method used (see IPCC AR6 WGII, Cross-Working Group Box ECONOMIC, [33]). The underlying reason for the large variety in economic impact assessments lies in how models translate sectoral impacts into quantified damages. In particular, the impact assessment will depend on the analyst's choice between aggregate damage functions and more granular, sector-specific approaches. Due to their highly simplified structure, IAMs often represent all temperature-related damages through a single, overarching damage function applied to total economic output (e.g. [19, 71]). This approach implicitly combines a wide range of climate impacts, including those on agriculture, labor productivity, health, and infrastructure, as well as other sectors affected by rising temperatures. The simplicity of an aggregated damage formulation makes them numerically capable of generating very large numbers of possible mitigation pathways, which then facilitates optimization and sensitivity analyses. Nevertheless, this approach to damage quantification has been criticized as potentially arbitrary, and susceptible to publication and replication biases [29, 30, 79]. This thesis aims to address this modeling culture of high aggregation and the problems that flow from it. In particular, regional and sectoral impacts become blurred, leading to transparency concerns and rendering 'invisible' potentially drastic differences in regional economic consequences. Thus, the second paper aims to assess economic damages with greater granularity, capturing variation in both region and sector. It quantifies the complete impact chain, from the bottom-up assessment of sectoral performance impacts to broader economic damages, as sectoral impacts propagate through regionally disaggregated world economies.

The first step towards more tractable assessment is the identification and quantification of sector-specific climate impacts. Roson and Sartori's work exemplifies this approach by providing a comprehensive set of country- and sector-specific damage functions [2],[1] capable of reuse in other economic analyses. Building on these foundations, Kompas et al. conduct a global assessment and apply these functions to estimate GDP impacts at the national level across all countries [81]. However, closer examination reveals notable gaps in Roson and Sartori's work. In the second paper, we address some of these methodological issues, refining the estimation of country-level heat-stress-induced labor productivity

[2]The term damage function in climate-economics represents a mathematical relationship between changes in economic activity and temperature increase [80]. In globally aggregated models, damage functions represent the change in total global economic activity, often in terms of GDP, as a response to climate change. In quantifying sectoral impacts, damage functions represent the changes in sectoral economic performance as a result of temperature changes.

losses. For the purposes of this thesis, our refinement serves as a case study of how sectoral damage functions are calculated.

Without revisiting methodological details here (see Paper 2, Section 2.1), our findings reaffirm that tropical and subtropical countries are expected to be disproportionately affected by future high humidity (e.g.,[82]). However, two significant sub-findings become evident when we examine losses as a function of global temperature increases. Firstly, losses are quadratically dependent on temperature increase, as opposed to the linear relationship assumed by Roson and Sartori. Secondly, based on 50 ensemble outcomes across four emissions scenarios, we explicitly demonstrate that the labor productivity loss damage function depends solely on temperature and is independent of the preceding emission pathway. As such, our findings contrast with previous studies, where scenario-independence was either assumed or not explored at all [83].

Having quantified labor productivity losses, we identify two additional sectoral impacts from recent literature to refine the country-level estimates by Roson and Sartori. These include agricultural yield changes from Li et al. and increased mortality due to higher temperatures from Bressler et al. [4, 84]. The final step is to translate these sector-specific impacts into overall GDP effects. Piontek et al. describe two distinct methodological approaches for this aggregation [85]. One approach is to assess GDP loss from each sector individually, and then the total economic effect being given as a sum of its parts (e.g. [17, 76, 86]). However, as Piontek et al. highlight, a key limitation of these approaches is that they ignore indirect effects. These indirect effects capture economic feedbacks in the form of endogenous economic adaptation (e.g., through labor force and capital relocation). They also include cascade impacts, where a climate shock in one part of the world affects other regions via global supply chains.

The second approach, which this thesis adopts, utilizes general equilibrium models (CGEs) to address these limitations by capturing economic adjustments and explicitly accounting for dynamics in international trade.

CGEs are economic models designed to simulate the complex global economy. CGEs do this by modeling value flows between domestic and foreign agents, including private firms and government entities, which represent countries and regions [87]. The use of CGEs for assessing climate impacts is well documented in the literature (e.g. [88–90]). However, as Cantele et al. showed [91], much of this literature relies on CGEs covering

only a limited number of regions and rarely disaggregating the world into more than 25 units. This severely limits the utility and real-world relevance of CGE-derived results about potential regional effects and inequalities in sharing the burden of climate change. In addition, most assessments either lack temporal dynamics (e.g. [92]) or adopt a recursively intertemporal approach with a limited time horizon, rarely exceeding the mid-21st century [93]. Moreover, the latter approach assumes myopic agents and intratemporal consumption optimization, making it inconsistent with IAMs that use intertemporal, forward-looking optimization to generate optimal mitigation pathways. Although there is some literature on the use of forward-looking CGEs, such studies typically represent only a handful of regions and often focus on single country analyses [94, 95]. The main limitation to wider use of CGEs in climate impact studies is the numerical challenges involved in solving these large models.

Following a series of developments in solution methods [96, 97], Kompas et al. study the above-mentioned limitations of CGE approaches. Using a partially forward-looking CGE model (GTAP-INT) [81], they quantified GDP losses stemming from rising temperatures for each country in the GTAP 9 database [98], incorporating the sectoral damage functions provided by Roson and Sartori [80]. In this paper we identify and resolve two issues in Kompas et al.'s work [81]. The first is the above-mentioned methodological issues in Roson and Sartori's study, which motivated the calculation of a revised labor productivity damage function. The second is that in GTAP-INT, only producers are forward-looking, meaning only producers could anticipate future conditions. For intertemporal consistency with IAMs, consumers should also possess the same foresight.

In the second paper of this thesis, we employ GTAP-INT 2 that modifies the previous version by enabling all economic agents to have forward-looking capabilities, thus providing a complete intertemporal CGE framework [99]. The Roson and Sartori damage quantifications have been replaced with a newly developed heat-related labor productivity loss function and two additional functions from recent literature, affecting agricultural yields and mortality changes due to climate change. After modeling a more complex world economy, consisting of 60 regions and 30 commodity groups, our results reveal significant disparities in regional GDP losses, with severe losses in some regions and potential benefits in others. Our results suggest these disparities could widen with increasing temperatures. This raises significant ethical concerns regarding the aggregation of these estimates into

a single global GDP loss figure, raising questions about standard operating procedures in IAM studies.

Some criticisms of using CGEs for calculating the effects of climate change refer to their structural inflexibilities, such as the inability to model changes in technology, investment, and consumption patterns. Furthermore, CGE models assume a perfect market response, which implies that their results can be interpreted as 'best case scenarios'. Nevertheless, we favor the CGE framework in this thesis because of its significant transparency benefits, with specific climate impacts and their integration into the economy rendered more tractable in CGEs. In the second paper, we focus on three impact channels, while openly acknowledging other channels we omit. This clarifies and qualifies the scope of our analysis. Thus, our approach not only addresses the methodological issues identified above, but also lays the groundwork for the application of a partial, temporally consistent, globally aggregated damage function in CBRA; a decision-making framework bridging the theoretical limitations discussed in Section 1.1. We demonstrate the practical feasibility of this bridging framework in the third and final paper of this thesis.

1.2.3 Decision-making under uncertainty: A unified Cost-Benefit-Risk-Assessment framework

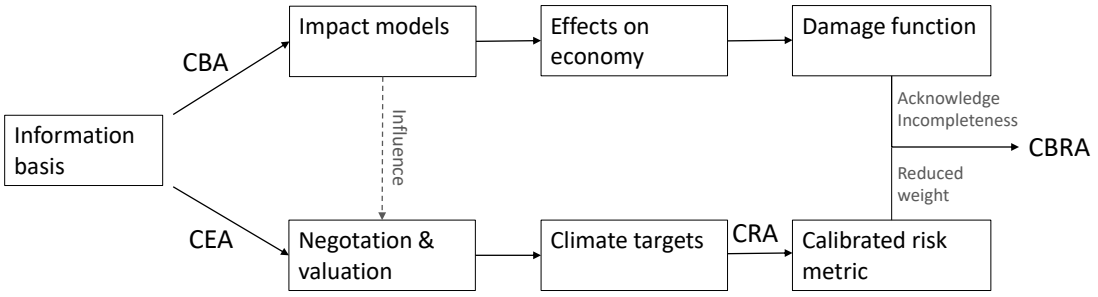

FIGURE 1.1: Logical flows leading to the representation of climate change effects in CBA, CEA, CRA, and CBRA frameworks. Economic impact modeling implicitly influences the negotiation and valuation processes involved in agreeing climate targets, while explicitly influencing the calculation of the damage function (see discussion in 1.2.2). The negotiation process encompasses all recognized uncertainties and results in the formulation of a climate target. CRA forms from the calibration of a risk metric in accordance with the agreed climate targets. Finally, CBRA combines CBA and CRA by observing the target with reduced weight and incorporating a partial damage function.

The third and final paper encapsulates the essence of the thesis: the construction and operationalization of CBRA, bringing its central premise into focus. Section 1.1 discussed

the research gap addressed by this paper. In summary, we start from a stance that two predominant, opposing schools of thought prevail in current IAM literature that focuses on identifying societally optimal policies, in the form of global emission mitigation pathways. Bridging the gap between target-based (CEA) and trade-off-based (CBA) approaches requires a framework that preserves guardrail targets while explicitly accounting for the economic damages caused by climate change [50, 51]. As discussed in 1.1, Cost-Risk Analysis (CRA) takes a critical step in this direction. CRA reinforces the utility maximization framework by introducing a penalty for exceeding temperature thresholds, thus mimicking the guardrail mechanisms of CEA [42, 43]. Yet, as climate damage quantification continues to advance, the rationale behind purely precautionary approaches grows less compelling. This emerging issue prompted Held to recently propose a bridging framework [52]. We call this Cost-Benefit-Risk Analysis (CBRA), which aims to systematically incorporate well-founded damage estimates into CRA. As such, CBRA represents a novel decision-making framework, unifying precautionary principles with robust (yet unavoidably incomplete) assessments of global economic damages. This unification is visualized in Figure 1.1, which also represents the respective logical sequence inherent in each of the above decision-making frameworks. The first and second papers in this thesis deal with intermediate steps in this sequence. Meanwhile, the third and final paper builds on the first two papers, but is directed at the consummation of the decision-making process; to our knowledge, we pioneer the operationalization of CBRA.

In addition to this methodological innovation, the third paper makes two other significant contributions to the climate economics literature. The initial contribution revisits fast and simple climate modeling by updating the central IAM used in CRA, MIND-L (Model of Investment and Technological Development including Learning) [37, 100, 101]. We replace this one-box model, which violated the carbon budget approach, with an improved climate module [70]. As in the first paper, we demonstrate the viability of the FaIR climate emulator as an efficient substitute in IAMs, vindicating an assertion by Dietz et al. [68]. A significant advantage is that FaIR adheres to the carbon budget approach. To tailor FaIR for use in CRA, traditionally based on decision-making under climate uncertainty captured in equilibrium climate sensitivity (ECS) distribution [72, 101], we have developed a probabilistic FaIR that accounts for ECS uncertainty only, reducing the whole uncertainty space into one parameter (ECS) (for details, see Section 2.3). With our probabilistic FaIR modification, we ensure that the analyses can be comparable with

previous work in MIND-L.

Building on the integration of the modified FaIR module—aligned with the carbon budget approach—we numerically demonstrate that CRA and CEA produce identical policy recommendations, consistent with the analytical prediction of Held (2019). Moreover, while this representation of uncertainty may be seen as oversimplified, since it does not capture the full uncertainty ensemble across all model parameters (as in [102], for example), we find the effect to be limited. It underestimates the temperature response of the full ensemble from Leach et al. by approximately 2.5 percentiles [1]. As such, this modified FaIR could be used in other IAMs that deal with climate uncertainty in the future.

A second contribution is the construction of a CGE-derived damage function. Building on the results from the second paper, this paper explicitly translates the global economic loss calculated in the second paper into a (partial) global damage function, implemented as an impact on the gross net production function in MIND-L. Somewhat surprisingly, studies employing this methodology remain scarce, despite recommendations by Piontek et al. [85]. This is notable given the arguments made in Section 1.2.2 supporting the use of CGE-based estimates to capture the global economic damage function, due to their ability to account for both direct and indirect effects on the economy. Furthermore, the existing CGE-derived damages come from either static or recursive CGE setups [103, 104]. In contrast, identifying optimal mitigation policies through intertemporal welfare optimization, as conducted in IAMs, assumes a forward-looking decision-maker, consistent with the temporal dynamics of GTAP-INT 2. Moreover, by incorporating impacts individually, we gain insight into the limitations and partial nature of global damage functions, which strengthens the case for adopting the hybrid target-based and trade-off-based approach embodied in CBRA.

The main, somewhat unexpected, discovery of the third paper is that CBRA can be interpreted as a mediator (or a translator) between the target-based approach and trade-off, damage assessment-based approach. More precisely, CBRA quantifies how many of the unknown risks embedded in climate targets under the precautionary principle are captured by explicitly (and potentially arbitrarily) quantified damage functions. We are therefore very interested to see future applications of CBRA in other domains, particularly other fields of decision-making under uncertainty.

1.3 Thesis outline

The thesis follows the following outline. Chapter 1 introduces the background and context of the thesis, and distinguishes the three themes addressed in the main body, which are presented in the form of three standalone papers — Paper 1, 2, and 3 — included as Chapters 2, 3, and 4, respectively. Chapter 5 discusses and summarizes the results from each paper, and provides the outlook for future research. Chapter 6 brings the three parts together, showing how they contribute to a common line of inquiry, and concludes the thesis.

Chapter 2

Carbon Budget Concept and its Deviation Through the Pulse Response Lens

This chapter is derived from the following publication:

- Avakumović, Vito. "Carbon budget concept and its deviation through the pulse response lens." Earth System Dynamics 15.2 (2024): 387-404

The carbon budget concept states that the global mean temperature (GMT) increase is roughly linearly dependent on cumulative emissions of CO_2*. The proportionality is measured as the transient climate response to cumulative emissions of carbon dioxide (TCRE). In this paper, the deviations of the carbon budget from the strict linear relationship implied by the TCRE is examined through the lens of a temperature response to an emission pulse (i.e., pulse response), and its relationship with a non-linear TCRE. Hereby, two sources of deviation are distinguished: emission scenario and climate state-dependence. The former stems from the scenario choice, i.e. the specific emission pathway for a given level of cumulative emissions, and the latter from the change in TCRE with changing climatic conditions. Previous literature argues for scenario independence using a stylized set of emission scenarios, and offers a way to fit a non-linear carbon budget equation. This paper shows how the pulse response, viewed as a Green's function, gives a unifying perspective on both scenario and state-dependence. Moreover, it provides an optimisation program*

that tests the scenario independence under the full range of emission pathways for a given set of constraints. In a setup chosen in this paper, the deviations stemming from emission pathway choices are less than 10% of the overall temperature increase and gradually diminish. Moreover, using the pulse response as a Green's function, the scenario-dependent effects of a reduced-complexity climate model were replicated to a high degree, confirming that the behavior of scenario-dependent deviations can be explained and predicted by the shape of the pulse response. Additionally, it is shown that the pulse response changes with climatic conditions, through which the carbon budget state-dependency is explained. Using a pulse response as an approximation for a state-dependent TCRE, an alternative method to derive a non-linear carbon budget equation is provided. Finally, it is shown how different calibrations of a model can lead to different degrees of carbon budget non-linearities. The analysis is done using FaIRv2.0.0, a simple climate emulator model that includes climate feedback modifying the carbon cycle, along with a one-box model used for comparison purposes. The Green's function approach can be used to diagnose both models' carbon budget scenario-dependency, paving the way for future investigations and applications with other and more complex models.

2.1 Introduction

The carbon budget concept, or the carbon budget approach, has gained prominence over the last decade due to its ability to determine allowable carbon dioxide emissions leading to a specific global mean temperature (GMT) increase. In essence, it assumes a direct link between the total cumulative carbon emissions and the temperature increase without the need to know the preceding emission pathway. Following the concurrent initial discoveries in the late 2000s (Allen et al. [53], Matthews et al. [54], Meinshausen et al. [55], Zickfeld et al. [56]), the concept received wider recognition after being included in the IPCC AR5 WG1 [1] [57], and after being presented as an explicit policy recommendation tool for limiting future climate change in IPCC AR6 WG1 (Table SPM.2) [58], where the 'remaining carbon budgets' indicate how much carbon may be emitted while still reaching low-temperature targets, assuming net-zero emissions afterward. By and large, since its emergence, the carbon budget has become 'a staple of climate policy discourse', having paved the way for various discourses, from policy proposals and international climate

[1] It was not labeled explicitly as a budget but rather presented implicitly through the emphasis on temperature dependency on cumulative emissions (see Figure AR5 SPM.10).

justice discussions to financial recommendations and even climate activism arguments for the immediate abandonment of fossil fuels, to name a few [105].

Formally, the carbon budget assumes the GMT increases nearly linearly with cumulative emissions, regardless of the preceding carbon emission scenario. Hence, a linear carbon budget equation:

$$T(t) = \Lambda F(t), \tag{2.1}$$

where $F(t) = \int_0^t E(\tau)\mathrm{d}\tau$ stands for cumulative emissions, and Λ is the proportionality constant, called the transient climate response to cumulative CO_2 emissions (TCRE). The (nearly) linear relationship emerges due to non-linearities cancelling each other out: a concave temperature dependency on the atmospheric carbon content and a convex atmospheric CO_2 dependency on cumulative emissions (Matthews et al. [54], Raupach [63]). The former stems from the radiative efficiency saturation of the atmospheric carbon, the latter from the declining ocean heat uptake and the weakening of natural carbon sinks [64].

When it comes to explicitly determining the remaining budget to reach a certain temperature target, a segmented framework had been devised by Rogelj et al. [106]. In essence, it determines what amount of cumulative emissions will lead to a given level of peak warming, if historical, non-CO_2 and Zero Emission Commitment (ZEC) warming are subtracted. ZEC is another metric closely related to TCRE and measures the warming (or cooling) that occurs after emission cessation [107]. MacDougall et al. [108] show that different models perform differently, with an inter-model range of ZEC 50 years following the emission cessation being -0.36 to 0.29 K. If ZEC were 0, then there would be no time delay in temperature response, and emissions would directly map to temperature according to TCRE. In reality, there is always some time lag between the input and the climate system's response (e.g., Ricke and Caldeira [109]). Regardless of ZEC, the linear segmented framework concept itself has been revisited by Nicholls et al. [110], who show that its assumption of a linear relationship between peak warming and cumulative emissions leads to lower budgets, albeit this effect is small in context of other uncertainties.

Hence, there is evidence that the relationship between the temperature and cumulative emissions (Equation (2.1)) can be non-linear, as either of the two (convex or concave)

mechanisms mentioned above could hypothetically outweigh the other under higher climatic stress (higher T). Indeed, Gillett et al. [59] show that the linear relationship overestimates temperature response in most Earth System Models (ESMs). Using the FaIR simple climate model (SCM), Leach et al. [1] quantify the TCRE drop to approximately 10% per 1000 PgC. Additionally, Leduc et al. [65] have shown that constant TCRE is a good approximation for temperature response under low-emission scenarios, while it overestimates the model's response to high-intensity scenarios; this reaffirms the need for TCRE to decrease in order for the relationship in Equation (2.1) to hold true. In the extant literature, Nicholls et al. [110] have derived the non-linear carbon budget equation by positing a logarithmic relationship between cumulative emissions and temperature increase with a multiplying factor that allows the relationship to be both convex and concave. In this paper, the change in TCRE with changing climatic conditions is referred to as (climate) *state-dependent carbon budget deviation*.

Further on, an alternative source of deviation from the budget approach that stems only from the choice of emission scenario, and not from the initial and final climate conditions of the system, is possible. In this paper, this type of deviation is referred to as an *emission scenario-dependent carbon budget deviation*. Previous literature, utilizing high-complexity climate models (ESMs), tends to argue in favour of scenario independence [59]. However, the problem with using ESMs to study the emission scenario effects is that these models are very costly from a computational standpoint, which means only a limited set of emission pathways are examined. Using a climate model of intermediate complexity, Herrington and Zickfeld [61] tested the robustness of the scenario independence with a set of 24 emission scenarios. Millar et al. [62] addressed this problem by forcing the simplified, globally aggregated climate model under various emission scenarios. However, to the best of the author's knowledge at the time of writing, the entire portfolio of emission scenarios that would yield the extreme cases of maximum possible scenario-dependent carbon budget deviations has yet to be investigated and scrutinized.

There is evidence that state- and scenario-dependent deviations are conditional on the model's complexity [111], suggesting that models with low linearity have a higher path dependence and vice versa. In this paper, the two effects are approached as separate entities, as the emission scenario-dependent carbon budget deviation implies the possibility of achieving a different temperature T by following a different emission pathway with the same total cumulative emissions F. On the other hand, it is exactly the change in F

(and consequently T) that drives the state-dependency of TCRE. As will be shown in this paper, with conclusions restricted to the model inspected, one can have one without the other, with the conditions given explicitly.

At its core, this study is focused on conducting a thorough assessment of deviations within the carbon budget approach, encompassing both scenario- and state-dependent deviations. The study introduces a novel concept termed the "pulse response representation", referring to the analysis of a temperature response to an emission pulse, under different climatic conditions. This conceptual framework proves to be a convenient and effective tool for explaining the observed deviations.

A reinterpretation of the carbon budget equation is suggested using a pulse response in the context of Green's function equation. It is shown that the linear carbon budget equation is only a special case of the Green's function equation. More importantly, the paper demonstrates that, by utilizing the pulse response as a Green's function, one can capture scenario-dependent deviation effects. Hence, it is revealed that, merely by assessing the shape of the pulse response, one can directly deduce to which extent the model adheres to carbon budget scenario independence.

The Green's function's validity is assessed through an optimization program functioning as the generator of scenario-dependent deviations. Specifically, the optimization program empowers users to assess the entire portfolio of emission scenarios, generating extreme cases of maximum scenario-dependent deviations within user-defined constraints. As such, the optimization program provides an enhanced approach in contrast to previous literature that tests predefined scenario sets instead.

Moreover, the paper translates the changing pulse response under varying climatic conditions into a state-dependent TCRE. The state-dependent TCRE, once explicitly quantified, is used to develop a non-linear carbon budget equation. This equation is capable of replicating the temperature dynamics seen in a reduced-complexity climate model, also reffered to as a simple climate model (SCM). Therefore, it is shown that one can deduce the model's degree of carbon budget non-linearity, only by examining its pulse response. Moreover, an alternative way of deriving the non-linear carbon budget equation to that put forward by Nicholls et al. [110]. The novelty of the method given in this paper is that a user does not assume any functional form but derives the change of TCRE from the change of the pulse response under changing climatic conditions.

Lastly, the paper shows how different parametrizations of the model lead to different behavior of the pulse response. Using the same logic as with inspecting the state-dependent TCRE, it is explained how the pulse response representation reveals whether a specific model's parametrization leads to concave, convex or linear carbon budget equation. This comes with a caveat since only a very limited parameter space has been inspected and the equation has been derived for only one parameter set. While the indications are clear, the validation across a larger parameter space is left for future work.

Overall, this paper offers a fresh perspective on how to approach the carbon budget and its deviations through the pulse response lens. It presents the pulse response in the role of Green's function, providing a unifying view on both the scenario and state-dependence of the carbon budget approach.

The paper is arranged as follows. In Section 2.2, the models are introduced and the Green's function framework is connected with the carbon budget equation. In Section 2.3, the pulse response representation in the context of Green's function is inspected and its implications for scenario and state-dependent deviations are revealed. Additionaly, Section 2.3 provides a method to derive a non-linear carbon budget equation using a changing pulse response as an approximation for state-dependent TCRE. In turn, Section 2.4 introduces the optimization program which generates the upper boundary scenario-dependent deviations and validates Green's approach; also, the non-linear budget equation is tested against the corresponding SCM. In Section 2.5, the findings are discussed in a broader context.

2.2 Models

The numerical optimization procedure introduced in Section 2.4. used to validate the Green's approach and generate carbon budget deviations requires a substantial number of model runs, so a computationally efficient model is a necessary choice. Hence, we restrict this analysis to a class of simple climate models, also known as climate emulators. We distinguish between and apply two approaches, the SCM approach and its corresponding Green's function approach. While the former is sufficient for numerical assessment of the carbon budget deviations, the latter mathematically formalizes the carbon budget

approach and offers a fresh perspective on the deviation through the pulse response representation. All of the runs are executed in the GAMS programming language, and the code for all models and runs is available online (https://doi.org/10.5281/zenodo.8314808).

2.2.1 FaIR model

By FaIR, I am referring to the FaIRv2.0.0 model as provided by Leach et al. [1]. The Cross-Chapter Box 7.1 in IPCC AR6 WG1 argues in favor of FaIR's value as a climate emulator [112]. For the purposes of this paper, two features of FaIR are crucial. The first is its ability to correctly capture the temperature response following a single carbon emission pulse, i.e., pulse response [113]; the second is its ability to incorporate climate feedback on the carbon cycle, with one of the effects being the modification of the changing pulse response with changing climatic conditions.

In essence, the FaIR model is a SCM designed to emulate the gas dynamics of different radiative forcers and their effect on the global mean temperature. Because we are interested only in the deviations from the carbon budget, the non-CO_2 forcers are left out of the analysis, utilizing only the carbon cycle system and its radiative forcing dynamics. The model's description and equations can be found in Leach et al. [1].

FaIRv2.0.0 consists of four carbon and three temperature components. Each carbon component has an associated decay timescale which dictates the dissipation of the carbon content into the shared permanent pool that represents the natural global carbon sink. Along with the global temperature increase, the sink's increased content creates a feedback mechanism, resulting in increased decay timescales and, therefore, increased atmospheric CO2 retention time. The atmospheric concentration gives rise to radiative forcing by combining a logarithmic and square root term, which translates into the temperature increase distributed between the components. Unless explicitly stated otherwise, FaIR is implemented with its default parametrization, with the default thermal and carbon cycle feedback parameters provided in [1], and with the default carbon cycle parameters presented in [113].

The effect of parameter uncertainty is addressed via a set of six FaIR calibrations. The parameters can be found in Tables 2 and 3 in [1], representing the thermal and carbon cycle feedback parameters tuned to CMIP6 models. Specifically, the sets used in this

paper are tuned to the MIROC-ES2L [114], BCC-CSM2-MR [115], MPI-ESM1-5 [116], CNRM-ESM2-1 [117], and ACCESS-ESM1-5 [118] models.

2.2.2 The one-box model

To see how drastically different pulse response affects the deviation, another SCM is introduced into the analysis. Employed as a climate module in climate-economy integrated assessment models like FUND [17], PAGE [119], and MIND [100], the one-box model consists of only one carbon and one temperature compartment, and it does not include any climate feedbacks. Since Joos et al. [120] have shown that three to four timescales attributed to individual compartments are necessary to correctly approximate the redistribution of CO_2 in the atmosphere, the one-box model is not sufficient to imitate ESMs fully. Nevertheless, Khabbazan and Held [121] have shown that different calibrations can be found with which it can emulate the temperature response of ESMs under RCP scenarios. The model's description and equations can be found in Petschel-Held et al. [70]. In this paper, the thermal parameters were chosen to fit the TCR and ECS values provided by FaIR's default parametrization, with the conversion formulae given in Khabbazan and Held [121].

Note that FaIR and one-box are not on equal footing, as the former is considered a state-of-the-art climate emulator, while the latter does not adhere to the carbon budget approach, as will be shown. Hence, the one-box model's pulse response should not be considered a correct representation of climate response, but rather a comparison tool. It is introduced in this article precisely because of its inexact pulse response behavior, in order to underscore how the pulse response is connected to carbon budget deviations. Also, it allows us to explore the effects of structural model uncertainty.

2.2.3 The Green's function framework

2.2.3.1 The Green's function formalism

Green's model is one equation motivated by Green's function formalism. Essentially, a Green's function $f_g(t-\tau)$ is a specific function unique to a set of linear differential equations $Lx(t) = y(t)$, where $y(t)$ is the input forcing and $x(t)$ is the state variable that

changes according to the forcing and the linear operator L. The advantage of Green's function is that it acts as a 'propagator' from the input variable (external forcing) to the output variable (change in state variable), allowing us to replace differential equations with just one equation, which reads as $x(t) = \int_{t_0}^{t} y(\tau) f_{\mathrm{g}}(t-\tau)\mathrm{d}\tau$.

Using the same formalism, Green's equation is proposed in the context of global mean temperature dynamics with a climate model in lieu of a set of linear differential equations (see Raupach [63]). Hence, we propose the following equation, imitating the Green's function formalism:

$$T(t) = \int_{t_0}^{t} E(\tau) f_{\mathrm{g}}(t-\tau)\mathrm{d}\tau. \tag{2.2}$$

The output variable is the global mean temperature change $T(t)$, and the input (forcing) variable is the emissions $E(t)$. Green's function $f_{\mathrm{g}}(t-\tau)$ modifies the contribution to a current temperature $T(t)$ stemming from the past emissions $E(\tau)$. According to Equation (2.2), the temperature in time t will depend on each emission contributing at time τ prior to t, with the effect modified by Green's function f_{g} dependent on how far the emission year τ is from t , hence $f_{\mathrm{g}}(t-\tau)$. Essentially, it is an integration scheme that counts the temporarily modified temperature contributions to each emission pulse, going backwards from moment t, with a resulting temperature being a superposition of modified contributions. Similar approaches can be found in the literature in Shine et al. [122] and Ricke and Caldeira [109]. The difference is that, in Equation (2.2), the temperature is deduced directly from emissions, without the need for quantifying the radiative forcing and/or atmospheric CO_2 response.

2.2.3.2 The pulse response as Green's function

To make use of Equation (2.2), one needs to choose an appropriate shape of Green's function f_{g}. Following the proposed definition, the chosen function is set to be a temperature evolution response following the 1 PgC emission pulse, or simply, the 'pulse response'. Therefore, in this paper, the terms 'Green's function', 'pulse response', and 'temperature evolution following the emission pulse' are interchangeable. Pulse response experiments are one of the generic experiments applied when evaluating climate models. As done in previous literature (Joos et al. [120], Millar et al. [113]), the pulse response is generated

by adding a unit emission pulse on prescribed emissions that keep a constant background atmospheric concentration background, as follows.

The model is forced by the idealized RCP6.0 CO_2-only emission scenario provided by the RCMIP protocol [66], starting from the year 1850. In the year of pulse response generation t_p, the emission pathway necessary to keep the level of atmospheric concentration $C_a(t_p)$ constant is generated. Using the derived emissions, two experiments are run: One with the generated emissions only and one with 1 PgC extra added in t_p. Thus, the pulse response (Green's function) is determined by subtracting the temperature evolution of the two runs.

The pulse response functions generated for different years (and hence, different climatic conditions) can be found in Figures 2.1 and 2.3, for the FaIR model standard parametrization, one-box model, and different FaIR parametrizations, respectively. In this paper, the set of different pulse responses generated under different climatic conditions is named a *pulse response representation*. Having a set of pulse responses (a representation) gives us information on both scenario- and state-dependency of a particular model, as will be discussed in the next section.

The Green's functions f_g utilized in Green's model (Equation (2.2)), and used in the optimization programs in Section 2.4, are generated at the year $t_p = 2020$ and depicted in blue in Fig 2.1, labeled 'pulse2020'.

2.3 Pulse response as carbon budget deviation indicator

In this section, the theory behind the pulse representation in form of Green's function and its ability to explicate carbon budget deviations is explored. The scenario-dependency is connected with the shape of the pulse response, whilst the state-dependency with changing of the pulse response under changing climatic conditions. The conclusions are validated numerically in Section 2.4. Firstly, the connection between Green's function (Equation (2.2)) and carbon budget equation as suggested by Equation (2.1) is examined, showing that the latter is merely a special case of the former.

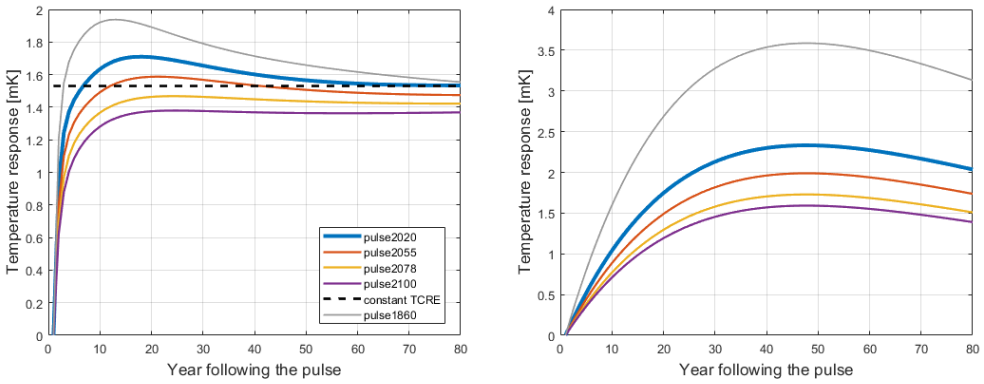

FIGURE 2.1: Temperature evolutions in response to 1 PgC emission pulse for different climatic conditions, i.e., pulse responses (colored lines) for FaIR (left panel) and one-box model (right panel), and the temperature response implied by Equation (2.1) (black dashed line, left panel). The numbers correspond to the year of an idealized RCP6.0 scenario in which the pulses were generated. Years 2020, 2055, 2078 and 2100 correspond to the FaIR generated background temperatures of 1, 1.5, 2 and 2.5 K, respectively, and 1860 to preindustrial climatic conditions. Constant TCRE is equal to 1.53 K EgC^{-1} and corresponds to the central TCRE estimates in Leach et al (2021) and AR6, respectively.

2.3.1 The carbon budget equation in the context of Green's formalism

Essentially, the linear carbon equation (Equation (2.1)) suggests an immediate temperature response to (cumulative) emissions, with the response that does not change in time or with climatic conditions. This implies that the pulse response introduced in the previous subsection should also be a constant function. In Figure 2.1, it is plotted as a dashed black line. Formally, a linear budget pulse response can be interpreted as a Heaviside function $\Theta(t)$ multiplied by a constant equal to Λ representing TCRE:

$$f_g^0(t-\tau) = \Lambda\Theta(t-\tau) = \begin{cases} 0 & t < \tau \\ \Lambda & t \geq \tau \end{cases}, \tag{2.3}$$

where τ is the timing of the emission pulse and is equal to the 0th year in Figure 2.1.

Proving that the Green's formalism can be considered an analogue to the carbon budget approach is simple. Inserting the idealized budget Green's function into Equation (2.2), one arrives precisely at the linear budget equation (Equation (2.1)):

$$T(t) = \int_{t_0}^{t} E(\tau) f_g^0(t-\tau)\mathrm{d}\tau = \int_{t_0}^{t} E(\tau)\Lambda\Theta(t-\tau)\mathrm{d}\tau = \Lambda\int_{t_0}^{t} E(t')\mathrm{d}t' = \Lambda F(t).$$

Therefore, if the temperature response always had the same (constant) shape as the dashed line in Figure 2.1, regardless of the underlying climatic conditions, the carbon budget would not show deviations – each unit of carbon emission would immediately add to the warming equally and regardless of when it was emitted. However, as shown in Figure 2.1, the FaIR-generated pulse responses are not a constant function, a fact that has implications for the carbon budget deviations.

2.3.2 Pulse response shape as a scenario dependency indicator

For now, the focus is on the pulse response functions that is used in Green's model (pulse 2020, Figure 2.1). In contrast to a constant step function, the initial response at the year of the emission pulse is zero. Then it steeply increases until reaching a maximum value of approximately 1.7 K, roughly 17 years following the pulse. Furthermore, following the peak, there is a slow relaxation of the response, which slowly reaches a constant response later in time.

To get a better feel for the deviations and how they are connected to the pulse, one can consider an extreme example. Say that all of the emissions are injected in one year. Total cumulative emissions will then amount to the value of the emissions injection only. Due to the pulse response, the temperature response will depend on what point in time the observer is at. Tracing the pulse response evolution, we can see a minimum magnitude of temperature in the first year of the pulse and the maximum temperature at the peak of the response, $\sim$17 years after the pulse. Effectively, these are two very different temperatures for the same cumulative emissions. The difference between the two temperatures is the maximum possible scenario-dependent carbon budget deviation. If the cumulative emissions then amount to 100 PgC, the pulse response scales accordingly, and the theoretical deviation between the minimum and maximum response is ˜0.17 K.

Finally, because of the gradual relaxation of the response, if the year in question is far enough from when we maximized the deviation, the deviation itself diminishes. In the extreme case presented in the previous paragraph, this can be intuitively seen as follows. Although there could have been a considerable difference in temperature stemming from the same cumulative emissions between the 0th (the injection year) and 17th year (the peak year) following the pulse, going forward in time, the temperature response difference between the 80th and 63rd year following the pulse (again, a 17-year

difference) is virtually non-existent. Hence, the carbon budget deviation 'fixes' itself as the system enters dynamic relaxation, i.e., the pulse response reaches a nearly constant value. Once it reaches the relaxation phase, the pulse response becomes very similar to the step-function response of the linear budget.

The Green's function derived from the one-box model is shown in Figure 2.1 (blue). Unlike its FaIR counterpart, the one-box model's pulse response peaks much later (roughly 45 years after the pulse). Additionally, and more importantly, it never reaches the relaxation phase in the form of a constant response in later years; it starts permanently decreasing after the peak instead. In the context of the discussion above, this means that, aside from its magnitude, even the sign of the one-box model's scenario-dependent deviations can change depending on the relative time we observe it. Repeating the thought experiment above, where we emit everything in one year, the observer will see a positive deviation comparing the initial (injection) year and the peak year ($\sim$45 years difference). If we go forward in time, specifically 45 years farther, the observer who was in the initial year now sees their temperature response at the peak, while the observer who was in the peak temperature year now sees a much lower temperature. Subtracting the two now yields a negative value, even though the deviation was previously positive.

In summary, the pulse response shape dictates both the deviation and its evolution, making it critical for the climate model's adherence to the carbon budget approach and its emission scenario independence. The FaIR model shows small, scenario-dependent deviations precisely because its pulse reaches an almost constant regime relatively quickly following a peak. Moreover, if a model cannot emulate reaching the temperature relaxation, it will also show much higher and more importantly, time-dependent emission scenario-dependent deviations.

2.3.3 Pulse response alteration as a state-dependency indicator

Until now, only a single pulse response (pulse2020) has been employed as Green's function and examined. However, the experiment shows that this pulse response changes with changing climatic conditions: Following the same procedure described in 2.3.2, pulse responses are generated later in the RCP emission run, for different t_p's accordingly. The

generated pulses are depicted in different colors in Figure 2.1 for both the FaIR and one-box models. The further analysis considers only the FaIR results, as the one-box model fails at criteria of pulse response relaxation, explored in the previous subsection.

When comparing the pulses (Figure 2.1), a general trend can be recognized. As the system is subjected to higher climatic stress in the form of higher cumulative emissions and higher temperatures, both the shape and the magnitude of the pulse response change. While all the pulse response variations show the aforementioned steep increase in the first few years following the pulse, the magnitude of the peak and the corresponding relaxation temperature level decrease with changing climatic conditions, with a visible 'flattening' of the curve.

2.3.3.1 State-dependent pulse response as a variable TCRE

As discussed in the introduction, the previous literature suggests that TCRE is not a constant value but slowly decreases with cumulative emissions. This can be interpreted as the carbon budget's state-dependency, which manifests in the non-linear carbon budget equation (Nicholls et al., 2020). This non-linearity can be identified by examining the change in pulse response shape with changing background climate conditions.

At the beginning of Section 2.3, it was shown how the step-function pulse response in Green's model translates into TCRE included in Equation (2.1). If the TCRE changes with background conditions, the carbon budget step-function pulse (black dashed line, Figure 2.1) should also change in magnitude following the climatic stress. Indeed, Figure 2.1 shows that the FaIR-generated pulse response decreases in magnitude with background conditions. If then the changing pulse is approximated with a changing step function, the decrease of the pulse response can be directly linked to the decrease of TCRE. A method for using a pulse response representation to explicitly quantify TCRE dependency on climatic conditions is developed, as follows.

To generalize the analysis, the additional pulses are generated under RCP4.5 and RCP8.5 emission scenarios, along with the already generated pulse responses under different climatic conditions under RCP6 (Figure 2.1). The first pulse of each run is generated at the benchmark year 2020 and the rest at the same temperature levels (1.5, 2 & 2.5 K), where possible.

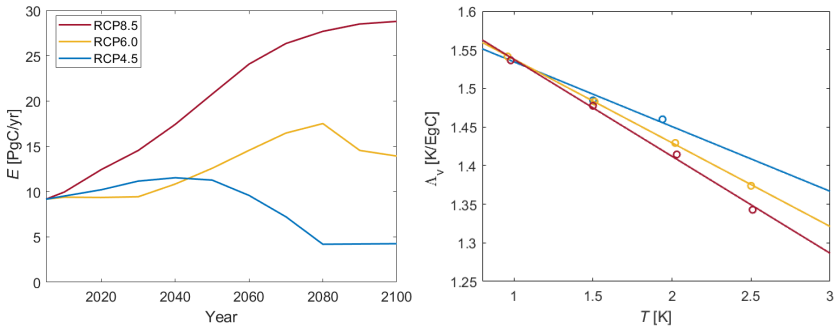

FIGURE 2.2: Right graph: TCRE approximations $\Lambda_v(T)$ generated from pulse response functions under different climatic conditions and emission scenarios. Scatter plots are actual values of Λ, while the line is the result of linear regression. The different colors represent the Λ_v's generated from different RCPs, which are plotted in the left graph.

Next, recalling the linear budget discussion, the generated pulses are to be approximated with the step function. Ignoring the temperature evolution dynamics in the early years of the pulse response, the pulse is transformed into a constant Λ_v by averaging it between years 70 and 80[2]. As shown in Figure 2.1, the pulse dynamics relax by that time, reaching relative constancy. With that approximation, however,the ability to express the time delay and scenario dependency is lost, as the shape of the pulse response function dictates the scenario dependency (Section 3.2). As they will be shown to be small, this aspect can be safely ignored.

After approximating the pulses, the corresponding cumulative emissions and temperature values (i.e., the background climatic conditions under which the original pulse was generated) are assigned to each value of generated Λ_v. By doing so, the $\Lambda_v(T, F)$ dependency is mapped, which, when reasoned in line with Equation (2.1)[3], can be considered a TCRE dependent on cumulative emissions and temperature increase, or simply, state-dependent TCRE.

In this way, the carbon budget's state dependency is made explicit: Examining each RCP case separately shows that Λ_v decreases linearly in T under the standard FaIR parametrization (Figure 2.2). Moreover, looking at the right figure, one can see that by adding 1 EgC into the system, $\Lambda_v(F)$ drops by roughly 10%, which is in keeping with the findings of Leach et al. [1].

[2]In this way, the approximation for each pulse resembles the black dashed line in relationship to the blue line in Figure 2.1.

[3]Note that Λ and Λ_v have the same function in the carbon budget equation. The difference is that Λ is a constant, while Λ_v is a function of temperature and cumulative emissions.

2.3.3.2 From pulse response to carbon budget equation

The RCP6-generated Λ_v (Figure 2.2, right panel, yellow dots) is chosen to derive the carbon budget's state dependency from the pulse response representation. The choice of RCP scenario does not constrain the conclusions of this exercise. Figure 2.2 suggests a linear relationship $\Lambda_v(T) = -\mathrm{a} \cdot T + \mathrm{b}$, with $\mathrm{a} = 0.1083$ EgC^{-1} and $\mathrm{b} = 1.646$ K EgC^{-1} derived via linear regression. Therefore, TCRE (here Λ_v) is reinterpreted through the lens of T dependency, as temperature is the main thermodynamic variable driving the climate system change. This way, assuming any functional form for the state depenency is avoided; rather, it is deducted from mapping $\Lambda_v(T)$ (Figure 2.2, right). The assumed linear relationship between TCRE and T suggests that TCRE can go to very low, and even negative values due to the negative linear coefficient. However, the linear form is derived and holds true for the values below 2400 PgC (approximately the cumulative emissions in RCP8.5 scenario at the year 2100). Hence, its domain of applicability is constrained within the theoretical TCRE bounds of 2000 PgC. Additionally, one can see that the assumed linear relationship suggests TCRE would reach zero at roughly $T = 15$ K, well above any projected future temperature increase.

Since Λ_v is, by definition, a temperature response to an emission pulse, the temperature change following the approximated pulse is interpreted as $\Delta T = \Lambda(T) \cdot E_{pulse}$. In words, the temperature change is equal to one unit of pulse emission scaled by temperature response to a pulse Λ_v. Given the fact that the emission pulse brings about a change in cumulative emissions, the aforementioned relation is rewritten in differential form as:

$$\mathrm{d}T = (-\mathrm{a} \cdot T + \mathrm{b})\mathrm{d}F. \tag{2.4}$$

By integrating Equation (2.4), one arrives at:

$$T(F) = \frac{\mathrm{b}}{\mathrm{a}} + (T_0 - \frac{\mathrm{b}}{\mathrm{a}})\mathrm{e}^{-a(F-F_0)}, \tag{2.5}$$

with T_0 and F_0 being the initial values at the time of the first pulse (pulse2020). Essentially, Equation (2.5) represents a non-linear carbon budget equation under a default FaIR parametrization. The validity of the equation is tested in Section 2.4.

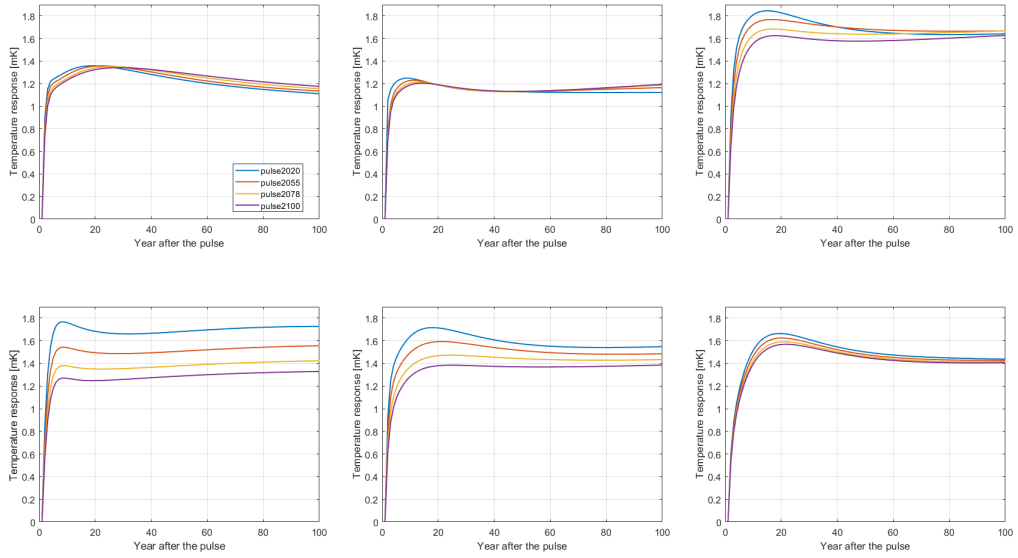

FIGURE 2.3: Pulse responses under different FaIR calibrations: MIROC-ES2L, BCC-CSM2-MR, MPI-ESM1-2-LR, ACCESS-ESM1-5, default parametrization, and CNRM-ESM2-1, respectively. Different parameter sets are each tuned to a specific ESM, with parameter values given in Tables 2 and 3 in Leach et al. [1]. Note that graph (e) matches the left graph in Figure 2.1, included here for comparison.

When plotted, one can see that $T(F)$ is a closely linear, slightly concave function within the F domain of interest[4]. Concavity comes from the (linearly) decreasing $\Lambda_v(T)$ (Figure 2.2, right). If, conversely, $\Lambda_v(T)$ increases with increasing T, the same derivation method as presented above would lead to a convex carbon budget equation. As will be shown in the next subsection, this is possible as pulse response, and subsequently $\Lambda_v(T)$, evolves differently under different FaIR parametrizations.

2.3.4 Uncertainty in pulse response

By considering the pulse response representation and its implications on the carbon budget framework under one FaIR parametrization, the effects of different model calibrations on pulse response and, thereby the carbon budget are evaluated in the final part of this section.

Figure 2.3 shows pulse responses generated as described in 2.2.3.2 under six different sets of FaIR parameters, each tuned to a different CMIP6 model, with Figure 2.3e being the default parametrization used in the rest of the analyses. We can see that every

[4]Note that here F represents the total cumulative emissions from the preindustrial era. One could rewrite the equation with $\Delta F = F - F_0$ to derive the temperature increase relative to the initial year $t_0 = 2020$.

calibration yields a distinct pattern of behavior. Using the framework introduced in the previous parts of this section, one can deduct how each calibration affects FaIR's adherence to the carbon budget approach.

To examine scenario dependency, one must examine pulse response shape (Section 2.3.2). Looking at Figure 2.3, we can see that all of the parametrizations show a relatively small scenario dependency, as all of them show pulse responses that peak in 10-20 years, followed by some degree of relaxation in the time domain of interest. In other words, one can imagine approximating them with a step function. Two parametrizations that stand out are MIROC-ES2L and ACCESS-ESM1-5. The former reaches a peak and then continually decreases just like the one-box model, although at a much slower rate (Figure 2.1b). Hence, the scenario-dependent deviations will not fully diminish and are likely to change sign. The same holds true for the latter, although in the other direction as the pulse response of ACCESS-ESM1-5, as the temperature gradually increases following the pulse.

In the context of state-dependent deviations, Figure 2.3 reveals an interesting effect of different FaIR parametrizations on the non-linearity type of carbon budget equation. In Section 2.3.4, it was shown that the changing TCRE under different climatic conditions can be reinterpreted as the changing pulse response through $\Lambda_v(T)$. Additionally, it was shown that a decreasing $\Lambda_v(T)$ (Fig 2.2b) leads to a concave non-linear carbon budget equation (Eqs. (2.4) and (2.5)). The opposite also holds true: If $\Lambda_v(T)$, and hence the pulse response increases in magnitude with higher temperatures, it results in a convex non-linear carbon budget equation. Ultimately, if the pulse response magnitude does not change with changing background conditions, the carbon budget equation is indeed linear[5]. With that in mind, one can easily deduct that not all the combinations of FaIR parameters lead to the concave carbon budget equation, as derived in Equation (2.5). For example, MIROC-ES2L tuned to FaIR indicates a slightly convex budget equation, while BCC-CSM2-MR and CNRM-ESM2-1 are closest to the linear carbon budget, while ACCESS-ESM1-5 shows larger concavity than the default FaIR setup inspected in the previous subsection.

Due to the constrained set of fully accessible parameter sets given in Leach et al. [1], only six calibrations are presented here. A larger set would provide some insights

[5]Note that a pulse relaxation is still a necessary requirement.

into which parameters in FaIR drive which types of behavior. Additionally, it would be interesting to see to which extent FaIR tuned to a CMIP6 model reproduces the pulse response representation behavior of its corresponding ESM under the same setup. To do so, one needs to run the pulse response experiments (Figure 2.3) with ESMs. If it were found to do so, one could potentially extend the pulse response framework with FaIR tuned to ESMs to analyze carbon budget deviations as produced by the corresponding ESM.

2.4 Numerical evaluation

In the previous section a theoretical background for inspecting carbon budget deviation through the lens of pulse response was established. The shape of the pulse response function is assumed to give information about the model's scenario-dependent deviations, and the method for deriving the non-linear carbon budget equation from the changing pulse response with changing climatic conditions is provided. In the first, brief part of this section, the state-dependent (non-linear) carbon budget equation is tested against its linear counterpart and FaIR. For the rest of this section the results of using an optimization scheme are presented. Using the optimization scheme in this context has a twofold role. Firstly, the pulse response's ability to capture scenario-dependent effects in a role of Green's function is confirmed with comparison to the corresponding SCM, validating the hypotheses given in the previous section. Secondly, the optimization scheme tests the full portfolio of possible emissions, providing the highest possible scenario-dependent deviation under given constraints.

The appendix introduces a modification to the Green's function approach that is necessary to compare diagnosed temperatures in the upper panels of Figure 2.5 (but not scenario-dependent deviations, lower panels) between the Green's approach and the FaIR model. The modification is a temperature leftover from emissions prior to an optimization year and is, in fact, ZEC (Appendix, Ch 3.).

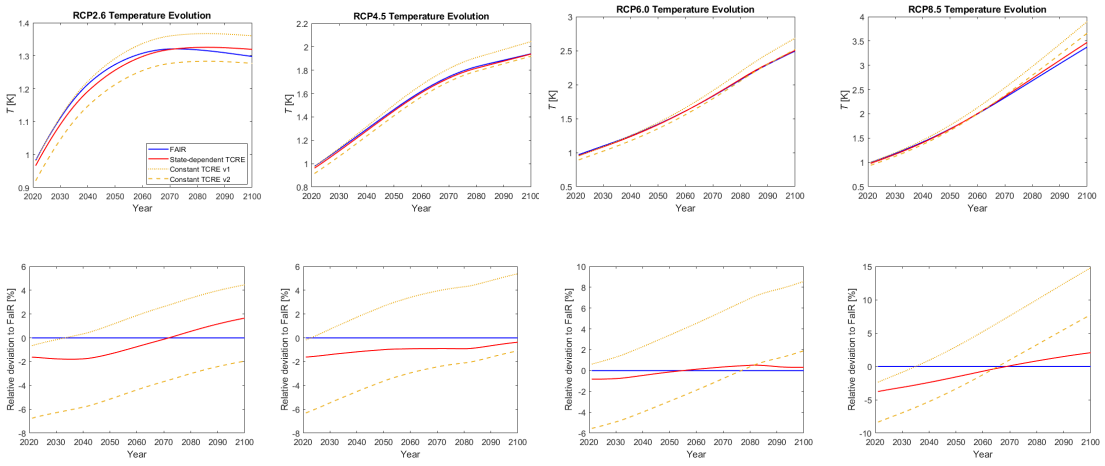

FIGURE 2.4: Top row: Temperature evolution under three RCP emission scenarios, calculated by FaIR model (blue), the derived non-linear carbon budget equation (Equation (2.5)) (red), and the linear carbon budget equation (Equation (2.1) with two different TCRE values) (yellow). Bottom row: Corresponding relative deviations of generated temperatures from FaIR-generated temperature, in percentages.

2.4.1 State-dependent carbon budget equation

To check if Equation (2.5) yields correct temperature dynamics, it is tested against the FaIR model under the aforementioned RCP scenarios. The resulting temperature pathways are plotted in the top row of Figure 2.4 (red) alongside the FaIR output (blue) and the linear carbon budget Equation (2.1) with two values of constant TCRE (yellow), while the bottom row shows the corresponding relative deviations from the FaIR-generated temperature pathway. The two TCRE values are TCRE_{v1}=$1.6 \cdot 10^{-6}$ K PgC^{-1}, and TCRE_{v1}=$1.53 \cdot 10^{-6}$ K PgC^{-1}.

Choosing a larger constant TCRE (v1) results in a more accurate temperature diagnosis in the first half of the century under lower cumulative emissions, with deviations increasing in step with rising emissions. The opposite is true for a smaller TCRE. In this sense, Equation (2.1) with a constant TCRE is a linearized version of FaIR in a similar way as the Green's function model but without the ability to generate scenario-dependent effects. Additionally, we can see that the state-dependent deviations are not transient like their scenario-dependent counterparts, but ever-increasing with the changing cumulative emissions. The highest detected absolute deviation is around $\sim$ 0.5 K for the end-of-the-century temperatures in the RCP8.5 run, which amounts to $\sim$ 15% relative deviation from the FaIR-generated temperature.

Unlike constant TCRE, Equation (2.5) replicates the FaIR generated temperatures in RCP2.6, RCP4.5, and RCP6 runs relatively well, with the relative deviation from FaIR being less than $\sim 2\%$ throughout the century. The largest absolute drift from the FaIR-generated temperature is around 0.1 K at the end of the century under the RCP8.5 scenario. However, this degree of drift is less than 3% in relative terms. Since RCP8.5 is arguably somewhere in the upper bound for possible emission pathways (and RCP2.6 arguably a very optimistic lower bound scenario), one can conclude that Equation (2.5) is a good emulator of FaIR under the single, default parametrization. The incorporation of different climate parameters in Equation (2.5) lies beyond the scope of this paper.

2.4.2 Scenario-dependent deviations

2.4.2.1 Optimization scheme

To test upper-bound scenario-dependent carbon budget deviations, the optimization program is formulated as follows:

$$\underset{\{E(t)\}}{(\mathrm{Max},\mathrm{Min})}[T(t^*)] \quad \text{s.t.} \int_{t_0}^{t^*} E(t)\mathrm{d}t = F_{\mathrm{tot}},\ \left|\frac{\mathrm{d}E(t)}{\mathrm{d}t}\right| \leq k,\ E(t) \geq 0,\ E(t_0) = E_0. \tag{2.6}$$

The program maximizes (or minimizes) the temperature variable in a given optimization year t^*. The minimum $T_{\mathrm{min}}(t^*)$ and maximum $T_{\mathrm{max}}(t^*)$ temperatures generated provide the upper and lower bounds for possible temperatures under given constraints. The maximum possible scenario-dependent carbon budget deviation T_{d} is then calculated by subtracting the two boundary temperatures, $T_{\mathrm{d}}(t^*) = T_{\mathrm{max}}(t^*) - T_{\mathrm{min}}(t^*)$.

In the optimization program (Equation (2.6)), the emission pathway assumes the role of the free control variable, except in the fixed initial condition $E(t_0) = E_0$. Hence, the novelty of testing scenario independence with the optimization program is that the emission pathway is generated, instead of being assumed as an input by the user. This way, the analysis does not rely on a limited number of emission scenarios but systematically runs through the whole portfolio of possible scenarios under given constraints. Three boundary conditions are implemented, whose values are subjectively chosen by the author, so that they provide a set of possible (not necessarily plausible) emission pathways. Restriction on total cumulative emissions F_{tot} ensures the same amount of cumulative

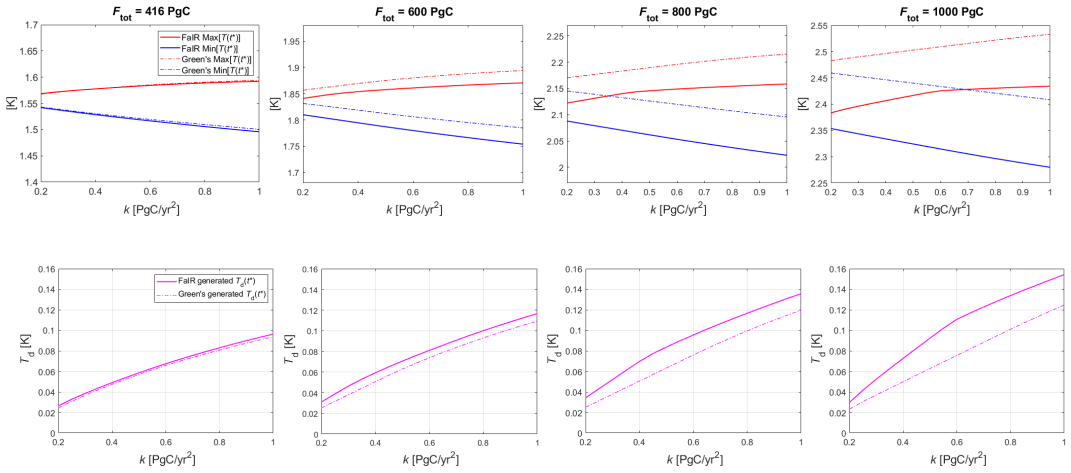

FIGURE 2.5: Top row: $T_{\max}$ (red) and $T_{\min}$ (blue) generated by the optimization program for the transient budget case, dependent on k, set up for different total cumulative emissions levels F_{tot} and $t^* = 2090$, with F_{tot} counted from the initial optimization year $t_0 = 2020$. The graphs are ordered by the magnitude of the associated F_{tot}. Y-axis domains all share the same relative interval of 0.3 K, but different absolute values. Lower panels: corresponding scenario-dependent deviations T_d plotted against the respective k values. In all graphs, the solid lines represent the FaIR output; the dashed lines represent Green's output.

emissions at the end of the each run, so that deviations stem only from scenario choice. The slope restriction k provides a bound on allowed emission change per year. The choice of boundary conditions and run configuration is further described in the supplementary material (S1,1).

Additionally, two different cases of scenario-dependent deviations are diagnosed and described in the supplementary. The "net-zero" case assumes that the emissions reach zero and that there are no emissions following the optimization year, while the "transient budget" case allows for emissions to evolve freely afterwards and allows for emissions to take any value in the optimization year.

2.4.2.2 Transient budget deviation

In Figure 2.5, the results of the optimizer in $t^* = 2090$ for four different F_{tot} choices in a transient budget setup are presented, explicitly showing the generated $T_{\max}(t^*)$ and $T_{\min}(t^*)$ dependent on k in the top row and and their corresponding $T_d(t^*)$ values in the bottom row. Note that F_{tot} are counted from the year $t_0 = 2020$, and not from preindustrial times like the variable F. For example, F_{tot} of 416 PgC, in addition to the pre-2020 emitted CO_2, amounts to 1000 PgC, which approximately corresponds to the

carbon budget allowed for adhering to 2 K increase with 67% probability, as suggested by the IPCC (Masson-Delmotte et al. (2021), Table SPM.2)[6].

Comparing the dashed and solid lines reveals that Green's approach using the pulse response as a Green's function diagnoses both $T_{\max}$ and $T_{\min}$[7], as well as scenario-dependent deviations, exhibiting deviations of the same order of magnitude as FaIR, with the Green's function approach being especially close to FaIR for lower cumulative emissions.

When comparing the effect of increasing cumulative emissions in Figure 2.5, some notable effects can be identified.

First, $T_{\mathrm{d}}(k)$ increases with higher cumulative emissions, in combination with the increase due to increasing allowed emission slope k. A comparison of the top to bottom graphs shows that the deviation increases by roughly 60%, in connection with the F_{tot} increase from 416 PgC to 1000 PgC. In the most extreme case with associated $F_{\mathrm{tot}} = 1000$ PgC, a deviation of $\sim$0.15 K, roughly 6.3% of overall temperature increase, is produced.

Next, as seen in the top row, the gap between FaIR's and its Green's counterpart's generated $T_{\max}$ and $T_{\min}$ steadily increases with higher cumulative emissions F_{tot}[8].

Furthermore, as shown in the bottom row, the difference in $T_{\mathrm{d}}(k)$ between the two models also increases with higher F_{tot}, albeit to a lesser extent. This effect can be attributed to the widening gap between the maximum and minimum temperature of the FaIR approach, which increases its $T_{\mathrm{d}}(k)$ to a larger extent than does Green's model (due to the constancy of Green's function). Both effects can be understood through the change of pulse response with changing climatic conditions. Namely, Green's approach uses one single pulse response as a Green's function throughout the run, albeit the pulse response changes under changing climatic conditions, i.e., higher cumulative emissions. The change in magnitude of the pulse response affects the drift between the FaIR and Green's generated $T_{\max}$ and $T_{\min}$, while the flattening of the response peak causes the drift between the diagnosed deviations T_d's.

[6]The generated temperatures are lower due to exclusion of non-CO_2 forcers and the choice of parametrization.

[7]Refer to the appendix for modification of Green's function to make this comparison possible.

[8]Note that the y-axis domains all share the same relative interval of 0.3 K, but different absolute values. In this way, the focus is shifted to the changing difference between the Green's model-generated and FaIR-generated temperature with increasing F_{tot}.

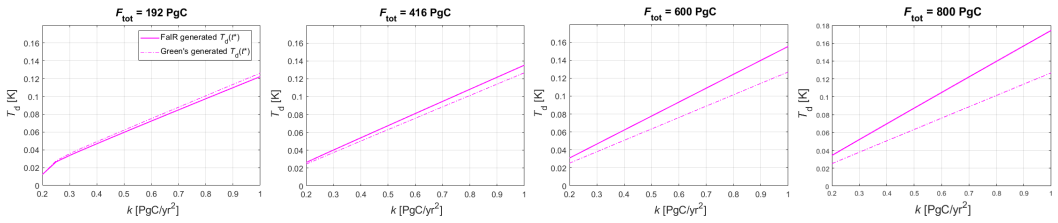

FIGURE 2.6: Scenario-dependent deviations, dependent on k, generated by the optimization program for the transient budget case with the allowed negative emissions, dependent on k, set up for different total cumulative emissions levels F_{tot} and $t^* = 2090$, with F_{tot} counted from the initial optimization year $t_0 = 2020$.

2.4.2.3 Effect of negative emissions

The effect of allowing negative emissions on the transient budget's scenario-dependent deviation is shown in Figure 2.6. The figure shows four different combinations of total allowed cumulative emissions F_{tot}, this time including a choice of $F_{\text{tot}} = 196$ PgC, which, when added to the cumulative pre-optimization emissions, reflects the carbon budget allowed for adhering to 1.5 K with 67% probability, as suggested by the IPCC (Masson-Delmotte et al. [58], Table SPM.2). Including negative emissions increases the generated T_d by roughly 0.04 K compared to the zero negative emissions scenario, in the highest k case for all F_{tot} combinations.

2.4.2.4 Scenario-dependent deviation time evolution

Because the optimization program, when set up as net-zero case, does not allow for emissions following the optimization year, it makes it possible to inspect the time evolution of the generated scenario-dependent deviation $T_d(t^*)$, as there are no further emissions to further modify the temperature.

Figures 2.7a and 2.7b show net-zero generated $T_d(t^*)$ with an additional, temporal dimension, instead of only k dependence in one year (Figure 2.5 (lower panels) and Figure 2.6). In this case, the optimization year is chosen to be $t^* = 2070$. The different shades of red depict the k range and their respective scenario-dependent deviations. The chosen F_{tot} for the run shown in Figure 2.7 is 416 GtC.

The net-zero budget case shows a significantly smaller initial $T_{\text{d}}(k)$ than its transient budget counterpart. The difference is due to lower minimum generated temperatures in the transient budget case, as a result of a non-constrained $E(t^*)$ and hence allowing

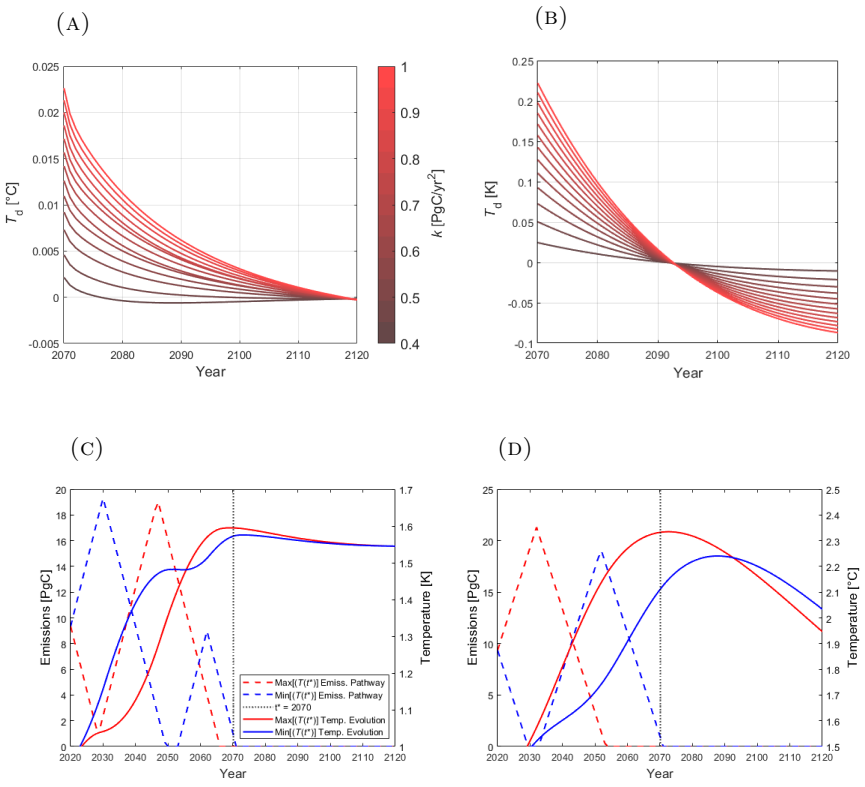

FIGURE 2.7: Graphs (a) and (b) show the temporal evolution of the net zero-case $T_{\mathrm{d}}(k)$ following the optimization year $t^* = 2070$, generated by FaIR and the one-box model respectively. The colors represent deviations corresponding to the different k allowed, with the darkest red being the lowest allowed (0.4 PgC yr^{-2}) and the brightest red being the highest (1 PgC yr^{-2}). The generated emission pathways and absolute temperature evolutions corresponding to the optimization runs (both min. & max.) under the same setup for one value $k = 1$ PgC yr^{-2} are shown in graphs (c) and (d), generated by FaIR and one-box respectively.

emissions to 'stack up' at the optimization year, while they are required to reach zero in the net zero counterpart. The pulse response discussion (Section 2.3) shows that if one wants to maximize the temperature response in a given year, they should stack the emissions ∼17 years before that year; conversely, to minimize the temperature response, they should stack the emissions as close as possible (within given constraints).

Further inspecting Figure 2.7a one can notice that, in FaIR, already small scenario-dependent deviations ultimately disappear if no additional carbon dioxide is added to the system; hence, the maximum deviations generated by the optimization program are only temporary. In contrast to FaIR, the one-box model's deviations (Figure 2.7b) do not 'die out' over time but decrease only to change sign, as predicted in Section 2.3.2.

The deviations' evolutions for $k = 1$ can be backtracked by examining the max. (red)

and min. (blue) generated temperature evolutions shown in Figures 2.7c and 2.7d, as the subtraction of the two yields the $T_{\mathrm{d}}(k)$. The FaIR-generated min. and max. temperature pathways are separated at t^* but eventually coincide, translating to a diminishing carbon budget deviation. Even though two temperatures are generated, they eventually reach the same level, just as the pulse relaxation discussed in the previous section suggests they should. Additionally, their cumulative emissions are equal, meaning that their pulse response is the same, so they reach the same level of constancy following the peak temperature response. The opposite is true for the one-box model counterpart. Because the one-box model's pulse response never reaches relaxation phase, i.e., keeps on decreasing following the peak, it makes a difference when we emit.

2.5 Discussion

To reiterate, this study focuses on evaluating deviations within the carbon budget approach, encompassing both its scenario- and state-dependent aspects. A novel method of analyzing these deviations is proposed in the form of a pulse response representation that explicates and distinguishes both forms of deviations by inspecting the evolution of temperature response to an emission pulse under different climatic conditions. The validity of examining the deviations through the lens of the pulse response has been tested by reinterpreting the pulse response as a Green's function of a set of differential equations that constitute a climate model [63]. Consequently, the introduced optimization program serves a dual role. It supplements the concurrent carbon budget literature by testing a full portfolio of possible, but not necessarily plausible, scenarios for scenario-dependent deviations under given constraints. Additionally, it confirms the ability of Green's function to capture scenario-dependent effects.

The analysis utilizes FaIR, the one-box model, and the associated Green's function models. The non-linearities appear in FaIR in both the carbon cycle feedback and in the temperature response saturation. As pointed out in the introduction, the interplay between the changing carbon cycle and temperature response produces the near-linearity of the carbon budget equation, with the former being convex and the latter a concave driver of the budget equation.

The second model used in the analysis is the one-box model, introduced as an example of a model with a dramatically different pulse response than FaIR, which facilitates comparison in the context of the pulse response behavior effect on the carbon budget approach deviations. In contrast to FaIR, the one-box model does not include climate feedbacks on the carbon cycle, so non-linearities arise only through the saturation in temperature response, which means that non-linearities are solely concave.

Moreover, the inclusion (or lack) of climate feedbacks has an effect on how the pulse response changes with changing climatic conditions. In the one-box model, the carbon cycle response stays the same regardless of background conditions, so the pulse response is modified only by logarithmic temperature response saturation. This manifests in the pulse changing magnitude but not shape. Conversely, including climate feedbacks changes the shape of the response function and modifies its magnitude. For a more detailed discussion on how the climate feedback changes the carbon cycle in FaIR in the context of decreased atmospheric CO_2 decay, see Millar et al. [113]. The effect of convex and concave drivers in context of pulse response representation and the non-linearities of the carbon budget equation (2.1) has been examined in Section 2.3.4.

To test whether pulse response behavior offers a trustworthy framework for explaining carbon budget deviations, it is employed as a Green's function in Equation (2.2). However, by proposing Equation (2.2) and using a FaIR-generated (or one-box-generated) Green's function, we assume that the climate model is a set of linear differential equations. Hence, although Green's model has been proven to capture scenario-dependent effects, the effects of climate change on the carbon budget approach cannot be explicitly captured with Equation (2.2). This effect is visible when comparing the FaIR's and Green's model optimization runs, as the two sets of generated temperatures have an ever-increasing gap with higher cumulative emissions (Figure 2.5, top row). One could modify Equation (2.2) so as to include a changing pulse response instead of a fixed f_g, but this remains theoretical; the implementation is unclear.

Regardless of Green's model's inability to correctly forecast (or hindcast, for the same reasons) temperature evolution, Section 2.4 shows that it is indeed capable of mimicking the scenario-dependent deviations of both FaIR and the one-box model. Even though there is an ever-increasing gap between temperatures generated by the SCM model and Green's model, the scenario-dependent deviations are well represented by Green's function

even for higher F_{tot}. Hence, one concludes that state and scenario dependencies can arise independently.

The distinction is crucial because non-linearities in the carbon budget and scenario-dependent deviations are distinct concepts, yet both contribute to carbon budget deviations individually. The key proposition is that state-dependent deviations manifest as non-linearities in the carbon budget equation, while scenario-dependent deviations could equally influence both linear and non-linear carbon budget equations. This distinction becomes intuitively evident when viewed through the pulse response lens, where these two effects are independent. In light of the findings in Section 2.4, we can consider two scenarios: one where the model, observed through the pulse response function, exhibits only state-dependent deviations (resulting in a non-linear carbon budget equation), and another where it exclusively displays scenario-dependent deviations while maintaining a linear carbon budget equation. In the case of state-dependent deviations, the pulse response resembles a step function that varies in magnitude with changing climatic conditions. Moreover, as illustrated through the derivation of Equation (2.5), if the pulse response (in this case, a step function) decreases in magnitude, the carbon budget equation becomes concave; conversely, if it increases in magnitude, the carbon budget equation becomes convex. On the contrary, for scenarios with scenario-dependency only (without non-linearities), the pulse response must not be a step function. Instead, it needs to exhibit some form of dynamic evolution that eventually leads to the relaxation of the pulse. The example would be the case when the pulse response (e.g., pulse2020) in Fig 2.1a would not change, thus always retaining the same shape regardless of climatic conditions. In that case the carbon budget equation would be linear (when viewed at the same point) even though it shows scenario-dependent deviations.

When it comes to validation of using pulse response as Green's function, the results show that the changing of the pulse under changing background conditions does not affect Green's model's ability to predict scenario dependency to a high degree. By combining these elements, the paper introduces the possibility of approximating the maximum scenario dependency of ESM models. This is achieved by utilizing their pulse response (acting as Green's function) and subjecting it to the optimization program, overcoming computational cost challenges that would otherwise render such an analysis infeasible. This claim remains to be validated in future work in a separate toolset, since the computational costs

also prevent the user from validating ESM's Green's function approach the same way it was done in this article.

When it comes to purely numerical findings in the context of scenario-dependent deviations, it was shown that how much we emit after the optimization year can dramatically affect the generated deviations. For FaIR, the largest possible deviation we acquire is approximately 0.15 K for the transient budget case. In the net-zero case, the largest deviation is well below 0.1 K. From the policy-relevant carbon budget viewpoint, this is good news, as it keeps the carbon budget approach resistant to scenario choice while complying with specific temperature targets and net-zero commitments. Regardless of the interpretation, the carbon budget scenario-dependent deviations identified are not permanent but a result of the optimization program in one year. The arguably small deviation diminishes relatively quickly if no further emissions are added to the system. Furthermore, scenario-dependent deviations increase with the higher cumulative emissions cap but do not depend on the optimization year (supplementary material S1.2). Moreover, allowing the system to produce negative emissions does not drastically increase scenario-dependent deviations. This shows us that the carbon budget approach is robust to scenario choice in FaIR.

The same conclusion cannot be made for the one-box model. As was shown, the one-box model produces up to 10 times larger scenario-dependent deviations, which evolve in time but do not disappear. The reasons for the dramatically different generated deviations are explained in detail in Section 2.3.2. Besides the one-box model discussed here, the shape comparison of pulse responses presented in Figure 1 in Dietz et al. (2001) Dietz et al. [68] shows that most simple climate models that are being used in climate-economic assessments have some potential for carbon budget scenario dependency – adding weight to the argument for replacing climate emulators with FaIR or any other model whose pulse response shows the right properties, if carbon budget adherence is of importance (presumably, it is).

Moving on, let us consider the connection between the ZEC metric and the pulse response. If ZEC is 0, as the central estimate in MacDougall et al. [108] suggests, this implies that temperature does not decrease or increase following the cessation of emissions. In the pulse response context, this requires that the pulse response is a step function, or close to it. Plotting the temperature leftover terms (Figure 2.8) explicitly shows the FaIR's

generated ZEC's under different climatic conditions (i.e., later in RCP run). FaIR initially produces a relatively small negative ZEC ($t_p = 2020$) that actually increases with changing climatic conditions, becoming slightly positive in $t_p = 2100$. This raises the question as to whether ZEC itself is a state-dependent value, i.e., whether the background climatic conditions dictate ZEC's value and to which extent. This question is left to be explored in more advanced models.

Concluding that the carbon budget is indeed unaffected by emission scenario choice confirms the carbon budget approach's value as a tool for directly mapping cumulative emissions to temperature increase. However, the question remains as to the functional form of the carbon budget equation. Section 2.4 provides a method as to how to deduct it from the pulse response representation. Namely, if TCRE is a constant, the carbon budget equation is linear. In Section 2.3, it was shown that the pulse response can be used as a proxy for TCRE, and that the pulse response decreases under changing climatic conditions in the default FaIR parametrization. A method was provided for deriving the non-linear carbon budget deviation from the changing pulse – a general method, which can be used for different models and different model calibrations. This offers an alternative approach to the non-linear carbon budget equation derived in Nicholls et al. (2020), as it does not assume a functional form of the non-linear carbon budget equation in advance, but derives it from TCRE dependency, building on Taylor expansion with respect to temperature, a key thermodynamic variable of the system investigated. As such, the method holds potential to be employed under different parametrizations and different models.

To address the lack of uncertainty in the analysis, Figure 2.3 shows different pulse response representations for different FaIR calibrations. Following the methodology explained above, one can deduct that under different parameter sets, FaIR can mimic various levels of carbon budget non-linearity and even full linearity, while keeping scenario-independence robust, as TCRE, which approximates the corresponding pulse responses, can change its magnitude in either direction. This is possible because of the inclusion of both feedbacks on the carbon cycle and the temperature saturation, which counteract each other and can be tuned separately, as mentioned at the beginning of the discussion section. Deriving the carbon budget equation explicitly for each calibration isn't pursued here, as doing so would not yield any new information, and the set is too small to make generalized conclusions on, e.g., how each FaIR parameter affects the (non)linearity of the

carbon budget approach. Among other questions raised, this is an interesting aspect for future research.

Finally, the tools used in this paper open a venue to inspect the deviations in other simple models. One promising candidate for developing the research further is the the Model for the Assessment of Greenhouse Gas Induced Climate Change (MAGICC), as it provides more detailed information about carbon cycle processes compared to FaIR. [123]. Given its relative simplicity, MAGICC presents an opportunity to be included in the optimization program, complementing the scenario-independence insights derived from the use of predefined emission scenario sets ([62], [110]). Even without the optimization program, the enhanced resolution of MAGICC in the context of the carbon cycle suggests that examining its pulse response representation under different parametrizations could potentially offer a more comprehensive understanding of the drivers of non-linearities in the carbon budget equation, in comparison to FaIR.

Conclusions

This article focuses on deviations from the carbon budget approach, seen as a linear mapping from cumulative emissions and temperature increase, and draws a clear distinction between carbon budget emission scenario-dependent and climate state-dependent deviation. Scenario-dependent deviations are the possible differences in resulting temperature that are solely due to the preceding emission choice. In contrast, state-dependent deviations underline the change in TCRE value, which depends on the change of background climatic conditions – specifically, the cumulative emissions and global mean temperature increase. Importantly, state-dependent TCRE leads to a non-linear carbon budget equation.

The innovative perspective towards inspecting the carbon budget deviations is provided in the form of inspecting the pulse response representation of a model, i.e., the changing temperature response to an emission pulse (pulse response) under changing climatic conditions. The shape of the pulse response dictates scenario dependency. On the other hand, the change of pulse response with background climatic conditions can be reinterpreted as the state-dependent TCRE, leading to the state-dependent deviations in the form of a non-linear carbon budget equation. The method used to derive the carbon

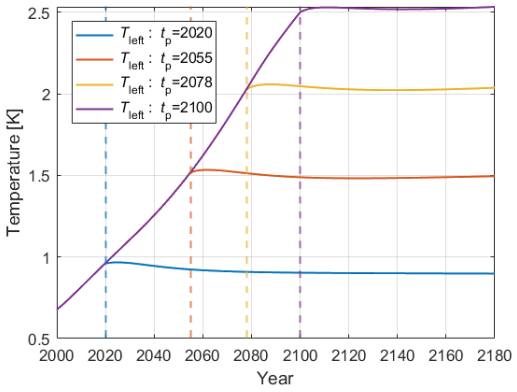

FIGURE 2.8: Temperature evolution run up to (RCP6.0 emission scenario) and following the emission cessation at different years t_p. The blue line represents $T_{\text{left}}(t)$, added to Green's integral to compensate for the temperature evolution leftover from prior to the optimization year $t_0 = 2020$.

budget equation from pulse response is universal and can be applied under different FaIR calibrations to see how individual climate drivers affect the non-linearity of the carbon budget. This, in combination with employing more complex models' pulse responses as Green's functions, opens a promising avenue for further research.

Finally, this article provides an optimization program that tests an entire portfolio of emission scenarios and diagnoses the maximal temperature differences under the same cumulative emissions within the user-defined constraints. As suggested by inspecting its pulse response, FaIR shows small and diminishing deviations compared to the total temperature increase, confirming the carbon budget's robustness when it comes to scenario choice.

Appendix: Temperature leftover in Green's function

When it comes to the magnitudes of $T_{\max}$ and $T_{\min}$, the Green's function approach requires an additional modification to make it (2), Green's approach responds only to emissions within the integral. That means that in the optimization run, which starts at t_0, it cannot capture the temperature response stemming from emissions predating t_0. Conversely, this is not a problem for the full SCM, since that 'leftover' temperature response is fed into the initial conditions of the run. To overcome this in Green's approach, the 'temperature leftover' parameter $T_{\text{left}}(t)$ to Equation (2.2), so it takes the form of $T(t^*) = \int_{t_0}^{t^*} E(\tau) f_{\text{g}}(t^* - \tau) \mathrm{d}\tau + T_{\text{left}}(t^*)$. Notice that the $T_{\text{left}}(t)$ term gets cancelled when

the deviation is calculated. The temperature leftover term is generated by feeding FaIR with RCP6.0 emissions until the year t_p, and then setting emissions to zero at the moment of pulse response generation. $T_{\text{left}}(t)$ is assessed as the temperature evolution after emission cessation. Hence, $T_{\text{left}}(t)$ is de facto ZEC by definition. Various temperature leftover values corresponding to different t_p years are shown in Figure 2.8. Note that the emission pathways and the years of emission cessation t_p correspond to those of pulse response generation (Figure 2.1).

Chapter 3

A Forward-Looking CGE Analysis of Climate Damages: Integrating Labor Productivity, Agricultural Yields, and Heat-Related Mortality

In this study, we examine the regional and sectorally disaggregated economic impacts of climate change on GDP, extending previous CGE assessments through more refined damage quantifications. First, we derive a new, country-level function for heat-related labor productivity, finding that losses follow a quadratic polynomial relationship with global mean temperature—independent of the emission pathway—and can become disproportionately large in tropical areas compared to cooler, drier regions. Next, we integrate these estimates with recent assessments of agricultural yield changes and heat-related mortality in the forward-looking CGE model GTAP-INT 2. Drawing on the GTAP 11 database (60 regions, 30 sectors), we run five emission scenarios out to 2200, revealing stark regional inequalities. The results reveal major regional inequalities, with poorer and more populous regions disproportionately affected, although certain countries experience modest benefits; emissions mitigation reduces both total economic losses and regional disparities. At the

global level, we estimate a cumulative GDP loss of about 18 trillion dollars by 2100 under a mid-range emission scenario. Weighing global GDP loss by the population affected, rather than by economic output, nearly doubles the estimated damages. Heat-related labor productivity losses alone account for approximately half of these total GDP damages. As our analysis includes only three major climate impact channels, our estimates remain conservative and incomplete, highlighting the need for further refinement and inclusion of additional climate impacts in future work.

3.1 Introduction

Earth's climate is changing at an unprecedented pace. From June 2023 to September 2024, global mean temperature surpassed all recorded levels for 16 consecutive months, alongside notable increases in ocean acidity, ice sheet loss, and sea level rise [124, 125]. Despite the Paris Agreement's ambition to keep warming below 2 °C [126], 2024 temperatures have already averaged about 1.5 °C above pre-industrial levels, and 2023 marked another record year for fossil fuel emissions [127].

These trends bring economic concerns. The top five greenhouse gas emitters alone have caused around $6 trillion climate-related damages since 1990 [128]. In 2010, heat-induced labor productivity losses cost the economy an estimated $311 billion [129], while natural disasters rose by 70% in 2000–2019 compared to the previous two decades, adding $1.34 trillion in damages [130]. Regionally, health-related costs of heatwaves in France reached $25.5 billion over 2015–2019 [131], whereas Nigeria's 2012 floods incurred $396 billion in losses through infrastructure damage, disease spread, and the resulting food insecurity [132].

Looking forward, however, projections of economic impacts of climate change vary significantly due to differing methodologies and impact coverages[77, 133]. According to the latest IPCC assessments, under 3 °C warming, global GDP outcomes can range from more than 50% losses to modest gains [33].

The IPCC identifies two distinct methodological approaches: statistical and structural. The statistical method implies identifying "economic impacts in a given sector or in aggregate, inferred from observed changes in economic factors, weather and climate, with responses and net results constrained by available data." [33]. In general, statistical

approaches project (in some cases substantially) higher losses [74, 86, 134, 135], compared to their methodological counterpart. However, we believe that they can overestimate the losses as they fail to account for economic readjustments following a climatic shock, since they simply sum assumed-to-be-independent sectoral impacts. For example, Burke et al. [86] assumes the economy to be made of separated (atomistic) industries that do not modify capital or labor in response to climate change, or that trade patterns within countries are not changing either; this means that the economy is kept under constant suboptimal performance leading to accumulation of losses that could be avoided (a part of it, at least) by allocating the workforce or investing in different industries that are more suitable to the new climate conditions, as one would expect to see in real-world economies. In this paper, we contribute to the literature on estimating the impacts of climate change through structural modeling [136, 137]. This approach simulates the economy by capturing climate impacts on production and its inputs, household consumption, investments, and, depending on the degree of spatial and sectorial aggregation, trade between sectors and regional economies. It accounts for feedback between the economy and climate impacts, as well as the interplay between different impacts and sectors, which captures indirect as opposed to direct costs only obtained by aggregating the damages independently [85].

In our view, the models that address these challenges fall within the category of computable general equilibrium (CGE) models, a subclass of economic models (EMs) designed to represent the global economy by simulating value flows among domestic and foreign agents, including households, private firms, and government entities representing countries or regions [87, 138]. Further strength of the CGE approach is its ability to treat each regional sector independently while capturing their interactions through transmission channels. This structure allows modelers to incorporate economic impacts that have been specifically calculated for individual sectors/regions, making them ideal for evaluating heterogeneous climate effects in a global economic framework [90].

Temporal dynamics in CGE models can be either static or dynamic. In the static setup, the shock is introduced in a single (baseline) year, with the resulting effects of the shock being a new equilibrium in that year, without exhibiting temporal evolution (e.g., [139]). The use of static CGE models in the context of climate change is well-documented in the literature [3, 103, 140]. However, static models cannot trace adjustment paths over time.

In contrast, dynamic models capture the temporal evolution of shocks, which can be addressed using either a recursive or an intertemporal (forward-looking) approach. Recursive dynamic models, often preferred for their lower computational requirements and greater numerical tractability, solve the model sequentially for each time step. Each period is treated as a separate static equilibrium, with information communicated intratemporally between neighboring time steps through linking variables such as savings and investment [141]. A systematic review conducted in 2023 [142] highlights that recursive models are by far the most commonly used temporal dynamics model setups in climate policy analyses, with static models ranking second. For instance, [104] revisits a study previously conducted using a static setup, demonstrating that the recursive approach reveals greater regional disparities in the results. However, the overall median aggregated global damage remains small (0.5% on roughly 2 °C increase). In recent times, a CGE model had been successfully integrated with a climate model for policy analysis [93]. However, this integration was limited in its time horizon (until 2060), likely due to computational challenges. While the recursive setup represents an improvement over the static counterpart for long-term policy evaluation, it applies deviations from the baseline as shocks to exogenous variables only at the current time step, with no influence from future shocks on present agent behavior. This assumes fully myopic agents who fail to anticipate future climate change—a simplification that, in our view, is not realistic.

This brings us to the final candidate: the intertemporal, forward-looking CGE framework. In contrast to the recursive approach, the intertemporal model solves for all time steps simultaneously, optimizing decisions across the entire time horizon while accounting for all future shocks. This approach enables forward-looking agents with perfect foresight but comes at a significantly higher computational cost. In this sense, the intertemporal CGE model functions similarly to a standard IAM, albeit without the integration of a climate module (as of yet). Experimentally, [143] explores the differences between the two approaches by setting up the same CGE model in both intertemporal and recursive forms, aiming to compare them. Their findings suggest that while the intertemporal framework is better suited for climate policy evaluations (e.g, borrowing and of GHG allowances), the recursive framework, with its lower computational costs, offers greater flexibility in representing system details, providing strong justification for its use. However, recent developments cast this conclusion in a new light. [91] systematically reviews the literature

on CGE models, comparing temporal dynamic approaches by analyzing their time horizons and the number of model components, such as regions and sectors, captured in their simulations. Contrary to the notion that recursive models offer superior flexibility and representation, this review reveals that one intertemporal model, GTAP-INT, stands out [144], including by far the most components and extending to the longest time horizon among the models examined, accounting for 139 countries, over 50 sectors and a time horizon past 2200.

The GTAP-INT model builds on the Global Trade Analysis Project (GTAP) static CGE model [3], with a series of technical modifications [96, 97], including an improved solving technique that enhances simulation speed and stability [144]. Its forward-looking nature stems from allowing producers to optimize capital investment decisions over time to maximize long-term profits, governed by capital accumulation equations and shadow pricing [97] (see Appendix A.1 for details). Using this advanced modeling framework [81], the damage functions for health impacts, sea-level rise, agricultural yield losses, and heat stress effects on labor productivity—estimated in [80]—are implemented to evaluate the economic consequences of different temperature pathways. These calculations assess climate-induced impacts across all countries included in the GTAP database, leveraging GTAP's highest level of regional resolution to date. However, two limitations motivate our update: (i) households are myopic in GTAP-INT (only producers are forward-looking), and (ii) the damage functions can be modernized using newer evidence and methods.

In this paper, we address both issues. We utilize GTAP-INT 2, an upgrade from GTAP-INT that incorporates a forward-looking household, completing the transition to a fully forward-looking GTAP model [99]. Moreover, we incorporate state-of-the-art climate impact assessments examining the effects of three distinct biophysical impacts of climate change, using damage functions that capture changes in agricultural yields, heat stress on labor productivity, and the effects of a changing climate on human health. For the overview of GTAP-INT 2 structure, and the specific modifications that extend GTAP from a static to an intertemporal (forward-looking) model—see Appendix A.1.

The paper's structure is as follows. In Section 3.2, we develop an improved country-level, heat-related labor productivity damage function. In Section 3.3, we provide a brief overview of additional impact channels, and outline the simulation setup. Section 3.4

presents the main results, followed by a discussion of their broader implications in Section 3.5.

3.2 Labor productivity damage function

labor is a fundamental driver of total production, playing a critical role in overall economic output. However, as climate change drives global temperatures upward, excessive heat exposure increasingly leads to fatigue, dehydration, and cognitive decline, thereby reducing workers' efficiency and labor productivity [145]. Sectors heavily reliant on outdoor labor, such as agriculture and construction, are particularly vulnerable, disproportionately affecting lower-income populations employed in these industries [146]. Consequently, heat-induced impacts on labor productivity act as a catalyst for deepening economic inequalities.

Previous studies within the GTAP intertemporal framework have utilized heat-related labor productivity damage functions from Roson and Sartori [80, 81]. Among various other climate change impacts, their work provides ready-to-use country-level labor productivity damage functions, formulated as linear functions of temperature. However, closer inspection of their methodology raises several concerns, including the use of base data at a monthly resolution, missing climate data on relative humidity, unclear country specifications, the absence of specific climate model projections, and an arbitrary choice of o linear upscaling of base results when constructing a damage function.

In this study, we revise their estimates by deriving updated country-level labor productivity assessments. Using daily climate projections, we demonstrate that the damage function follows a quadratic rather than a linear form and explicitly show that it is independent of the preceding emission pathway, supporting a purely temperature-dependent relationship.

3.2.1 Methodology

The climate variables used in the analysis are daily average gridded temperature and relative humidity levels, obtained from the Max Planck Institute for Meteorology Earth System Model (MPI-ESM 1.2) [147]. These data are provided under four different CMIP6

projection scenarios (SSPs) as well as a historical run serving as the baseline scenario. To account for uncertainty, we analyze 50 ensemble members of MPI-ESM model runs separately. By incorporating the full range of ensemble members, we capture the internal variability of the climate system. Unlike relying on multi-model means, which can obscure important variability and extreme events, this approach preserves the full spectrum of potential future scenarios, offering a more realistic risk assessment—albeit at the cost of potential model biases. As a compromise between the available data and an effort to capture more emission scenarios with a full uncertainty ensemble, the chosen grid resolution is 250 km. The model output is publicly available and distributed by the World Climate Research Program [148]. Population data are sourced from NASA's Socioeconomic Data and Applications Center [149], using gridded world population estimates for the year 2020. We opted for 30 arc-minute resolution (approximately 40 km grid length)and upscaled it to match the climate data resolution, ensuring spatial consistency necessary for country-level population weighting. Since we are upscaling population counts within grids, a natural choice was to set each upscaled grid's value as the sum of its finer-scale components. The country-level data is represented as the sum of the population-weighted grids within each country's borders. First, we generate separate grids for each country, preserving original population values within national boundaries while setting values outside to zero. Given the high temperature gradient between coastal and maritime grids, we adopt a conservative approach in delineating borders, ensuring that the selected grids predominantly capture land areas. Out of the 177 countries distinguishable by region masking python package[1], 25 were omitted in the analysis due to their size being smaller than the grid size (e.g., Palestine or Taiwan). Once the countries are separated, we assign a population-based weight to each grid within a country, calculated as the grid's population count divided by the total national population (i.e., the sum of all grids within the country's borders). These "weighting masks" are applied to the climate data, generating separate population-weighted grid datasets for each country. Country-level variables are then derived by summing all population-weighted climate data within each country's borders, ensuring a more accurate representation of population heat exposure.

The method of acquiring the labor productivity losses from the daily average temperature and relative humidity data is motivated by Kjellström et al.[150]. Before doing the country masking, daily Wet-Bulb Globe Temperature (WBGT) values are calculated for

[1]Documentation available at https://regionmask.readthedocs.io/en/stable/, accessed 23/09/2024.

each grid following the approximation given by the Australian Bureau of Meteorology [151], such that

$$WBGT = 0.567 \cdot T_a + 3.94 + 0.393 \cdot \frac{RH}{100} \cdot 6.105 \cdot exp\left(\frac{17.27 \cdot T_a}{237.7 + T_a}\right), \tag{3.1}$$

where T_a is the average daily surface temperature (in °C), and RH the average daily relative humidity (in %). This WBGT measure does not, however, account for sun exposure or wind speed, both of which influence human heat stress. Nevertheless, due to data limitations, we adopt this as the best available approximation. The WBGT grids are then population-weighted and aggregated as described earlier, yielding daily country-level WBGT values.

After preprocessing the country-level WBGT data, the next step is getting a daily WBGT frequency distribution in the baseline period (1990-2009) and five projected time periods (years 2015-2034, 2035-2054, 2055-2074, 2075-2094 and 2094-2100). For each country and each timeslice, the daily occurrences of WBGT values are counted with a precision of two decimal places and grouped into bins, yielding the WBGT frequency distribution. Using these frequency distributions, we calculate the productivity decrease relative to baseline for each timeslice, as follows.

To estimate work ability from WBGT, we adopt a WBGT-based work ability metric as a pragmatic choice, balancing methodological robustness with practical applicability. While advanced physiological models, such as Predicted Heat Strain (PHS) or Universal Thermal Climate Index (UTCI), can account for cumulative physiological strain and provide more detailed assessments, they require significantly more data and computational resources. In contrast, WBGT-based metrics are well-established and widely used in occupational heat stress assessments, offering a straightforward and empirically validated approach to estimating heat-related productivity losses [152]. WBGT is translated into ability to work using an approximated Hothaps work ability function

$$f_h(WBGT) = 0.1 + \frac{0.9}{1 + (WBGT/\alpha_1)^{\alpha_2}}. \tag{3.2}$$

Three different parameter sets (α_1,α_2) are equal to (34.64, 16.64) for low, (32.93, 17.81) for moderate, and (30.94, 16.64) for high workload, as given by [152]. Then, the total workability W_h within a a given time period is calculated using the sum of daily work

ability values, determined by the frequency WBGT occurrances and their corresponding work ability estimates:

$$W_h = \sum_i \frac{n_i \cdot f_h(WBGT_i)}{N}, \tag{3.3}$$

where N is the total number of days in the time period, and n_i the count of the days with corresponding WBGT value $WBGT_i$. Finally, productivity loss is quantified as a relative change in total work ability compared to the baseline period (total) work ability. By measuring workability loss relative to the baseline, we account for historical, endogenous, and country-specific adaptations to higher WBGT conditions, ensuring that the assessment reflects existing resilience to heat stress in different regions.

3.2.2 Country-level labor Productivity Loss

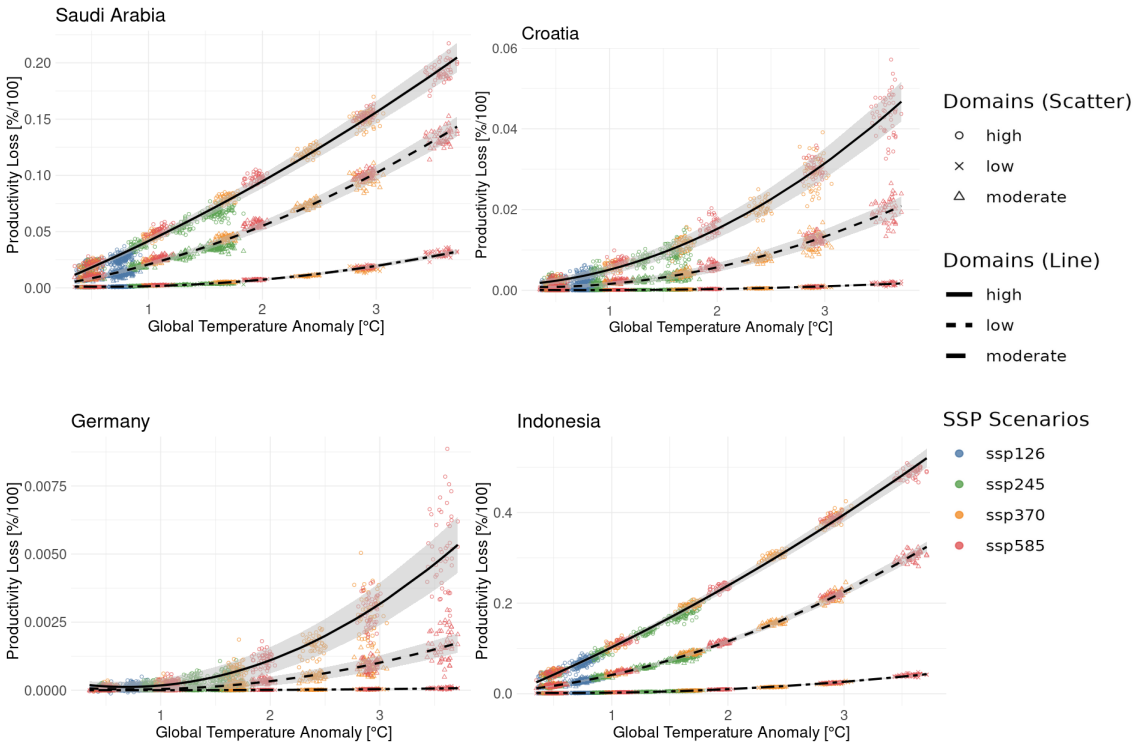

FIGURE 3.1: Labor productivity losses for four selected countries as a function of the global mean temperature anomaly relative to the 1990–2019 baseline. The colored scatter points depict results from 50 ensemble members, differentiated by three workload domains and four CMIP6 emission scenarios. The black line represents the quadratic fit across all outcomes, while the grey shaded area indicates the 5th–95th percentile range.

Figure 3.1 presents the relative change in productivity loss as a function of the global mean temperature anomaly for four selected countries representing different world regions and distinct climatic zones. In this figure, we aggregate data from all SSPs and workload domains into a single plot for each country, shifting the time dependence to a dependence on global temperature anomaly. The global mean anomaly refers to the temperature increase relative to the baseline period (1990–2009).

Each point in the scatter plot represents the productivity loss calculated from an individual ensemble member for a specific SSP and workload domain. These points cluster around certain temperature values, reflecting the average global temperature of the ensemble member during the time period of calculation. Due to internal climate variability, each ensemble member exhibits slight deviations in the corresponding global temperature anomaly within a given time period. As a result, the data points are spread rather than aligning along a single vertical line. This dispersion contrasts with a time-based plot, where calculations performed for five distinct time periods would appear as discrete vertical groupings.

Aligning the results to a temperature-based x-axis reveals that labor productivity loss follows a purely quadratic function of temperature, independent of the preceding emission scenario and consistent across all countries. In this paper, we define emission pathway dependency as a variable that not only exhibits a relationship with temperature but also varies depending on the emission pathway under which it is observed. For each country, we fit a quadratic (second-degree polynomial) regression of productivity loss on global temperature anomaly, pooling across SSPs and ensemble members. The resulting coefficients form the country-level damage function, provided in the supplementary materials. These coefficients can be directly applied as damage functions in country-level economic assessments that are interested in linking labor productivity loss to climate change. Additionally, the supplementary materials include a heatmap that illustrates the labor productivity loss for each country per incremental 1-degree increase in global mean temperature across all three workload domains. Our results indicate a drastic impact on tropical countries, generally much higher than previous assessments at elevated temperatures. This greater loss under higher temperatures is due to the quadratic, rather than previously assumed linear, relationship of losses with temperature. However, in contrast to their tropical and subtropical counterparts, countries located at latitudes higher than those of

the subtropical belt, or at high altitudes like Bhutan, experience relatively negligible labor productivity losses.

In our study, we categorize the agriculture and construction sectors as high workload domains, manufacturing and industry as medium workload domains, and the service sector as a low workload domain, following definitions from the International labor Organization [153]. We apply these categorizations and corresponding damage functions to the sectors in GTAP-INT 2 [99].

Alongside the labor productivity loss damage function, we incorporate two additional damage functions sourced from recent literature to ensure the most up-to-date assessment.

3.3 Other damages and simulation setup

Implementation details of the climate impacts as economic shocks, and their propagation through the GTAP-INT 2 system, are provided in Appendix (A.2).

3.3.1 Effects on agricultural yields

The impacts of climate change on agriculture is incorporated as changes in yields, seen as changes in productivity, in the agricultural sectors of examined regions. Changes on agricultural yields are based on a study done by Li et al. [4]. The authors conducted a meta-analysis to understand how climate factors affect crop yields, focusing on four main crops (maize, rice, soy and wheat) and the effects of temperature, rainfall, and CO_2 on crop productivity. The study evaluated the performance of statistical models in crop yield damage prediction, taking into account the correlation between different studies and quantifying the magnitude of both modeling, sampling and missing data uncertainty. In this study, we consider only the average calculated values for each crop's yield in selected regions due to the deterministic nature of GTAP-INT 2. The yield changes are calculated as average changes in crops' productivity for 20-year periods in 21st century, under 3 different emission scenarios (RCP2.6, RCP4.5 and RCP8.5), which we then interpret as regional yield changes dependent on global mean temperature corresponding to the 20-year averages.

In general, the findings reveal a pronounced and consistent decline in maize production, projected to be the largest and most uniform globally throughout the 21st century. In contrast, trends in rice, soy, and wheat yields exhibit substantial regional variability, with production losses differing by region and timing across these crops. Additionally, certain regions and crops show an initial increase in production under climate change up to an optimal temperature threshold, followed by a decline. Moreover, when analyzing the yield change dependency on average global temperature levels, we noticed a recurring emission pathway dependency pattern for all four crops. This emission pathway dependent behavior is in stark contrast with the labor productivity loss damage function counterpart. Namely, while yield changes show relatively similar temperature dependency between RCP4.5 and RCP8.5, they are more adversely affected by climate change at the same temperatures under RCP2.6. Hence, when incorporating the yield losses as damage function in GTAP-INT 2, we opt for a functional form that connects yield loss with temperature under RCP8.5 scenario as a conservative estimate, with (piecewise) linear interpolation of given discrete estimates. Finally, the damages (yield changes) on agricultural products that are not assessed by Li et al. are taken from the older estimates given by [80].

3.3.2 Effects on human health

We interpret the impact of climate change on human health as an increase of mortality rate in regions of interest due to increase in global (and hence, regional) temperatures. The mortality rate change is incorporated in the model as a change in both the population, effecting the welfare through the household module, and the labor force availability, which directly effects the productivity of every sector examined. We base our quantification of the impact on human health on the study conducted by Bressler et al. [84]. This study builds upon the foundational work of Gasparrini et al. [154], which originally projected the effects of climate change on heat- and cold-related mortality for a selected set of countries. Bressler et al. extend these projections to a global scale, allowing for a more comprehensive assessment of climate-related health impacts worldwide.

Gasparrini et al. assess country-specific statistical relationships between daily temperature and mortality using a 21-day nonlinear distributed lag model[155], over a baseline period 1984-2015. The countries are selected based on data availability, capturing a whole spectrum of climatic and economic conditions and roughly 40% of global population. The

obtained statistical relationships (i.e., response functions) are then combined with future projections of daily temperatures for two time periods and four RCPs in order to estimate future projections of mortality changes for the countries available by data. Bressler et al. use this set of projections to extrapolate mortality changes in countries not included in the initial sample, using each country's specific wealth and regional climate characteristics as a basis for this extrapolation. Finally, the heat- and cold-related mortalities are assessed separately, and the resulting net mortality serves as a basis damage function, which incorporate in GTAP-INT 2.

The damage function is based on a linear interpolation that links country-level temperatures with net mortality changes. Bressler et al. calculate mortality rates for two time slices—the mid-century and the end of the century—across four Representative Concentration Pathway (RCP) scenarios: RCP 2.6, 4.5, 6.0, and 8.5. These mortality estimates, paired with the associated country-level temperature projections for each scenario and time period, form the basis for the interpolation in the damage function. We use the the calculated country-specific temperature coefficients (supplementary material, Table S2.5) to link the global mean temperature with country-level temperature.

It is important to note that Bressler et al. conduct two distinct assessments of future mortality changes: one that includes assumptions about future income growth and the endogenous adaptation resulting from this growth, and one that does not. This approach contrasts with the original calculations by Gasparrini et al., which did not account for potential adaptation from income growth. In our study, we choose the no-income-adaptation scenario for two main reasons.

Firstly, our model is designed to assess the impacts on the economy assuming constant population and GDP, making it logically consistent to evaluate mortality impacts without considering income-driven adaptation. Secondly, we believe that incorporating future income-based adaptation could yield misleading results, as it relies solely on a single socio-economic pathway, which may not represent the broader range of possible future outcomes. With this assumptions, most countries, with a few exceptions in Northern European, experience an increase in mortality as a result of climate change.

Finally, our damage function provides a conservative estimate of climate change impacts on human health, as it does not include extreme events or additional health threats. While we assess the direct effects of local temperature variability on mortality, impacts on

morbidity and the spread of disease vectors—considered in some prior assessments—are excluded. By focusing on well-substantiated effects, we aim to maintain a rigorous standard, even with this more limited scope.

3.3.3 Run specifications

In this paper, we assess damages relative to the baseline economy, which we define as the present-day economy. This means that baseline population and GDP remain fixed at their current values, independent of any predefined socio-economic pathway. Economic changes occur solely due to shocks from damage functions driven by the concurrent global mean temperature anomaly, measured relative to the present day. The baseline model data, including GDP and population, is sourced from the GTAP 11 database [156].

Economic pathways are thus determined by global temperature dynamics. We shock the model using five different emission scenarios (RCP2.6, RCP4.5, RCP6.0, RCP7.0, and RCP8.5)[2], capping temperature increases after 2150 to maintain a constant climate thereafter. This choice prevents forward-looking agents, as defined in GTAP-INT 2, from anticipating what we consider to be highly uncertain and potentially extreme temperatures in high-emission scenarios by the late 22nd century, which would be difficult to account for meaningfully. Since the GTAP database reflects real-world economic conditions, it inherently accounts for damages accrued to date. By using this as a baseline, we introduce temperature pathways so that anomalies are relative to the present day (supplementary, Figure S2.5). This ensures consistency with the damage functions, which are also formulated as anomalies from present-day conditions (1990–2009 for the labor productivity function).

The model divides the world into 60 regions, encompassing individual countries and aggregated country groups, with economic activity captured across 30 sectors. A full list of represented sectors and regions, along with their corresponding baseline population and GDP, is provided in the supplementary material. The regional aggregation was determined for computational efficiency rather than normative considerations, as this configuration was found to be optimal in the present setup, with future work intended to expand the coverage.

[2]Note that here we switch from SSP to RCP definitions to align with the fact that we utilize temperature pathways rather than socio-economic scenarios.

For regions consisting of multiple countries, we apply regional damage functions based on the average impact across all included countries for each of the three damage types, ensuring consistency with the country-scale nature of the damage functions.

3.4 Results

TABLE 3.1: Projected climate damages in (counterfactual) 2100 by region and RCP scenario (% GDP)

Country	**RCP2.6**	**RCP4.5**	**RCP6.0**	**RCP7.0**	**RCP8.5**	**Damage Type**
Argentina	-0.60	-2.01	-2.59	-3.78	-5.45	All Damages
Argentina	-0.05	-0.14	-0.20	-0.35	-0.64	Labour Product.
Australia	-0.13	-0.59	-0.73	-0.85	-1.32	All Damages
Australia	-0.06	-0.24	-0.34	-0.54	-0.83	Labour Product.
Austria	-0.09	0.39	0.70	1.63	2.17	All Damages
Austria	-0.00	0.07	0.13	0.37	0.55	Labour Product.
Belgium	-0.09	0.34	0.62	1.48	1.90	All Damages
Belgium	-0.01	0.02	0.06	0.25	0.36	Labour Product.
Brazil	-1.05	-3.58	-4.68	-7.07	-10.29	All Damages
Brazil	-0.26	-0.91	-1.29	-2.26	-3.82	Labour Product.
Canada	-0.10	-0.66	-0.82	-0.95	-1.52	All Damages
Canada	-0.02	-0.00	-0.00	0.05	-0.01	Labour Product.
Caribbean	-2.94	-8.76	-11.19	-16.52	-23.54	All Damages
Caribbean	-2.25	-7.14	-9.28	-14.12	-20.47	Labour Product.
China and Hong Kong	-1.22	-3.95	-5.12	-7.67	-11.08	All Damages
China and Hong Kong	-0.24	-0.91	-1.28	-2.28	-3.74	Labour Product.
Costa Rica	-1.78	-6.02	-8.03	-12.89	-19.81	All Damages
Costa Rica	-1.25	-4.49	-6.17	-10.48	-16.72	Labour Product.
Croatia	-0.64	-1.75	-2.28	-3.51	-5.61	All Damages
Croatia	-0.05	-0.10	-0.13	-0.19	-0.41	Labour Product.
Czechia	-0.11	0.20	0.43	1.16	1.51	All Damages
Czechia	0.02	0.12	0.20	0.45	0.67	Labour Product.
Denmark	-0.06	0.31	0.57	1.41	1.88	All Damages
Denmark	-0.02	-0.02	0.00	0.16	0.26	Labour Product.
Ethiopia	-1.37	-4.56	-5.93	-8.74	-12.41	All Damages
Ethiopia	-0.05	-0.02	-0.04	-0.07	-0.29	Labour Product.
Finland	0.22	0.72	1.03	1.95	2.52	All Damages
Finland	0.01	0.10	0.18	0.46	0.71	Labour Product.
France	-0.20	-0.06	0.09	0.70	0.88	All Damages

Continued on next page

Table 3.1 – Continued from previous page

Country	RCP2.6	RCP4.5	RCP6.0	RCP7.0	RCP8.5	Damage Type
France	-0.01	0.04	0.07	0.26	0.36	Labour Product.
Gabon	-1.56	-4.87	-6.26	-9.36	-14.29	All Damages
Gabon	-0.72	-2.75	-3.73	-6.11	-9.90	Labour Product.
Germany	-0.07	0.23	0.43	1.09	1.42	All Damages
Germany	-0.00	0.04	0.07	0.24	0.35	Labour Product.
Ghana	-3.37	-12.07	-15.79	-23.82	-32.78	All Damages
Ghana	-1.78	-6.93	-9.32	-14.90	-21.69	Labour Product.
India	-3.18	-11.27	-14.70	-22.14	-30.35	All Damages
India	-1.24	-4.80	-6.45	-10.36	-15.13	Labour Product.
Indonesia	-1.54	-8.63	-11.96	-19.98	-30.83	All Damages
Indonesia	-1.67	-6.67	-9.16	-15.59	-24.79	Labour Product.
Iran (Islamic Republic of)	-1.42	-4.29	-5.43	-7.78	-11.04	All Damages
Iran (Islamic Republic of)	-0.17	-0.54	-0.74	-1.22	-2.01	Labour Product.
Ireland	0.01	0.40	0.65	1.40	1.85	All Damages
Ireland	-0.02	-0.05	-0.05	0.01	0.04	Labour Product.
Italy	-0.46	-0.89	-1.01	-1.13	-1.73	All Damages
Italy	-0.01	0.04	0.07	0.16	0.13	Labour Product.
Japan	-0.81	-2.01	-2.52	-3.61	-5.62	All Damages
Japan	-0.33	-1.09	-1.48	-2.41	-3.84	Labour Product.
Malaysia	-1.81	-6.53	-8.88	-14.82	-23.28	All Damages
Malaysia	-1.04	-4.28	-6.10	-11.09	-18.47	Labour Product.
Netherlands	-0.07	0.39	0.68	1.52	1.97	All Damages
Netherlands	-0.04	-0.04	-0.03	0.09	0.13	Labour Product.
Portugal	-0.57	-1.29	-1.57	-2.12	-3.24	All Damages
Portugal	-0.05	-0.14	-0.20	-0.32	-0.66	Labour Product.
Republic of Korea	-0.75	-2.14	-2.75	-4.14	-6.45	All Damages
Republic of Korea	-0.34	-1.23	-1.68	-2.75	-4.26	Labour Product.
Rest of EFTA	0.17	0.70	1.00	1.91	2.55	All Damages
Rest of EFTA	-0.02	-0.05	-0.05	0.03	0.08	Labour Product.
Rest of EU25	-0.26	-0.51	-0.57	-0.57	-1.01	All Damages
Rest of EU25	-0.01	0.02	0.03	0.10	0.08	Labour Product.
Rest of East Asia	-0.51	-1.73	-2.28	-3.49	-5.39	All Damages
Rest of East Asia	-0.23	-0.82	-1.16	-2.02	-3.31	Labour Product.
Rest of Eastern Africa	-2.35	-7.86	-10.23	-15.36	-21.41	All Damages
Rest of Eastern Africa	-0.51	-2.05	-2.85	-4.84	-7.56	Labour Product.
Rest of Eastern Europe	-0.19	-0.72	-0.93	-1.32	-2.14	All Damages
Rest of Eastern Europe	0.02	0.12	0.17	0.29	0.34	Labour Product.
Rest of Europe	-0.79	-1.98	-2.40	-3.14	-4.30	All Damages

Continued on next page

Table 3.1 – Continued from previous page

Country	RCP2.6	RCP4.5	RCP6.0	RCP7.0	RCP8.5	Damage Type
Rest of Europe	-0.01	0.04	0.07	0.19	0.24	Labour Product.
Rest of Former Soviet Union	-1.15	-3.23	-4.04	-5.63	-7.80	All Damages
Rest of Former Soviet Union	-0.05	-0.17	-0.24	-0.40	-0.68	Labour Product.
Rest of North Africa	-1.49	-4.80	-6.19	-9.15	-12.93	All Damages
Rest of North Africa	-0.26	-0.94	-1.32	-2.27	-3.68	Labour Product.
Rest of North and Central America	-0.89	-2.50	-3.16	-4.51	-6.74	All Damages
Rest of North and Central America	-0.21	-0.77	-1.06	-1.76	-2.91	Labour Product.
Rest of Oceania	-0.38	-1.15	-1.53	-2.47	-4.21	All Damages
Rest of Oceania	-0.22	-0.79	-1.08	-1.77	-2.76	Labour Product.
Rest of South America	-0.84	-3.28	-4.33	-6.65	-9.75	All Damages
Rest of South America	-0.35	-1.51	-2.09	-3.47	-5.38	Labour Product.
Rest of South and SE	-2.58	-8.70	-11.37	-17.32	-24.69	All Damages
Rest of South and SE	-1.22	-4.64	-6.29	-10.24	-15.42	Labour Product.
Rest of Southern African Custo	-1.11	-3.35	-4.26	-6.15	-8.68	All Damages
Rest of Southern African Custo	-0.08	-0.28	-0.41	-0.75	-1.28	Labour Product.
Rest of Western Africa	-2.06	-7.60	-10.08	-15.64	-22.25	All Damages
Rest of Western Africa	-0.73	-3.03	-4.24	-7.36	-11.46	Labour Product.
Rest of Western Asia	-1.60	-5.11	-6.58	-9.74	-13.62	All Damages
Rest of Western Asia	-0.63	-2.24	-3.00	-4.76	-7.02	Labour Product.
Rest of World	0.06	0.66	0.96	1.73	2.17	All Damages
Rest of World	-0.01	0.00	0.03	0.17	0.27	Labour Product.
Russian Federation	-0.55	-1.45	-1.74	-2.19	-2.97	All Damages
Russian Federation	-0.01	-0.02	-0.02	0.02	0.05	Labour Product.
Saudi Arabia	-1.68	-5.56	-7.21	-10.80	-15.43	All Damages
Saudi Arabia	-0.71	-2.65	-3.58	-5.81	-8.83	Labour Product.
Slovakia	-0.15	-0.05	0.08	0.53	0.64	All Damages
Slovakia	0.03	0.15	0.22	0.43	0.63	Labour Product.
Slovenia	-0.45	-0.82	-0.91	-0.91	-1.40	All Damages
Slovenia	-0.06	-0.14	-0.18	-0.24	-0.45	Labour Product.
South Africa	-0.80	-2.36	-2.99	-4.25	-5.93	All Damages
South Africa	-0.02	-0.02	-0.03	-0.03	-0.11	Labour Product.
South-Central Africa	-2.01	-7.09	-9.34	-14.43	-20.91	All Damages
South-Central Africa	-0.56	-2.48	-3.47	-5.98	-9.42	Labour Product.
Spain	-0.56	-1.25	-1.51	-1.99	-3.00	All Damages
Spain	-0.05	-0.11	-0.17	-0.27	-0.60	Labour Product.
Sweden	0.08	0.64	1.02	2.20	2.92	All Damages
Sweden	-0.00	0.07	0.14	0.46	0.73	Labour Product.
Switzerland	-0.11	0.27	0.53	1.36	1.82	All Damages

Continued on next page

Table 3.1 – Continued from previous page

Country	RCP2.6	RCP4.5	RCP6.0	RCP7.0	RCP8.5	Damage Type
Switzerland	-0.03	-0.05	-0.04	0.09	0.16	Labour Product.
Thailand	-1.64	-5.49	-7.24	-11.33	-16.83	All Damages
Thailand	-0.85	-2.89	-3.96	-6.73	-10.64	Labour Product.
Türkiye	-0.60	-1.72	-2.26	-3.57	-6.13	All Damages
Türkiye	0.01	0.11	0.16	0.36	0.43	Labour Product.
Ukraine	-0.31	-1.91	-2.59	-3.92	-5.80	All Damages
Ukraine	-0.00	0.05	0.07	0.15	0.14	Labour Product.
United Arab Emirates	-2.08	-6.28	-7.97	-11.48	-16.01	All Damages
United Arab Emirates	-1.49	-4.89	-6.33	-9.50	-13.34	Labour Product.
United Kingdom of Great Britain	0.02	0.39	0.61	1.26	1.65	All Damages
United Kingdom of Great Britain	-0.01	0.00	0.02	0.14	0.21	Labour Product.
United States of America	-0.33	-1.09	-1.41	-2.08	-3.31	All Damages
United States of America	-0.10	-0.35	-0.52	-0.98	-1.76	Labour Product.
Viet Nam	-2.35	-9.27	-12.42	-19.59	-27.78	All Damages
Viet Nam	-1.10	-4.13	-5.73	-9.80	-15.08	Labour Product.

Figure 3.2 illustrates GDP changes worldwide, segmented into the 60 analyzed regions, with each region's GDP changes shown relative to its own economy, all damages included. Antarctica is excluded due to its negligible socioeconomic activity. The upper panel presents transient GDP deviations from the baseline under RCP7.0 for the years 2035, 2050, 2075, and 2100, reflecting each economy's ongoing adjustment to temperature shocks over time. In contrast, the lower panel depicts the quasi-equilibrium states of each regional economy at the terminal year of the simulations for the four adjusted RCP scenarios.

Comparing the two panels reveals several key insights. Firstly, long-term impacts on GDP are consistently more negative than transient impacts, regardless of the region or pathway. Secondly, while most regions experience negative economic consequences across all scenarios, some (particularly Scandinavian countries) show consistent GDP benefits. Additionally, other higher-latitude countries, such as Canada, Belgium, and Germany, exhibit initial economic benefits in the transient phase but face economic losses in the long-term equilibrium. Notably, this trend also extends to Australia, which follows a similar pattern despite being outside the higher-latitude zone. Lastly, both panels highlight significant regional disparities, with tropical and subtropical regions being the most severely affected. These disparities grow more pronounced as total losses increase, underscoring the systematic inter-regional inequities.

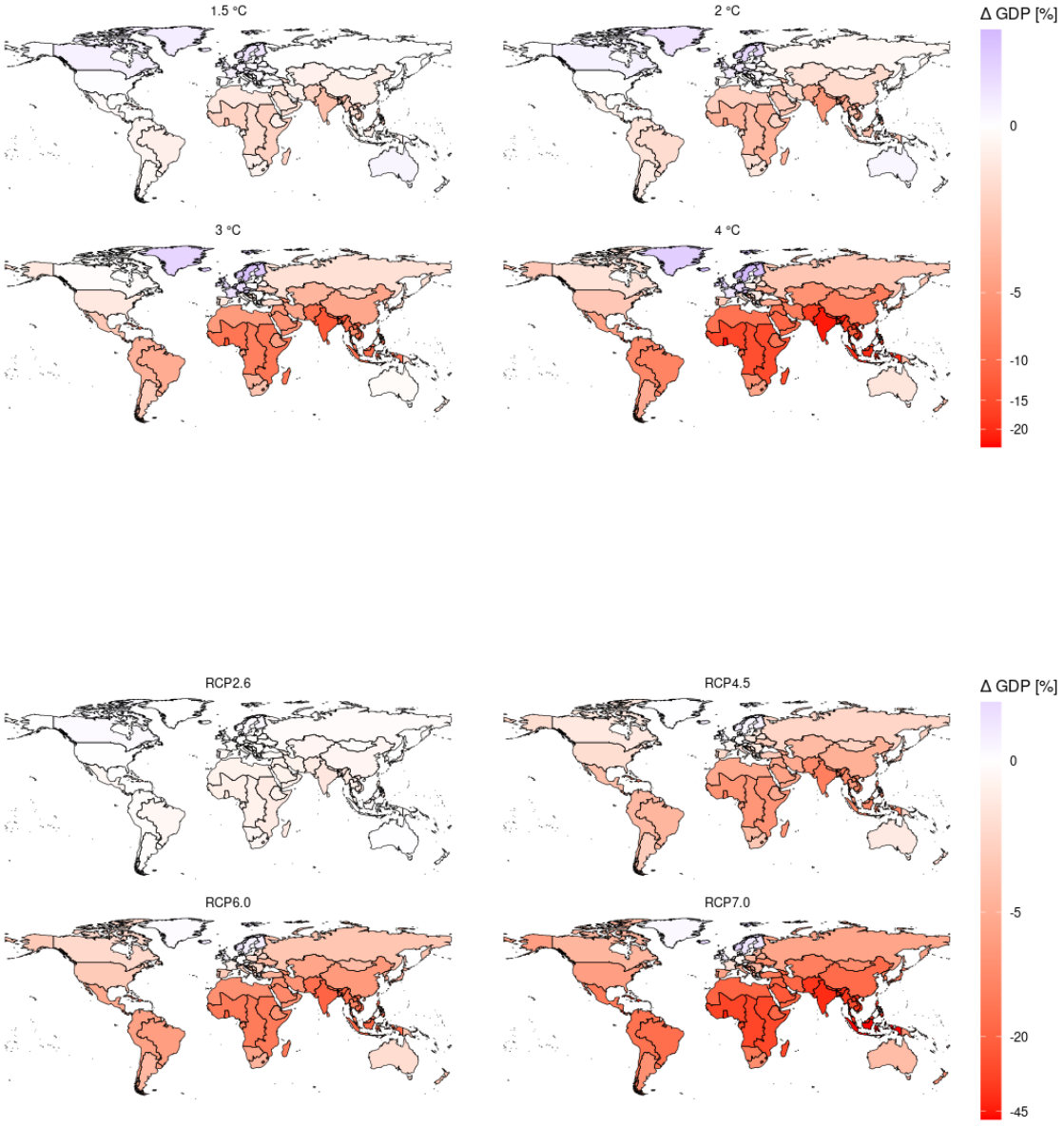

FIGURE 3.2: Climate change-induced GDP effects for each region included in this analysis. The upper panel provides four snapshots of annual GDP changes under the RCP7.0 scenario for the years 2035, 2050, 2075, and 2100, respectively. The lower panel shows long-term impacts under four different RCP scenarios.

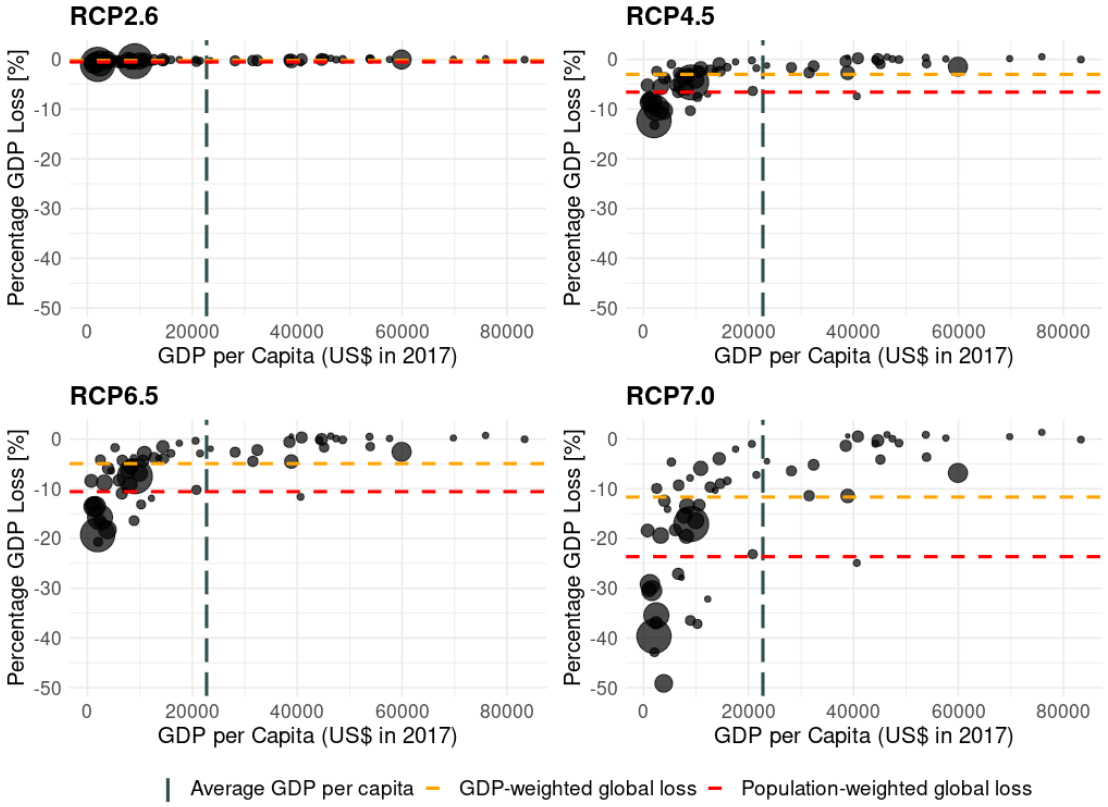

FIGURE 3.3: Long-term regional GDP percentage losses under four RCP scenarios, plotted against the baseline GDP per capita of the corresponding region. Each circle represents a region included in the model run, with its size proportional to the region's population. The vertical dashed line indicates the global average of regional baseline GDP per capita, while the yellow and red horizontal dashed lines represent global GDP percentage losses, weighted by GDP and population, respectively.

Figure 3.3 delves deeper into regional heterogeneity, illustrating the long-term climate change impacts on GDP for the four RCP scenarios (as in Figure 3.2, lower panel). It examines the relationship between regional GDP losses and baseline GDP per capita, with each circle representing a region. The size of the circles reflects the population of the corresponding region. Two key patterns emerge from this representation. Firstly, while most regions experience negative impacts from long-term climate change, low-income countries (those with low GDP per capita) are disproportionately affected, with both losses and disproportionality increasing alongside temperature (higher RCPs). Secondly, the most populous regions tend to fall on the lower end of the GDP per capita spectrum. This emphasizes that negative impacts tend to affect a larger number of people than one might infer from a spatial map of losses alone. Moreover, Figure 3.3 starkly emphasizes on the importance of mitigation in context of shared burden of impacts – while in RCP2.6 scenario most of the losses are avoided for all the regions of the world, the long-term

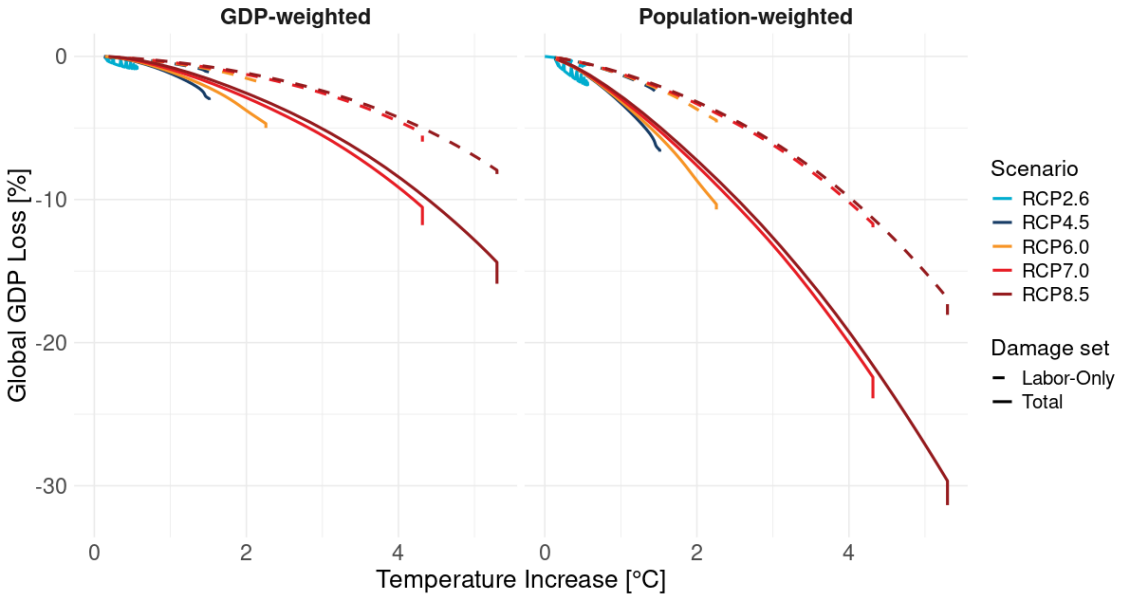

FIGURE 3.4: Globally aggregated GDP losses per degree of global mean temperature change for all five adjusted RCP scenarios, using unweighted, population-weighted, and GDP-weighted methods. The kink at the end of each slope represents the system's adjustment to long-term impacts at the constant temperature.

regional GDP losses following RCP7.0 can reach almost 50% in Indonesia followed by Ghana and India with both roughly around 40% GDP loss. On the opposite side of the GDP per capita scale, Switzerland, Ireland the Rest of EFTA countries are not effected by climate change even under a high temperature scenario. Drawing a vertical dashed line that represents the global average of regional GDP per capita, one can see that the regions with the lower GDP per capita experiences proportionally larger losses, with increasing difference scaled with higher emission scenarios, compared to the regions on the higher-than-average. Population size plays a critical role, as the most populous regions tend to have lower GDP per capita, with the exception of the United States (60k US$ GDP per capita). Finally, the figure clearly touches down on the importance of the mitigation when it comes to reducing the regional GDP loss inequalites, as seen by RCP2.6 scenario case where all of the countries tend to cluster around the same horizontal line.

Zooming out to the global scale, Figure 3.4 presents globally aggregated GDP losses per degree of global mean temperature change (relative to the present day) across all five adjusted RCP scenarios. With two different GDP loss aggregation methods applied, the figure provides insight into how climate-induced economic damages vary depending on the chosen weighting approach. Solid lines represent the case where all three damage

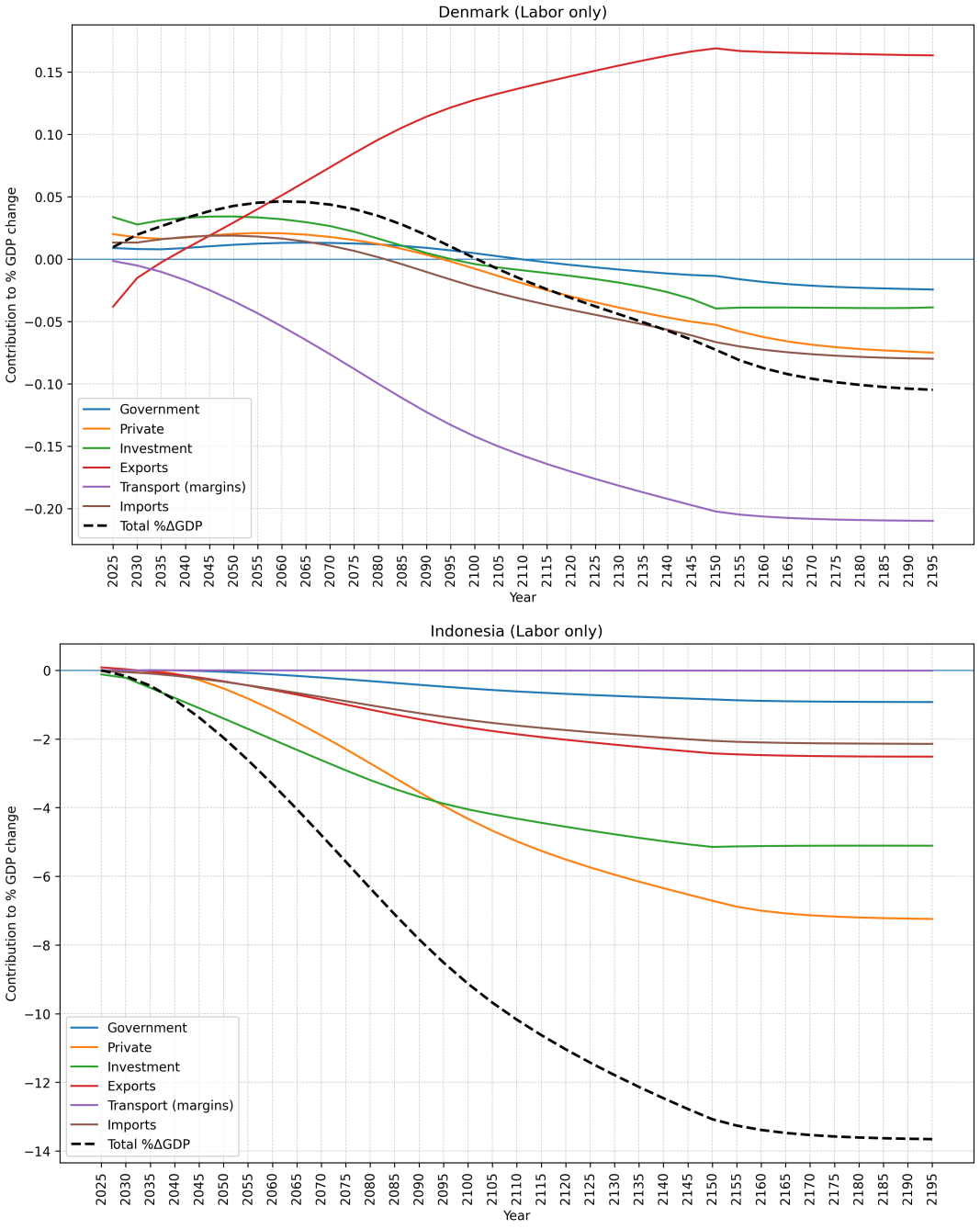

FIGURE 3.5: Decomposition of GDP-contributing impacts under labor-productivity damages only (RCP6.0). Contribution of demand components to the percent change in GDP for Denmark (top) and Indonesia (bottom), with the dashed line showing total GDP change (as reported in the rest of the Results section). While labor-productivity losses are always negative, the figure shows that positive (or less negative) GDP change amid climate change can come from increased exports (Denmark case). We also see that international transport margins decrease as the world economy slows. Indonesia experiences losses across all components (imports buffer the loss only slightly). Indonesia does not supply international transport services in GTAP-INT 2; hence its transport margin term remains zero.

components are included, while the dashed lines depict losses considering only labor productivity damages, isolating the economic consequences of reduced worker efficiency due to rising temperatures. The kink at the end of each slope represents the adjustment of the system to long-term impacts, during which we keep the temperature constant, allowing economic damages to stabilize over time.

The first panel applies a GDP-weighted aggregation method, where each region's GDP loss is weighted by its share of global GDP. This approach prioritizes regions with larger economic contributions, emphasizing the proportional impact of climate change on the overall global economy. By assigning greater weight to wealthier regions, it reflects the economic significance of losses relative to baseline GDP levels. The second panel uses a population-weighted aggregation method, where regional GDP losses are weighted by population before being aggregated globally. This method provides a more representative measure of global damages by aligning the results with the proportional impact of climate change on the total number of people affected. The comparison between these two methods reveals a clear pattern: the population-weighted global loss is approximately twice as large as the GDP-weighted loss. This aligns closely with the findings of Figures 3.1 and 3.2, reinforcing the conclusion that poorer and more populous regions bear a disproportionately high share of climate-induced economic losses. Separating the damage contributions on the global scale, both panels show that the labor productivity loss impact on GDP contributes to roughly half of the total damages. Table 3.1 provides more regional detail and shows that this proportion varies substantially between regions. Additionally, Figure 3.4 reveals that the global GDP losses exhibit a small degree of temperature pathway dependency: stronger mitigation pathways tend to show slightly higher losses for the same level of temperature increase compared to weaker mitigation counterparts. Running the model with only labor productivity damages (which are pathway independent, see Figure 3.1), drastically reduces this pathway dependency, but does not eliminate it entirely.

Table 3.1 explicitly presents each region and its corresponding GDP losses (%) in the year 2100 under all five temperature scenarios, for both cases: one where all three damage components are included and one where only labor productivity damages are considered. Furthermore, Table 3.1 confirms the masking effect of globally aggregated phenomena, particularly regarding the proportion of labor productivity-derived damages relative to total damages. While the globally aggregated view suggests that labor productivity losses

contribute to the half of the total GDP loss, this ratio is rarely observed at the regional level.

Generally, Northern European countries benefit as global mean temperature increases, while the rest of the world, including Southern Europe, experiences negative impacts to varying degrees. Some of these benefits stem from reduced cold-related mortality and positive effects on certain crops in these regions. However, focusing on labor productivity damages only suggests additional drivers, particularly those linked to trade dynamics that GTAP captures. Since the labor productivity damage function itself can only generate losses, yet Northern European countries still benefit in these simulations, the most plausible explanation is that production losses in highly affected regions are compensated by increased trade from minimally affected countries, such as Denmark.

Indeed, Figure 3.5 points in this direction. It shows a decomposed GDP identity and how each element changes under the assumption of labor productivity damage only. Since Denmark's labor productivity loss due to climate change is negligible (see supplementary Figures S2.1 to S2.3), it does not drastically affect Denmark's economy (in contrast to the Indonesian case). As other countries are more severely affected, their production levels drop while demand remains similar, increasing the need for imported goods. Countries that are barely affected, like Denmark, can (and will) expand exports and, in this regard, benefit from climate change.

However, because the global economy slows, total international trade also declines. Countries that are suppliers of international transport services therefore lose GDP from reduced global demand for transport, even if their own merchandise exports rise. Denmark is one such supplier, so it incurs a loss via the international transport channel (Figure 3.5). This pattern appears for other regions with a positive supply share in the GTAP international transport account. By contrast, Indonesia has no transport-supply share in the GTAP database, so the figure shows no movement for that channel.

Before progressing to the discussion, this portion of the results section provides picked examples of losses under the RCP6.0 scenario. Regional snapshots of losses for each scenario, specifically for the years 2035, 2050, 2075, and 2100, as well as the corresponding long-term damages, are detailed in the supplementary material.

In the United States, initial GDP gains shift to rapid declines, with damages quadrupling by 2100 to roughly 275 billion USD per year (1.4% of GDP, see Table 3.1), assuming no economic growth, which would further increase these numbers. In China, damages remain steady through much of the century but escalate sharply in the long term, reaching roughly 645 billion USD in 2100. In present-day dollar terms, GTAP-INT 2 estimates that in 2100 (RCP6.0, roughly 3 °C compared to preindustrial temperature) warming would result in a global loss in that single year of approximately 2.6 trillion USD (3.22% of global GDP), based on GDP-weighted aggregated losses. If aggregated for every year until 2100, the cumulative loss amounts to over 17.6 trillion USD, not taking into account the damages that accrued up to the present day. In this context, COP29 pledge of 300 billion USD might seem insufficient.

The highest share of global loss are China, India and USA, with roughly 25%, 15% and 10% of total losses in present-day USD in 2070 (RCP6.0), followed by the Rest of South and Southeast Asia and Indonesia with 7% and 5%[3]. This reflects the fact primarily that these countries have a large contribution to global GDP combined with non-negligible losses. Relative to their own economies, the same countries experience roughly 2.7%, 9%, 0.5%, 6.5% and 5.8% losses respectively, with the country with the highest damages relative to its own economy is Ghana (roughly over 9.2%, placing India the second on this tier). On the other side of the scale, five countries that have the lowest share of global loss are in this order: Germany, UK, France, Netherlands and Sweden, de facto observing gain. These regional discrepancies in climate impacts reflect how interpretations can differ depending on the perspective used and highlights the challenges in accurately quantifying and communicating global climate change losses. It also further emphasizes the unequal and often disproportionate distribution of damages across regions.

3.5 Discussion

The literature often presents the economic effects of climate change through relative changes in global GDP. However, estimates vary depending on the methodological approach, and a clear consensus has yet to be reached. This study, incorporating the latest

[3]Note that the "Rest of" regions have disproportionally higher shares due to its GDP and the corresponding loss stemming from a conglomerate of countries.

climate impact assessments on agricultural yields and human mortality, alongside an improved labor productivity loss function, produces estimates that fall on the higher end of global damage projections derived from CGE modeling. Importantly, the regionally disaggregated approach that estimates losses at the regional level before aggregating them to a global scale, underscores that focusing exclusively on the global picture obscures critical regional disparities. If the global community is to effectively mitigate losses in a way that international equity is adequately addressed, adopting a more granular, region-specific perspective is essential.

Firstly, changing the global aggregation method from weighting regions by their associated GDP to weighting them by population increases the relative global GDP loss by approximately a factor of two. Even though losses measured this way are not directly applicable in global economic assessments—such as damage functions on global production in optimizing IAMs—because the units are not aligned, it nonetheless indicates underlying ethical implications and raises a key question: if shifting the focus to how climate change impacts the global population (i.e., the GDP losses that population will experience), rather than focusing on overall global capital (regardless of who is affected), doubles the total impact, should this be of concern to policymakers? If so, it would be informative to investigate how this weighting choice influences other global assessments that are calculated as aggregates from regional losses (e.g., [86]).

The second, more concerning reason to question global climate damage assessments is that they obscure the stark differences evident in disaggregated regional and country-level effects. For example, in this study, we demonstrate that a roughly 2°C temperature increase from the present day (projected for the year 2085 under RCP7.0) results in a GDP-weighted global GDP decline of 2.5%. At the same time, when looking at the country level, the effects vary significantly. For example, Indonesia observes a relative decline of over 13%, whereas Sweden, in contrast, gains from climate change with a relative GDP increase of 2%. This adds another fundamental question: who does the 5% global loss actually represent, given that the global economy is inherently granular and functions primarily at the national level?

Even more concerning is that the disparity in economic losses between countries widens as total losses and global temperatures rise, as illustrated in Figure 3.3. These findings

further confirm the unequal (and arguably, unjust) distribution of climate change damages. As a general trend, poorer and more populous countries will bear increasingly greater burdens with each additional increment of unmitigated global warming. However, our results indicate that the mitigation does make a difference. Observing the RCP2.6 scenario, both the total losses and the large discrepancies in regional economic impacts are effectively mitigated.

Aggregation matters not only for GDP levels but also for decomposing losses by damage channel. In the global aggregate (Figure 3.4), labor-productivity losses account for roughly half of total GDP losses, alongside agriculture and heat-related mortality. However, as Table 3.1 illustrates, this proportionality varies significantly at the country level, making it impossible to derive a universal rule. This cross-country variation reflects differences in climate exposure (country-unique climate damage functions) and economic structure (production, preferences, and trade); input–output and trade linkages transmit shocks unevenly across sectors, yielding country-specific decompositions. Taken together, the main trend of economic impacts in terms of GDP loss can be read from the damage functions, while trade dynamics reshape it, sometimes substantially. The country damage mixes (supplementary Tables S2.1–S2.5) and the labor-productivity-only case (Figure 3.5, Table 3.1) are informative in this regard and help explain observed differences.

Results consistently show that long-term GDP losses exceed transient ones, across all regional aggregation levels. While each country's outcome reflects its own mix of climate damages and sectoral structure, this pattern is structural in GTAP-INT 2 due to intertemporal dynamics (see Appendix A.1.6 and A.1.7 for details). First of all, capital accumulation dynamics amplify losses. In the transient horizon, damages make production less efficient (workers are less productive; yields are lower), so output falls. Anticipating lower future returns leads to lower investments, so capital accumulation slows, making the future capital stock is smaller, and hence, further reducing future output. Forward-looking households, seeing a less rewarding future, save less and consume more today, widening the gap between transient and long-run GDP.

To situate our study, Cantele et al. [91] map CGE climate studies by regional/sectoral coverage and time horizon; our configuration (60 regions, 30 sectors, multi-century horizon) lies at the high-resolution end of that spectrum and enables the heterogeneity documented here.

Because GTAP-INT 2 directly succeeds GTAP-INT [81], a brief comparison of the two studies using the two related models is warranted. Structurally, GTAP-INT 2 adds forward-looking households alongside firms, which could, in principle, temper losses via consumption–saving adjustments. In practice, however, we predominantly find larger GDP losses than [81]. The primary reason is the implementation of updated damage functions (labor productivity, agriculture, heat-related mortality) that impose stronger impacts at higher temperatures. We exclude sea-level-rise (SLR) damages from Roson & Sartori [80] due to representation limits; in their framework SLR contributes only a small share of total costs ("limited incidence on total land" and a low land-income share in GDP). Excluding SLR would, if anything, reduce our totals, so the larger losses here are best explained by the updated damages rather than by the change in timing assumptions.

In agriculture, the impact functions are improved: Li et al. [4] estimate crop-yield impacts at the grid-cell level and then aggregate to countries, rather than extrapolating from broad climate regions by latitude (as in Roson Sartori, whose functions underpin the GTAP-INT study). A detailed, country-by-country comparison is beyond our scope and does not point consistently in one direction (see Supplementary Tables S2.2–S2.4). Nevertheless, agricultural changes remain a material contributor to GDP outcomes, particularly in countries with a high agriculture share in GDP.

When it comes to human health, the main modification in GTAP-INT 2 is that changes in mortality affect production through changes in labor availability (separately from labor productivity) on the production side, and also alter population, which enters the household-welfare component. Moreover, this study accounts for potential positive effects on human health due to lower cold-related deaths, which is particularly relevant and observed in high-latitude countries in the Northern Hemisphere. These effects, combined with improvements in agricultural yields, contribute to small but detectable positive GDP effects, by increasing effective labor supply (and thus lowering unit labor costs for firms) while simultaneously affecting welfare through population dynamics.

In contrast, the labor productivity impacts are exclusively negative, as the Hothaps work ability function considers productivity losses only at elevated WBGT levels. A key finding in interpreting the results is that country-level labor productivity losses are independent of the emission scenario, depending solely on the global mean temperature change. This contrasts with other climate impacts, which vary with emission pathways.

This independence enables the creation of a precise temperature-dependent damage function for labor productivity, which exhibits a clear quadratic relationship with temperature. This represents a significant improvement over the previous labor productivity loss damage function in Roson and Sartori, which estimated losses for a 1°C increase and then linearly interpolated damages for higher temperature levels. Comparing the two assessments shows that the labor productivity damages are comparable at lower temperatures, but escalate more sharply at higher temperatures in the new estimates.

These impacts are particularly severe for tropical and subtropical countries, where increased humidity and higher temperatures combine to exacerbate losses. In fact, high humidity levels in these regions are the key driver of labor productivity losses as temperatures increase globally (albeit at different rates—see supplementary Table S2.5). This can lead to more than two orders of magnitude larger labor productivity losses (in percentage terms) when, for example, comparing Indonesia to Germany. Moreover, the most affected regions tend to have a larger share of employment in high and moderate workload sectors, such as agriculture, industry, and manufacturing, which are more vulnerable to productivity losses. In contrast, service sectors, which dominate in the developed Global North, are less affected—additionally contributing to regional disparities.

Before concluding words, we would like to emphasize that this study provides only a partial view of the overall economic impact of climate change in terms of GDP, serving as a conservative, lower-bound estimate. The list of currently unrepresented impact channels is still extensive, and their inclusion, along with extreme events not covered here, would likely result in a significant increase in the estimated damages, on both global and local level. This caveat is particularly relevant for countries that appear to benefit from climate change. Unaccounted factors such as storm surges, sea level rise effects on coastal infrastructure, and a potential weakening of the AMOC, which could excessively cool Scandinavia, would disproportionately disadvantage northern Europe. For most others, our conservative estimate already presents more than enough cause for concern.

3.6 Conclusion and outlook

"All models are wrong, but some are useful" as a phrase is already clichéd in discussing the topics of models and their limitations in capturing complex realities; however, it remains

true. The strength of CGEs lies in their high regional and sectoral resolution, crucial for representing diverse regional economies and their interactions and capturing both direct and indirect effects of different economic shocks.

This paper examines the economic impacts of climate change using a forward-looking, highly disaggregated CGE model. We develop a country-level labor productivity loss damage function and translate it into regional and global GDP losses, alongside two additional impact channels—agriculture and human health. The results confirm and highlight the stark regional discrepancies in climate change effects on GDP while reaffirming that mitigation pays off, both in reducing total losses and narrowing regional inequalities.

Future outlook promises further development in increasing the regional and sectoral aggregation, and in improving the climate damage representation as well. Additional interesting venue is taking steps toward becoming a fully coupled Integrated Assessment Model (IAM). Currently, temperature change is assumed to be an exogenous input, while in reality, it is driven by emissions generated by the economy. The next step in advancing GTAP-INT 2 is to endogenize emissions, and consequently temperature change, by linking a climate module with the economic system.

Chapter 4

Modified Cost-Risk Analysis as a Bridge Between Target-Based and Trade-Off-Based Decision-Making Frameworks

This study introduces Cost-Benefit-Risk Analysis (CBRA), a novel decision-making framework that bridges target-based and trade-off-based approaches by incorporating explicit climate damages while maintaining a reduced-weight risk function. CBRA refines Cost-Risk Analysis (CRA) by introducing a partial global damage function derived from a forward-looking, regionally and sectorally disaggregated Computable General Equilibrium (CGE) model. This allows us to assess how much of the precautionary risk embedded in climate targets is captured by explicit economic losses. We implement CBRA in the integrated assessment model MIND, incorporating a modified version of the FaIR climate model that accounts for climate sensitivity uncertainty. Our findings reveal that explicit damages from agriculture, labor productivity, and human health explain 58% of the risk captured by a 2°C target under a 65% safety level. Furthermore, we demonstrate that when MIND is updated with FaIR, CRA fully replicates Cost-Effectiveness Analysis (CEA), confirming their conceptual equivalence. These results suggest that as damage estimates improve, a greater share of precautionary risk is accounted for within cost-benefit models, reducing the need for rigid precautionary targets and narrowing the gap between CBA and CEA.

However, uncertainty in climate sensitivity remains a dominant factor, highlighting the need for a more precise understanding of the climate system response to guide policy.

4.1 Introduction

As greenhouse gas emissions continue to drive global temperature increases [157] [158], global society faces a fundamental dilemma: reducing emissions requires significant present-day efforts, while inaction risks uncertain but potentially severe socio-economic consequences [159]. How should a rational decision-maker respond?

Climate economics has been grappling with this question for over 30 years, with one of the earliest and most prominent approaches framing the problem in terms of cost-benefit analysis (CBA). In the context of climate change, CBA aims to balance the costs of present-day mitigation efforts against the benefits of avoiding future losses from climate change caused socio-economic impacts. Central to the implementation of CBA are globally aggregated integrated assessment models (IAMs), which use simplified representations of the climate and economic systems to link the effects of policy decisions on the climate with feedback from climate changes on the economy [160]. These simplified representations are essential for computational feasibility, as they make it possible to implement optimization procedures that evaluate a wide range of potential policy pathways [12]. However, policy recommendations derived from research utilizing CBA remains contentious.

Using the DICE IAM, which couples a simplified global carbon cycle and temperature model with a neoclassical economic growth framework as a single, global economy, W. Nordhaus demonstrated that the optimal policy involves only modest mitigation efforts until later in the century, with the global warming considered optimal for society exceeding 3 °C by the end of the century [161][162][27]. Using the same model but with modified parameters and an improved climate representation, Hänsel et al. argued that optimal mitigation is likely to align more closely with limiting warming to 2 °C, providing cost-benefit-based support for the goals of the Paris Agreement [28]. Opposedly, M. Weitzman argued that the fat-tailed nature of the climate sensitivity probability distribution justifies a de-facto immediate cessation of emissions, as the potential catastrophic consequences would far outweigh the associated (and enormous) present-day costs [29]. The stark differences in results across the literature highlight that, despite its strong theoretical

foundation, CBA outcomes depend on underlying model assumptions which are often subject to considerable uncertainties [23][30].

In light of the difficulties and uncertainties in quantifying future socio-economic damages from climate change—a key trade-off in CBA—some economists have proposed bypassing this aspect of the framework altogether. Instead, they advocate a target-based approach known as cost-effectiveness analysis (CEA). Guided by the precautionary principle, this framework assumes adherence to a predefined temperature target and does not directly quantify the resulting climate impacts or damages [37] [35]. The decision-maker's role is to identify the least costly pathway for achieving and maintaining this target. However, Schmidt et al. demonstrated that this framework encounters significant conceptual challenges when a decision-maker considers future learning about the system [42]. Namely, the absence of explicitly represented negative climate impacts in the model can lead to situations where a decision-maker chooses to disregard new information, hence undermining adaptive decision-making processes. To address this limitation, cost-risk analysis (CRA) was introduced.

CRA is a hybrid decision-making tool that integrates precautionary motivated decision-making with a modified trade-off based framework. As demonstrated by Neubersch et al., it allows a target-oriented decision-maker to incorporate anticipated future learning while preserving dynamic consistency [72]. However, similar to its predecessor, CEA, it operates under the assumption that the economic impacts of climate change are entirely unknown, with all the risk concentrated in the domain beyond the target threshold. Since the uncertainty surrounding climate damages is inherently epistemic, it is reasonable to assume that the scientific community is gradually advancing in its understanding. With more consolidated impact assessments now emerging, a relevant question arises: can these insights be incorporated into CRA? If the impact knowledge base becomes sufficiently comprehensive, this integration could allow for a complete transition from target-based approaches to a fully impact-informed CBA. At the same time, we can envision a utility maximization framework that accounts for the partiality of impact knowledge while still incorporating the unknown effects embodied in the target. Such a framework could serve as a transitional approach, bridging the gap between these two contrasting decision-making approaches. In this paper, we develop and implement such a modification to CRA, first theoretically proposed by Held [52].

In this paper, we operationalize the CRA modification and label it Cost-Benefit-Risk Analysis (CBRA), a hybrid decision-making framework that bridges CRA and CBA by incorporating partial climate impact information while preserving a precautionary target. We put CBRA into action, refining it into a structured framework that integrates precautionary and cost-benefit perspectives within a unified decision-making model. To implement this framework, we update an integrated assessment model (IAM) previously used in CRA assessments by incorporating a modified FaIR climate model. This updated version includes a simplified uncertainty scheme specifically designed for this study to account for uncertainty in climate sensitivity. While tailored for our analysis, this approach can also be applied in other climate-economic contexts that explore climate response sensitivity using FaIR. We explicitly demonstrate that, when an improved climate module is employed, CRA fully replicates CEA, as analytically predicted by Held [45].

Furthermore, we develop a partial damage function using output from a forward-looking computable general equilibrium (CGE) model and demonstrate how CBRA can assess the extent to which a damage function accounts for the initially perceived risk of exceeding a predefined target, as determined by the precautionary community. To identify the threshold where a damage function fully replaces the precautionary perception of risk, we calibrate it within a pure CBA framework to align with the predefined target, mirroring the calibration approach applied to CRA in previous studies. By doing this, we show that it provides a way to directly compare the two schools of thought, quantifying the extent to which the climate impacts represented in the damage function were implicitly assumed by the precautionary community when setting a climate target.

Following the introduction, the paper proceeds as follows. The first part of Section 4.2 defines each decision-making framework in greater detail, provides their formal descriptions, and briefly introduces the model used to test the frameworks. The remainder of the Section 4.describes modifications to the FaIR model to incorporate climate sensitivity uncertainty and outlines the context and specification of the tailor-made damage function. Section 4.3 presents the results, while Section 4.4 examines their implications in detail.

4.2 Methodology

4.2.1 Decision-making frameworks

4.2.1.1 Cost-effectiveness analysis (CEA)

Cost-effectiveness analysis is a target-driven decision-making framework that seeks to identify the least costly policy recommendation while adhering to predetermined targets. In the context of climate economics, these targets often include temperature targets, net-zero emission targets, or renewable energy benchmarks. A key feature of this framework is that it does not evaluate the benefits of achieving these targets (e.g., avoided damages), as it does not include the quantification of damages. Instead, the targets themselves encapsulate these considerations, having been established through multiple lines of evidence and consensus. A prominent example that we inspect in this paper is a 2 °C target, reached by political consensus [163] [126], and rationalized by Jaeger and Jaeger [164]. Being a product of a precautionary principle, this target acts as a safeguard against potentially harmful and deeply unknown events, whose likelihood and impacts remain highly uncertain [165]. In this paper, we use the probabilistic extension of the conventional CEA framework by employing chance-constrained programming (CCP), a probabilistic variant of CEA [166] [36] [40]. While we refer to this approach as CEA for simplicity, CCP offers a general framework for incorporating uncertainty into decision-making. Held et al. [37] were the first to apply CCP specifically to address uncertainties in climate response and resource availability in the context of adhering to temperature targets. Switching from the fully deterministic CEA to a probabilistic version implies deciding on the probability level at which the target will be adhered to. While the deterministic version typically relies on the chosen percentile value of uncertain parameters (if a probability distribution is assigned to them), the probabilistic approach explicitly prescribes the "safety" P_g —the percentage probability that the temperature increase will remain below a target value. The following equation represents the general structure of the probabilistic CEA for our purposes:

$$\max_{[x(t)]} W := \int_0^{t_{\text{end}}} U(t, [x(t)], 0) e^{-\rho t} \mathrm{d}t \quad \text{s.t.} \quad P_\gamma(T_{\max}(\gamma, [x(t)]) \leq T_g) = P_g \tag{4.1}$$

Hence, the decision-maker maximizes the inter-generational welfare aggregate W by varying the control variable $x(t)$, subject to the probabilistic constraint adhering to the desired safety P_g, such that the all-time maximum of temperature $T_{\max}(\gamma, [x(t)]) = \max_t T(\gamma, [x(t)])$, determined by the control variable pathway $[x(t)]$ and the state of the world (uncertain parameter) γ, does not exceed the target temperature the target temperature T_g with probability P_g. The utility function U is model-dependent, driven by consumption determined by the control variable $x(t)$, and exponentially discounted for future time steps using a discount rate ρ. The zero term in the parenthesis reflects the fundamental assumption of CEA, where the damages are set to 0 and the impacts are captured solely through the temperature target rather through a damage function. In the context of climate change economics, the emissions pathway $E(t)$ is determined through policy optimization, where the optimal control variable $[x(t)]$ pathway defines an emissions policy that satisfies the target criteria while maximizing welfare.

4.2.1.2 Cost-benefit analysis (CBA)

While CEA focuses on adhering to predetermined targets, cost-benefit analysis operates on the opposite end of the spectrum, emphasizing trade-offs between the contemporary mitigation costs and avoided future damages. This framework assumes that decision-makers possess a complete formulation of the damages associated with climate change and can therefore conduct the necessary evaluation. However, while it is a predominant school of thought in economics, its core assumption that decision-makers know the socioeconomic consequences of climate change is open to scrutiny (see Section 4.2.4). The intertemporal welfare optimization equation is given by:

$$\max_{[x(t)]} W := \int_0^{t_{\text{end}}} \int_\gamma p(\gamma) U(t, [x(t)], D(T(\gamma, [x(t)]))) e^{-\rho t} \mathrm{d}\gamma \mathrm{d}t. \tag{4.2}$$

Compared to its CEA counterpart, any constraint is omitted, and mitigation is driven by balancing consumption losses from climate change against those from mitigation efforts. The consumption loss from climate change, and consequently welfare, is indirectly influenced by impacts captured in the damage function $D(T(\gamma, [x(t)]))$, with probability distribution of uncertain parameter $p(\gamma)$. The damage function depends on the temperature anomaly, introducing a negative feedback mechanism that incentivizes mitigation efforts and helps regulate the temperature.

4.2.1.3 Cost-risk analysis (CRA)

Cost-risk analysis integrates elements of both CEA and CBA, offering a hybrid decision-making framework. Its mathematical structure builds on unconstrained utility maximization, while maintaining the precautionary element of adhering to the temperature target. The precautionary principle is embodied by introducing a negative utility term that represents the perceived risk of crossing the predetermined target. On a fundamental level, CRA can be interpreted as the trade-off between mitigation costs and the decision-maker's aversion to crossing the target, described by the following welfare optimization equation:

$$\max_{[x(t)]} W := \int_0^{t_{\text{end}}} \int_\gamma p(\gamma) \left(U(t, [x(t)], 0) - \beta R(T(\gamma, [x(t)]))\right) e^{-\rho t} \mathrm{d}\gamma \mathrm{d}t. \tag{4.3}$$

The equation reveals that CRA assumes no knowledge of the socioeconomic impacts of climate change, as the damage function is zero. In this case, mitigation efforts are guided by the negative utility driven by the risk function R, which is designed to fully capture the deeply uncertain risk associated with crossing the temperature target. Hence, the risk function incorporates the precautionary principle from CEA but frames it as a trade-off rather than a strict boundary. The β parameter quantifies the decision-makers aversion to crossing the target, reflecting the perceived severity of the associated risk. In this paper, the risk metric is calibrated by running the model such that the temperature target T_g is met with a P_g safety level, referencing the preference implicit in the Cancun Accord (UNFCCC, 2010) to stay below 2°C with a "likely" probability (65%) [167], as suggested in previous CRA literature [42]. Previous literature has shown that the risk function can take any convex shape, which guarantees a single optimal solution, while the calibration procedure ensures that the risk perception remains consistent regardless of its functional form [48]. We adopt the kink-linear risk function as the most conservative convex option to intuitively reflect target-oriented preferences $R(T) = (T - T_g)\Theta(T - T_g)$, where $\Theta(T - T_g)$ is a step function. This function has a value of zero for temperatures below the target and increases linearly once the target is exceeded.

4.2.1.4 Cost-benefit-risk analysis (CBRA)

Cost-benefit-risk analysis represents a novel hybrid concept in decision-making theory, conceptualized by Held [52]. It describes a situation where the rational decision-maker

has acquired partial information of climate damages while still accounting for unknown effects in the form of the temperature target motivated by the precautionary principle. Hence, this framework combines elements of CRA and CBA, as mathematically formulated in the following welfare optimization equation:

$$\max_{[x(t)]} W := \int_0^{t_{\text{end}}} \int_\gamma p(\gamma)\,(U(t,[x(t)],D(T(\gamma,[x(t)])))-k\beta R(T(\gamma,[x(t)])))\,e^{-\rho t}\mathrm{d}\gamma\mathrm{d}t. \tag{4.4}$$

Compared to CRA, one can notice that the damage function is reintroduced to affect the utility function. However, the decision-maker accounts for the possibility of incomplete knowledge about climate damages by retaining the risk function, which represents the aversion towards unknown risks of crossing the target. This aversion, embodied by the risk function R, is scaled by a parameter k, reflecting the extent of unaccounted-for damages.

In this paper, we treat k in two distinct ways. In one approach, we conduct a sensitivity analysis by varying k from 0 to 1, thereby encompassing the full range of possible knowledge states regarding climate impacts. A value of k=0 implies that the damage function fully captures the impacts. In the second approach, we recalibrate the model within the CBRA framework following the same procedure used for CRA. Specifically, we determine a value of k that ensures the simulated trajectory remains within the predefined safety margin for the temperature target. Since this framework includes a damage function that incentivizes mitigation efforts alongside the risk function, the resulting risk-weighting parameter takes a lower value than 1.

This approach allows a researcher to test what proportion of the perceived risk is quantified in the damage function. The choice of the damage function used in this paper is introduced in subsection 4.2.4.

4.2.2 MIND Model

The Model of Investment and Technological Development (MIND) is a globally aggregated Ramsey-type economic growth model that incorporates a detailed representation of the renewable energy sector, fossil fuel extraction, and fossil energy production. Initially introduced by Luderer et al. [168], the model has been enhanced over time by subsequent studies to address uncertainty and incorporate learning mechanisms [37] [101]. A key

advancement of MIND in comparison to other IAMs (e.g., DICE [161]) lies in its treatment of the energy system, where it incorporates an endogenous learning-by-doing mechanism, improving the representation of technological progress within the energy sector.

In this paper, we provide an improvement to the MIND model by updating the climate module, which provides a feedback mechanism between energy production choices and global mean temperature change. We replace the one box climate model, originally introduced by Petschel-Held et al. (1999) [70], with a modified version of FaIRv2.0[1] [169]. As part of this update, we modified FaIR to include a tailored uncertainty scheme for climate sensitivity that allows the user to do probabilistic analysis and to assess the effects of learning about uncertain climate sensitivity, as detailed later in this section. This choice of uncertainty scheme ensures compatibility with previous literature using the MIND model while significantly reducing computational demands compared to optimization with the full uncertainty ensemble for each parameter (e.g., [102]).

The production function, representing the global economic output in terms of GDP, is modeled as a constant-elasticity-of-substitution (CES) function that depends on labor, capital and energy as input factors. Consumption, and by extension the utility U, is determined at each step by the decision-maker's allocation of output between consumption and investment. In MIND, the control variable represents investments in various technologies, including renewables as a mitigation mechanism. These decisions are governed by inter-temporal welfare optimization, whose formulation depends on the decision-making framework, as discussed above. When damages are introduced into MIND, the production function is modified by the damage function, resulting in a net reduced production function given by $Y_{\text{net}(T)} = (1 - \frac{D(T)}{100}) \cdot Y_{\text{gross}}$. This reduction propagates through the system, affecting utility and ultimately diminishing intertemporal welfare.

Apart from the introduction of the new climate module, the configuration of the MIND model used in this paper remains consistent with the version presented in the work of Neubersch et al. [72].

[1] Hereafter referred to as just FaIR.

4.2.3 Probabilistic FaIR

FaIR belongs to the category of climate models of reduced complexity, also known as climate emulators. It represents the climate system as a global aggregate, enabling computational efficiency that is essential for performing optimization procedures required in climate policy evaluations. The first version of FaIR was introduced by Millar et al. [170]. It builds on the four carbon compartments proposed by Joos et al. [171], which were shown to effectively replicate the carbon dynamics of fully resolved climate systems. FaIR extends this framework by incorporating a feedback parameter that accounts for the saturation of carbon sinks, modifying the carbon retention time in each compartment. The total content of these compartments defines the atmospheric carbon concentration[2], which is then translated into radiative forcing, driving temperature increases.

Temperature dynamics in FaIR were initially modeled using two temperature compartments, following the framework proposed by Geoffroy et al. [172]. FaIRv2 [169] introduced a third temperature compartment and adjusted the feedback mechanism. To incorporate uncertainty about climate sensitivity, we modify the temperature dynamics to depend explicitly on the chosen climate sensitivity value. The temperature dynamics are dictated by following equations:

$$\frac{\mathrm{d}S_j(t)}{\mathrm{d}t} = \frac{q_j F(t) - S_j(t)}{d_j}, \quad T(t) = \sum_{j=1}^{3} S_j(t), \tag{4.5}$$

where $S_j(t)$ are the temperature compartments, whose sum gives a total temperature increase $T(t)$, providing a mode representation of the energy balance model matrix (see Leach et al. for details). The temperature change is driven by the radiative forcing parameter F, which depends on the atmospheric carbon content and is redistributed across the temperature compartments according to their response timescales d_j and response coefficients q_j. In this representation, the equilibrium climate sensitivity and transient climate response are given by:

$$\mathrm{ECS} = F_{2\times\mathrm{CO}_2} \cdot \sum_{j=1}^{3} q_j, \quad \mathrm{TCR} = F_{2\times\mathrm{CO}_2} \cdot \sum_{j=1}^{3} \left\{ q_j \left(1 - \frac{d_j}{t_{2\times\mathrm{CO}_2}} \left[1 - e^{-\frac{t_{2\times\mathrm{CO}_2}}{d_j}} \right] \right) \right\}, \tag{4.6}$$

[2]The compartments are not physical entities but rather a fitting mechanism designed to emulate Earth System Models.

where $F_{2\times CO_2}$ represents the radiative forcing at a doubling of atmospheric CO_2 concentration, and $t_{2\times CO_2}$ denotes the timescale for CO_2 doubling in a stylized scenario with 1% annual increase from preindustrial levels, which corresponds to approximately 70 years. In their paper, Leach et al. derived the default parametrization by first fixing d_j's and q_1 to default values based on a central value within the constrained ensemble, and then quantifying the parameters q_2 and q_3 by setting the ECS and TCR to central values within the constrained ensemble (3.24 °C and 1.79 °C, respectively) and solving the equations above to obtain q_2 and q_3. We follow the same approach to derive the probabilistic FaIR used in this paper, treating ECS as the uncertain parameter.

To ensure the model depends solely on ECS, we express TCR as a function of ECS by employing an equation from the literature that defines the relationship between TCR and ECS. Nijsse et al. (2020) demonstrated an approximate relationship between TCR and ECS based on CMIP6 and CMIP5 models given as $\text{ECS} = \text{TCR}/(1 - e' \cdot \text{TCR})$, with $e' = 0.24$ [173]. Rearranging this equation to express TCR as a function of ECS, and using $e' = 0.25$, derived from the default FaIR TCR and ECS values, we combine it with the equations above that ECS, TCR, q_j's and d_j's. While fixing d_j's and q_1 to the same default values as suggested by Leach et al., we derive the relationships between q_2(ECS) and q_3(ECS) to construct the probabilistic FaIR that varies with climate sensitivity.

The climate sensitivity probability distribution is modeled as a log-normal distribution, following the approach suggested by previous studies [48] [174]. To parameterize this distribution, we use the constrained ECS estimates from Table 7 in Leach et al., which provide median values along with likely and 5%–95% ranges. These estimates are derived from methodologies that integrate observational data with outputs from CMIP6. First, we acquire the μ and σ for our log-normal distribution by solving the cumulative distribution equation for the 50% and 95% percentile values provided in Table 7 in [169]. This choice ensures the median of the distribution aligns with the central value reported by Leach et al, while also bringing it closer to the IPCC AR6 very likely range of 2 to 5 °C compared to the original Leach et al. version [175]. The distribution is then numerically sampled by dividing it into equally probable intervals using the inverse cumulative distribution function and then representing each interval by its expected value, calculated analytically ([48]). This calculation is given by: $\theta_n = \frac{\bar{\theta}N}{2}\left(\text{Erf}\left[\frac{\sigma}{\sqrt{2}} + \text{InverseErfc}\left(\frac{2(n-1)}{N}\right)\right] - \text{Erf}\left[\frac{\sigma}{\sqrt{2}} + \text{InverseErfc}\left(\frac{2n}{N}\right)\right]\right)$, where θ_n represents the n-th sampled climate sensitivity, N is the total number of samples, and n

is the n-th sample. The parameter $\bar{\theta}$ is the mean climate sensitivity, and σ corresponds to the scale parameter of the log-normal distribution.

The parameterized distribution used in this study, along with the N=20 sampled numerical values representing different states of the world (i.e., various climate sensitivity outcomes), is visualized in the left panel of Figure 4.1. The right panel shows the model results for the idealized scenario of an abrupt fourfold increase in atmospheric CO_2 concentration, with the 20 states of the world corresponding to those shown in the left panel, represented by consistent coloring. This simulation can be directly compared to the same experiment and the full FaIR uncertainty range calibrated to fit the CMIP6 range, as shown in Figure 8b of Leach et al. [169]. Notably, for the central (default) value, the two model runs align almost perfectly. However, our uncertainty scheme exhibits a slight bias toward a lower response, systematically underestimating temperature outcomes by approximately 2.5 percentiles, as indicated by the abrupt-4xCO_2 experiment. This bias arises from modeling climate sensitivity as a log-normal distribution, which, while useful, does not fully capture the complexity of the uncertainty space. In this study, the distribution is parameterized to align with constrained estimates of central and upper percentiles, which produces biases at the lower end of distribution. Another source of deviation stems from the approximation used to relate TCR to ECS, which, although effective for central cases, may introduce inaccuracies at the tails of the distribution. Overall, simplifying the representation of systematic uncertainty into a single variable, climate sensitivity, introduces further bias. Nevertheless, the uncertainty space is sufficiently well-represented, and the use of a single-variable representation remains a practical and effective simplification.

4.2.4 Damage function specification

To operationalize the CBRA framework, it is essential to select an appropriate damage function. In this section, we present our choice and derivation of a partial damage function, which reflects decision-makers' incomplete information about the socioeconomic effects of climate change. This partial knowledge, in turn, motivates the adoption of CBRA as a decision-making framework.

Quantifying the total damage function had been open to the debate ever since integrated assessments models started looking into optimal mitigation policies, with the ranges of total production losses from climate change varying drastically, depending on

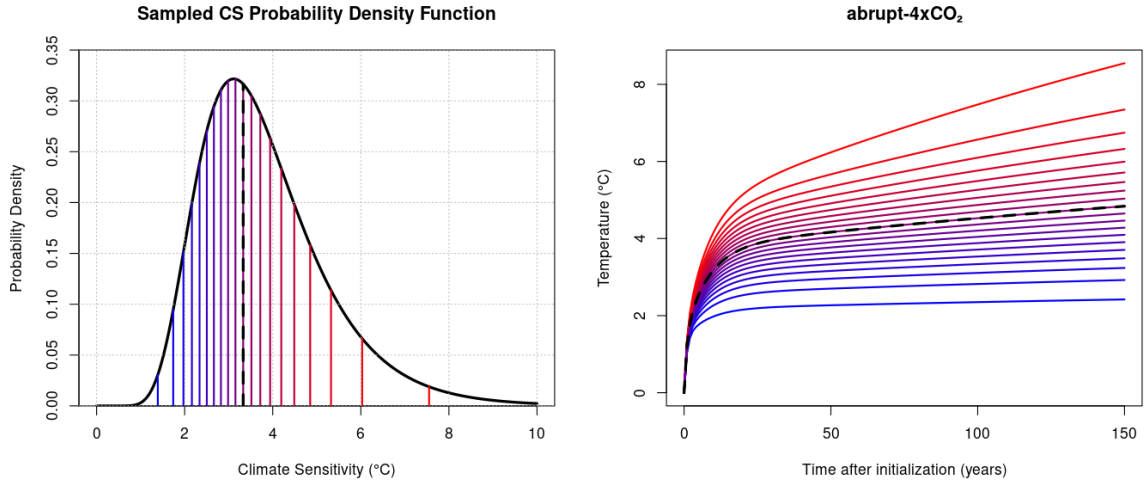

FIGURE 4.1: Left: The parameterized log-normal distribution and the N=20 sampled values representing different climate sensitivity outcomes. The first (1.39 °C) and the last (7.55 °C) values correspond approximately to the 2.5th and 97.5th percentiles, respectively, of the log-normal distribution ($\mu = 1.27412$ and $\sigma = 0.371725$). Right: Model run for an abrupt fourfold increase in CO_2, with colors corresponding to the states of the world (i.e., climate sensitivity outcomes) shown in the left panel.

the methodical approach, best depicted by the IPCC AR6's collection of different damage function calculations, shown in AR6 WGII Cross-Working Group Box [33]. Moreover, Horward and Sterner showed that many of the damage functions found in the literature suffer from different types of biases, i.e, replication, omitted variable and publication biases, which presumably led to overconfidence in our assessments [79]. In this paper, we quantify the damage function using the output of a computable general equilibrium (CGE) model, following one of the suggestions of Piontek et al. [176]. In this paper, we argue that CGE model output is the superior choice for calculating damage functions in IAMs compared to upscaling local estimates, for several reasons.

Firstly, CGE models are promising due to their ability to simulate the propagation of climate damages across sectors and represent a heterogeneous economy that dynamically responds to structural changes induced by climate impacts. The first argument builds on the fact that CGE models capture the entire economic impact chain, translating climate change effects on specific sectors and regions into their final impact on globally aggregated production. This approach incorporates internal economic feedback mechanisms, providing a comprehensive representation of the full channel of damage propagation, including both direct and indirect climate change related GDP effects. We find this an important factor, as indirect impacts can effect the economy across different sectors, locations and time, all three covered by a CGE. Crucially to notice is that this global production impact

aligns with the level of aggregation at which IAMs apply their damage functions. In contrast, upscaling local estimates of direct impacts bypasses these feedbacks by aggregating localized impacts without accounting for their propagation through the broader economy, inevitably missing critical economic readjustments resulting from these changes. Since IAMs apply damage functions directly to total global production, it is essential that these functions capture the systemic responses reflected in CGE models. This, we argue, makes CGE-calculated damage functions a more consistent and accurate foundation for use in IAMs.

Moreover, CGE models provide a transparent framework for identifying explicitly included impact channels, making exclusions clear and highlighting the partial nature of the damage assessment. This transparency enables more informed result interpretations. Moreover, CGE models can explicitly model damages in certain sectors while leaving others intact, reinforcing the partial nature of total damages and making it qualitatively accessible.

There have been few attempts in the literature to derive global damage functions from CGE models [103, 104], with existing studies primarily relying on either recursive or static temporal dynamics. Static setup involves shocking the model (e.g., with a temperature change) in a single year and using the resulting equilibrium for that year to represent the damage, avoiding any temporal evolution. Recursive models, on the other hand, account for the propagation of temperature shock throughout a time period but assume fully myopic agents who optimize consumption only between two consecutive time steps. Both approaches are misaligned with the temporal dynamics of globally aggregated policy-optimizing IAMs, which determine optimal policies by simultaneously optimizing over the entire time period. In this paper, we introduce the first intertemporal, forward-looking CGE-derived damage function. To the best of our knowledge, this makes our approach the only dynamically consistent CGE-derived damage function currently available for use in IAMs.

To derive the damage function, we use the results from Avakumović et al.[177] (in prep.). The study divides the global economy into 60 regions and 30 commodity sectors and, using three different sources of climate impacts, calculates total regional GDP losses. These regional losses are then aggregated into global GDP loss, providing the necessary data to construct a ready-to-use damage function for integration into MIND. The CGE

model employed is GTAP-INT 2.0, a fully intertemporal model in which both firms and households act as forward-looking agents. This study pioneers the application of a fully intertemporal CGE to assess the economic effects of climate change, achieving temporal dynamic consistency with globally aggregated IAMs such as MIND and DICE, in contrast to static or recursive approaches.

Avakumović et al. apply shocks through three distinct impact channels: the effects of climate change on human health via changes in mortality [178], impacts on the agricultural sector through yield changes [4], and heat-related labor productivity losses [177]. Figure 4.2 illustrates the globally aggregated GDP loss for 5 emission pathways (solid lines), with regional contributions weighted by GDP before aggregation.

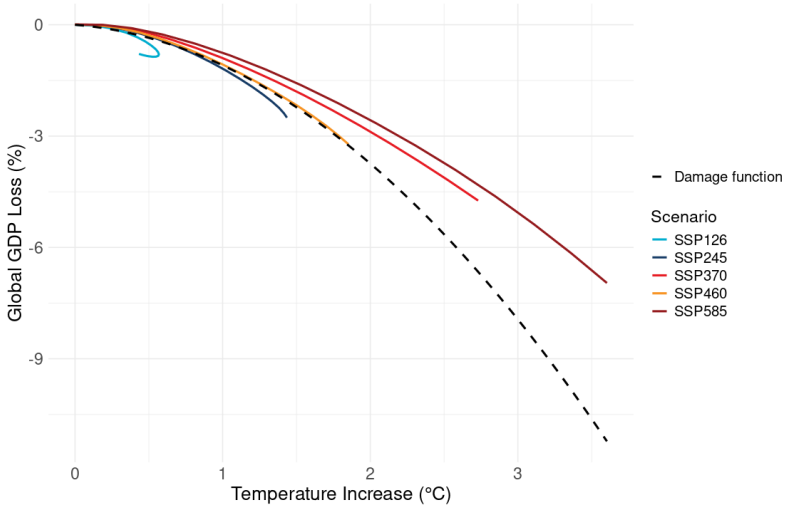

FIGURE 4.2: Globally aggregated GDP loss across five emission pathways (solid lines), with regional contributions weighted by GDP. The black dashed line represents the derived quadratic damage function, estimated based on model-simulated GDP losses under the SSP460 pathway. This function accounts for the combined impacts of climate change on human health, agriculture, and labor productivity.

Unlike previous CGE-derived damage functions, which estimate damages at a specific year under varying temperature levels, we derive the damage function (black dashed line) based on globally aggregated GDP losses simulated by the model for each year under the SSP460 pathway. This pathway was selected as it represents a mid-range emission-intensive scenario within our set. We assume a quadratic functional form to describe the evolution of total GDP losses as a function of temperature, expressed as: $D(T) = a \cdot T^2 + b \cdot T$, yielding coefficients $a = 0.772$ $(1/°\text{C})^2$ and $b = 0.301$ $(1/°\text{C})$. It is important to note that the results from Avakumović et al. suggest that the contemporary global damage function depends on the emission scenario. This challenges the conventional

approach of presenting global damage functions as solely temperature-dependent (see, for example, [79]). However, addressing this issue is beyond the scope of this study and is left for future research.

For comparison purposes, we employ an additional damage function used in study by Hänsel et al. [28], which represents the best estimate from a meta-analysis conducted by Howard and Sterner [79], given in a form of $D(T) = 1.0038 \cdot T^2$.

4.3 Results

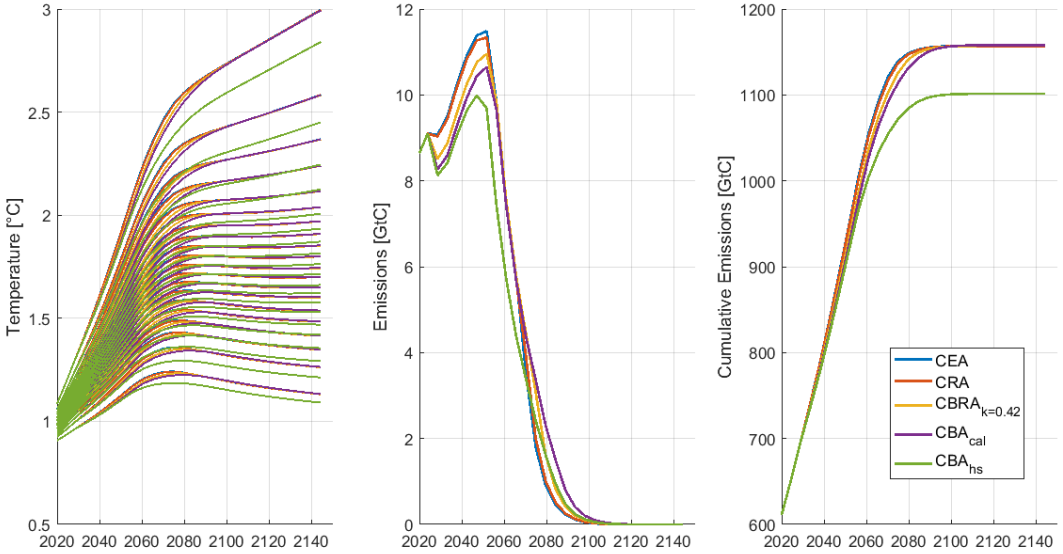

FIGURE 4.3: Comparative analysis of temperature pathways, emission trajectories, and cumulative emissions across the decision-making frameworks: CEA, CRA, $\mathrm{CBRA_{k\,=\,0.42}}$, $\mathrm{CBA_{hs}}$, and $\mathrm{CBA_{cal}}$. Each emission pathway corresponds to 20 possible temperature pathways per framework, reflecting the sampling of 20 distinct climate sensitivity outcomes. CRA and CBRA are calibrated to assess the weight of the risk function, while $\mathrm{CBA_{cal}}$ is calibrated to evaluate the damage function itself, disregarding risk considerations. The calibration for CRA, CBRA, and $\mathrm{CBA_{cal}}$ is performed to adhere to the 2 °C target under a 65% safety level, requiring 65% of the temperature pathways to remain below 2 °C. Notably, $\mathrm{CBA_{hs}}$ cannot be calibrated in this manner because the Howard and Sterner damage function inherently results in more stringent emission reductions, making it incompatible with the specified safety threshold.

Figure 4.3 presents multiple optimization runs across all four decision-making frameworks. The first panel illustrates the temperature pathways for each climate sensitivity within each framework, the middle panel depicts the corresponding emission pathways, and the right panel shows the resulting cumulative emissions. The CEA, CRA,

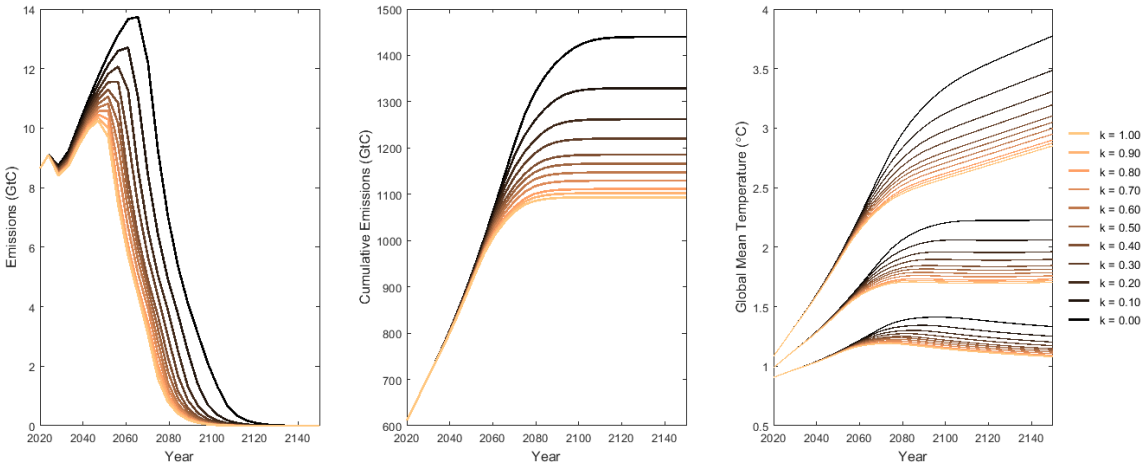

FIGURE 4.4: Sensitivity analysis of the CBRA framework with respect to the risk-weighting parameter k, incorporating CGE-generated, partial damage function. The left and center panels display emission pathways and cumulative emissions, respectively, for varying k values. The right panel illustrates corresponding temperature pathways for three climate sensitivity levels: the lowest (2.5th percentile), median (50th percentile), and the highest (97.5th percentile). The temperature pathways cluster into three distinct groups, indicating that uncertainty in climate sensitivity dominates over variations in k when it comes to overall temperature outcomes.

$\text{CBRA}_{\text{k = 0.42}}$ and CBA_{cal} are set to adhere to the 2 °C with 65% safety, each operating under distinct equations as described in the methodology section.

Remarkably, an important first observation is that CEA and CRA (blue and red) yield virtually identical policy recommendations in terms of both emissions and cumulative emissions pathways, with a maximum deviation of 1.3% at peak emissions (around the mid-century) and negligible differences before and after. In terms of temperature and cumulative emissions, the peak deviations are 0.40 % and 0.36% respectively, further confirming their alignment.

In $\text{CBRA}_{k=0.42}$ run (yellow), a partial CGE-generated damage function is incorporated to reduce the production function, and the calibration follows the same approach as in CRA. This process reduces the multiplier factor in front of the risk function to $k = 0.42$, compared to the pure CRA value. The results indicate that the partial damage function accounts for $1 - k = 0.58$ (or 58%) of the perceived risk in CRA, which otherwise assumes no damages to production. While cumulative emissions and temperature pathways align with the CEA and CRA counterparts by the end of the century, temporary deviations of 1.86% in cumulative emissions and 1.96% in temperature occur at intermediate stages before full convergence. The emission pathway in CBRA exhibits

more pronounced deviations within the century, likely due to differences in the structural formulation of temperature feedback within the model, as similarly observed in the CBA runs.

Moving forward, CBA_{hs} (green) represents the case of using a fully-fledged CBA that incorporates the damage function provided by Horward and Sterner (HS) [79]. The resulting cumulative emissions—and consequently, the temperature change—are lower than those in the CEA, as well as in the calibrated CRA and CBRA counterparts. The 65% percentile of the final temperature distribution is approximately 0.2 °C lower than the the 2°C required by the calibration processes in other cases. This corresponds to a 10% decrease in generated temperatures across all states of the world, which can also be traced to a 10% decrease in cumulative emissions, reflecting the direct link between cumulative emissions and temperature outcomes. Moreover, calibrating CBRA with the HS damage function is not feasible for any value of positive k, as the resulting pathways consistently fall below the safety threshold. This suggests that the damages represented by the HS function are more severe than the perceived risk embedded in the CRA-based risk function.

Finally, CBA_{cal} represents the case, within the fully-fledged CBA framework, we assumed an unknown quadratic damage function $D(T) = a \cdot T^2$, and then calibrate a so that the model run adheres 2°C with 65% safety, resulting in $a = 0.896(1/\text{C})^2$. The pure CBA run under this newly specified damage function yields the same cumulative end-of-century emissions and temperature pathways, while the emissions pathway closely aligns with the CBRA counterpart but exhibits slight deviations due to differences in the structural representation of temperature feedback mechanisms (i.e., exclusion of the risk function). Nonetheless, when comparing CEA and the three calibrated runs (CRA, CBRA and CBA_{cal}), the overall policy recommendations remain highly consistent, as reflected in the key climate policy variable of interest: temperature increase. The largest temperature difference among the four occurs between the CBA_{cal} and CEA, reaching a maximum of less than 0.07 °C around 2075 for the highest climate sensitivity value, before diminishing quickly thereafter. In contrast, the temperature difference between CEA and CBA_{hs} in the same year is 0.15°C and continues to grow over time.

Having examined how the choice of framework affects various outcomes, Figure 4.4 shows the sensitivity analysis of CBRA with respect to the risk-weighting parameter

k. This parameter indicates what proportion of unknown risk remains unaccounted for, given that the partial damage function captures only a fraction of the total damages while the remainder is embedded in the risk function. This exercise explores the full spectrum of possible damage representation, ranging from the assumption of complete damage knowledge at k = 0 to the scenario where, even with the incorporation of a partial function, the risks associated with crossing the target remain fully unaccounted for, as reflected by k=1. Notably, the calibrated CBRA run from Figure 4.4 falls between the pathways associated with k=0.4 and k=0.5, which serves as a useful point of reference to compare with CBRA run in Figure 4.3.

Examining the left and center panels of Figure 4.4, we observe that incorporating the risk of exceeding the target imposes a significantly stronger constraint on emissions than the partial damage function. This is evident from the differences in final cumulative emissions (center panel): reducing k from 1 to 0.3, which represents a 70% decrease in the weight of the risk function, results in a change of just over 100 GtC in final cumulative emissions. However, a further reduction of k from 0.3 to 0, a 30% decrease, leads to a more substantial variation of over 200 GtC. This indicates that the final reduction to zero has a disproportionately larger impact on emissions compared to the initial decrease in weighting the risk of crossing the target. The right panel of Figure 4.4 presents temperature pathways in the CBRA run across the full range of k values, considering three climate sensitivity levels: the lowest, median, and highest in our set. The clustering of runs corresponding to different k values into three distinct groups suggests that uncertainty in climate sensitivity has a more pronounced impact on overall temperature outcomes than uncertainty in climate damages. Consequently, this indicates that climate sensitivity uncertainty plays a more dominant role in shaping policy advice.

4.4 Discussion

This study represents the first operationalization and formal naming of cost-benefit-risk analysis, a hybrid decision-making framework originally proposed by Held [52]. Designed to bridge the gap between the target-based, precautionary-principle-driven cost-effectiveness analysis and the trade-off-based cost-benefit analysis, CBRA builds upon the cost-risk analysis. By incorporating the negative utility from crossing the temperature target through a risk function, as well as introducing an (incomplete) damage function

akin to that in CBA, CBRA captures both the quantifiable economic damages and the residual uncertainties associated with exceeding predefined climate thresholds.

In that sense, CBRA is a hybrid between CRA and CBA, representing a situation where the decision-maker acknowledges that some of the fully unknown socioeconomic feedbacks assumed by the precautionary decision-maker are actually known and can be quantified, while at the same time recognizing that their knowledge is only partial. This partial knowledge leaves the unquantifiable impacts embodied in the less-weighted negative utility stemming from crossing the target. By integrating these components, CBRA provides a flexible yet structured framework for navigating between purely precautionary and fully damage-informed decision-making approaches, making it an attractive tool for addressing the evolving landscape of climate impacts research. Moreover, while this study applies CBRA within the context of climate economics, the underlying logic of bridging target-based and trade-off-based decision-making could, in principle, be extended to other domains where policy decisions must balance precautionary constraints with evolving impact assessments. Since CRA has thus far been used exclusively in the context of climate targets, we hope that the newly revealed properties of CRA will encourage its application in broader decision-making contexts.

Another notable feature of CBRA is its potential to act as a mediator between precautionary and cost-benefit-oriented schools of thought. By employing CBRA, one can quantitatively assess how much of the implicit climate damage was assumed by proponents of precautionary climate targets, while also accounting for uncertainties such as climate sensitivity. Our results demonstrate that the partial damage function, which incorporates three categories of climate impacts (agriculture, human health, and labor productivity) propagated through a CGE model, accounts for 58% of the unknown risks associated with crossing the 2°C target under a 65% safety level. This methodology can be extended to any damage function or target/safety level combination to evaluate their interrelation. Besides the reasons of internal consistency between discussed in the methodology, another feature of forward-looking CGE models that makes it paramount for the damage function assessment is its ability to be explicit with the user what climate impact channels are being quantified (in our case three). One could imagine turning on and off a specific sectoral damage to gain new insights on how do different permutations of included damages affect the total damage function, and with that potentially gain more insight into the completeness (or lack of) of the estimated damages.

Furthermore, we showed that CBRA can be used to calibrate a damage function that fully encapsulates the risks embodied in a climate target, provided that the mathematical form of the damage function is known. For example, if we adopt a quadratic form for the damage function, as suggested by Howard and Sterner [79], our calibration process yields $D(T) = 0.896 \cdot T^2$. This calibrated function aligns closely with the risks implicit in the 2°C target under the given safety level. While the emission pathway shows some differences, likely due to the functional form and its incorporation in the welfare equation, by the end of the century it converges perfectly in terms of cumulative emissions and resulting temperatures. Importantly, this calibration proposes k = 0, which means that the risk function is fully eliminated. This indicates that all risks are assumed to be captured by the calibrated damage function, marking a complete transition from CBRA to pure CBA framework, where decision-making is driven entirely by trade-offs between mitigation costs and quantified damages.

Moreover, we showed that it is not possible to calibrate the model to fit the target if the best-fit damage function from Howard and Sterner is employed ($D(T) = 1.0038 \cdot T^2$), since for every possible non-negative value of k the resulting safety will be above the required 65% as the strength of the damage function will require it to do so. This clearly means that, in comparison to the impacts assessed by Howard and Sterner, the precautionary community in fact expected less damages on the economy when assuming the 2 °C target (with 65% safety). Using CBRA framework, one could theoretically quantify how much of the risk of crossing the target was omitted by the precautionary decision-maker if the calibration is done with k allowed to be negative. This is not done in our analysis since it leads to a counterintuitive framework where the decision-maker gains utility from crossing the target.

To sum up, CBRA's flexibility is demonstrated across the spectrum of k values. When $0 < k < 1$, it represents cases where assumed risks in the target exceed the quantified effects in the damage function. When k = 0, it transitions to pure CBA. The range $k < 0$, while not explored in our analysis due to its counterintuitive implication of utility gains from crossing the target, theoretically represents cases where the damage function overestimates climate impacts compared to the precautionary perspective. Hence, CBRA serves as a "translator" between the two opposing schools of thought in climate economics.

A pivotal innovation in bridging decision-making frameworks is the incorporation of a

temperature target within the utility maximization framework through the introduction of CRA. This paper demonstrates that updating the climate module enables CRA to fully replicate CEA, as Held [45] anticipated. The updated module conforms to the carbon budget approach [179], ensuring that any change in cumulative emissions directly impacts temperature outcomes, independent of previous emission trajectories. This adjustment in climate response behavior prevents further emissions once the temperature target is exceeded, as temperatures stabilize at levels dictated by cumulative emissions rather than decreasing to allow additional emissions. This confirms that CRA operates as a robust, standalone target-based approach, seamlessly integrating trade-off considerations within its framework.

CBRA effectively aligns the trade-off-based and target-based communities in achieving similar long-term goals for temperature and cumulative emissions by the end of the century. This alignment underscores that while the frameworks converge on the critical metrics of temperature and cumulative emissions, set by the temperature-based targets, they offer varied recommendations on the pathways for achieving these emissions. In terms of interpreting the damage functions as the quantification of assumed targets, this is not an issue since the precautionary principle dictates the maximum levels of warming, not how we reach there. Nevertheless, we hypothesize that these variations in emissions recommendations may be attributed to differences in how damage functions are integrated within the models and the functional form of the damages themselves, potentially affecting the structural dynamics between temperature and economic outputs. Future research should explore how diverse formulations of damage functions and their application methods within models can influence these pathways.

Building on our findings, we have quantitatively demonstrated—while accounting for the caveats discussed in this paper—that incorporating only three impact channels in our analysis (agricultural yield losses, changes in human mortality, and heat-related labor productivity losses) accounts for up to 58% of the risk perceived by the target-based community under a 2°C climate target. Given the vast number of additional impact channels that could further amplify GDP losses—too numerous to list in full—this suggests that the target itself may be overly conservative in capturing the full spectrum of potential risks. This, in turn, raises the question of whether the global community should have initially pursued more stringent climate targets, if large losses were to be avoided.

Finally, Figure 4.4 illustrates that the separation of temperature pathways for different risk-weighting parameter k values across three levels of climate sensitivity highlights how uncertainties in climate sensitivity dominate policy recommendations, surpassing the influence of perceived risks or the depth of damage understanding. While damage function research remains essential, its impact may be overshadowed by uncertainty in climate response to emissions, given that damage functions are convex in temperature. This reemphasizes on the need to refine our understanding of climate sensitivity, given its non-linear amplification of damages, and reinforces the central role of climate science in shaping effective policy.

Conclusion

To conclude, this paper makes several contributions to the field of decision-making in global mitigation efforts. It presents the first operationalization of CBRA, an extension of the purely target-driven CRA, enabling the incorporation of well-known socioeconomic impacts through a damage function on production. This hybrid framework bridges trade-off-based and target-based approaches while maintaining the dynamic consistency of the utility maximization framework, thereby avoiding the structural limitations of traditional target-based methods such as CEA.

We updated the MIND model with the FaIR climate module, incorporating a novel, simplified uncertainty scheme developed in this study. This scheme condenses the entire uncertainty space of climate parameters into a single variable—climate sensitivity. Such an approach is particularly advantageous in optimization procedures that require a high number of iterations to determine an optimal value, as it significantly enhances computational feasibility by allowing variations in climate sensitivity without the need to sample an entire ensemble of model-related parameters. By implementing a new climate module, we explicitly show that the CRA almost perfectly replicates the policy recommendations of the CEA counterpart.

Furthermore, we introduced, to our knowledge, the first-ever damage function derived from a forward-looking, regionally and sectorally disaggregated global CGE model on globally aggregated production. In this paper, we argue that calculating global losses directly from the CGE run is preferable to aggregating local impacts and scaling them up,

as the latter approach overlooks economic interactions that shape the final production response. Additionally, CGE-derived damages provide transparency regarding their origin, enabling explicit tracking of the contribution of different impact channels and clarifying the partiality of total damages. However, we emphasize that the temporal structure of CGE models must be carefully considered to ensure consistency with the forward-looking nature of policy-optimizing IAMs.

By incorporating a CGE-derived partial damage function that reflects the latest assessments of climate impacts on agriculture, human health, and labor productivity, we demonstrate that CBRA can quantify how much of the unknown risks embedded in climate targets under the precautionary principle are captured by explicitly quantified damage functions. In doing so, CBRA serves as a bridge between fully target-based and fully trade-off-based approaches, effectively acting as a translator between these two opposing schools of thought.

Chapter 5

Discussion & Outlook

5.1 Discussion

5.1.1 Paper 1

The "carbon budget approach" is one of the central concepts in this dissertation. This approach is premised on a "nearly linear" relationship in the Earth's climate system, whereby global mean temperature increases proportionally with cumulative emissions of CO_2, independent of the preceding emissions scenario [64]. Due to its simplicity in relating the primary driver of climate change to the corresponding climate response, the carbon budget approach has gained prominence in policy discourse, providing a clear account on exactly how much of the total carbon is allowed to emit for the society to adhere to the predetermined temperature target [105]. In the context of the decision-making theory that this thesis also contributes to, it is a crucial element that unifies CRA- and CEA-generated policy advice, first theorized by Held [73] and numerically shown in the third paper of this thesis.

The proportionality factor underpinning the carbon budget approach is formally called transient climate response to cumulative emissions of carbon dioxide (TCRE). If the carbon budget approach is to hold, TCRE must be preserved various possible preceding emissions scenarios. We refer to this as scenario-independency. In addition, the possibility that TCRE varies with preceding cumulative emissions implies that the carbon budget follows a non-linear relationship—a condition we refer to as state-dependency. Thus,

for the carbon budget approach to remain valid, it must satisfy scenario-independency. However, it need not assume state-independency, as the relationship between cumulative emissions and temperature can still be captured through a non-linear carbon budget equation, should TCRE prove to be state-dependent.

Previous literature has addressed both scenario-dependence and non-linearity in the carbon budget equation (i.e., state-dependent TCRE) to a limited extent. Several scholars have tested the latter using a restricted set of emission scenarios [59, 60, 62]. However, to our knowledge, the full portfolio of potential scenario-dependent deviations in the carbon budget has not been systematically examined prior to this thesis. To address this gap, we develop an optimization program to determine the minimum and maximum temperature outcomes for a given cumulative emissions level. This allows us to systematically explore the extent of scenario-dependence. Using a simplified climate emulator (FaIR v2, with default parameterization as in [1]), scenario-dependent deviations reach approximately 8% of the total temperature increase when negative emissions are allowed (and are lower otherwise), but remain short-lived. Moreover, these deviations diminish rapidly over time, reaffirming the validity of the carbon budget approach when using FaIR. In contrast, our calculations show that the one-box model—a climate module implemented in a variety of IAMs [17, 18, 72] —can produce substantially larger and more persistent deviations than its FaIR counterpart. Our findings show the critical importance of climate model selection in climate economic analyses. This should raise concerns among IAM modellers, for so long as the carbon budget approach remains policy relevant.

In this paper, we unify the treatment of scenario- and state-dependency through the lens of the pulse response function—i.e., the temperature response to a single emission pulse. We demonstrate that this framework serves a dual purpose: it enables the assessment of scenario-dependent deviations without requiring an optimization program, and it provides a basis for deriving the (non)linear carbon budget equation. In the first paper, we formalize this approach as the "pulse response representation", defined as the analysis of a temperature response to an emission pulse generated under varying climatic conditions. The novelty of this framework lies in its diagnostic power: the shape of the pulse response indicates the degree to which a model is susceptible to scenario-dependence, while changes in the pulse response under different climatic conditions reflect the presence and nature of state-dependence—and thus the non-linearity of the carbon budget equation.

To test the hypothesis that the shape of the pulse response reveals scenario-dependent deviations, we reinterpret the pulse response using the Green's function formalism and apply it within the optimization program. The results are consistent with those from full simulations using FaIR, thereby numerically confirming the hypothesis. Our findings show that FaIR's pulse response peaks approximately 17 years after an emission pulse, followed by a modest decline and gradual relaxation—explaining its small, diminishing scenario-dependent deviations. By contrast, the one-box model lacks a relaxation phase, which accounts for its failure to reproduce the carbon budget property.

Aside from scenario-dependency, pulse response representation also contributes to understanding the state-dependency of TCRE, which gives rise to non-linearities in the carbon budget equation. Previous work on non-linear carbon budget equations is limited, with the only example we are aware of presented by Nicholls et al. [110]. However, their approach assumes a specific functional form for the non-linear relationship. Our hypothesis is that the non-linearity of the carbon budget equation arises from the temperature-dependence of TCRE, which can be diagnosed through changes in the pulse response. To explore this, we propose approximating the pulse response with a step function that mimics TCRE. This enables the derivation of a non-linear carbon budget equation without assuming its form in advance.

This approach is novel in that it grounds the derivation in the thermodynamic structure of the system by applying a Taylor expansion with respect to temperature, rather than fitting an arbitrary curve. Under the default FaIR parameterization, the pulse response declines in magnitude, implying a corresponding decline in TCRE. This leads to the derivation of a concave carbon budget equation. The resulting equation closely replicates the full FaIR model, with deviations of only 2% across all four RCP emissions scenarios tested. In contrast, a linear carbon budget equation assuming constant TCRE yields relative deviations of up to 15% from FaIR-generated temperature projections. These results support our claim that state-dependency in TCRE—and the resulting non-linearity in the carbon budget—can be meaningfully diagnosed and incorporated through this pulse-based method.

Additionally, we derived pulse response representations for eight different calibrations of the FaIR model, each tuned to a distinct Earth System Model (ESM) [1]. The results show that while all calibration variants exhibit scenario-independency and hence adhere to

the carbon budget approach, they differ in the degree of non-linearity, ranging from fully linear behavior to slightly convex responses. Moreover, using a simplified climate model, MacDougall suggested that the models with low linearity have a higher path dependence and vice versa [111]. Our results suggest that these two are independent, but more models and calibrations need to be tested. In the outlook part of the conclusion section, future research perspectives following this article are suggested.

In short, this paper quantified potential carbon budget deviations resulting from the standard parametrization of the FaIR model; provided robust confirmation of the scenario-independency of the carbon budget approach; and derived a non-linear carbon budget equation. As such, this paper offers various tools for the climate research and policymaking community to assess their climate model's adherence to the carbon budget approach. These tools include the optimization framework (which assists in identifying extreme cases of scenario-dependency) and the pulse response representation (which illuminates the extent of scenario- and state-dependency). In addition, this thesis confirms FaIR's adherence to carbon budget approach, particularly in comparison to other climate emulators commonly used in Integrated Assessment Models (IAMs). Thus, taken together, this thesis strengthens the case for the use of FaIR in climate-economic assessments, as previously suggested by Kikstra et al. and Dietz et al. [68, 180]. We implement FaIR in the MIND model [72] in the third paper of this thesis.

5.2 Paper 2

The second paper estimates future climate change-related economic damage, expressed primarily as losses in GDP at the regional—and, in many cases, national—level. These estimates are derived using the latest climate impact assessments within a Computable General Equilibrium (CGE) model. Section 1.2.2 provides a detailed rationale for employing CGEs in this context. We argued that CGEs offer advantages over alternative bottom-up methods that sum sector-specific impacts in isolation (i.e., direct effects on the economy). In contrast, CGEs aim to maintain structural consistency with the real-world economy by accounting for interactions between impacted sectors and regions following as the economic response to the initial, sector and region specific shocks. These interactions capture indirect effects, such as shifts and disruptions in interregional trade patterns, labor and capital reallocations in response to shocks. By bringing together both direct

and indirect impacts, CGEs deliver a more comprehensive picture of climate impacts and their propagation as economic impacts through the world economy.

Another central idea in this thesis is the development of a decision-making framework that explicitly acknowledges the inherent incompleteness of global climate damage estimates. As a corollary, it is essential to be transparent about which impacts are—and are not—included in any damage estimate. CGE-based damage functions render it straightforward to identify the specific impact channels assumed by the analyst, and thereby reveal the partial scope of the assessment. This clarity is critical when integrating these estimates into hybrid approaches such as CBRA, which depend on a clear distinction between quantified damages and remaining, unquantified risks. In practice, sectoral and regional granularity in impact assessments deliver more policy relevant information, especially if the aim is targeted, equity-based climate adaptation and compensation for the future damages. By capturing heterogeneous impacts, higher granularity allows models to reflect regional differences in exposure and vulnerability, while also considering sector-specific sensitivities (e.g., the agricultural sector is more sensitive to heat stress than the IT sector). Such heterogeneous factors are expected to exacerbate existing socioeconomic inequalities and amplify the uneven distribution of future climate-driven economic losses, as shown in the second paper of this thesis. Estimating economic damages using a CGE model is done in two steps. First, sector-specific climate impacts are derived from bottom-up quantifications that connect observed climate stressors with the subsequent performance of specific economic sectors. Each of these impacts is then translated into a temperature-dependent, sector-specific damage function. In the second step, these damage functions are integrated into a CGE framework, forcing the stylized economic system to dynamically adjust to model-imposed temperature changes and hence producing resultant changes in GDP. This article contributes to the existing literature on the economic modeling of climate impacts by refining impact calculations and testing them in a CGE.

5.2.1 Impact quantification: new heat-related labor productivity loss assessment

Roson and Sartori present a suite of climate-damage functions linking temperature changes to distinct, country-specific socio-economic impacts [80]. However, closer inspection reveals methodological limitations that warrant refinement. In this article, we focus on

heat-related labor productivity losses—a damage function ultimately affecting almost all economic sectors by reducing labor output, the key element in production. We identified the following list of inconsistencies in their methodology: reliance on monthly data (too low temporal resolution), approximation of humidity variable (instead of using the available data), not relying on climate projections but assuming a linear temperature–damage relationship. As a response, this thesis developed a refined, country-level labor productivity loss damage function.

Our refined approach is as follows. We use daily temperature and humidity data from an ESM with 50 ensemble variations to account for climate variability. We match these climate data with gridded population data to derive country-level, population-weighted projections of wet-bulb globe temperature (WBGT). WGBT is a key variable for assessing heat exposure effects on the labor force. Drawing on empirical relationships provided by the literature, we then translate WBGT into three categories of work ability, corresponding to different work requirements (Bröde et al. 2018). The loss of labor productivity is then defined as a relative change in work ability per unit time, compared to some baseline period. This metric thereby indicates regional labor adaptation to changing climatic conditions, from historical baselines. By analyzing multiple emissions scenarios and all ensemble outcomes, we confirm the temperature–damage relationship for labor productivity across 151 countries and three categories of workloads. Our results indicate a robust relationship between temperature increases and labor productivity losses that does not depend on any specific emission scenario. This suggests labor productivity losses are a rare example of impact-to-damage functions that can be modeled as a function of temperature alone (unlike, for example, agricultural sector losses [4]).

Our derived loss functions reconfirm (and exacerbate) regional discrepancies in labor productivity losses. In general, our results suggest tropical regions are most severely affected, while regions above the subtropical belt suffer comparably minor/negligible losses. For example, under a 3°C warming scenario, Indonesia is projected to experience up to 100 times greater losses than Germany—albeit losses in Germany remain extremely low. This suggests that labor productivity losses are driven by higher humidity levels and are therefore highly sensitive to temperature increases. Moreover, due to the quadratic nature of the relationship, higher temperatures lead to substantially larger labor productivity losses under our refined approach, compared to previous estimates [80].

5.2.2 GDP loss calculation: CGE estimates

We then translate our country-level climate impact quantifications into region-specific GDP projections. To do this, we employ GTAP-INT 2 [99], an intertemporal, fully forward-looking extension of the standard Global Trade Analysis Project model [3]. This extension was enabled by a series of methodological advances in solution methods [96, 97]. GTAP-INT 2 stands out for incorporating a higher degree of sectoral and regional detail compared to typical CGE-based climate studies [91], while at the same time adopting forward-looking dynamics.

We set up GTAP-INT 2 by representing the global economy as disaggregated into 60 regions and 30 sectors or commodity groups. This disaggregation is detailed in the supplementary materials. We quantify GDP effects as changes relative to the baseline economy, given by the GTAP 11 database [156] and keeping the GDP and population constant at current levels. Economic changes thus emerge solely from temperature-dependent damage functions that shock sectoral performance, represented here by five different future temperature scenarios (RCP2.6, RCP4.5, RCP6.0, RCP7.0, and RCP8.5). Although most of these 60 regions match individual countries, some constitute multi-country aggregates (particularly in Africa, Central Asia, and South America). For these aggregates, we calculated the damage function as the average of the associated country-level damage estimates.

The labor productivity damage function, as expected, directly affects labor productivity across all production sectors. We categorized the workload required for different sectors following International Labor Organization guidelines: agriculture and construction-related sectors fall under high workload, manufacturing and industry under medium, and services under low workload. In addition to labor productivity losses, we include two further impact channels: agricultural damages via changes in crop yields, and human health damages via changes in mortality rates (affecting both labor supply and population), based on recent impact studies [4, 84]. While labor productivity losses consistently impose negative effects on the economy, changes in yields and mortality rates may be either positive or negative, depending on the region. If these impacts are realized, we would expect them to contribute to a further widening of existing global inequalities.

Our results show overall negative economic impacts, but with notable regional differences and disparities. In terms of long-term effects, China, India, and the United States

together account for roughly half of global GDP losses in absolute terms. However, several tropical and subtropical regions (e.g., Indonesia) face much larger relative losses, exceeding 40–50% of their baseline GDP under more severe scenarios (e.g., RCP7.0). Meanwhile, certain high-latitude and generally wealthier countries (e.g., parts of Northern Europe) experience net gains or minimal losses. Notably, when simulating climate change impacts through labor productivity damages alone, we observe an effect not captured by direct damages: labor productivity loss is always a loss, yet some Northern European countries exhibit slight GDP gains. Since the labor productivity function produces only losses, these gains must arise from trade interactions, specifically shifts in production and market share away from more severely affected regions. This type of adjustment would not occur without the propagation mechanisms embedded in the CGE framework. The regional disparities are further exacerbated by the sectoral composition of each economy; the most affected countries are often more dependent on primary sectors, while less affected countries tend to have service-based economies. Moreover, we show that the gap in regional effects increases as the global temperature increases. Conversely, our results emphasize that stronger mitigation policies substantially diminish these geographic imbalances: both total global damages and relative regional losses are markedly reduced under lower-emissions scenarios.

When aggregating country and regional damage data into global GDP losses, the information on disparities (unsurprisingly) disappears. As an example, we demonstrate that a roughly 2°C temperature increase results in a global GDP decrease of 5% . Under this global scenario, Indonesia could observe a relative GDP decrease of over 13%, whereas Sweden could gain a relative GDP increase of 2%. Moreover, we show that the population-weighted global loss aggregate is double the GDP-weighted counterpart. While the latter is commonly used in global assessments (e.g., in damage functions in IAMs) because it represents overall economic impacts, the former better captures the relative burden on the global population. Finally, we show that across all emissions scenarios, labor productivity losses alone account for about half of the total globally-aggregated GDP decline. However, this share varies significantly by region, further reinforcing the value of more granular analyses.

Despite these limitations, a globally aggregated perspective is necessary for evaluations in globally aggregated IAMs, as they observe the world as a single unit. In the final article, we adopt such an aggregate approach to address the more foundational question of how

to apply a unified decision-making framework that reconciles the target-based and trade-off-based strategies, which are central to global climate policy discourse.

5.3 Paper 3

Cost–Risk Analysis (CRA) was initially proposed by Schmidt et al. [42]. This decision-making tool is distinguished by the fact it is the only tool enabling commitments to climate targets in the evaluation of climate policies, while also accounting for the possibility of resolving climate sensitivity uncertainty through anticipated future learning. CRA thereby addresses key limitations of the target-based Cost-Effectiveness Analysis (CEA) framework. Whereas CEA is dynamically inconsistent under deep uncertainty, CRA introduces a guardrail principle into the utility maximization framework, via a calibrated risk function that captures the decision-maker's aversion to exceeding the temperature target. At the same time, the CRA approach also addresses limitations of Cost-Benefit Analysis (CBA). In particular, CBA is characterized by very strong assumptions about the completeness of climate impact knowledge and clear trade-off analysis between future impacts and current mitigation costs. By contrast, CRA interprets preferences as the result of negotiation and valuation based on multiple lines of evidence [126, 164]. In its current form, CRA assumes complete ignorance about quantification of climate damages, aligning philosophically with the precautionary principle underlying the formulation of climate targets. However, it is reasonable to expect that, over time, the scientific method will progressively yield a clearer understanding about climate damages (e.g. [181, 182]). To address this possibility, Held introduced a new framework that would allow CRA to incorporate new knowledge alongside incomplete knowledge about impacts, by retaining the (reduced-weight) risk function to represent what is still unknown or unrepresented about damages [52]. In the third article, we build on this work by considering one potential application of this new modified framework, which we call Cost-Benefit-Risk Analysis (CBRA).

The final article of this thesis offers three distinct contributions. First, it introduces a tailored uncertainty framework within the FaIR climate emulator by condensing the full uncertainty space of climate response parameters into a single uncertain variable: equilibrium climate sensitivity (ECS). This modified version of FaIR is then integrated into the Model of Investment and Technological Development (MIND), a globally aggregated,

Ramsey-type integrated assessment model (IAM). Second, and building on the second article, we introduce what is, to our knowledge, the first global damage function derived from a forward-looking computable general equilibrium (CGE) model. We explicitly interpret this damage function as partial, reflecting the inclusion of only three impact channels (labor productivity, agriculture and human health). Third, by incorporating this incomplete damage function into MIND, where it directly influences total economic output, we present what we believe to be the first operationalization of CBRA. This modified CRA framework bridges the gap between quantified economic losses and the residual uncertainties inherent in climate impact assessments, acknowledging that precaution remains necessary in light of incomplete knowledge about climate damages. We now turn to examine each of these three contributions in the third article in more detail, before considering possibilities for future research.

The first contribution builds on the work presented in the first article. Recall that there we showed the climate module previously used in the MIND model and in earlier CRA analyses [46, 47, 72] does not adhere to the carbon budget approach. This is because it fails to allow the temperature response to reach the relaxation phase following an emission pulse. To enhance the robustness of our analysis and those of future MIND users, we replaced this module with FaIR 2 [1].

To make FaIR suitable for decision-making under uncertainty, we modified the model to treat equilibrium climate sensitivity (ECS) as an uncertain parameter. This approach is consistent with CRA studies that explore learning about ECS as a reduced-form representation of broader climate system uncertainty. It also constitutes a novel way of representing uncertainty within the FaIR framework. Specifically, we parameterized ECS using a log-normal distribution calibrated to constrained estimates from Leach et al. [1], and expressed transient climate response (TCR) [1] as a function of ECS, following Nijsse et al. [173]. In line with the derivation of FaIR's standard parameterizations [1], we then made two of the model's response coefficients dependent on ECS. To ensure comparability with previous studies (e.g. [72]), we discretized the ECS distribution into 20 intervals, each representing 5 percent of the probability mass, and used the midpoints of these intervals as representative ECS values, that is, 20 discrete states of the world. This simplified, single-parameter uncertainty scheme significantly reduces the computational cost and simplifies the model implementation, compared to sampling the full FaIR parameter

[1] TCR is not the same as TCRE.

space, as conducted by Smith et al. [102]. At the same time, it closely reproduces the temperature response of more complex climate models. For example, it differs by only 2.5 percentile points across the full uncertainty distribution in the abrupt 4xCO_2 experiment, as reported by Leach et al.[1]. Finally, we note that these modifications to FaIR are not limited to the MIND model or to CRA applications. They could be readily adopted in other integrated assessment or optimization models where a simple and computationally efficient representation of climate uncertainty is required.

The second contribution expands upon the literature on global damage function derivations for IAMs, drawing on estimates from CGE models. We improve upon previous studies employing CGEs (e.g. [89, 183]), which typically rely on static or recursive temporal dynamics and estimate damage functions by varying temperature in a single reference year. By contrast, in this study we employ a forward-looking CGE model (GTAP 2) to derive damage functions. We do this by first running the model under different emissions scenarios to simulate annual GDP impacts over time. We then approximate transient GDP losses across each year in the simulation and match these annual GDP changes to the corresponding annual temperature levels. This process yields a time-consistent relationship between temperature and GDP loss, which we use to construct the damage function. This ensures temporal consistency between the derived damage functions and the forward-looking intertemporal optimization structure of IAMs used to generate optimal climate policies. Following established practice in the IAM literature [27, 101], we incorporate the resulting (partial) damage function into the MIND model by directly reducing total global production. We consider such CGE-based approaches superior to bottom-up methods that aggregate only direct impacts without capturing broader economic feedback effects, as discussed above. Simply put, if IAMs simulate production as a total economy aggregate, then model damage functions should also aggregate both direct and indirect effects on the economy. However, one of our interesting findings is that the damage function derived from CGEs is not solely temperature dependent, but varies with the underlying emissions scenario. This calls into question the traditional IAM representation of damage as solely a function of temperature. We merely highlight this important finding here without further discussion, leaving it open for more detailed consideration and future research.

The third contribution is the first-ever, to our knowledge, construction and operationalization of CBRA. Incorporating the above-mentioned improvements in MIND, the

results of this article, as a pioneering application of CBRA, can be separated into two categories. First, we conduct a sensitivity analysis on the reduced weight of the risk function in response to the incorporation of (partial) damages. This is motivated by the unresolved question of what share of the socio-economic consequences, which originally warranted the precautionary approach, is now explicitly represented in our damage function. We varied the weight of the risk function between 0 and 1. A weight of 0 assumes that the damage function fully captures all relevant climate impacts, effectively reverting the framework to a full-fledged CBA. A weight of 1 preserves the original CRA structure, where the risk function reflects all uncertainty, and the damage function simply adds an additional incentive for mitigation. By varying the weight in this way, we show that the risk of exceeding the temperature guardrail continues to impose a stronger constraint on emissions than the partial damage function alone.In particular, if the weighting is reduced from 1 to 0.3 (a 70% reduction in the risk component), the resulting increase in recommended optimal cumulative emissions is less than half the additional increase observed when reducing the weight further from 0.3 to 0. This asymmetry highlights that even when the guardrail is considered with reduced weight, it continues to act as a strong driver of mitigation. Notwithstanding this result, we find that uncertainty in climate sensitivity is a more significant driver of variation in projected temperatures, far outweighing the influence of uncertainty in the relative contributions of risk and damages.

The second category of the third contribution lays down a framework which reinterprets CBRA as a bridge between the target-based approaches embodied in CEA and the trade-off approaches embodied in CBA. The precautionary principle underpins the use of temperature targets in climate policy. In this context, CBRA enables us to extract the explicit quantification of damages that was implicitly assumed by a precautionary-motivated decision-maker when the target was originally defined. Moreover, if the damage function is indeed an incomplete picture of total impacts, we showed that, through the proper calibration procedure, one can quantify what proportion of the unknown risks embodied in the agreed-upon temperature target has been covered by the (partial) damage function. In the first step of this bridge, we showed that when calibrated to reflect the preferences of climate policymakers under a binding temperature target, CRA produces effectively identical policy recommendations as CEA (the maximum deviation briefly peaks at about 1% of total emissions). This result numerically confirms the theoretical proof provided by

Held [73]. As such, CRA can now be considered firmly established as a viable decision-making framework: consistent with the target-based approach, yet grounded in a utility maximization framework.

Moving to the next step in the bridge, we use the same calibration procedure in CBRA as described above. This procedure matches the preferences of a precautionary-motivated decision-maker consistent with the temperature target. Under this calibration, the weight on the risk function is reduced to 0.42. The resulting emissions pathway deviates only slightly from the CRA and CEA counterparts, peaking at a 10 percent difference in emissions, which declines over time, and a temporary temperature difference of just under 2 percent. All other model components remain fixed, allowing for direct comparison across the three approaches. We interpret this result as showing that our partial damage function, quantified from impacts on labor productivity, agriculture, and human health, accounts for approximately 58 percent of the initially perceived risk embodied in the temperature target. In other words, CBRA enables us to assess how much of the impact uncertainty that originally motivated the precautionary use of a strict temperature target is now explicitly captured through quantified damages.

Finally, we went a step further and brought CBRA back to a fully-fledged CBA by setting the risk function weight to zero. We find that, by using the same calibration technique and assuming a simple quadratic form for the damage function, one can approximate the level of damages implicitly assumed by policymakers and scientists when defining the global temperature goal. When compared to several recent damage functions as benchmarks [28, 133], our calibrated function yields lower damage estimates. This raises an inevitable rhetorical question: was the international community cautious enough in adopting the global temperature targets?

5.4 Outlook

In the context of carbon budget research, we have presented a pulse response framework that can be straightforwardly applied to different climate models. If a model satisfies the condition of scenario-independency (either through the shape of its pulse response or by direct test using an optimization program), then the generation of pulse dynamics under varying climatic conditions can reveal non-linearities in the corresponding model's

carbon budget equation. In this regard, the next promising candidate is the Model for the Assessment of Greenhouse Gas Induced Climate Change (MAGICC) [184]. This is because MAGICC provides detailed information about carbon cycle processes, yet remains relatively simple. By examining its pulse response under different parameterizations, future research could improve our understanding of the carbon cycle processes that drive non-linear behaviour.

When it comes to labor productivity loss assessments, we noted that the current empirical studies suggest that the work ability (negatively) changes only with higher WBGTs. Intuitively, one could imagine that work ability also drops with very low temperatures. If this possibility was also included in future analyses, this could provide even more regional disparities between the colder, higher latitudes and the hotter, humid (sub)tropics. Moreover, another natural step could be to repeat the labor productivity loss assessment following the same methodology as in the second article. However, future research could include a suite of models and their mean climate values, instead of one model and its full ensemble. In addition, one could use a much higher model resolution to test how (and if) it affects the outcomes.

In the context of future CBRA applications, numerous avenues remain to be explored, as this study represents only the first implementation of the approach. In climate mitigation research, it would be interesting to examine how both the CBRA and CRA frameworks incorporate compliance with emissions targets (i.e., net-zero targets), instead of temperature targets. If the carbon budget relationship holds, does this also imply an equivalence between temperature-based and emissions-based targets?

To date, both CRA and CBRA have been applied exclusively in climate mitigation studies. However, given their general mathematical structure, these frameworks could be readily applied in other fields of economics and, more broadly, in decision-making under uncertainty. In these ways, future research could establish CRA alongside more traditional decision-making approaches.

Chapter 6

Conclusion

Anthropogenic climate change compels trade-offs between near-term mitigation costs and uncertain, potentially severe long-term damages from rising temperatures. The established decision-making framework for generating a rational mitigation policy is cost-benefit analysis (CBA), a trade-off based method founded on expected utility maximization. However, it relies on an unmet assumption of complete knowledge of future climate impacts and their socio-economic damages. An alternative, Cost-Effectiveness Analysis (CEA) offers a framework for identifying the least-cost mitigation pathway consistent with global temperature targets, reflecting a precautionary response to deep uncertainty about the future socio-economic impacts of climate change. Yet, when the possibility of future learning events is introduced, CEA becomes dynamically inconsistent. Therefore, Schmidt et al. (2011) introduced Cost-Risk Analysis (CRA) to overcome this limitation by embedding the temperature target within the utility maximization framework, using a risk function that imposes a utility penalty for target exceedance. Nonetheless, given the ongoing progression of climate impact research, the rationale for strictly target-oriented approaches is called into question. To accommodate this, Held (2024) proposed a modification of CRA that enables the consistent integration of matured impact modeling components. This thesis provides a pioneering operationalization of the modified CRA, hereby named Cost-Benefit-Risk Analysis (CBRA), interpreted as a bridging framework between strictly target-based approaches (from CEA to CRA) and fully trade-off-based CBA. In doing so, it also advances two foundational components of climate economics—climate modeling and climate impact assessment—both of which serve as essential building blocks in the construction of CBRA.

Paper 1 establishes a fundamental condition from climate physics under which CEA and CRA are expected to yield equivalent policy recommendations, thereby providing a necessary basis that legitimizes CRA as a dynamically consistent extension of CEA within target-based frameworks. Held (2019) proposed a theorem that under the condition that the cumulative emissions directly translate to the temperature increase (i.e., carbon budget approach), that CEA and CRA provide equivalent results. Using the FaIR 2 climate emulator in an optimization program that tests the boundaries of the carbon budget assumption, Paper 1 confirms the robustness of the carbon budget approach, contributing a novel method that examines the full portfolio of scenarios that could lead to potential deviations. Moreover, it shows that if a temperature response to an emission pulse is interpreted as a Green's function, it can mimic the deviations posed by the full model. In addition, the results demonstrate that the equational form of the carbon budget approach—and the degree of its nonlinearity—can be derived by examining how the pulse response changes under different climatic conditions, offering a novel method for deriving the carbon budget equation.

Having established that FaIR 2 adheres to the carbon budget approach, Paper 3 introduces a modified version of FaIR 2 with a simplified uncertainty scheme that captures the full parameter uncertainty space to a high precision (2.5 percentile) through a single uncertain variable: climate sensitivity. This modification not only enables the implementation of FaIR 2 for direct intercomparison between decision-making frameworks, but also offers the broader community a computationally tractable tool for probabilistic analysis under climate uncertainty. By replacing the previous climate module in MIND (which does not adhere to the carbon budget approach, as shown in Paper 1) with FaIR, we numerically confirm the result proposed by Held (2019), demonstrating that CEA and CRA yield equivalent policy recommendations, and hence, establishing CRA as a legitimate, dynamically consistent extension of CEA.

With the first bridge established between CEA and CRA, Paper 2 lays the groundwork for CBRA by addressing climate impact quantification, an essential step in extending CRA toward CBA. The analysis is structured around two stages of climate-economic impacts: sectoral disruptions and their transmission into GDP based economic damages. Using Earth System Model climate data, combined with the population data and the empirical relationships that connect climate indices with ability to work, we calculated the country-level labor productivity loss related to the increasing heat-stress. This impact, together

with two others from recent literature—agricultural yield losses and mortality changes—is implemented in GTAP-INT 2, a regionally and sectorally disaggregated forward-looking computable general equilibrium (CGE), and applied across several temperature pathways to assess resulting economic damages. The results show large regional disparities in the GDP losses, while also allowing aggregation to global GDP loss estimates.

Building on these findings, Paper 3 develops what is, to our knowledge, the first forward-looking CGE-derived damage function aligned with the intertemporal optimization framework that underpins IAMs. Moreover, the segmented structure and transparency of the included impacts make it possible to explicitly identify and quantify a partial damage function—one that reflects only well-understood impacts and thus serves as a tractable input for CBRA.

Finally, Paper 3 provides the first operationalization of CBRA. It explores two distinct approaches for identifying the extent to which the explicitly quantified impacts, captured in the form of a partial damage function, account for the unknown risks embedded in the risk function. In the sensitivity approach, by varying the weighting parameter of the risk function, we show that the risk constraint imposes a stronger limitation on allowable emissions than the partial damage function. Moreover, the results indicate that uncertainty in the climate response has a greater influence on temperature outcomes than uncertainty in climate damages. In the second, calibration approach, we calibrate CBRA to adhere to the climate target with the same probability as CRA and CEA counterparts. This lowers the weighting parameter and allows us to quantify exactly how much of the initially perceived unknown risks embodied in a temperature target is covered by the partial damage function. Put differently, it enables one to determine what fraction of the guardrail-type uncertainty or "unknown risk" has been replaced by explicit, data-driven damage estimates.

To conclude, this thesis, while centered on the development of CBRA, addresses three pivotal facets of climate economics: how cumulative greenhouse gas emissions drive global temperature rise, how physical climate responses translate into economic damages, and how precautionary targets can be systematically integrated with cost-benefit reasoning.

Appendix: GTAP-INT 2 description and model setup

A.1 GTAP-INT 2 overview

A.1.1 Why GTAP INT-2?

Global Trade Analysis Project (GTAP) model is a multiregional, multisectorial, computational general equilibrium (CGE) model [3]. In short, CGEs are designed to represent the global economy by simulating value flows (in monetary terms) among domestic and foreign agents, including households, private firms, and governments. The economic effects of climate change are modeled as an output change between a counterfactual baseline scenario and a scenario where sectors are modified by preassembled damage functions (shocks) that affect the specific component in response to the temperature increase.

The temporal dynamics in CGE models can be either static or dynamic. In the static setup [3], the shocks are introduced in a single baseline year, with the resulting effects of the shock being a new equilibrium within the same timestep. Hence, the main issue with the static approach is that it cannot analyze how pathways evolve over time. In contrast, dynamic models capture the temporal evolution of shocks, which can be addressed using either a recursive or an intertemporal (forward-looking) approach. Recursive dynamic models, often preferred for their lower computational requirements and greater numerical tractability, solve the model sequentially for each time step. Each period is treated as a separate static equilibrium, with information communicated intratemporally between neighboring time steps through linking variables such as savings and investment [141].

A systematic review conducted in 2023 [142] highlights that recursive models are by far the most commonly used temporal dynamics model setups in climate policy analyses, with static models ranking second. While the recursive setup represents an improvement over the static counterpart for long-term policy evaluation, it applies deviations from the baseline as shocks to exogenous variables only at the current time step, with no influence from future shocks on present agent behavior. This assumes fully myopic agents who fail to anticipate future climate change—a simplification that, in our view, contradicts reality. This is especially problematic in the context of climate change impacts research, as it assumes that actors will have no access to the very knowledge produced to inform their decisions. Ignoring this undermines the relevance of such analyses in this field, creating a disconnect between research and actionable policy-making.

In contrast to the recursive approach, the forward-looking intertemporal model solves for all time steps simultaneously, optimizing decisions across the entire time horizon while accounting for all future shocks. This approach enables forward-looking agents with perfect foresight but comes at a significantly higher computational cost.

The CGE used in this analysis, GTAP-INT 2, is a forward-looking intertemporal model that builds on the static GTAP through series of technical modifications, introduced sequentially in [96, 97]. In the remainder of this appendix, GTAP-INT 2 is introduced in broad terms only, starting from the original GTAP framework and then highlighting the forward-looking modifications. The full set of equations that constitute the model is exhaustive and can be found elsewhere (in the original literature).

A.1.2 Structure of GTAP

The GTAP model is a global model of the world economy, where each region and its economic activity flow between the associated agents is illustrated in Figure A.1.

The main building block of GTAP is a regional household associated with each region covered by the model setup. The functioning of GTAP can be understood by zooming in one such regional household, while treating all of the other regions (and their households) under collectively as the “Rest of the world”. Each of these other regions operates according to the same structure, with an identical household structure and associated economic activities. Hence, we can understand the whole GTAP if we understand one

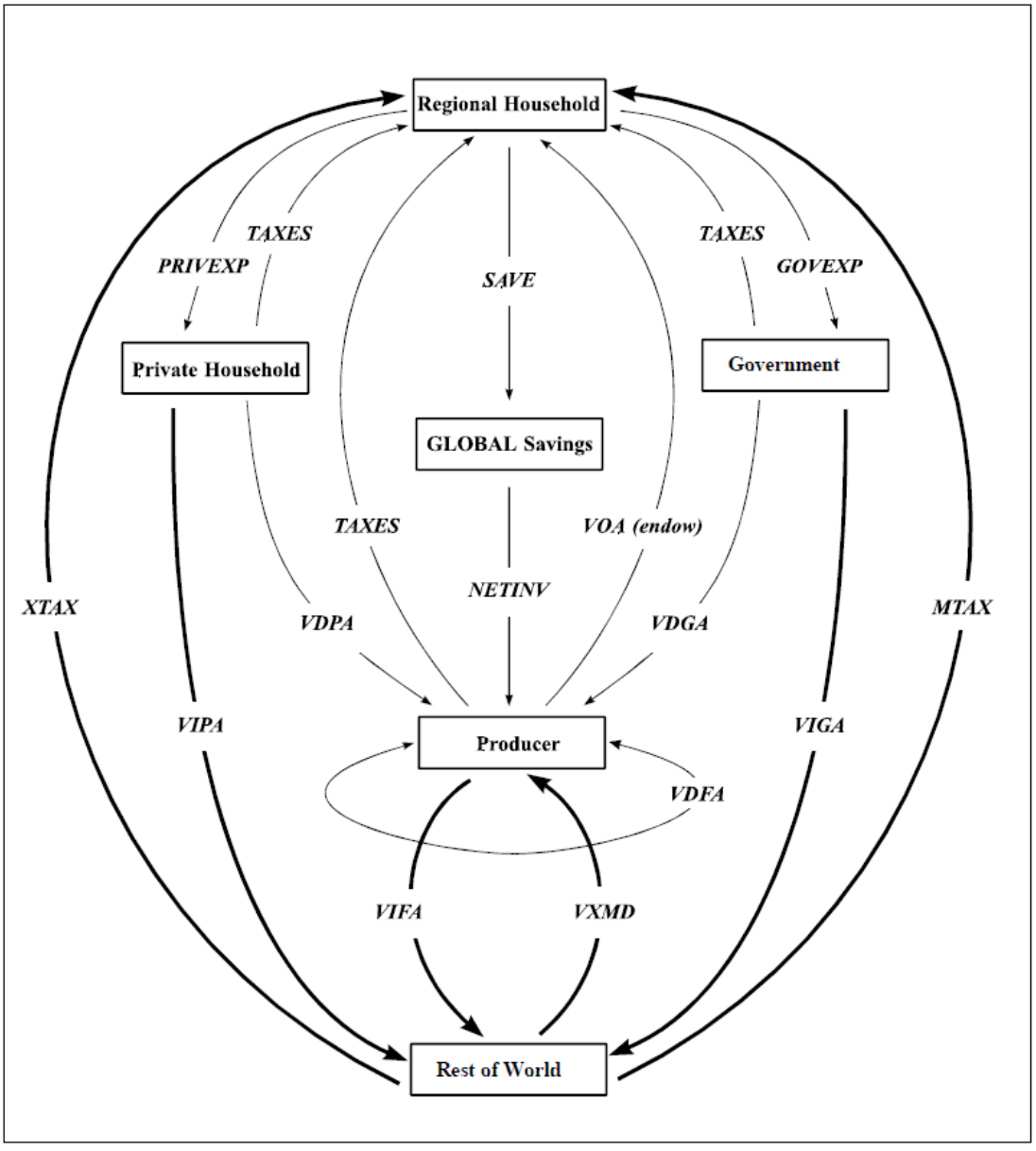

FIGURE A.1: A schematic representation of the GTAP model. The diagram illustrates the structure of economic flows for a single region, with the rest of the world represented as an aggregate external region. Taken from Brockmeier (2001) [2].

regional household, consisting of private household, government and the domestic producers (hereby called firms), further called "agents", and the interconnections between them. Two global agents are missing in the figure, the global transport sector and the world bank, introduced later in the appendix, as they play a crucial role in linking regions and, in the case of the world bank, in the intertemporal features of GTAP – INT 2.

The starting point of the model's value flow can be the regional household's income (arbitrary choice just for demonstration purposes). This income comes from selling regional endowments. These are the primary factors of production that firms can buy only domestically, typically distinguished between perfectly mobile ones (such as labor and capital), and sluggish ones (such as land). Additional income to the regional household comes from taxes on trade flows with other regions, including export taxes (XTAX) and import taxes (MTAX).

The regional income is allocated across three compartments dictated by private (PRIVEXP), government (GOVEXP), and saving (SAVE) expenditure (demand). The private household and government spend the allocated income to consume goods and services, with their corresponding demands VDPA and VDGA. Both agents pay TAXES, so their expenditures are net values of the income allocations, while at the same time these taxes are allocated to the total pot of regional disposable income.

Moving to the firms, they receive payments from private and government households from product consumption (VDPA, VDGA), as well as from the demand of other firms for intermediate goods (VDFA) used as the input in the production tree (Section A.1.3). Investments into firms come indirectly from regional households through the global savings sector which pools the investments from all regions into one pot, and redistributes it back to the regional firms (NETINV). Firms sell their products both in the domestic and the foreign markets. In the figure, imports (VIFA) and exports (VXMD) represent the flow of intermediate goods between the regional and foreign firms.

Equilibrium in GTAP is maintained through four main sets of conditions. First, market-clearing equations ensure that for every good and (primary) factor, total demand matches total supply. Second, zero-profit conditions guarantee that firms' output prices cover their costs without leaving excess profits. A third set links the different price concepts, connecting market prices with import, export, and purchasers (agents) prices. Finally, the regional income–expenditure identity makes sure that disposable income is fully

allocated across private consumption, government spending, and savings. Each equation type is accompanied by a slack variable that allows for partial equilibrium settings, and exploring the problems where we exogenously fix certain variables (different closures) and hence deviate from the perfect market setting. Taken together with the basic (but extensive) accounting identities, these conditions keep the circular flow of income consistent; simply put, all income earned in production is exactly matched by expenditure, taxes, and savings. While these equations taken together ensure consistency, they don't model the behavior of the system which dictates the choice of economic activities. The behavioral content comes from corresponding demand structures introduced in later sections, both for firms and households separately.

GTAP solves the whole system in percentage-change (linearized) form, with lowercase variables denoting proportional changes around the benchmark. This linearization allows large shocks to be applied gradually via decomposition methods (Euler's and Gragg's approaches [185]). Hence, the shocks to the model (in this work, the sectoral temperature change impacts) are also introduced as percentage changes.

A.1.3 Firm behavior in GTAP

Figure A.2 illustrates the "Technology Tree", a schematic representation of the production structure in GTAP. It displays the assumed nested technology under which firms operate in the model. The production technologies in GTAP are assumed to be separable and exhibit constant returns to scale. Within each nest, inputs are combined according to a constant elasticity of substitution (CES) function. While this assumption makes the model tractable, it can also be seen as restrictive, since it rules out increasing returns or scale effects that might be relevant in real-world production. Each industry can be conceptualized in this way, with the tree branching into its constituent inputs as shown in the figure.

On the top of the tree sits the sectoral output of the firm qo(j,s). The output is produced combining two aggregates: the bundle of value-added (i.e., primary factor or endowment) and intermediate inputs. At this highest level, the model does not apply the usual CES specification but instead uses a Leontief function, which requires these two bundles to be combined in fixed proportions (not allowing substitution). This means that

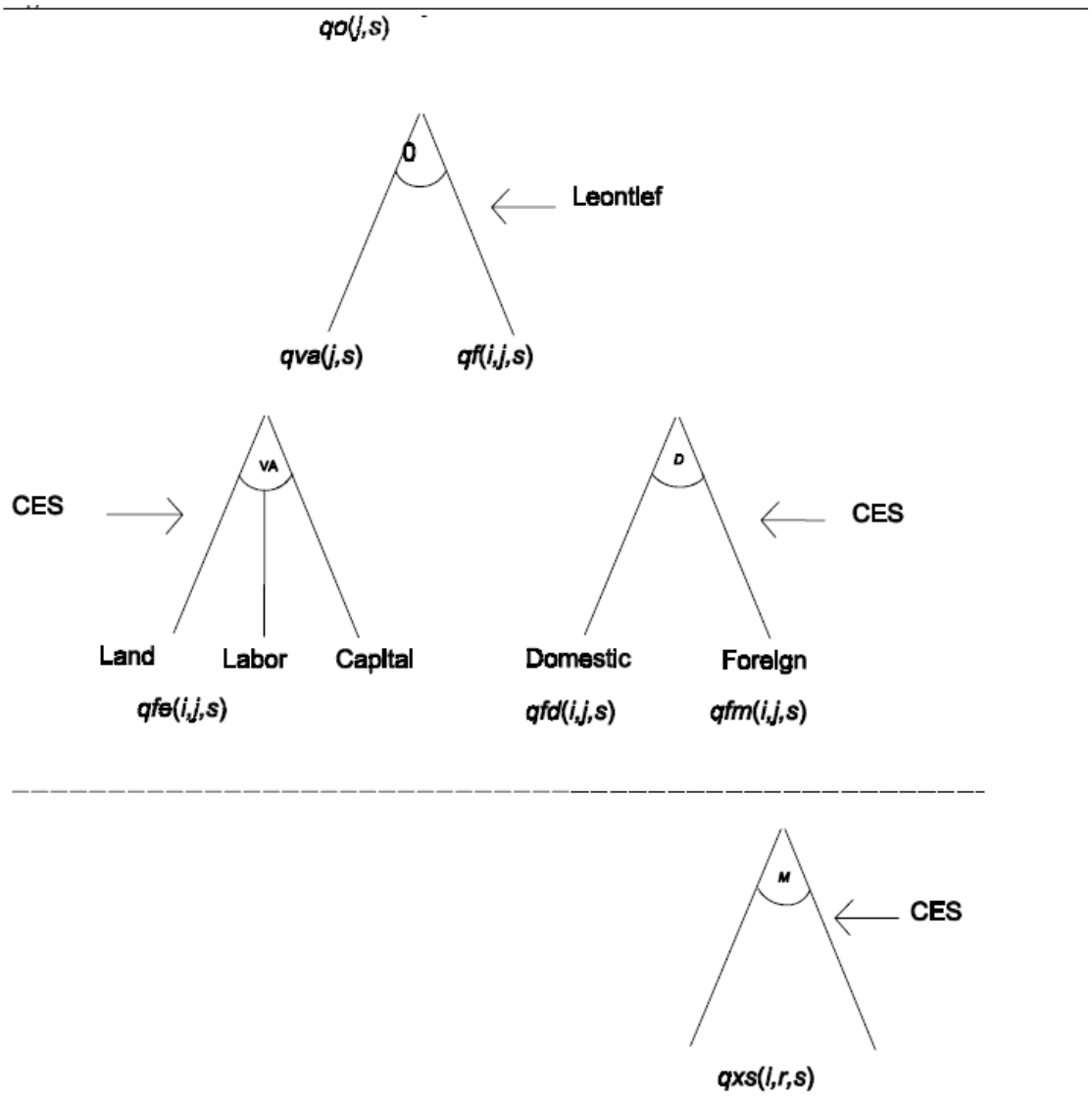

FIGURE A.2: A schematic representation of production structure in GTAP. Taken from Hertel (1997) [3].

the overall ratio of value-added to intermediates is fixed and cannot adjust in response to changes in relative prices.

Below the top nest, firms have more flexibility in the input choice. The value-added bundle is composed of primary factors (endowments): land, labor, and capital. The substitution is possible according to the CES function. In practice, this means that the demand for each factor depends only on how its price compares to the others. For example, if labor productivity falls, the firm can substitute capital for labor to maintain the same

level of output. Parallel to value-added, the intermediate-input bundle is a CES mix of domestic and imported tradeable commodities. These are themselves the outputs of other firms, but in this context they appear as inputs into the production of the final good. Furthermore, imported goods are distinguished by their country of origin and combined through the Armington CES specification. In this setup, otherwise identical commodities are treated as imperfect substitutes depending on their source, so the effective price of an imported good reflects not only the world market price but also the specific origin of supply.

The nested structure of the technology tree implies that firms' choice of production factor mix is separable across the bundles. In practice, this means that the mix of endowments is determined independently of the prices of intermediate inputs. With the additional assumption of constant returns to scale, the absolute level of output is also irrelevant. As a result, only the relative prices of endowments enter the demand equations for the components of the value-added bundle. The same logic of separability applies on the intermediate side, and both for domestic and imported goods separately.

The mathematical representation of the firm behavior is summarized in Tables 2.10. and 2.11 of Hertel (1997) [3]. For each nest in the production structure, there are two types of equations.

The first one determines the unit cost of the composite good produced in that nest. It is built on the net-zero profit condition, which ensures the sum of input and output prices to be equal. The composite good price in one nest enters a higher one to determine the demand. At the top (final output) level, total net-zero profit condition introduces a slack variable. This variable is set to zero by default, but it preserves model consistency if an output price is fixed exogenously. In such a case, the slack absorbs the gap between the fixed price and non-fixed unit cost of production, allowing the model to remain solvable. This option can be used to represent a partially regulated or policy-driven sector, though the closure which is used in this study retains the standard competitive specification.

The second type of equations specifies the conditional demand for inputs within each nest, derived from the CES form of the production function. In general, the demand for an input in the CES composite takes the form: $q_i = +q + \sigma(p - p_i)$, which holds for any number of inputs in the composite. Here, q_i and p_i are percentage changes in quantity and price of input i, q and p the percentage changes for the composite good (the

output of the nest). The good i's demand is dictated by two mechanisms. First, due to constant returns to scale, when the demand for the composite good rises, demand for each good i rises equiproportionally (expansion effect). Secondly, if the input's i price goes up relative to the composite price, demand for i shrinks, while it increases for others, dictated by σ (substitution effect). The elasticity of substitution σ is calibrated from the real-world data. Note, that in the top-level nest (the demand between the value added and intermediate), the conditional demand equation drops out, leaving only the expansion effect.

A.1.4 Household behavior in GTAP

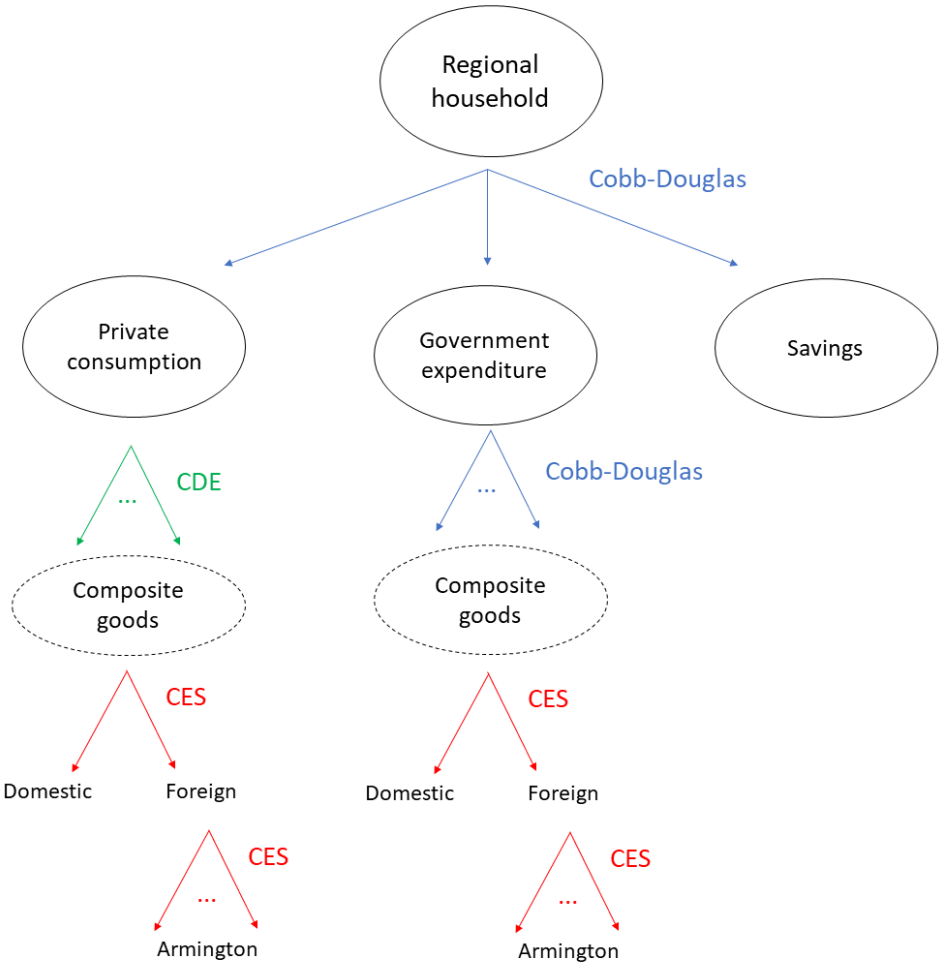

FIGURE A.3: A schematic representation of the regional household expenditure structure in GTAP.

Figure A.3 illustrates an "Expenditure Tree", a schematic representation of the income flow of the regional household in GTAP, providing the households' demand structure (the analogue of the firm's technology tree). As discussed in Section A.1.2, a regional household is represented as a single representative agent (distinct from the firm/producer), which receives primary factor incomes and tax revenues. The income is allocated across three top-level categories: private consumption, government consumption, and savings. Preferences over these categories are formalised through an aggregate (Cobb-Douglas) utility function. Nota bene, since the standard GTAP model is static, the savings were tweaked following the approach of Howe (1975) [186]. The savings in this context are not actual accumulations of wealth but rather a modelling device that mimics the expenditure pattern of an intertemporal optimisation problem within a static framework (see [3] for details). Moreover, the mathematical structure of the expenditure tree is analogous to its firm-side counterpart: at each nest two equations govern the demand flow, namely the budget constraint (analogous to the zero-profit condition for firms) and the conditional demand equations.

At the top of the expenditure tree, the income is disposed across the three top-level categories according to the Cobb-Douglas (per capita) utility conditional demand. That means that income flows are partitioned into constant shares of total income across the categories (private, government, savings), implying a fixed budget share. The changes in expenditures on savings and government activities are a function of regional income and prices (budget constraint). Moreover, slack variables are included that allow either savings or government utility to be exogenised (swapped with slacks), in which case the budget constraint ensures that private household expenditure adjusts residually. Hence, the top nest guarantees that the household's total income is fully allocated, while providing closure flexibility through the slack variables to treat either savings or government demand as exogenous.

Government branch. Once the government's aggregate expenditure is specified, GTAP first constructs a composite price index for government purchases. This index can be thought of as the "average price" of one unit of government demand, based on the mix of commodities it buys. Multiplying this index by the chosen real level of government demand gives the total nominal expenditure. GTAP then allocates this spending across commodities, according to the Cobb-Douglas substitution scheme. Once the demand for each commodity has been established, the remainder of the government's tree branching

is analogous to that of the firms. Each commodity composite is split into domestic vs. imported components with the usual Armington structure, and imported demand is further allocated across source regions. The associated price-link equations ensure consistency between import prices (CIF) and export prices (FOB) when goods cross borders. Importantly, Armington substitution parameters are commodity-specific but common across the agents: what distinguishes the agent's demand of the imported goods are their associated benchmark import shares.

The private household demand system differs from others due to its nonhomothetic nature. In Cobb-Douglas or CES systems (homothetic) the demand for all goods scales proportionally with income. On the contrary, nonhomothetic elasticity embodied in the Constant Difference of Elasticities (CDE) demand system allows budget shares to vary with income. As an example, poorer households devote a large share of their income to necessities such as food, while richer households spend proportionally less on these items, even as their absolute consumption may rise. The CDE system is calibrated in GTAP to match observed own-price and income elasticities. Private utility is defined on a per-capita basis, so the utility index measures welfare changes per person in each region and thereby accounts for the population dynamics (unlike other agents). Once the CDE system has determined the allocation of spending across commodity composites, the structure mirrors that of other agents (government and firms).

A.1.5 Investments, world bank and global transport

In a static CGE model like GTAP [3], investment is not determined intertemporally (as discussed above), so it does not accumulate into the capital stock that could be later used to expand the future productive capacity. Hence, there is a closure problem: how to reconcile savings, investment, and the current account (trade balance plus international transfer receipts). Hertel (1997) explains that GTAP users can choose alternative "macroeconomic closures", whereby they can fix either savings or investment, with the others adjusting accordingly. The default closure is that global savings equals global investment, with regional trade balances fixed, and private consumption adjusting residually. The fictional global institution "world bank" ensures that regional savings are collected into a global pool and reallocated as investment demand across regions. While the treatment of fixed

capital formation and the allocation of investment across regions in a static model is documented Hertel (1997) [3], these mechanisms do not carry over to GTAP-INT 2, where they are embedded directly in the intertemporal optimisation problem. The key shifts from static accounting devices towards forward-looking dynamics that constitute GTAP-INT 2 will be discussed in detail in the following section.

Before moving on, we close this section with a look at the global transportation sector, which has the same structure in both the static and intertemporal versions of GTAP. Together with the "world bank," it is one of the two global (non-regional) sectors. It fills the gap between the supply and demand for international transport services: on the demand side, this appears as the difference between CIF and FOB values on traded goods, while on the supply side, the services originate from all regions and are pooled together through a Cobb–Douglas setup. These services are produced within regional economies by regional firms. The global transport sector is an accounting device that aggregates these regional contributions into a single composite international transport good. Since there are no reliable data linking exports of transport services to specific shipping routes, GTAP combines these contributions into a single composite international transport commodity. The transport sector uses only intermediate inputs (such as fuel) and no primary factors. The global bundle of transport services is then distributed across bilateral trade flows in proportion to their value, thereby accounting for the trade margins that reconcile export (Free on Board, FOB) and import (Cost, Insurance, and Freight, CIF) prices. In each bilateral flow, the importing region bears the cost of the margin.

A.1.6 Forward-looking firms

In GTAP-INT 2, the firm's forward-looking, intertemporal behavior is modeled the same as in GTAP–INT. The behavior fundamentally differs from the static version in terms of how investment behavior is modeled. Instead of treating investment as a static residual (standard GTAP closure), firms in each region maximize long run investments, and all individual capital stocks are treated as variables: $\max_{I_{r,t}} \int_0^\infty \left[P^K_{r,t} K_{r,t} - TI_{r,t} P^I_{r,t}\right] e^{-\int_0^t [R_s - g_s]\, ds}\, dt$, subject to capital accumulation equation $\dot{K}_{r,t} = I_{r,t} - [\delta_{r,t} + g_t] K_{r,t}$, where $P^K_{r,t}$ and $K_{r,t}$ are the rental price of capital and a capital stock of region r at timestep t; $TI_{r,t}$, $I_{r,t}$ and $P^I_{r,t}$ are total investment expenditure, capital increment (from investment activities) and price of investment; R_t is the global interest rate, and g_t and $\delta_{r,t}$ are long run growth rate

and depreciation rate. The setup is very standard in the intertemporal growth theory: the objective function maximizes the present value of profits (capital rents – total investment costs), with the exponential discounting at the world interest rate corrected for growth (Ramsey condition: interest rate = preference rate + growth of consumption). An additional assumption in this setup is the convex adjustment function in investment increment (more than 1 unit of investment is necessary for 1 unit of capital increase), reflecting installation frictions, learning costs, or limits to scaling capacity $TI_{r,t} = I_{r,t}\left[1 + \frac{\phi_{r,t} I_{r,t}}{2K_{r,t}}\right]$, where $\phi_{r,t}$ is (positive) adjustment cost coefficient.

The solution to this optimization problem with a Hamiltonian yields a system of motion equations that are embedded in the model, one is the aforementioned capital accumulation equation, and the other describes how the shadow price of capital (the Lagrangian multiplier of the Hamiltonian) evolves over time. The convex adjustment cost ensures a smooth accumulation. This system can be solved numerically by imposing two terminal conditions. We assume that the model reaches a steady state sufficiently far in the future such that (i) the capital stocks are constant (net investment equals depreciation) and (ii) the shadow value of capital is constant (return on capital converges to discount rate adjusted for depreciation). In this way, GTAP-INT 2 explicitly incorporates the intertemporal behavior of firms.

Finally, to make the model operational, an appropriate baseline scenario is required. In static and recursive setups, the GTAP database can serve as a baseline, since each period is solved independently and sequentially (in the recursive case). In contrast, the intertemporal models require the entire path of the economy to be internally consistent with the optimization problem. In other words, the baseline needs to be constructed so that both the capital accumulation and shadow price equation(s) hold throughout the entire time horizon. This is done by introducing a corresponding slack variable as a multiplier to both equations. This allows the baseline to be defined either as a steady state, where slack variable is set to zero and capital and its shadow value remain constant, or as a non-steady state, where slack variable is 1 and the economy gradually transitions from the observed state toward a steady state. If, by chance, the database is not a steady state and we force slack to 0, then the baseline path is generally infeasible.

A.1.7 Forward-looking household

In GTAP-INT 2, household behavior is extended beyond the static and recursive setups (and also GTAP-INT) by making households explicitly forward-looking. In the standard model [3], savings are included in the upper-level Cobb–Douglas utility function alongside private and government consumption, so that expenditure equations only mimics an intertemporal trade-off without households solving an actual dynamic problem. GTAP-INT 2 replaces this approximation with a full intertemporal household optimisation problem, where a representative regional household (Figure A.3) maximizes intertemporal utility subject to budget and wealth accumulation constraints. The full derivation of the household problem is provided in Ha et al. (2025) [187]; here we highlight only the key elements needed to understand the model.

GTAP-INT 2 adopts the household wealth accumulation structure from the recursive GTAP framework (GDyn) [141]), in which wealth is defined as the value of equity owned in domestic firms with the equity held in the global trust. The global trust is an additional institution not present in the static GTAP, and it works as an intermediary between regional households and foreign firm equity. It pools and redistributes international ownership claims, while ensuring accounting consistency. The household wealth accumulates through increased ownership of domestic firms and global trust equity, thereby linking saving with the capital stock. The households' wealth allocation between domestic firms and claims in the global trust is governed by constant elasticities, so that households can diversify their equities but only within limits determined by the elasticity of substitution, which ensures stable but responsive ownership shares.

With these modifications, the intertemporal (forward-looking) household behavior is defined as follows. The household maximizes its intertemporal utility function

$$\max_{U^P_{r,t}, U^G_{r,t}, QSAV_{r,t}, X_{r,t}} \int_0^\infty C_{r,t} \left(U^P_{r,t}\right)^{B^P_{r,t}} \left(U^G_{r,t}\right)^{B^G_{r,t}} e^{-\int_0^t [\theta_s - g_s]\, ds}\, dt$$

, subject to budget constraint and the wealth accumulation constraint; where $\theta_{r,t}$ is the social discount rate and g_s is the growth of the economy, $E_P(.)$ and $E_G(.)$ are private and government expenditure functions ($X_{r,t}$ is total expenditure variable), $P^P_{r,t}$ and $P^G_{r,t}$ are private and government consumption prices, $NWI_{r,t}$ is the net of wealth household income, $Y_{r,t} is the return on household equity wealth$, $W_{r,t} the household wealth$ $PSAV_{r,t}$ and $QSAV_{r,t}$

price and quantity of savings. The utility function in the integral takes a Cobb–Douglas form, aggregating the sub-utilities of private and government consumption. The parameter C is a normalization constant, while B_P and B_G are the calibrated budget share parameters corresponding to private and government sub-utilities, U_P and U_G, respectively. Operationally, the utilities are coded in GTAP-INT 2 (in percentage change form) as UELASPRIV(r,t) * u_p(r,t) = yp(r,t) - ppriv(r,t) - pop(r,t) and u_g(r,t) = yg(r,t) - pgov(r,t) - pop(r,t) where yp and y, g are nominal private and government expenditures, $ppriv$ and $pgov$ the corresponding price indices, and pop the population. Hence, the utilities are expressed in real, per-capita terms. $UELASPRIV(r,t)$ term is the elasticity for the private CDE block (see Section A.1.4).

The Hamiltonian approach to this optimization problem yields its own set of motion equations that solve the intertemporal problem. The first is the law of motion for household wealth (above), denoting that $NWI_{r,t}$ is exogenous and equals the sum of non-capital endowment incomes, and indirect and direct taxes. The second is the shadow value of wealth equation (the Lagrangian multiplier of the Hamiltonian), which also captures the marginal utility of saving, and links present vs. future consumption. Lastly, the intraperiod condition ties the current saving decisions to the shadow value: households increase their saving until the opportunity cost of current consumption equals the marginal utility benefit of additional wealth. To solve this set of equations, terminal (boundary) conditions are required. The first one ties firm wealth to firm's capital stock and the second one is simply a steady-state restriction on the household side (far in the future, wealth stops accumulating).

Finally, the forward-looking household problem requires an internally consistent baseline, as in the case of forward-looking firms. Accordingly, slack variables are attached to each household motion equation. However, in this thesis, the issue of baseline is circumvented: the baseline itself is taken to be constant across all timesteps, matching the GTAP 11 database [188], which by construction is already in equilibrium.

A.2 GTAP-INT 2 simulation setup

Chapter 3 examines the propagation of climate impacts in GTAP-INT 2 via three channels: agricultural output efficiency (yield change) shocks, labor productivity (labor-augmenting

efficiency) shocks, and human health (mortality) shocks to population/labor availability. This section documents the simulation design (baseline and included impacts), and the model closure that governs the macro responses (leading to GDP change through which the results in Chapter 3 are reported as the variable of interest).

Under the GTAP-INT 2 closure, the macroeconomic aggregates that (in expenditure form) make up regional GDP[1] respond as follows. Private consumption (C) and saving/wealth are endogenous and determined by the forward-looking household block (App. A.1.7). Investment (I) is endogenous and determined by forward-looking firm block with convex adjustment costs (App. A.1.6); capital is fixed only at the initial time step and thereafter evolves endogenously. Government consumption (G) is endogenous, with the private–government split fixed by exogenous top-nest (Cobb–Douglas) shares (Figure A.3). Tradeables (X, M) clear via Armington/CET with the standard goods-market slack tradslack held exogenous, so prices (not quantities) eliminate demand–supply gaps; globally, saving equals investment. Endowments: non-capital factors (labor, land/resources) are fixed in quantity, so factor prices/real wages adjust; capital evolves after t0. Exogenous drivers: the population path, tax wedges (gaps between buyer and seller prices), technology shifters (e.g., labor-augmenting productivity), and the price anchor are held exogenous.

All reported economic changes from climate impacts are expressed as deviations of the climate-change scenario (where impact functions modify the system) from a baseline scenario. The baseline is built as a time-invariant replication of the GTAP 11 database [188], with all variables held constant over the whole time horizon. In this case, the slack variables attached to the household and firm motion equations (see previous section) are set to 0, enforcing a steady-state path in which both the capital stock and its shadow value remain constant (the motion equations are set to 0, mirroring the static setup). Since the GTAP database already represents a world economy in equilibrium, this steady-state configuration provides a feasible and internally consistent baseline.

In the climate-change scenario, the slack variables on the firm and household motion equations are set to 1, restoring intertemporal adjustment in a non-steady state (i.e., after the system is shocked out of the steady state by climate impacts). The non-steady state is created by "shocking" the steady state (baseline) as follows:

[1] Following the GDP identity $GDP_{r,t} = C_{r,t} + I_{r,t} + G_{r,t} + X_{r,t} - M_{r,t}$

- **Labor productivity (all sectors).** Sector (c) and region (r) specific labor-augmenting efficiency $A_L(c, r, t)$ is shocked (tiered by high/medium/low workload). A fall in A_L means the same unit of labor provides less to output: unit cost rises in the value-added nest (left nest in Figure A.2); as cost share of labor rises, firms substitute away from labor toward other inputs guided by CES; the sector's producer price increases, reducing the total output; trade adjusts (imports rise / exports fall case-dependently). Since non-capital endowment quantities are fixed (closure), employment does not drop; instead, real wages fall to equilibrate labor supply and demand, and the contraction manifests in higher costs, lower output, and trade reallocation. Lower profitability reduces investment incentives, thereby slowing capital accumulation, while the forward-looking household adjusts consumption/saving intertemporally (e.g., if anticipated future returns on capital are lower, the households shift a proportion of savings to consumption).

- **Agricultural output efficiency (yields).** Sector (c) and region (r) specific output-augmenting efficiency $A_O(c, r, t)$ is shocked, specifically for agricultural sectors (interpreting yield changes as sectoral productivity). A fall in A_O means less output from the same inputs. This leads to unit cost rising at the top of the production tree A.2 (scaling both the value added and the intermediates' branches); the agricultural output is modified, modifying the sector's producer price; downstream users and trade adjust (imports rise / exports fall, case-dependent). Unlike labor productivity damages, agricultural damages can be both positive and negative, and the sign can also depend on the temperature levels. Endowment quantities are fixed, so real wages adjust to clear factor markets. Intermediate inputs are not fixed: the total quantity of intermediate goods scales in proportion to output at the top (Leontief nest), while input composition can substitute within the CES intermediates bundle, and reallocate between domestic/imported sources. Macro propagation to investment/consumption follows the mechanism already described for labor-productivity shocks.

- **Human health (mortality).** Two components are shocked: first, regional population, which rescales per-capita private and government indices and the size of household absorption, thereby affecting the household utility function. A change in population modifies per-capita measures and scale but does not, by itself, alter factor-market clearing. Secondly, labor availability is modified as a change in

the labor endowment. It operates through the same mechanism as for labor productivity: labor becomes relatively scarcer (if mortality increases, decreasing labor availability), wages adjust to equilibrate factor markets, production costs rise, and firms substitute away from labor in line with CES substitution possibilities, with the propagation through the model detailed above (labor productivity). An important distinction is that in some cases mortality impacts can increase labor availability (e.g. under reduced mortality), in which case the sign of these effects is reversed.

Supplementary 1: Carbon Budget Concept and its Deviation Through the Pulse Response Lens

S1.1 Scenario-dependent deviations - experimental setup

Optimization scheme - boundary conditions

The first boundary condition sets the total cumulative emissions at the year of optimization t^* to a fixed value F_{tot}, counting from the initial year t_0, chosen as the year 2020 in RCP6.0. The condition on F_{tot} ensures that the deviation from the carbon budget stems only from the difference between the emission pathways, as it fixes the cumulative emissions to be equal at the end of both the minimization and the maximization run.

The second boundary condition provides the upper bound on the rate of change in emissions per year, effectively setting the allowed absolute slope of the emission pathway to be less than or equal to a prescribed value k. Hence, a trivial solution (e.g., emitting all of the emissions in one year) is avoided. The emission slope k is chosen such that it its upper bound is 1 PgC/yr^2, roughly corresponding to the emission reduction rate if the annual emissions were linearly reduced to zero between the years 2020 and 2030.

The combination of the restriction on k with the F_{tot} restriction will affect the run's feasibility. The higher the cumulative emissions and the lower the k is, the less feasible the run is. Moreover, the additional requirement that the emissions reach net-zero by t^*

further negatively affects the feasibility. The feasibility limiting value of k will correspond to the run where both $T_{\max}(t^*)$ and $T_{\min}(t^*)$ are equal, as they come from the only possible and feasible scenario; hence, the scenario-dependent carbon deviation $T_{\mathrm{d}}(t^*)$ is zero for that specific k. The higher k is, the more the range of possible pathway combinations increases, as does T_{d}.

The last boundary condition excludes negative emissions. This condition is utilized since Green's approach uses a pulse response generated under positive emissions. Nevertheless, for the sake of completeness, negative emissions will be allowed in the last part of the section to see how doing so affects the deviations.

Two settings of the scenario-dependent deviations

To examine the carbon budget interpretation, we distinguish between two additional sets of conditions that differ depending on how much we emit after the optimization year (t^*).

The first carbon budget interpretation is addressed as a net-zero budget case, which corresponds to the situation in which all of the carbon has been emitted up until the point in time of interest, and there are no other emissions afterward. This interpretation coincides more with a carbon budget as addressed by the IPCC, which indicates how much more carbon can be emitted while still reaching specific targets. In the corresponding emission scenario set, the emissions are bound to reach zero by the year t^* and stay zero from there onwards ($E(t \geq t^*) = 0$). Note, however, that this is not the case of calculating the ZEC deviations, even though the requirement is emission cessation. ZEC tells us what the temperature evolution will be following emission cessation. In the optimization program, however, one derives two maximally different possible temperatures in a specific year, stemming from different preceding emission choices, and the deviation comes from deducting the two. ZEC affects both boundary temperature cases equally, so when the two are subtracted to get the deviation $T_d(t^*)$, the effect of ZEC is also subtracted.

On the other hand, there is the transient budget case, in which only the momentary relationship between the current cumulative emissions and current temperature increase is of interest (as given by Equation (2.1), for example). Therefore, in the optimization year t^*, emissions are free to take any value in transient budget case (within the limits of other constraints). The additional constraint on the emission pathway negatively affects

the feasibility. Therefore, the transient budget case has more possible emission pathway combinations available compared to net zero, which means a higher expected T_{d}.

Deviation time evolution

The optimization procedure (Equation (2.6)) calculates the extreme case of scenario-dependent deviations in one specific year t^* only. To see whether these deviations are persistent in time, an additional experiment is designed, one unique to the net-zero approach. For unit of k specified in the setup above, the system is left to evolve for the next 50 years following the optimization year ($t^* = 2070$), without adding new emissions. Hence, $T_{\mathrm{d}}(k)$ is allowed to evolve freely in time, while keeping cumulative emissions at the same level. In this way, one can see how the scenario-dependent deviation obtained in t^* changes in time.

Run configuration

Preceding the initialization of the optimization program, the FaIR model was historically forced from the preindustrial period (the year 1850) until 2020 under the RCP6.0 emission scenario. The quasi-historical run is dynamically separated from the optimization run since, in the former, emissions are prescribed, not generated by the program. The two runs coincide in the year 2020, where the values of the historical run's variables are translated into the initial conditions of the variables of the FaIR's optimization run. Hence, $t_0 = 2020$ in Equation (2.6) and the initial emissions value of the optimizer run equals to $E_0 = E_{\mathrm{RCP6.0}}(2020)$. The initial temperature at t_0 is $T_0 = 0.96$ K, with the associated cumulative emissions counting $F_0 = 584$ PgC.

S1.2 Optimization year sensitivity

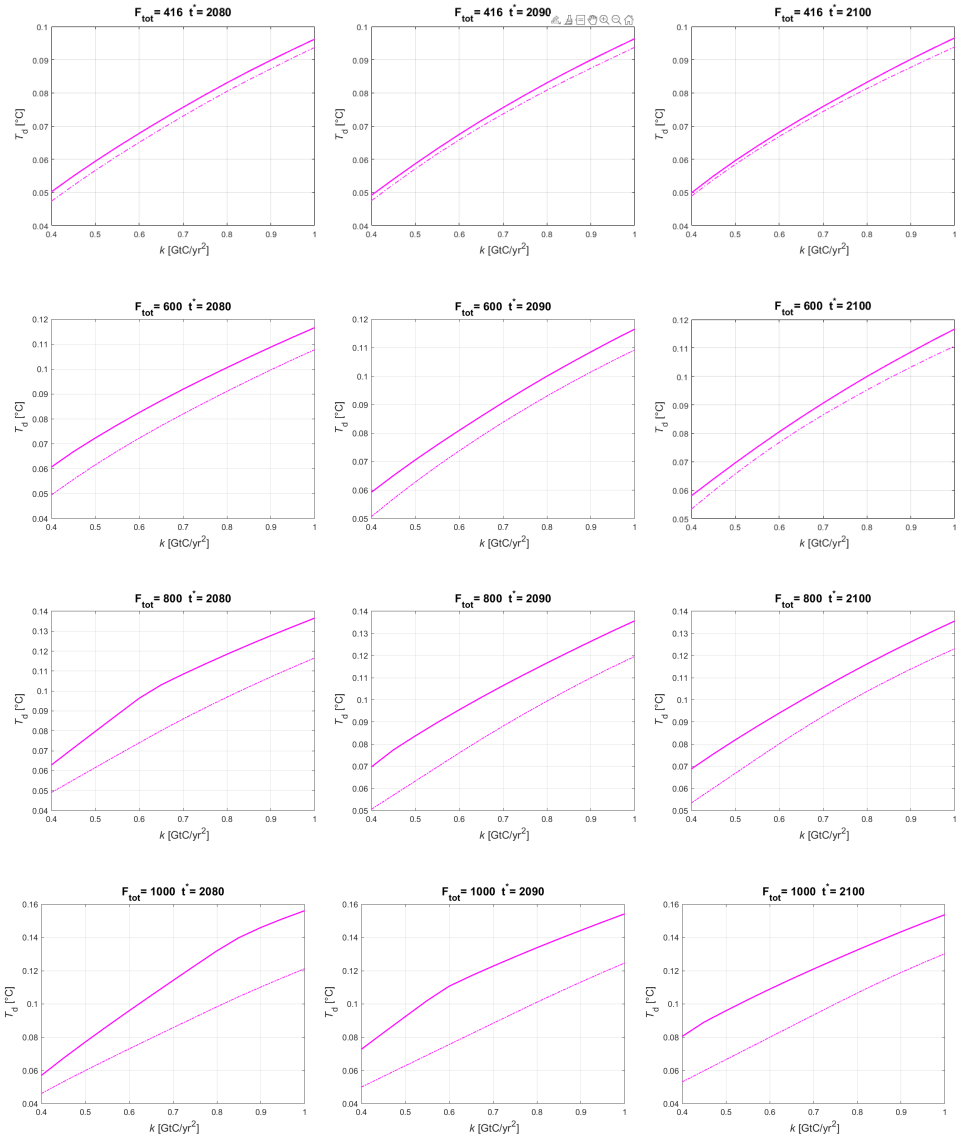

FIGURE S1.4: Maximal scenario dependent deviations for different optimization years and total cumulative emission choices, under transient budget case. One can detect that the optimization year choice does not affect the generated deviations, except for feasibility limit that becomes more prominent the lesser t^*, or prominently, the higher F_{tot} is.

Supplementary 2: A Forward-Looking CGE Analysis of Climate Damages: Integrating Labor Productivity, Agricultural Yields, and Heat-Related Mortality

S2.1 Labor Productivity

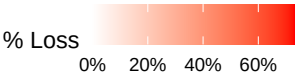

	1°C	2°C	3°C	4°C	5°C
Afghanistan	0.000 (0.000, 0.000)	0.000 (0.000, 0.000)	0.001 (0.000, 0.001)	0.002 (0.002, 0.002)	0.004 (0.003, 0.004)
Algeria	0.010 (0.008, 0.011)	0.028 (0.025, 0.031)	0.056 (0.051, 0.060)	0.093 (0.087, 0.100)	0.140 (0.131, 0.150)
Angola	0.015 (0.013, 0.016)	0.043 (0.041, 0.046)	0.087 (0.083, 0.092)	0.146 (0.140, 0.153)	0.221 (0.212, 0.229)
Argentina	0.005 (0.005, 0.006)	0.016 (0.015, 0.018)	0.033 (0.031, 0.036)	0.057 (0.053, 0.060)	0.087 (0.082, 0.092)
Armenia	0.000 (0.000, 0.000)	0.000 (0.000, 0.001)	0.002 (0.002, 0.003)	0.006 (0.005, 0.006)	0.010 (0.009, 0.011)
Australia	0.003 (0.002, 0.004)	0.010 (0.009, 0.011)	0.021 (0.019, 0.023)	0.036 (0.033, 0.039)	0.055 (0.051, 0.059)
Austria	0.000 (0.000, 0.000)	0.001 (0.000, 0.001)	0.003 (0.002, 0.004)	0.007 (0.006, 0.008)	0.013 (0.011, 0.015)
Azerbaijan	0.004 (0.003, 0.005)	0.013 (0.011, 0.014)	0.027 (0.025, 0.030)	0.048 (0.045, 0.052)	0.075 (0.070, 0.081)
Bangladesh	0.064 (0.059, 0.070)	0.139 (0.129, 0.150)	0.217 (0.200, 0.234)	0.298 (0.273, 0.323)	0.382 (0.348, 0.416)
Belarus	0.000 (0.000, 0.001)	0.001 (0.001, 0.002)	0.004 (0.003, 0.005)	0.007 (0.006, 0.009)	0.012 (0.010, 0.014)
Belgium	0.000 (0.000, 0.000)	0.000 (0.000, 0.001)	0.001 (0.001, 0.001)	0.002 (0.002, 0.003)	0.004 (0.003, 0.005)
Benin	0.091 (0.084, 0.099)	0.204 (0.190, 0.218)	0.318 (0.295, 0.340)	0.432 (0.398, 0.465)	0.547 (0.501, 0.593)
Bhutan	0.000 (0.000, 0.000)	0.001 (0.000, 0.001)	0.004 (0.003, 0.005)	0.010 (0.009, 0.011)	0.018 (0.016, 0.019)
Bolivia	0.000 (0.000, 0.000)	0.000 (0.000, 0.000)	0.000 (0.000, 0.001)	0.001 (0.001, 0.002)	0.003 (0.002, 0.003)
Bosnia and Herz.	0.005 (0.004, 0.006)	0.015 (0.013, 0.017)	0.031 (0.028, 0.034)	0.054 (0.049, 0.059)	0.083 (0.077, 0.090)
Botswana	0.010 (0.009, 0.011)	0.031 (0.028, 0.034)	0.066 (0.061, 0.070)	0.115 (0.108, 0.121)	0.177 (0.168, 0.186)
Brazil	0.020 (0.019, 0.022)	0.057 (0.053, 0.060)	0.110 (0.105, 0.116)	0.181 (0.174, 0.189)	0.270 (0.259, 0.280)
Brunei	0.077 (0.073, 0.080)	0.189 (0.182, 0.196)	0.335 (0.324, 0.347)	0.515 (0.499, 0.532)	0.729 (0.706, 0.752)
Bulgaria	0.005 (0.004, 0.006)	0.015 (0.013, 0.017)	0.032 (0.028, 0.035)	0.055 (0.051, 0.060)	0.086 (0.080, 0.093)
Burkina Faso	0.093 (0.088, 0.098)	0.186 (0.177, 0.196)	0.272 (0.256, 0.288)	0.350 (0.327, 0.374)	0.422 (0.390, 0.454)
Burundi	0.000 (0.000, 0.000)	0.002 (0.001, 0.003)	0.010 (0.008, 0.012)	0.025 (0.022, 0.027)	0.045 (0.041, 0.049)
Cambodia	0.092 (0.087, 0.097)	0.198 (0.189, 0.207)	0.317 (0.302, 0.331)	0.448 (0.427, 0.469)	0.592 (0.563, 0.622)
Cameroon	0.044 (0.041, 0.048)	0.115 (0.108, 0.121)	0.206 (0.195, 0.216)	0.318 (0.303, 0.333)	0.451 (0.430, 0.472)
Canada	0.000 (0.000, 0.000)	0.002 (0.002, 0.003)	0.009 (0.008, 0.010)	0.020 (0.018, 0.022)	0.035 (0.032, 0.037)
Central African Rep.	0.061 (0.055, 0.066)	0.143 (0.133, 0.153)	0.241 (0.225, 0.257)	0.355 (0.331, 0.378)	0.484 (0.452, 0.515)
Chad	0.070 (0.065, 0.074)	0.152 (0.143, 0.160)	0.236 (0.222, 0.250)	0.322 (0.302, 0.343)	0.411 (0.383, 0.439)
China	0.021 (0.019, 0.023)	0.053 (0.049, 0.056)	0.093 (0.088, 0.098)	0.143 (0.136, 0.150)	0.202 (0.192, 0.212)
Colombia	0.016 (0.014, 0.018)	0.051 (0.048, 0.055)	0.106 (0.100, 0.113)	0.181 (0.172, 0.190)	0.275 (0.263, 0.288)
Congo	0.075 (0.068, 0.082)	0.186 (0.173, 0.200)	0.320 (0.298, 0.342)	0.477 (0.444, 0.509)	0.655 (0.611, 0.700)
Costa Rica	0.099 (0.091, 0.107)	0.225 (0.210, 0.240)	0.371 (0.347, 0.394)	0.536 (0.502, 0.571)	0.722 (0.674, 0.770)
Côte d'Ivoire	0.081 (0.076, 0.086)	0.186 (0.176, 0.195)	0.300 (0.285, 0.316)	0.423 (0.401, 0.446)	0.555 (0.524, 0.587)
Croatia	0.005 (0.004, 0.006)	0.015 (0.013, 0.018)	0.031 (0.028, 0.035)	0.054 (0.048, 0.059)	0.082 (0.075, 0.090)
Cuba	0.122 (0.117, 0.128)	0.249 (0.240, 0.259)	0.374 (0.359, 0.390)	0.498 (0.474, 0.521)	0.619 (0.587, 0.650)
Czechia	0.000 (0.000, 0.000)	0.001 (0.001, 0.002)	0.003 (0.003, 0.004)	0.007 (0.006, 0.009)	0.013 (0.011, 0.014)
Dem. Rep. Congo	0.027 (0.024, 0.030)	0.074 (0.068, 0.079)	0.142 (0.133, 0.152)	0.234 (0.220, 0.247)	0.347 (0.329, 0.366)
Denmark	0.000 (0.000, 0.000)	0.000 (0.000, 0.001)	0.001 (0.001, 0.001)	0.002 (0.001, 0.003)	0.003 (0.002, 0.004)
Djibouti	0.109 (0.104, 0.115)	0.227 (0.217, 0.238)	0.350 (0.333, 0.367)	0.477 (0.452, 0.502)	0.609 (0.575, 0.644)
Dominican Rep.	0.101 (0.096, 0.106)	0.213 (0.204, 0.222)	0.332 (0.318, 0.347)	0.460 (0.438, 0.481)	0.595 (0.565, 0.625)
Ecuador	0.006 (0.005, 0.008)	0.031 (0.027, 0.034)	0.073 (0.068, 0.079)	0.135 (0.127, 0.142)	0.215 (0.205, 0.226)
Egypt	0.031 (0.028, 0.034)	0.075 (0.069, 0.081)	0.129 (0.119, 0.138)	0.192 (0.178, 0.205)	0.265 (0.246, 0.283)
Eritrea	0.037 (0.034, 0.041)	0.093 (0.087, 0.099)	0.166 (0.156, 0.176)	0.257 (0.243, 0.272)	0.367 (0.346, 0.387)
eSwatini	0.010 (0.008, 0.012)	0.029 (0.027, 0.032)	0.061 (0.056, 0.066)	0.105 (0.098, 0.111)	0.160 (0.151, 0.170)
Ethiopia	0.000 (0.000, 0.000)	0.002 (0.001, 0.003)	0.012 (0.011, 0.014)	0.029 (0.027, 0.031)	0.052 (0.049, 0.056)
Fiji	0.098 (0.090, 0.105)	0.212 (0.198, 0.227)	0.332 (0.309, 0.355)	0.457 (0.424, 0.490)	0.587 (0.541, 0.633)
Finland	0.000 (0.000, 0.000)	0.000 (0.000, 0.000)	0.000 (0.000, 0.001)	0.001 (0.001, 0.001)	0.001 (0.001, 0.002)
France	0.000 (0.000, 0.001)	0.003 (0.002, 0.004)	0.008 (0.006, 0.009)	0.015 (0.013, 0.018)	0.026 (0.023, 0.029)
Gabon	0.068 (0.064, 0.072)	0.174 (0.166, 0.182)	0.310 (0.297, 0.322)	0.475 (0.456, 0.493)	0.669 (0.644, 0.694)
Georgia	0.001 (0.000, 0.001)	0.004 (0.003, 0.004)	0.010 (0.009, 0.011)	0.019 (0.018, 0.021)	0.032 (0.030, 0.034)
Germany	0.000 (0.000, 0.000)	0.001 (0.001, 0.002)	0.003 (0.002, 0.004)	0.006 (0.005, 0.008)	0.011 (0.009, 0.012)
Ghana	0.101 (0.095, 0.108)	0.215 (0.202, 0.227)	0.328 (0.308, 0.348)	0.441 (0.412, 0.470)	0.554 (0.513, 0.594)
Greece	0.009 (0.008, 0.010)	0.025 (0.023, 0.028)	0.051 (0.046, 0.055)	0.085 (0.079, 0.091)	0.128 (0.119, 0.136)
Guatemala	0.041 (0.036, 0.045)	0.113 (0.104, 0.122)	0.217 (0.203, 0.232)	0.355 (0.333, 0.376)	0.525 (0.496, 0.554)
Guinea	0.075 (0.071, 0.079)	0.171 (0.163, 0.179)	0.279 (0.267, 0.292)	0.400 (0.382, 0.418)	0.532 (0.508, 0.557)
Guinea−Bissau	0.098 (0.092, 0.105)	0.205 (0.193, 0.218)	0.317 (0.297, 0.338)	0.433 (0.403, 0.463)	0.554 (0.512, 0.595)
Guyana	0.105 (0.098, 0.112)	0.227 (0.214, 0.240)	0.361 (0.340, 0.382)	0.507 (0.476, 0.538)	0.666 (0.623, 0.709)
Haiti	0.116 (0.111, 0.121)	0.242 (0.232, 0.251)	0.371 (0.356, 0.386)	0.505 (0.483, 0.527)	0.643 (0.612, 0.673)
Honduras	0.063 (0.057, 0.069)	0.167 (0.156, 0.178)	0.292 (0.274, 0.310)	0.438 (0.412, 0.465)	0.605 (0.569, 0.641)
Hungary	0.002 (0.001, 0.003)	0.007 (0.006, 0.009)	0.017 (0.014, 0.019)	0.031 (0.027, 0.034)	0.049 (0.044, 0.054)
India	0.059 (0.057, 0.062)	0.130 (0.125, 0.134)	0.204 (0.197, 0.212)	0.284 (0.273, 0.295)	0.369 (0.354, 0.384)
Indonesia	0.102 (0.097, 0.108)	0.239 (0.229, 0.248)	0.396 (0.380, 0.411)	0.574 (0.551, 0.597)	0.772 (0.741, 0.804)
Iran	0.003 (0.003, 0.004)	0.012 (0.011, 0.014)	0.028 (0.026, 0.031)	0.051 (0.047, 0.055)	0.080 (0.075, 0.085)
Iraq	0.027 (0.024, 0.029)	0.064 (0.059, 0.068)	0.108 (0.101, 0.116)	0.161 (0.150, 0.171)	0.221 (0.207, 0.236)
Ireland	0.000 (0.000, 0.000)	0.000 (0.000, 0.000)	0.000 (0.000, 0.000)	0.000 (0.000, 0.001)	0.001 (0.000, 0.001)
Israel	0.018 (0.016, 0.021)	0.045 (0.040, 0.050)	0.081 (0.073, 0.089)	0.126 (0.115, 0.138)	0.180 (0.165, 0.196)
Italy	0.002 (0.001, 0.003)	0.008 (0.006, 0.009)	0.019 (0.017, 0.021)	0.036 (0.032, 0.039)	0.058 (0.053, 0.062)
Japan	0.023 (0.021, 0.025)	0.055 (0.051, 0.059)	0.095 (0.088, 0.101)	0.143 (0.134, 0.152)	0.199 (0.186, 0.212)
Jordan	0.018 (0.016, 0.020)	0.046 (0.042, 0.050)	0.083 (0.077, 0.089)	0.129 (0.120, 0.138)	0.185 (0.173, 0.198)
Kazakhstan	0.000 (0.000, 0.000)	0.002 (0.001, 0.002)	0.007 (0.006, 0.008)	0.014 (0.013, 0.015)	0.025 (0.023, 0.026)
Kenya	0.002 (0.002, 0.003)	0.016 (0.014, 0.017)	0.043 (0.040, 0.045)	0.083 (0.079, 0.087)	0.137 (0.131, 0.142)
Kosovo	0.002 (0.001, 0.003)	0.008 (0.007, 0.009)	0.019 (0.017, 0.021)	0.036 (0.033, 0.039)	0.058 (0.054, 0.062)
Laos	0.058 (0.054, 0.062)	0.132 (0.125, 0.139)	0.220 (0.209, 0.231)	0.321 (0.305, 0.337)	0.436 (0.413, 0.458)
Latvia	0.000 (0.000, 0.000)	0.001 (0.000, 0.001)	0.002 (0.001, 0.002)	0.003 (0.002, 0.004)	0.005 (0.004, 0.006)
Lesotho	0.000 (0.000, 0.000)	0.000 (0.000, 0.000)	0.001 (0.000, 0.001)	0.001 (0.001, 0.002)	0.003 (0.002, 0.003)
Liberia	0.063 (0.058, 0.069)	0.161 (0.152, 0.171)	0.276 (0.260, 0.292)	0.407 (0.383, 0.430)	0.554 (0.522, 0.586)

	1°C	2°C	3°C	4°C	5°C
Libya	0.019 (0.017, 0.022)	0.049 (0.045, 0.054)	0.090 (0.083, 0.097)	0.141 (0.131, 0.152)	0.203 (0.189, 0.218)
Lithuania	0.000 (0.000, 0.000)	0.001 (0.001, 0.001)	0.003 (0.002, 0.003)	0.005 (0.004, 0.006)	0.008 (0.007, 0.010)
Madagascar	0.015 (0.014, 0.017)	0.040 (0.037, 0.043)	0.078 (0.073, 0.082)	0.128 (0.121, 0.135)	0.190 (0.181, 0.199)
Malawi	0.021 (0.019, 0.023)	0.055 (0.051, 0.059)	0.104 (0.098, 0.110)	0.167 (0.158, 0.176)	0.246 (0.233, 0.258)
Malaysia	0.093 (0.088, 0.098)	0.223 (0.213, 0.233)	0.380 (0.364, 0.396)	0.564 (0.541, 0.587)	0.775 (0.744, 0.807)
Mali	0.082 (0.078, 0.086)	0.168 (0.160, 0.176)	0.255 (0.242, 0.267)	0.343 (0.325, 0.361)	0.432 (0.407, 0.457)
Mauritania	0.071 (0.067, 0.075)	0.143 (0.136, 0.151)	0.217 (0.204, 0.229)	0.291 (0.272, 0.309)	0.366 (0.340, 0.391)
Mexico	0.002 (0.002, 0.003)	0.013 (0.012, 0.014)	0.032 (0.030, 0.034)	0.060 (0.057, 0.062)	0.096 (0.093, 0.100)
Moldova	0.001 (0.001, 0.002)	0.006 (0.005, 0.007)	0.015 (0.013, 0.017)	0.028 (0.024, 0.031)	0.045 (0.040, 0.049)
Mongolia	0.000 (0.000, 0.000)	0.001 (0.001, 0.002)	0.004 (0.003, 0.004)	0.008 (0.007, 0.009)	0.013 (0.012, 0.015)
Morocco	0.009 (0.007, 0.010)	0.025 (0.023, 0.027)	0.050 (0.047, 0.054)	0.084 (0.079, 0.090)	0.128 (0.120, 0.135)
Mozambique	0.030 (0.028, 0.033)	0.078 (0.073, 0.083)	0.143 (0.136, 0.151)	0.226 (0.215, 0.237)	0.325 (0.310, 0.341)
Myanmar	0.047 (0.044, 0.049)	0.111 (0.105, 0.116)	0.191 (0.182, 0.199)	0.285 (0.273, 0.298)	0.396 (0.378, 0.413)
Namibia	0.006 (0.005, 0.007)	0.022 (0.020, 0.024)	0.048 (0.045, 0.050)	0.083 (0.079, 0.087)	0.128 (0.123, 0.133)
Nepal	0.001 (0.001, 0.001)	0.007 (0.006, 0.008)	0.019 (0.018, 0.020)	0.037 (0.035, 0.038)	0.060 (0.058, 0.062)
Netherlands	0.000 (0.000, 0.000)	0.001 (0.000, 0.001)	0.002 (0.001, 0.002)	0.003 (0.003, 0.004)	0.006 (0.005, 0.007)
New Zealand	0.000 (0.000, 0.000)	0.000 (0.000, 0.000)	0.001 (0.001, 0.001)	0.002 (0.002, 0.002)	0.004 (0.003, 0.004)
Nicaragua	0.078 (0.073, 0.083)	0.184 (0.174, 0.194)	0.304 (0.288, 0.321)	0.439 (0.415, 0.463)	0.589 (0.556, 0.622)
Niger	0.077 (0.071, 0.083)	0.157 (0.146, 0.168)	0.236 (0.219, 0.254)	0.316 (0.290, 0.342)	0.396 (0.361, 0.432)
Nigeria	0.083 (0.078, 0.088)	0.183 (0.175, 0.192)	0.290 (0.276, 0.304)	0.402 (0.382, 0.423)	0.521 (0.492, 0.549)
North Korea	0.012 (0.011, 0.014)	0.032 (0.029, 0.035)	0.059 (0.054, 0.064)	0.094 (0.086, 0.101)	0.135 (0.125, 0.145)
North Macedonia	0.001 (0.001, 0.002)	0.007 (0.006, 0.008)	0.017 (0.015, 0.019)	0.032 (0.029, 0.034)	0.052 (0.048, 0.055)
Oman	0.073 (0.068, 0.077)	0.150 (0.142, 0.158)	0.228 (0.215, 0.241)	0.309 (0.290, 0.328)	0.391 (0.365, 0.417)
Pakistan	0.050 (0.047, 0.053)	0.104 (0.098, 0.109)	0.156 (0.147, 0.165)	0.208 (0.194, 0.221)	0.259 (0.240, 0.277)
Panama	0.096 (0.090, 0.102)	0.220 (0.209, 0.231)	0.368 (0.350, 0.385)	0.538 (0.512, 0.564)	0.731 (0.695, 0.767)
Papua New Guinea	0.037 (0.035, 0.039)	0.100 (0.096, 0.104)	0.192 (0.185, 0.198)	0.312 (0.302, 0.322)	0.461 (0.447, 0.474)
Paraguay	0.055 (0.050, 0.060)	0.130 (0.121, 0.140)	0.218 (0.203, 0.233)	0.319 (0.296, 0.341)	0.432 (0.401, 0.463)
Peru	0.000 (0.000, 0.000)	0.000 (0.000, 0.000)	0.001 (0.000, 0.001)	0.002 (0.001, 0.002)	0.003 (0.002, 0.004)
Philippines	0.130 (0.125, 0.136)	0.276 (0.265, 0.286)	0.419 (0.402, 0.437)	0.561 (0.536, 0.587)	0.702 (0.666, 0.737)
Poland	0.000 (0.000, 0.001)	0.002 (0.001, 0.003)	0.005 (0.004, 0.006)	0.010 (0.008, 0.011)	0.016 (0.014, 0.018)
Portugal	0.007 (0.005, 0.008)	0.020 (0.018, 0.022)	0.040 (0.037, 0.044)	0.069 (0.063, 0.074)	0.104 (0.097, 0.112)
Romania	0.003 (0.002, 0.004)	0.010 (0.009, 0.012)	0.024 (0.021, 0.027)	0.043 (0.039, 0.047)	0.068 (0.062, 0.074)
Russia	0.000 (0.000, 0.000)	0.000 (0.000, 0.001)	0.002 (0.001, 0.002)	0.004 (0.004, 0.005)	0.008 (0.007, 0.009)
S. Sudan	0.065 (0.061, 0.069)	0.156 (0.148, 0.163)	0.265 (0.252, 0.277)	0.392 (0.374, 0.411)	0.538 (0.513, 0.564)
Saudi Arabia	0.042 (0.038, 0.045)	0.095 (0.089, 0.101)	0.156 (0.146, 0.166)	0.226 (0.211, 0.240)	0.303 (0.284, 0.323)

	1°C	2°C	3°C	4°C	5°C
Senegal	0.084 (0.076, 0.091)	0.178 (0.163, 0.193)	0.285 (0.261, 0.308)	0.404 (0.369, 0.438)	0.535 (0.488, 0.583)
Serbia	0.003 (0.002, 0.004)	0.010 (0.009, 0.012)	0.023 (0.020, 0.026)	0.041 (0.038, 0.045)	0.066 (0.060, 0.071)
Sierra Leone	0.085 (0.080, 0.090)	0.198 (0.188, 0.208)	0.323 (0.307, 0.339)	0.460 (0.436, 0.484)	0.608 (0.575, 0.641)
Slovakia	0.001 (0.000, 0.001)	0.003 (0.002, 0.004)	0.008 (0.007, 0.010)	0.016 (0.013, 0.018)	0.026 (0.023, 0.029)
Slovenia	0.003 (0.002, 0.004)	0.010 (0.008, 0.012)	0.022 (0.019, 0.025)	0.040 (0.036, 0.044)	0.063 (0.057, 0.068)
Somalia	0.100 (0.095, 0.106)	0.228 (0.218, 0.238)	0.366 (0.350, 0.383)	0.516 (0.492, 0.540)	0.677 (0.644, 0.710)
Somaliland	0.060 (0.056, 0.064)	0.145 (0.137, 0.152)	0.249 (0.237, 0.261)	0.372 (0.354, 0.389)	0.514 (0.490, 0.539)
South Africa	0.000 (0.000, 0.001)	0.003 (0.002, 0.004)	0.011 (0.010, 0.012)	0.024 (0.022, 0.026)	0.041 (0.039, 0.044)
South Korea	0.025 (0.023, 0.028)	0.058 (0.053, 0.062)	0.096 (0.089, 0.103)	0.139 (0.128, 0.149)	0.186 (0.172, 0.201)
Spain	0.004 (0.003, 0.005)	0.014 (0.012, 0.016)	0.032 (0.029, 0.035)	0.057 (0.053, 0.061)	0.090 (0.084, 0.095)
Sri Lanka	0.140 (0.134, 0.145)	0.297 (0.286, 0.309)	0.455 (0.437, 0.473)	0.613 (0.586, 0.639)	0.770 (0.734, 0.807)
Sudan	0.049 (0.045, 0.052)	0.113 (0.106, 0.119)	0.188 (0.177, 0.198)	0.274 (0.259, 0.289)	0.372 (0.350, 0.393)
Suriname	0.100 (0.093, 0.106)	0.228 (0.216, 0.241)	0.374 (0.354, 0.394)	0.537 (0.507, 0.566)	0.716 (0.676, 0.757)
Sweden	0.000 (0.000, 0.000)	0.000 (0.000, 0.000)	0.000 (0.000, 0.001)	0.001 (0.001, 0.001)	0.001 (0.001, 0.002)
Switzerland	0.000 (0.000, 0.000)	0.000 (0.000, 0.000)	0.001 (0.001, 0.002)	0.003 (0.002, 0.004)	0.006 (0.005, 0.006)
Syria	0.024 (0.021, 0.026)	0.057 (0.053, 0.062)	0.100 (0.093, 0.107)	0.151 (0.141, 0.161)	0.211 (0.197, 0.224)
Tajikistan	0.000 (0.000, 0.000)	0.000 (0.000, 0.000)	0.001 (0.000, 0.001)	0.002 (0.001, 0.002)	0.003 (0.003, 0.004)
Tanzania	0.009 (0.008, 0.010)	0.030 (0.028, 0.033)	0.063 (0.059, 0.067)	0.107 (0.101, 0.112)	0.162 (0.154, 0.170)
Thailand	0.072 (0.067, 0.076)	0.159 (0.151, 0.168)	0.261 (0.248, 0.275)	0.377 (0.358, 0.397)	0.508 (0.481, 0.536)
Tunisia	0.018 (0.016, 0.021)	0.046 (0.041, 0.050)	0.082 (0.075, 0.089)	0.128 (0.118, 0.138)	0.183 (0.169, 0.197)
Turkey	0.002 (0.002, 0.003)	0.010 (0.008, 0.011)	0.023 (0.021, 0.025)	0.041 (0.039, 0.044)	0.066 (0.062, 0.070)
Turkmenistan	0.008 (0.007, 0.009)	0.022 (0.020, 0.024)	0.044 (0.041, 0.047)	0.074 (0.069, 0.078)	0.111 (0.104, 0.118)
Uganda	0.013 (0.011, 0.014)	0.041 (0.038, 0.044)	0.085 (0.081, 0.090)	0.145 (0.138, 0.152)	0.220 (0.210, 0.230)
Ukraine	0.002 (0.001, 0.002)	0.006 (0.005, 0.007)	0.015 (0.012, 0.017)	0.027 (0.024, 0.030)	0.043 (0.039, 0.048)
United Arab Emirates	0.067 (0.062, 0.073)	0.138 (0.128, 0.148)	0.210 (0.194, 0.226)	0.284 (0.260, 0.307)	0.359 (0.327, 0.392)
United Kingdom	0.000 (0.000, 0.000)	0.000 (0.000, 0.000)	0.001 (0.000, 0.001)	0.002 (0.001, 0.002)	0.003 (0.002, 0.003)
United States of America	0.012 (0.011, 0.013)	0.035 (0.033, 0.038)	0.071 (0.067, 0.075)	0.118 (0.112, 0.124)	0.177 (0.169, 0.185)
Uruguay	0.016 (0.013, 0.018)	0.039 (0.034, 0.043)	0.068 (0.060, 0.076)	0.104 (0.093, 0.116)	0.147 (0.132, 0.163)
Uzbekistan	0.003 (0.003, 0.004)	0.011 (0.010, 0.013)	0.025 (0.023, 0.027)	0.045 (0.042, 0.048)	0.070 (0.066, 0.074)
Venezuela	0.113 (0.105, 0.120)	0.253 (0.239, 0.267)	0.400 (0.377, 0.422)	0.552 (0.519, 0.585)	0.710 (0.665, 0.756)
Vietnam	0.067 (0.063, 0.071)	0.148 (0.140, 0.156)	0.241 (0.229, 0.254)	0.347 (0.329, 0.365)	0.465 (0.440, 0.489)
W. Sahara	0.040 (0.036, 0.044)	0.090 (0.082, 0.098)	0.145 (0.133, 0.157)	0.205 (0.187, 0.224)	0.271 (0.246, 0.296)
Yemen	0.033 (0.030, 0.035)	0.082 (0.076, 0.087)	0.147 (0.138, 0.156)	0.228 (0.215, 0.241)	0.326 (0.308, 0.344)
Zambia	0.010 (0.009, 0.011)	0.030 (0.027, 0.032)	0.060 (0.057, 0.064)	0.102 (0.097, 0.107)	0.155 (0.148, 0.162)
Zimbabwe	0.010 (0.009, 0.011)	0.029 (0.027, 0.032)	0.060 (0.056, 0.064)	0.103 (0.097, 0.109)	0.157 (0.149, 0.165)

FIGURE S2.1: Heatmap showing country-level losses (high workload).

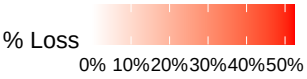

	1°C	2°C	3°C	4°C	5°C
Afghanistan	**0.000** (0.000, 0.000)	**0.000** (0.000, 0.000)	**0.000** (0.000, 0.000)	**0.001** (0.000, 0.001)	**0.001** (0.001, 0.001)
Algeria	**0.003** (0.002, 0.004)	**0.011** (0.009, 0.012)	**0.024** (0.022, 0.027)	**0.044** (0.041, 0.048)	**0.071** (0.066, 0.075)
Angola	**0.004** (0.003, 0.004)	**0.013** (0.012, 0.014)	**0.029** (0.028, 0.031)	**0.052** (0.050, 0.055)	**0.082** (0.079, 0.086)
Argentina	**0.002** (0.001, 0.002)	**0.005** (0.005, 0.006)	**0.012** (0.011, 0.013)	**0.021** (0.020, 0.022)	**0.033** (0.031, 0.035)
Armenia	**0.000** (0.000, 0.000)	**0.000** (0.000, 0.000)	**0.001** (0.000, 0.001)	**0.002** (0.001, 0.002)	**0.003** (0.003, 0.003)
Australia	**0.001** (0.001, 0.001)	**0.003** (0.003, 0.004)	**0.007** (0.006, 0.008)	**0.012** (0.011, 0.014)	**0.020** (0.018, 0.021)
Austria	**0.000** (0.000, 0.000)	**0.000** (0.000, 0.000)	**0.001** (0.001, 0.001)	**0.002** (0.002, 0.003)	**0.004** (0.004, 0.005)
Azerbaijan	**0.001** (0.001, 0.001)	**0.004** (0.004, 0.005)	**0.010** (0.009, 0.011)	**0.019** (0.018, 0.021)	**0.031** (0.029, 0.033)
Bangladesh	**0.052** (0.047, 0.057)	**0.119** (0.110, 0.128)	**0.196** (0.182, 0.211)	**0.284** (0.262, 0.306)	**0.381** (0.351, 0.411)
Belarus	**0.000** (0.000, 0.000)	**0.000** (0.000, 0.001)	**0.001** (0.001, 0.002)	**0.003** (0.002, 0.003)	**0.004** (0.003, 0.005)
Belgium	**0.000** (0.000, 0.000)	**0.000** (0.000, 0.000)	**0.000** (0.000, 0.000)	**0.001** (0.000, 0.001)	**0.001** (0.001, 0.001)
Benin	**0.048** (0.043, 0.053)	**0.122** (0.113, 0.131)	**0.214** (0.200, 0.229)	**0.326** (0.305, 0.347)	**0.456** (0.427, 0.486)
Bhutan	**0.000** (0.000, 0.000)	**0.000** (0.000, 0.000)	**0.001** (0.001, 0.001)	**0.003** (0.002, 0.003)	**0.005** (0.005, 0.005)
Bolivia	**0.000** (0.000, 0.000)	**0.000** (0.000, 0.000)	**0.000** (0.000, 0.000)	**0.000** (0.000, 0.001)	**0.001** (0.001, 0.001)
Bosnia and Herz.	**0.001** (0.001, 0.002)	**0.005** (0.004, 0.006)	**0.013** (0.011, 0.014)	**0.023** (0.021, 0.025)	**0.037** (0.034, 0.040)
Botswana	**0.003** (0.002, 0.003)	**0.010** (0.009, 0.011)	**0.024** (0.022, 0.026)	**0.046** (0.042, 0.049)	**0.073** (0.069, 0.078)
Brazil	**0.006** (0.005, 0.007)	**0.020** (0.019, 0.022)	**0.044** (0.041, 0.046)	**0.077** (0.074, 0.081)	**0.120** (0.115, 0.125)
Brunei	**0.028** (0.026, 0.030)	**0.083** (0.079, 0.088)	**0.174** (0.167, 0.181)	**0.299** (0.289, 0.310)	**0.460** (0.446, 0.474)
Bulgaria	**0.001** (0.001, 0.002)	**0.005** (0.004, 0.006)	**0.012** (0.011, 0.014)	**0.023** (0.021, 0.025)	**0.038** (0.035, 0.040)
Burkina Faso	**0.061** (0.057, 0.065)	**0.138** (0.130, 0.145)	**0.223** (0.211, 0.235)	**0.316** (0.299, 0.334)	**0.418** (0.394, 0.442)
Burundi	**0.000** (0.000, 0.000)	**0.000** (0.000, 0.001)	**0.003** (0.002, 0.003)	**0.007** (0.006, 0.008)	**0.013** (0.012, 0.014)
Cambodia	**0.045** (0.042, 0.048)	**0.111** (0.104, 0.117)	**0.200** (0.190, 0.210)	**0.313** (0.299, 0.328)	**0.450** (0.430, 0.471)
Cameroon	**0.016** (0.014, 0.017)	**0.048** (0.045, 0.051)	**0.099** (0.094, 0.104)	**0.168** (0.161, 0.176)	**0.256** (0.246, 0.267)
Canada	**0.000** (0.000, 0.000)	**0.001** (0.000, 0.001)	**0.003** (0.002, 0.003)	**0.006** (0.006, 0.007)	**0.011** (0.011, 0.012)
Central African Rep.	**0.024** (0.021, 0.027)	**0.066** (0.061, 0.072)	**0.128** (0.119, 0.136)	**0.208** (0.196, 0.221)	**0.308** (0.291, 0.325)
Chad	**0.034** (0.031, 0.037)	**0.088** (0.082, 0.094)	**0.158** (0.149, 0.167)	**0.244** (0.230, 0.257)	**0.346** (0.327, 0.365)
China	**0.008** (0.007, 0.009)	**0.025** (0.023, 0.027)	**0.051** (0.048, 0.054)	**0.087** (0.082, 0.091)	**0.132** (0.126, 0.139)
Colombia	**0.004** (0.003, 0.005)	**0.015** (0.014, 0.017)	**0.035** (0.032, 0.037)	**0.063** (0.059, 0.066)	**0.100** (0.095, 0.104)
Congo	**0.028** (0.024, 0.031)	**0.082** (0.076, 0.089)	**0.164** (0.153, 0.175)	**0.272** (0.255, 0.288)	**0.406** (0.384, 0.428)
Costa Rica	**0.045** (0.040, 0.049)	**0.118** (0.109, 0.126)	**0.221** (0.207, 0.236)	**0.357** (0.336, 0.377)	**0.523** (0.494, 0.551)
Côte d'Ivoire	**0.037** (0.034, 0.040)	**0.101** (0.095, 0.106)	**0.186** (0.177, 0.196)	**0.295** (0.281, 0.309)	**0.426** (0.407, 0.445)
Croatia	**0.002** (0.001, 0.002)	**0.006** (0.005, 0.007)	**0.013** (0.012, 0.015)	**0.024** (0.022, 0.027)	**0.039** (0.036, 0.043)
Cuba	**0.069** (0.065, 0.072)	**0.157** (0.151, 0.164)	**0.262** (0.251, 0.273)	**0.382** (0.367, 0.398)	**0.519** (0.497, 0.540)
Czechia	**0.000** (0.000, 0.000)	**0.000** (0.000, 0.000)	**0.001** (0.001, 0.001)	**0.002** (0.002, 0.003)	**0.004** (0.004, 0.005)
Dem. Rep. Congo	**0.008** (0.007, 0.009)	**0.025** (0.022, 0.027)	**0.054** (0.050, 0.057)	**0.094** (0.089, 0.100)	**0.147** (0.140, 0.155)
Denmark	**0.000** (0.000, 0.000)	**0.000** (0.000, 0.000)	**0.000** (0.000, 0.000)	**0.001** (0.000, 0.001)	**0.001** (0.001, 0.001)
Djibouti	**0.069** (0.065, 0.073)	**0.157** (0.149, 0.165)	**0.262** (0.249, 0.275)	**0.384** (0.365, 0.403)	**0.523** (0.498, 0.549)
Dominican Rep.	**0.049** (0.046, 0.052)	**0.118** (0.112, 0.124)	**0.206** (0.197, 0.216)	**0.314** (0.300, 0.328)	**0.441** (0.422, 0.461)
Ecuador	**0.002** (0.001, 0.002)	**0.009** (0.008, 0.010)	**0.023** (0.021, 0.025)	**0.044** (0.041, 0.046)	**0.071** (0.068, 0.075)
Egypt	**0.013** (0.011, 0.015)	**0.039** (0.035, 0.042)	**0.077** (0.071, 0.083)	**0.129** (0.121, 0.138)	**0.195** (0.183, 0.207)
Eritrea	**0.014** (0.013, 0.016)	**0.041** (0.038, 0.045)	**0.083** (0.077, 0.089)	**0.139** (0.131, 0.147)	**0.210** (0.198, 0.221)
eSwatini	**0.003** (0.002, 0.004)	**0.010** (0.009, 0.012)	**0.024** (0.022, 0.026)	**0.044** (0.041, 0.048)	**0.071** (0.066, 0.075)
Ethiopia	**0.000** (0.000, 0.000)	**0.001** (0.000, 0.001)	**0.003** (0.003, 0.004)	**0.008** (0.008, 0.009)	**0.015** (0.014, 0.016)
Fiji	**0.053** (0.049, 0.057)	**0.129** (0.121, 0.136)	**0.221** (0.209, 0.234)	**0.331** (0.313, 0.350)	**0.459** (0.434, 0.484)
France	**0.000** (0.000, 0.000)	**0.001** (0.000, 0.001)	**0.003** (0.002, 0.003)	**0.005** (0.004, 0.006)	**0.009** (0.008, 0.010)
Gabon	**0.024** (0.022, 0.026)	**0.074** (0.070, 0.078)	**0.152** (0.146, 0.159)	**0.260** (0.250, 0.270)	**0.397** (0.384, 0.410)
Georgia	**0.000** (0.000, 0.000)	**0.001** (0.001, 0.001)	**0.003** (0.003, 0.003)	**0.006** (0.006, 0.007)	**0.011** (0.010, 0.011)
Germany	**0.000** (0.000, 0.000)	**0.000** (0.000, 0.000)	**0.001** (0.001, 0.001)	**0.002** (0.002, 0.002)	**0.004** (0.003, 0.004)
Ghana	**0.055** (0.051, 0.059)	**0.132** (0.124, 0.141)	**0.228** (0.215, 0.241)	**0.342** (0.323, 0.362)	**0.475** (0.448, 0.501)
Greece	**0.003** (0.002, 0.003)	**0.009** (0.008, 0.011)	**0.022** (0.020, 0.024)	**0.040** (0.037, 0.043)	**0.064** (0.059, 0.068)
Guatemala	**0.013** (0.011, 0.016)	**0.045** (0.041, 0.049)	**0.100** (0.093, 0.107)	**0.178** (0.168, 0.188)	**0.280** (0.265, 0.294)
Guinea	**0.034** (0.031, 0.036)	**0.091** (0.086, 0.096)	**0.171** (0.163, 0.179)	**0.274** (0.262, 0.286)	**0.400** (0.384, 0.416)
Guinea−Bissau	**0.055** (0.050, 0.060)	**0.132** (0.123, 0.141)	**0.229** (0.213, 0.244)	**0.345** (0.322, 0.367)	**0.481** (0.450, 0.512)
Guyana	**0.048** (0.044, 0.052)	**0.120** (0.112, 0.128)	**0.217** (0.204, 0.230)	**0.339** (0.321, 0.358)	**0.487** (0.461, 0.512)
Haiti	**0.060** (0.057, 0.063)	**0.142** (0.136, 0.148)	**0.244** (0.234, 0.254)	**0.366** (0.351, 0.380)	**0.507** (0.487, 0.527)
Honduras	**0.024** (0.021, 0.027)	**0.075** (0.070, 0.081)	**0.152** (0.143, 0.161)	**0.253** (0.240, 0.266)	**0.379** (0.361, 0.397)
Hungary	**0.001** (0.000, 0.001)	**0.002** (0.002, 0.003)	**0.006** (0.005, 0.007)	**0.012** (0.011, 0.014)	**0.020** (0.018, 0.022)
India	**0.034** (0.033, 0.036)	**0.085** (0.081, 0.088)	**0.149** (0.143, 0.154)	**0.227** (0.219, 0.235)	**0.319** (0.308, 0.330)
Indonesia	**0.041** (0.039, 0.044)	**0.116** (0.110, 0.121)	**0.225** (0.216, 0.234)	**0.370** (0.357, 0.382)	**0.549** (0.532, 0.567)
Iran	**0.001** (0.001, 0.001)	**0.004** (0.003, 0.005)	**0.010** (0.009, 0.011)	**0.019** (0.018, 0.021)	**0.032** (0.029, 0.034)
Iraq	**0.012** (0.011, 0.014)	**0.034** (0.031, 0.037)	**0.066** (0.061, 0.071)	**0.108** (0.101, 0.115)	**0.160** (0.151, 0.169)
Israel	**0.007** (0.006, 0.009)	**0.021** (0.018, 0.024)	**0.043** (0.038, 0.047)	**0.072** (0.065, 0.079)	**0.109** (0.100, 0.118)
Italy	**0.000** (0.000, 0.001)	**0.002** (0.002, 0.003)	**0.007** (0.006, 0.008)	**0.013** (0.012, 0.015)	**0.022** (0.020, 0.024)
Japan	**0.009** (0.008, 0.010)	**0.026** (0.024, 0.029)	**0.053** (0.049, 0.057)	**0.089** (0.084, 0.095)	**0.135** (0.127, 0.143)
Jordan	**0.007** (0.006, 0.008)	**0.021** (0.019, 0.023)	**0.043** (0.040, 0.046)	**0.073** (0.068, 0.079)	**0.112** (0.105, 0.119)
Kazakhstan	**0.000** (0.000, 0.000)	**0.001** (0.000, 0.001)	**0.002** (0.002, 0.002)	**0.004** (0.004, 0.005)	**0.008** (0.007, 0.008)
Kenya	**0.001** (0.000, 0.001)	**0.004** (0.004, 0.005)	**0.013** (0.012, 0.014)	**0.025** (0.024, 0.027)	**0.043** (0.041, 0.044)
Kosovo	**0.000** (0.000, 0.001)	**0.002** (0.002, 0.003)	**0.007** (0.006, 0.007)	**0.013** (0.012, 0.014)	**0.022** (0.020, 0.023)
Laos	**0.027** (0.025, 0.030)	**0.071** (0.067, 0.076)	**0.135** (0.127, 0.142)	**0.217** (0.206, 0.228)	**0.318** (0.303, 0.333)
Latvia	**0.000** (0.000, 0.000)	**0.000** (0.000, 0.000)	**0.001** (0.000, 0.001)	**0.001** (0.001, 0.001)	**0.002** (0.001, 0.002)
Lesotho	**0.000** (0.000, 0.000)	**0.000** (0.000, 0.000)	**0.000** (0.000, 0.000)	**0.000** (0.000, 0.000)	**0.001** (0.001, 0.001)
Liberia	**0.027** (0.024, 0.030)	**0.081** (0.076, 0.086)	**0.158** (0.149, 0.166)	**0.258** (0.245, 0.270)	**0.380** (0.363, 0.398)
Libya	**0.007** (0.006, 0.008)	**0.022** (0.019, 0.024)	**0.046** (0.042, 0.050)	**0.080** (0.074, 0.086)	**0.124** (0.116, 0.132)
Lithuania	**0.000** (0.000, 0.000)	**0.000** (0.000, 0.000)	**0.001** (0.001, 0.001)	**0.002** (0.001, 0.002)	**0.003** (0.002, 0.003)

	1°C	2°C	3°C	4°C	5°C
Madagascar	**0.004** (0.004, 0.005)	**0.013** (0.012, 0.014)	**0.028** (0.026, 0.030)	**0.050** (0.047, 0.053)	**0.077** (0.073, 0.081)
Malawi	**0.006** (0.005, 0.007)	**0.019** (0.018, 0.021)	**0.041** (0.038, 0.044)	**0.072** (0.068, 0.076)	**0.111** (0.106, 0.117)
Malaysia	**0.037** (0.034, 0.040)	**0.107** (0.101, 0.112)	**0.214** (0.206, 0.223)	**0.359** (0.346, 0.371)	**0.541** (0.524, 0.559)
Mali	**0.048** (0.045, 0.051)	**0.113** (0.107, 0.118)	**0.192** (0.183, 0.201)	**0.285** (0.272, 0.299)	**0.394** (0.375, 0.412)
Mauritania	**0.051** (0.048, 0.054)	**0.112** (0.106, 0.118)	**0.180** (0.171, 0.190)	**0.256** (0.241, 0.270)	**0.338** (0.318, 0.357)
Mexico	**0.001** (0.000, 0.001)	**0.004** (0.003, 0.004)	**0.010** (0.009, 0.010)	**0.019** (0.018, 0.020)	**0.031** (0.030, 0.032)
Moldova	**0.000** (0.000, 0.001)	**0.002** (0.001, 0.002)	**0.005** (0.004, 0.006)	**0.010** (0.009, 0.012)	**0.017** (0.015, 0.019)
Mongolia	**0.000** (0.000, 0.000)	**0.000** (0.000, 0.000)	**0.001** (0.001, 0.001)	**0.002** (0.002, 0.003)	**0.004** (0.004, 0.005)
Morocco	**0.003** (0.002, 0.003)	**0.009** (0.008, 0.010)	**0.020** (0.019, 0.022)	**0.037** (0.034, 0.039)	**0.058** (0.055, 0.061)
Mozambique	**0.010** (0.009, 0.012)	**0.031** (0.029, 0.033)	**0.065** (0.061, 0.069)	**0.111** (0.105, 0.117)	**0.170** (0.162, 0.178)
Myanmar	**0.020** (0.019, 0.022)	**0.056** (0.053, 0.060)	**0.110** (0.104, 0.115)	**0.181** (0.172, 0.189)	**0.270** (0.258, 0.281)
Namibia	**0.002** (0.001, 0.002)	**0.006** (0.006, 0.007)	**0.015** (0.014, 0.016)	**0.028** (0.027, 0.030)	**0.046** (0.044, 0.048)
Nepal	**0.000** (0.000, 0.000)	**0.002** (0.002, 0.002)	**0.006** (0.005, 0.006)	**0.011** (0.011, 0.012)	**0.019** (0.018, 0.020)
Netherlands	**0.000** (0.000, 0.000)	**0.000** (0.000, 0.000)	**0.001** (0.000, 0.001)	**0.001** (0.001, 0.001)	**0.002** (0.001, 0.002)
New Zealand	**0.000** (0.000, 0.000)	**0.000** (0.000, 0.000)	**0.000** (0.000, 0.000)	**0.001** (0.000, 0.001)	**0.001** (0.001, 0.001)
Nicaragua	**0.030** (0.027, 0.033)	**0.082** (0.076, 0.088)	**0.156** (0.146, 0.166)	**0.251** (0.237, 0.265)	**0.368** (0.348, 0.387)
Niger	**0.048** (0.044, 0.052)	**0.112** (0.104, 0.120)	**0.188** (0.175, 0.200)	**0.276** (0.258, 0.295)	**0.377** (0.352, 0.403)
Nigeria	**0.040** (0.037, 0.043)	**0.103** (0.097, 0.108)	**0.186** (0.177, 0.195)	**0.290** (0.277, 0.304)	**0.415** (0.397, 0.433)
North Korea	**0.004** (0.004, 0.005)	**0.014** (0.012, 0.016)	**0.030** (0.027, 0.033)	**0.052** (0.048, 0.056)	**0.080** (0.074, 0.086)
North Macedonia	**0.000** (0.000, 0.001)	**0.002** (0.002, 0.002)	**0.006** (0.005, 0.006)	**0.011** (0.010, 0.012)	**0.019** (0.017, 0.020)
Oman	**0.057** (0.054, 0.061)	**0.125** (0.118, 0.131)	**0.199** (0.188, 0.210)	**0.280** (0.264, 0.295)	**0.366** (0.345, 0.388)
Pakistan	**0.036** (0.034, 0.038)	**0.081** (0.077, 0.086)	**0.132** (0.125, 0.139)	**0.188** (0.178, 0.198)	**0.249** (0.235, 0.263)
Panama	**0.039** (0.035, 0.042)	**0.105** (0.098, 0.111)	**0.204** (0.193, 0.214)	**0.335** (0.319, 0.351)	**0.499** (0.478, 0.521)
Papua New Guinea	**0.011** (0.010, 0.012)	**0.035** (0.033, 0.037)	**0.076** (0.073, 0.079)	**0.133** (0.129, 0.138)	**0.207** (0.201, 0.213)
Paraguay	**0.029** (0.025, 0.032)	**0.077** (0.070, 0.083)	**0.142** (0.132, 0.153)	**0.225** (0.210, 0.241)	**0.325** (0.304, 0.346)
Peru	**0.000** (0.000, 0.000)	**0.000** (0.000, 0.000)	**0.000** (0.000, 0.000)	**0.000** (0.000, 0.001)	**0.001** (0.001, 0.001)
Philippines	**0.068** (0.065, 0.072)	**0.165** (0.159, 0.172)	**0.284** (0.273, 0.295)	**0.424** (0.408, 0.440)	**0.586** (0.565, 0.608)
Poland	**0.000** (0.000, 0.000)	**0.001** (0.000, 0.001)	**0.002** (0.001, 0.002)	**0.003** (0.003, 0.004)	**0.006** (0.005, 0.006)
Portugal	**0.002** (0.002, 0.003)	**0.007** (0.006, 0.008)	**0.017** (0.015, 0.019)	**0.031** (0.028, 0.033)	**0.049** (0.045, 0.052)
Romania	**0.001** (0.000, 0.001)	**0.003** (0.003, 0.004)	**0.009** (0.008, 0.010)	**0.017** (0.015, 0.019)	**0.028** (0.025, 0.030)
Russia	**0.000** (0.000, 0.000)	**0.000** (0.000, 0.000)	**0.001** (0.000, 0.001)	**0.001** (0.001, 0.001)	**0.002** (0.002, 0.003)
S. Sudan	**0.025** (0.023, 0.028)	**0.072** (0.068, 0.076)	**0.142** (0.135, 0.149)	**0.235** (0.225, 0.244)	**0.350** (0.337, 0.364)
Saudi Arabia	**0.021** (0.019, 0.023)	**0.055** (0.051, 0.059)	**0.102** (0.095, 0.109)	**0.162** (0.152, 0.172)	**0.234** (0.221, 0.248)
Senegal	**0.049** (0.044, 0.054)	**0.115** (0.106, 0.125)	**0.200** (0.185, 0.215)	**0.303** (0.281, 0.325)	**0.424** (0.394, 0.455)

	1°C	2°C	3°C	4°C	5°C
Serbia	**0.001** (0.000, 0.001)	**0.003** (0.003, 0.004)	**0.009** (0.007, 0.010)	**0.016** (0.015, 0.018)	**0.027** (0.025, 0.029)
Sierra Leone	**0.040** (0.037, 0.043)	**0.109** (0.103, 0.115)	**0.204** (0.194, 0.213)	**0.323** (0.309, 0.337)	**0.468** (0.448, 0.487)
Slovakia	**0.000** (0.000, 0.000)	**0.001** (0.001, 0.001)	**0.003** (0.002, 0.003)	**0.006** (0.005, 0.007)	**0.010** (0.008, 0.011)
Slovenia	**0.001** (0.000, 0.001)	**0.003** (0.003, 0.004)	**0.008** (0.007, 0.010)	**0.016** (0.014, 0.018)	**0.026** (0.024, 0.029)
Somalia	**0.046** (0.043, 0.050)	**0.121** (0.115, 0.127)	**0.220** (0.210, 0.230)	**0.344** (0.330, 0.358)	**0.493** (0.473, 0.513)
Somaliland	**0.025** (0.022, 0.027)	**0.070** (0.066, 0.075)	**0.140** (0.133, 0.147)	**0.234** (0.223, 0.244)	**0.351** (0.337, 0.365)
South Africa	**0.000** (0.000, 0.000)	**0.001** (0.001, 0.001)	**0.003** (0.003, 0.004)	**0.007** (0.007, 0.008)	**0.012** (0.012, 0.013)
South Korea	**0.012** (0.010, 0.013)	**0.032** (0.029, 0.034)	**0.060** (0.056, 0.065)	**0.097** (0.091, 0.104)	**0.143** (0.134, 0.152)
Spain	**0.001** (0.001, 0.001)	**0.005** (0.004, 0.005)	**0.012** (0.011, 0.013)	**0.022** (0.021, 0.024)	**0.037** (0.034, 0.039)
Sri Lanka	**0.073** (0.069, 0.077)	**0.180** (0.173, 0.188)	**0.314** (0.302, 0.326)	**0.475** (0.457, 0.492)	**0.662** (0.638, 0.687)
Sudan	**0.021** (0.019, 0.023)	**0.057** (0.053, 0.060)	**0.109** (0.103, 0.115)	**0.177** (0.168, 0.186)	**0.261** (0.249, 0.273)
Suriname	**0.043** (0.039, 0.047)	**0.115** (0.108, 0.122)	**0.216** (0.204, 0.228)	**0.346** (0.329, 0.363)	**0.505** (0.482, 0.529)
Switzerland	**0.000** (0.000, 0.000)	**0.000** (0.000, 0.000)	**0.000** (0.000, 0.001)	**0.001** (0.001, 0.001)	**0.002** (0.001, 0.002)
Syria	**0.010** (0.009, 0.011)	**0.029** (0.027, 0.032)	**0.059** (0.055, 0.062)	**0.098** (0.093, 0.104)	**0.148** (0.141, 0.156)
Tajikistan	**0.000** (0.000, 0.000)	**0.000** (0.000, 0.000)	**0.000** (0.000, 0.000)	**0.001** (0.000, 0.001)	**0.001** (0.001, 0.001)
Tanzania	**0.002** (0.002, 0.003)	**0.009** (0.008, 0.010)	**0.020** (0.019, 0.021)	**0.036** (0.034, 0.038)	**0.056** (0.054, 0.059)
Thailand	**0.035** (0.032, 0.038)	**0.089** (0.083, 0.094)	**0.163** (0.154, 0.172)	**0.259** (0.245, 0.272)	**0.375** (0.357, 0.394)
Tunisia	**0.007** (0.006, 0.008)	**0.021** (0.018, 0.023)	**0.043** (0.039, 0.047)	**0.074** (0.068, 0.079)	**0.113** (0.105, 0.121)
Turkey	**0.001** (0.000, 0.001)	**0.003** (0.002, 0.003)	**0.008** (0.007, 0.009)	**0.015** (0.014, 0.016)	**0.025** (0.023, 0.026)
Turkmenistan	**0.002** (0.002, 0.003)	**0.008** (0.007, 0.009)	**0.018** (0.017, 0.020)	**0.033** (0.031, 0.035)	**0.052** (0.049, 0.055)
Uganda	**0.003** (0.003, 0.004)	**0.012** (0.011, 0.013)	**0.028** (0.026, 0.029)	**0.049** (0.047, 0.052)	**0.077** (0.074, 0.081)
Ukraine	**0.000** (0.000, 0.001)	**0.002** (0.001, 0.003)	**0.005** (0.004, 0.006)	**0.010** (0.009, 0.011)	**0.017** (0.015, 0.018)
United Arab Emirates	**0.055** (0.050, 0.060)	**0.117** (0.108, 0.127)	**0.183** (0.169, 0.198)	**0.253** (0.232, 0.275)	**0.327** (0.297, 0.357)
United Kingdom	**0.000** (0.000, 0.000)	**0.000** (0.000, 0.000)	**0.000** (0.000, 0.000)	**0.000** (0.000, 0.001)	**0.001** (0.001, 0.001)
United States of America	**0.004** (0.003, 0.004)	**0.014** (0.012, 0.015)	**0.032** (0.030, 0.034)	**0.058** (0.055, 0.061)	**0.093** (0.089, 0.097)
Uruguay	**0.007** (0.006, 0.009)	**0.019** (0.016, 0.022)	**0.037** (0.032, 0.041)	**0.060** (0.053, 0.066)	**0.088** (0.079, 0.097)
Uzbekistan	**0.001** (0.001, 0.001)	**0.004** (0.003, 0.004)	**0.009** (0.008, 0.010)	**0.017** (0.016, 0.018)	**0.027** (0.025, 0.029)
Venezuela	**0.051** (0.047, 0.056)	**0.137** (0.128, 0.145)	**0.248** (0.234, 0.262)	**0.387** (0.366, 0.407)	**0.552** (0.524, 0.579)
Vietnam	**0.033** (0.030, 0.035)	**0.083** (0.078, 0.088)	**0.152** (0.144, 0.160)	**0.241** (0.229, 0.252)	**0.349** (0.332, 0.365)
W. Sahara	**0.022** (0.020, 0.025)	**0.057** (0.051, 0.062)	**0.100** (0.092, 0.109)	**0.154** (0.141, 0.166)	**0.216** (0.199, 0.234)
Yemen	**0.012** (0.011, 0.014)	**0.036** (0.033, 0.039)	**0.074** (0.069, 0.079)	**0.125** (0.117, 0.132)	**0.189** (0.179, 0.199)
Zambia	**0.003** (0.002, 0.003)	**0.009** (0.008, 0.010)	**0.020** (0.019, 0.022)	**0.036** (0.034, 0.038)	**0.057** (0.054, 0.060)
Zimbabwe	**0.003** (0.002, 0.003)	**0.009** (0.008, 0.010)	**0.021** (0.020, 0.023)	**0.039** (0.036, 0.042)	**0.062** (0.059, 0.066)

FIGURE S2.2: Heatmap showing country-level losses (moderate workload).

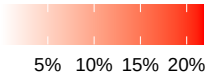

	1°C	2°C	3°C	4°C	5°C
Algeria	0.000 (0.000, 0.000)	0.001 (0.000, 0.001)	0.002 (0.002, 0.002)	0.004 (0.003, 0.004)	0.007 (0.006, 0.007)
Angola	0.000 (0.000, 0.000)	0.000 (0.000, 0.001)	0.001 (0.001, 0.001)	0.003 (0.002, 0.003)	0.004 (0.004, 0.005)
Argentina	0.000 (0.000, 0.000)	0.000 (0.000, 0.000)	0.001 (0.001, 0.001)	0.001 (0.001, 0.001)	0.002 (0.002, 0.002)
Australia	0.000 (0.000, 0.000)	0.000 (0.000, 0.000)	0.000 (0.000, 0.000)	0.001 (0.001, 0.001)	0.001 (0.001, 0.001)
Azerbaijan	0.000 (0.000, 0.000)	0.000 (0.000, 0.000)	0.001 (0.001, 0.001)	0.001 (0.001, 0.001)	0.002 (0.002, 0.002)
Bangladesh	0.013 (0.010, 0.015)	0.038 (0.033, 0.043)	0.080 (0.072, 0.087)	0.137 (0.126, 0.148)	0.210 (0.195, 0.226)
Benin	0.005 (0.003, 0.006)	0.017 (0.015, 0.020)	0.041 (0.037, 0.045)	0.075 (0.070, 0.081)	0.121 (0.114, 0.129)
Bosnia and Herz.	0.000 (0.000, 0.000)	0.000 (0.000, 0.000)	0.001 (0.001, 0.001)	0.002 (0.002, 0.002)	0.003 (0.003, 0.003)
Botswana	0.000 (0.000, 0.000)	0.000 (0.000, 0.001)	0.001 (0.001, 0.002)	0.003 (0.003, 0.003)	0.005 (0.004, 0.005)
Brazil	0.000 (0.000, 0.000)	0.001 (0.001, 0.001)	0.003 (0.002, 0.003)	0.005 (0.005, 0.006)	0.009 (0.008, 0.009)
Brunei	0.001 (0.001, 0.002)	0.006 (0.005, 0.007)	0.017 (0.016, 0.019)	0.035 (0.033, 0.037)	0.059 (0.056, 0.062)
Bulgaria	0.000 (0.000, 0.000)	0.000 (0.000, 0.000)	0.001 (0.001, 0.001)	0.002 (0.001, 0.002)	0.003 (0.002, 0.003)
Burkina Faso	0.008 (0.007, 0.009)	0.028 (0.026, 0.031)	0.065 (0.061, 0.069)	0.117 (0.111, 0.123)	0.186 (0.178, 0.194)
Cambodia	0.004 (0.003, 0.005)	0.014 (0.012, 0.016)	0.033 (0.030, 0.036)	0.063 (0.059, 0.067)	0.102 (0.096, 0.108)
Cameroon	0.001 (0.000, 0.001)	0.003 (0.003, 0.004)	0.009 (0.008, 0.009)	0.017 (0.016, 0.018)	0.028 (0.027, 0.030)
Central African Rep.	0.001 (0.001, 0.002)	0.005 (0.005, 0.006)	0.014 (0.012, 0.015)	0.026 (0.024, 0.028)	0.042 (0.040, 0.044)
Chad	0.002 (0.002, 0.003)	0.011 (0.009, 0.012)	0.028 (0.026, 0.031)	0.054 (0.051, 0.058)	0.090 (0.085, 0.095)
China	0.000 (0.000, 0.001)	0.002 (0.002, 0.002)	0.006 (0.005, 0.006)	0.011 (0.010, 0.012)	0.019 (0.018, 0.020)
Colombia	0.000 (0.000, 0.000)	0.000 (0.000, 0.001)	0.001 (0.001, 0.002)	0.003 (0.003, 0.003)	0.005 (0.005, 0.005)
Congo	0.001 (0.001, 0.002)	0.006 (0.005, 0.007)	0.016 (0.015, 0.017)	0.031 (0.029, 0.033)	0.051 (0.048, 0.054)
Costa Rica	0.003 (0.002, 0.004)	0.012 (0.011, 0.014)	0.031 (0.028, 0.034)	0.059 (0.055, 0.063)	0.097 (0.091, 0.102)
Côte d'Ivoire	0.003 (0.002, 0.003)	0.011 (0.010, 0.013)	0.029 (0.026, 0.031)	0.055 (0.051, 0.058)	0.089 (0.084, 0.094)
Croatia	0.000 (0.000, 0.000)	0.000 (0.000, 0.000)	0.001 (0.001, 0.001)	0.002 (0.002, 0.002)	0.003 (0.003, 0.004)
Cuba	0.007 (0.006, 0.008)	0.026 (0.024, 0.028)	0.060 (0.057, 0.063)	0.109 (0.104, 0.114)	0.174 (0.167, 0.180)
Dem. Rep. Congo	0.000 (0.000, 0.000)	0.001 (0.001, 0.001)	0.003 (0.003, 0.003)	0.006 (0.005, 0.006)	0.010 (0.009, 0.010)
Djibouti	0.010 (0.008, 0.012)	0.034 (0.031, 0.037)	0.076 (0.071, 0.081)	0.137 (0.130, 0.145)	0.218 (0.208, 0.227)
Dominican Rep.	0.004 (0.003, 0.005)	0.014 (0.013, 0.016)	0.034 (0.031, 0.036)	0.062 (0.058, 0.065)	0.099 (0.094, 0.104)
Ecuador	0.000 (0.000, 0.000)	0.000 (0.000, 0.000)	0.001 (0.001, 0.001)	0.002 (0.002, 0.002)	0.003 (0.003, 0.003)
Egypt	0.001 (0.000, 0.001)	0.004 (0.003, 0.005)	0.013 (0.011, 0.015)	0.026 (0.024, 0.029)	0.045 (0.041, 0.049)
Eritrea	0.001 (0.000, 0.001)	0.003 (0.003, 0.004)	0.009 (0.008, 0.010)	0.017 (0.016, 0.018)	0.028 (0.026, 0.030)
eSwatini	0.000 (0.000, 0.000)	0.001 (0.000, 0.001)	0.002 (0.001, 0.002)	0.003 (0.003, 0.004)	0.005 (0.005, 0.006)
Fiji	0.006 (0.005, 0.006)	0.019 (0.018, 0.021)	0.043 (0.041, 0.046)	0.077 (0.074, 0.081)	0.122 (0.117, 0.127)
Gabon	0.001 (0.001, 0.001)	0.005 (0.004, 0.006)	0.014 (0.013, 0.015)	0.027 (0.026, 0.029)	0.045 (0.043, 0.047)
Ghana	0.006 (0.004, 0.007)	0.020 (0.018, 0.023)	0.047 (0.043, 0.051)	0.087 (0.081, 0.093)	0.140 (0.131, 0.148)
Greece	0.000 (0.000, 0.000)	0.001 (0.000, 0.001)	0.002 (0.001, 0.002)	0.003 (0.003, 0.004)	0.006 (0.005, 0.007)
Guatemala	0.000 (0.000, 0.001)	0.003 (0.002, 0.003)	0.008 (0.008, 0.009)	0.017 (0.016, 0.018)	0.029 (0.027, 0.031)
Guinea	0.002 (0.001, 0.003)	0.010 (0.008, 0.011)	0.025 (0.023, 0.027)	0.048 (0.046, 0.051)	0.080 (0.076, 0.084)
Guinea−Bissau	0.006 (0.004, 0.007)	0.021 (0.018, 0.024)	0.050 (0.045, 0.054)	0.092 (0.086, 0.099)	0.148 (0.139, 0.157)
Guyana	0.003 (0.003, 0.004)	0.013 (0.011, 0.014)	0.031 (0.028, 0.033)	0.057 (0.053, 0.061)	0.092 (0.087, 0.097)
Haiti	0.005 (0.005, 0.006)	0.020 (0.018, 0.021)	0.046 (0.043, 0.049)	0.085 (0.081, 0.089)	0.136 (0.130, 0.142)
Honduras	0.001 (0.001, 0.002)	0.006 (0.005, 0.007)	0.016 (0.014, 0.017)	0.031 (0.029, 0.033)	0.051 (0.048, 0.053)
Hungary	0.000 (0.000, 0.000)	0.000 (0.000, 0.000)	0.000 (0.000, 0.000)	0.001 (0.001, 0.001)	0.001 (0.001, 0.002)
India	0.003 (0.003, 0.004)	0.013 (0.012, 0.014)	0.031 (0.029, 0.033)	0.059 (0.056, 0.062)	0.095 (0.091, 0.099)
Indonesia	0.002 (0.002, 0.003)	0.010 (0.009, 0.011)	0.026 (0.025, 0.028)	0.051 (0.049, 0.054)	0.084 (0.081, 0.088)
Iran	0.000 (0.000, 0.000)	0.000 (0.000, 0.000)	0.001 (0.000, 0.001)	0.001 (0.001, 0.001)	0.002 (0.002, 0.002)
Iraq	0.001 (0.000, 0.001)	0.004 (0.003, 0.004)	0.010 (0.009, 0.011)	0.020 (0.018, 0.021)	0.033 (0.031, 0.035)
Israel	0.000 (0.000, 0.001)	0.002 (0.001, 0.003)	0.006 (0.005, 0.007)	0.011 (0.010, 0.013)	0.018 (0.016, 0.020)
Italy	0.000 (0.000, 0.000)	0.000 (0.000, 0.000)	0.000 (0.000, 0.000)	0.001 (0.001, 0.001)	0.001 (0.001, 0.001)
Japan	0.000 (0.000, 0.001)	0.002 (0.002, 0.003)	0.006 (0.005, 0.007)	0.013 (0.011, 0.014)	0.021 (0.019, 0.023)
Jordan	0.000 (0.000, 0.001)	0.002 (0.001, 0.002)	0.005 (0.004, 0.006)	0.010 (0.009, 0.011)	0.017 (0.015, 0.018)
Kenya	0.000 (0.000, 0.000)	0.000 (0.000, 0.000)	0.000 (0.000, 0.000)	0.001 (0.001, 0.001)	0.002 (0.002, 0.002)
Kosovo	0.000 (0.000, 0.000)	0.000 (0.000, 0.000)	0.000 (0.000, 0.000)	0.001 (0.001, 0.001)	0.001 (0.001, 0.001)
Laos	0.002 (0.001, 0.003)	0.008 (0.007, 0.009)	0.020 (0.018, 0.022)	0.039 (0.036, 0.042)	0.063 (0.059, 0.067)
Liberia	0.002 (0.001, 0.002)	0.008 (0.007, 0.009)	0.020 (0.019, 0.022)	0.039 (0.036, 0.041)	0.063 (0.060, 0.066)
Libya	0.000 (0.000, 0.000)	0.002 (0.001, 0.002)	0.005 (0.004, 0.006)	0.010 (0.009, 0.011)	0.018 (0.016, 0.019)
Madagascar	0.000 (0.000, 0.000)	0.001 (0.000, 0.001)	0.001 (0.001, 0.002)	0.003 (0.003, 0.003)	0.005 (0.004, 0.005)
Malawi	0.000 (0.000, 0.000)	0.001 (0.001, 0.001)	0.003 (0.002, 0.003)	0.005 (0.005, 0.005)	0.008 (0.008, 0.009)
Malaysia	0.002 (0.001, 0.003)	0.009 (0.008, 0.010)	0.025 (0.023, 0.027)	0.050 (0.047, 0.053)	0.084 (0.080, 0.087)
Mali	0.005 (0.004, 0.006)	0.018 (0.016, 0.020)	0.044 (0.041, 0.048)	0.083 (0.079, 0.088)	0.135 (0.128, 0.141)
Mauritania	0.009 (0.007, 0.010)	0.028 (0.025, 0.030)	0.060 (0.056, 0.063)	0.104 (0.099, 0.110)	0.162 (0.155, 0.170)
Mexico	0.000 (0.000, 0.000)	0.000 (0.000, 0.000)	0.000 (0.000, 0.000)	0.001 (0.001, 0.001)	0.001 (0.001, 0.001)
Moldova	0.000 (0.000, 0.000)	0.000 (0.000, 0.000)	0.000 (0.000, 0.000)	0.001 (0.001, 0.001)	0.001 (0.001, 0.001)
Morocco	0.000 (0.000, 0.000)	0.000 (0.000, 0.001)	0.001 (0.001, 0.001)	0.003 (0.002, 0.003)	0.004 (0.004, 0.005)
Mozambique	0.000 (0.000, 0.001)	0.002 (0.002, 0.002)	0.005 (0.005, 0.006)	0.010 (0.009, 0.011)	0.016 (0.015, 0.017)
Myanmar	0.001 (0.001, 0.002)	0.005 (0.005, 0.006)	0.014 (0.013, 0.015)	0.027 (0.025, 0.029)	0.044 (0.041, 0.046)
Namibia	0.000 (0.000, 0.000)	0.000 (0.000, 0.000)	0.001 (0.001, 0.001)	0.001 (0.001, 0.001)	0.002 (0.002, 0.002)
Nepal	0.000 (0.000, 0.000)	0.000 (0.000, 0.000)	0.000 (0.000, 0.000)	0.000 (0.000, 0.000)	0.001 (0.001, 0.001)
Nicaragua	0.002 (0.001, 0.002)	0.006 (0.005, 0.007)	0.016 (0.014, 0.018)	0.030 (0.027, 0.032)	0.048 (0.045, 0.052)
Niger	0.005 (0.004, 0.007)	0.022 (0.019, 0.024)	0.053 (0.048, 0.057)	0.099 (0.093, 0.105)	0.160 (0.151, 0.168)
Nigeria	0.003 (0.002, 0.004)	0.012 (0.011, 0.013)	0.031 (0.029, 0.033)	0.059 (0.056, 0.063)	0.097 (0.092, 0.102)
North Korea	0.000 (0.000, 0.000)	0.001 (0.001, 0.001)	0.003 (0.003, 0.003)	0.006 (0.005, 0.006)	0.010 (0.009, 0.011)
North Macedonia	0.000 (0.000, 0.000)	0.000 (0.000, 0.000)	0.000 (0.000, 0.000)	0.001 (0.000, 0.001)	0.001 (0.001, 0.001)
Oman	0.014 (0.012, 0.016)	0.043 (0.040, 0.047)	0.091 (0.086, 0.096)	0.157 (0.150, 0.165)	0.242 (0.231, 0.253)
Pakistan	0.006 (0.005, 0.007)	0.020 (0.019, 0.022)	0.045 (0.042, 0.047)	0.080 (0.076, 0.084)	0.126 (0.120, 0.131)

	1°C	2°C	3°C	4°C	5°C
Panama	0.002 (0.001, 0.003)	0.009 (0.008, 0.011)	0.024 (0.022, 0.026)	0.046 (0.043, 0.050)	0.077 (0.072, 0.081)
Papua New Guinea	0.000 (0.000, 0.000)	0.002 (0.002, 0.002)	0.005 (0.004, 0.005)	0.009 (0.009, 0.009)	0.015 (0.014, 0.015)
Paraguay	0.003 (0.002, 0.004)	0.011 (0.009, 0.013)	0.028 (0.025, 0.031)	0.053 (0.048, 0.057)	0.086 (0.080, 0.092)
Philippines	0.006 (0.005, 0.007)	0.023 (0.021, 0.025)	0.054 (0.051, 0.057)	0.100 (0.096, 0.104)	0.160 (0.154, 0.165)
Portugal	0.000 (0.000, 0.000)	0.000 (0.000, 0.001)	0.001 (0.001, 0.001)	0.002 (0.002, 0.003)	0.004 (0.004, 0.005)
Romania	0.000 (0.000, 0.000)	0.000 (0.000, 0.000)	0.000 (0.000, 0.001)	0.001 (0.001, 0.001)	0.002 (0.002, 0.002)
S. Sudan	0.001 (0.001, 0.002)	0.006 (0.005, 0.007)	0.016 (0.015, 0.017)	0.031 (0.029, 0.032)	0.051 (0.048, 0.053)
Saudi Arabia	0.001 (0.001, 0.002)	0.007 (0.006, 0.008)	0.020 (0.018, 0.021)	0.038 (0.036, 0.041)	0.063 (0.060, 0.067)
Senegal	0.006 (0.004, 0.007)	0.019 (0.017, 0.022)	0.044 (0.041, 0.048)	0.081 (0.075, 0.087)	0.129 (0.121, 0.137)
Serbia	0.000 (0.000, 0.000)	0.000 (0.000, 0.000)	0.000 (0.000, 0.001)	0.001 (0.001, 0.001)	0.002 (0.002, 0.002)
Sierra Leone	0.003 (0.002, 0.004)	0.013 (0.011, 0.014)	0.032 (0.030, 0.034)	0.061 (0.058, 0.064)	0.100 (0.095, 0.104)
Slovakia	0.000 (0.000, 0.000)	0.000 (0.000, 0.000)	0.000 (0.000, 0.000)	0.000 (0.000, 0.000)	0.001 (0.000, 0.001)
Slovenia	0.000 (0.000, 0.000)	0.000 (0.000, 0.000)	0.001 (0.000, 0.001)	0.001 (0.001, 0.001)	0.002 (0.002, 0.002)
Somalia	0.004 (0.003, 0.004)	0.014 (0.013, 0.016)	0.034 (0.032, 0.037)	0.064 (0.061, 0.068)	0.104 (0.100, 0.109)
Somaliland	0.001 (0.001, 0.002)	0.006 (0.005, 0.007)	0.017 (0.015, 0.018)	0.033 (0.031, 0.035)	0.056 (0.053, 0.059)
South Korea	0.001 (0.000, 0.001)	0.003 (0.003, 0.004)	0.009 (0.008, 0.010)	0.018 (0.017, 0.020)	0.030 (0.028, 0.032)
Spain	0.000 (0.000, 0.000)	0.000 (0.000, 0.000)	0.001 (0.001, 0.001)	0.001 (0.001, 0.002)	0.002 (0.002, 0.003)
Sri Lanka	0.007 (0.006, 0.008)	0.026 (0.024, 0.029)	0.063 (0.060, 0.067)	0.117 (0.112, 0.123)	0.189 (0.182, 0.196)
Sudan	0.001 (0.001, 0.002)	0.005 (0.005, 0.006)	0.014 (0.013, 0.016)	0.028 (0.026, 0.030)	0.047 (0.044, 0.049)
Suriname	0.003 (0.002, 0.004)	0.011 (0.010, 0.013)	0.028 (0.026, 0.031)	0.054 (0.050, 0.057)	0.087 (0.083, 0.092)
Syria	0.000 (0.000, 0.001)	0.003 (0.002, 0.003)	0.008 (0.007, 0.009)	0.016 (0.015, 0.018)	0.028 (0.026, 0.029)
Tanzania	0.000 (0.000, 0.000)	0.000 (0.000, 0.000)	0.001 (0.001, 0.001)	0.002 (0.001, 0.002)	0.003 (0.002, 0.003)
Thailand	0.003 (0.002, 0.004)	0.011 (0.009, 0.013)	0.026 (0.024, 0.029)	0.050 (0.046, 0.053)	0.080 (0.075, 0.086)
Tunisia	0.000 (0.000, 0.001)	0.002 (0.001, 0.002)	0.005 (0.004, 0.006)	0.010 (0.009, 0.011)	0.018 (0.016, 0.019)
Turkey	0.000 (0.000, 0.000)	0.000 (0.000, 0.000)	0.000 (0.000, 0.000)	0.001 (0.001, 0.001)	0.001 (0.001, 0.001)
Turkmenistan	0.000 (0.000, 0.000)	0.000 (0.000, 0.001)	0.001 (0.001, 0.001)	0.003 (0.002, 0.003)	0.004 (0.004, 0.005)
Uganda	0.000 (0.000, 0.000)	0.000 (0.000, 0.000)	0.001 (0.001, 0.001)	0.002 (0.002, 0.002)	0.004 (0.003, 0.004)
Ukraine	0.000 (0.000, 0.000)	0.000 (0.000, 0.000)	0.000 (0.000, 0.000)	0.001 (0.000, 0.001)	0.001 (0.001, 0.001)
United Arab Emirates	0.023 (0.020, 0.026)	0.060 (0.055, 0.066)	0.112 (0.103, 0.121)	0.177 (0.164, 0.190)	0.255 (0.237, 0.273)
United States of America	0.000 (0.000, 0.000)	0.001 (0.001, 0.001)	0.002 (0.002, 0.003)	0.005 (0.005, 0.006)	0.009 (0.008, 0.010)
Uruguay	0.001 (0.000, 0.001)	0.002 (0.001, 0.003)	0.005 (0.004, 0.006)	0.009 (0.008, 0.010)	0.014 (0.013, 0.016)
Uzbekistan	0.000 (0.000, 0.000)	0.000 (0.000, 0.000)	0.000 (0.000, 0.001)	0.001 (0.001, 0.001)	0.002 (0.001, 0.002)
Venezuela	0.004 (0.003, 0.004)	0.015 (0.014, 0.017)	0.039 (0.036, 0.042)	0.075 (0.070, 0.079)	0.122 (0.116, 0.128)
Vietnam	0.003 (0.002, 0.003)	0.010 (0.008, 0.011)	0.024 (0.022, 0.026)	0.046 (0.042, 0.049)	0.074 (0.070, 0.079)
W. Sahara	0.002 (0.002, 0.003)	0.009 (0.008, 0.010)	0.021 (0.019, 0.023)	0.039 (0.037, 0.042)	0.063 (0.060, 0.067)
Yemen	0.001 (0.000, 0.001)	0.003 (0.002, 0.003)	0.007 (0.007, 0.008)	0.014 (0.013, 0.015)	0.023 (0.022, 0.025)
Zambia	0.000 (0.000, 0.000)	0.000 (0.000, 0.000)	0.001 (0.001, 0.001)	0.002 (0.002, 0.002)	0.003 (0.003, 0.003)
Zimbabwe	0.000 (0.000, 0.000)	0.000 (0.000, 0.000)	0.001 (0.001, 0.001)	0.002 (0.002, 0.002)	0.004 (0.003, 0.004)

FIGURE S2.3: Heatmap showing country-level losses (low workload). Unaffected countries are left out of this table.

TABLE S2.1: Polynomial coefficients for country-level labour productivity damage function $Loss(T) = a_0 + a_1T + a_2T^2$

Country	a_0(low)	a_1(low)	a_2(low)	a_0(moderate)	a_1(moderate)	a_2(moderate)	a_0(high)	a_1(high)	a_2(high)
Fiji	0.002492	-0.002132	0.005218	-0.005162	0.049709	0.008614	-0.012063	0.107242	0.002507
Tanzania	0.000083	-0.000169	0.000135	0.000418	-0.000403	0.002315	-0.001129	0.004509	0.005621
W. Sahara	0.001348	-0.002075	0.002897	-0.002329	0.019950	0.004763	-0.003918	0.041644	0.002677
Canada	0.000033	-0.000070	0.000032	0.000613	-0.001356	0.000706	0.001631	-0.003711	0.002070
United States of America	0.000418	-0.000833	0.000508	0.001946	-0.002435	0.004131	0.000475	0.005439	0.005974
Kazakhstan	0.000017	-0.000036	0.000018	0.000352	-0.000806	0.000454	0.000992	-0.002347	0.001417
Uzbekistan	0.000073	-0.000140	0.000089	0.000715	-0.001045	0.001266	0.001034	-0.000487	0.002858
Papua New Guinea	0.000539	-0.000906	0.000751	0.003906	-0.001042	0.008342	0.002502	0.020207	0.014280
Indonesia	0.002982	-0.004938	0.004243	0.002304	0.021562	0.017571	-0.012909	0.104964	0.010421
Argentina	0.000069	-0.000120	0.000096	0.000703	-0.000574	0.001409	0.001036	0.001096	0.003207
Chile	0.000000	-0.000000	0.000000	0.000003	-0.000007	0.000003	0.000012	-0.000025	0.000010
Dem. Rep. Congo	0.000367	-0.000644	0.000505	0.002921	-0.001162	0.006014	0.002714	0.013050	0.011175
Somalia	0.002850	-0.004147	0.004884	-0.003340	0.037364	0.012368	-0.015991	0.110744	0.005576
Kenya	0.000064	-0.000148	0.000090	0.000987	-0.002624	0.002186	0.002105	-0.006433	0.006665
Sudan	0.001688	-0.002935	0.002396	0.000733	0.011901	0.008042	-0.004271	0.047201	0.005597
Chad	0.002874	-0.004911	0.004450	-0.003371	0.029726	0.008025	-0.010012	0.078634	0.001116
Haiti	0.003653	-0.004325	0.006152	-0.001898	0.052083	0.009944	-0.005286	0.119283	0.002063
Dominican Rep.	0.002781	-0.003246	0.004498	-0.000087	0.039703	0.009714	-0.003183	0.100151	0.003888
Russia	0.000005	-0.000011	0.000005	0.000159	-0.000338	0.000154	0.000529	-0.001133	0.000523
Bahamas	0.000000	0.000000	0.000000	0.000000	0.000000	0.000000	0.000000	0.000000	0.000000
Falkland Is.	0.000000	0.000000	0.000000	0.000000	0.000000	0.000000	0.000000	0.000000	0.000000
Norway	-0.000000	0.000000	-0.000000	-0.000000	0.000000	-0.000000	-0.000000	0.000000	-0.000000
Greenland	0.000000	0.000000	0.000000	0.000000	0.000000	0.000000	0.000000	0.000000	0.000000
Fr. S. Antarctic Lands	0.000000	0.000000	0.000000	0.000000	0.000000	0.000000	0.000000	0.000000	0.000000
Timor-Leste	0.000000	0.000000	0.000000	0.000000	0.000000	0.000000	0.000000	0.000000	0.000000
South Africa	0.000025	-0.000053	0.000027	0.000576	-0.001296	0.000733	0.001728	-0.003969	0.002369
Lesotho	0.000002	-0.000004	0.000002	0.000070	-0.000140	0.000056	0.000252	-0.000502	0.000200
Mexico	0.000052	-0.000117	0.000072	0.000565	-0.001554	0.001535	0.000621	-0.002661	0.004357
Uruguay	0.000373	-0.000493	0.000663	0.000310	0.004017	0.002707	-0.000725	0.013017	0.003319
Brazil	0.000313	-0.000541	0.000445	0.002131	-0.000721	0.004870	0.001476	0.010151	0.008704
Bolivia	0.000002	-0.000004	0.000001	0.000082	-0.000157	0.000058	0.000305	-0.000585	0.000215
Peru	0.000002	-0.000005	0.000002	0.000096	-0.000184	0.000067	0.000360	-0.000685	0.000249
Colombia	0.000196	-0.000386	0.000267	0.001448	-0.001704	0.004265	-0.000449	0.006356	0.009759
Panama	0.002943	-0.004662	0.003880	0.004991	0.017232	0.016332	-0.005563	0.090015	0.011456
Costa Rica	0.003301	-0.004857	0.004708	0.002932	0.026193	0.015551	-0.006510	0.095569	0.010042
Nicaragua	0.001473	-0.002144	0.002310	-0.000439	0.019922	0.010736	-0.013074	0.083761	0.007334
Honduras	0.001419	-0.002812	0.002531	-0.002859	0.014226	0.012417	-0.019639	0.072389	0.010517
El Salvador	0.000000	0.000000	0.000000	0.000000	0.000000	0.000000	0.000000	0.000000	0.000000
Guatemala	0.001151	-0.002207	0.001546	0.004965	-0.003184	0.011620	0.001725	0.022613	0.016406
Belize	0.000000	0.000000	0.000000	0.000000	0.000000	0.000000	0.000000	0.000000	0.000000
Venezuela	0.003372	-0.005747	0.005885	-0.007000	0.045134	0.013317	-0.022143	0.131891	0.002924
Guyana	0.002892	-0.003724	0.004316	0.001831	0.033653	0.012671	-0.004359	0.103627	0.006084
Suriname	0.002704	-0.004096	0.004206	0.000245	0.028291	0.014550	-0.011836	0.102935	0.008545
France	0.000024	-0.000049	0.000026	0.000380	-0.000760	0.000491	0.000927	-0.001816	0.001353
Ecuador	0.000122	-0.000269	0.000170	0.001211	-0.003076	0.003421	0.000960	-0.003908	0.009353
Puerto Rico	0.000000	0.000000	0.000000	0.000000	0.000000	0.000000	0.000000	0.000000	0.000000
Jamaica	0.000000	0.000000	0.000000	0.000000	0.000000	0.000000	0.000000	0.000000	0.000000
Cuba	0.004218	-0.004560	0.007686	-0.004306	0.065030	0.007907	-0.006535	0.129975	-0.000989
Zimbabwe	0.000164	-0.000299	0.000201	0.001616	-0.001659	0.002750	0.002242	0.001736	0.005859
Botswana	0.000232	-0.000440	0.000270	0.002134	-0.002814	0.003416	0.002837	0.000221	0.006925
Namibia	0.000087	-0.000176	0.000120	0.000738	-0.001173	0.002026	0.000277	0.001018	0.004920
Senegal	0.003392	-0.003462	0.005720	0.000962	0.038715	0.009191	0.001718	0.075595	0.006230
Mali	0.003894	-0.005401	0.006305	-0.001718	0.042606	0.007290	-0.001983	0.083827	0.000585
Mauritania	0.002572	-0.000472	0.006485	-0.002825	0.050621	0.003493	-0.000572	0.071186	0.000410
Benin	0.002936	-0.003879	0.005502	-0.007343	0.045741	0.009395	-0.020552	0.111493	0.000399
Niger	0.004300	-0.006365	0.007495	-0.002969	0.044918	0.006221	-0.001959	0.079056	0.000127
Nigeria	0.003110	-0.005064	0.004768	-0.002644	0.032207	0.010266	-0.011310	0.091392	0.003004
Cameroon	0.000946	-0.001723	0.001443	0.001776	0.004601	0.009262	-0.004684	0.038610	0.010514

Continued on next page

Table S2.1 (continued)

Country	a_0(low)	a_1(low)	a_2(low)	a_0(moderate)	a_1(moderate)	a_2(moderate)	a_0(high)	a_1(high)	a_2(high)
Togo	0.000000	0.000000	0.000000	0.000000	0.000000	0.000000	0.000000	0.000000	0.000000
Ghana	0.003991	-0.004645	0.006351	-0.003662	0.049574	0.009213	-0.013121	0.114338	-0.000192
Côte d'Ivoire	0.002600	-0.004308	0.004323	-0.003492	0.029486	0.011278	-0.015696	0.091850	0.004474
Guinea	0.002636	-0.004504	0.003992	-0.000441	0.022701	0.011480	-0.008514	0.077523	0.006134
Guinea-Bissau	0.003851	-0.005027	0.006781	-0.001927	0.047226	0.009868	-0.004182	0.100336	0.002250
Liberia	0.001596	-0.002959	0.003058	-0.003868	0.019423	0.011481	-0.018257	0.073454	0.008197
Sierra Leone	0.002687	-0.004520	0.004779	-0.004065	0.031496	0.012569	-0.016456	0.095509	0.005882
Burkina Faso	0.003614	-0.003844	0.008067	-0.007553	0.064431	0.004129	-0.006982	0.103952	-0.003649
Central African Rep.	0.001277	-0.001958	0.002020	0.001000	0.013502	0.009578	-0.006428	0.059229	0.007757
Congo	0.001545	-0.002686	0.002516	-0.000005	0.014567	0.013335	-0.014427	0.077976	0.011194
Gabon	0.001647	-0.002917	0.002328	0.003426	0.006144	0.014507	-0.008422	0.061838	0.014729
Eq. Guinea	0.000000	0.000000	0.000000	0.000000	0.000000	0.000000	0.000000	0.000000	0.000000
Zambia	0.000122	-0.000224	0.000159	0.001140	-0.000966	0.002437	0.001046	0.003321	0.005487
Malawi	0.000318	-0.000536	0.000430	0.002035	-0.000068	0.004389	0.001333	0.012102	0.007354
Mozambique	0.000587	-0.000999	0.000833	0.002157	0.001713	0.006373	-0.000693	0.022100	0.008627
eSwatini	0.000259	-0.000473	0.000303	0.001957	-0.002142	0.003184	0.002539	0.001407	0.006022
Angola	0.000168	-0.000315	0.000229	0.001443	-0.001064	0.003447	0.000788	0.006228	0.007545
Burundi	0.000027	-0.000057	0.000025	0.000902	-0.001924	0.000854	0.003168	-0.006786	0.003032
Israel	0.000705	-0.001266	0.000963	0.001252	0.002162	0.003874	0.000251	0.013287	0.004552
Lebanon	0.000000	0.000000	0.000000	0.000000	0.000000	0.000000	0.000000	0.000000	0.000000
Madagascar	0.000179	-0.000290	0.000242	0.001728	-0.000470	0.003119	0.002417	0.006520	0.006206
Palestine	0.000000	0.000000	0.000000	0.000000	0.000000	0.000000	0.000000	0.000000	0.000000
Gambia	0.000000	0.000000	0.000000	0.000000	0.000000	0.000000	0.000000	0.000000	0.000000
Tunisia	0.000751	-0.001384	0.000947	0.001680	0.001127	0.004218	0.000590	0.013105	0.004677
Algeria	0.000332	-0.000639	0.000382	0.001798	-0.001921	0.003141	0.001518	0.003614	0.004834
Jordan	0.000653	-0.001210	0.000885	0.001348	0.001514	0.004127	0.000057	0.013347	0.004744
United Arab Emirates	-0.001616	0.017444	0.006780	-0.002965	0.056304	0.001941	-0.001313	0.067760	0.000872
Qatar	0.000000	0.000000	0.000000	0.000000	0.000000	0.000000	0.000000	0.000000	0.000000
Kuwait	0.000000	0.000000	0.000000	0.000000	0.000000	0.000000	0.000000	0.000000	0.000000
Iraq	0.001142	-0.002079	0.001683	0.000294	0.006861	0.005011	-0.002192	0.025097	0.003914
Oman	0.002929	0.001805	0.009198	-0.004060	0.058115	0.003195	-0.002664	0.074418	0.000865
Vanuatu	0.000000	0.000000	0.000000	0.000000	0.000000	0.000000	0.000000	0.000000	0.000000
Cambodia	0.003706	-0.004775	0.004898	0.003558	0.029593	0.011957	-0.001266	0.086944	0.006353
Thailand	0.002777	-0.003559	0.003814	0.002911	0.021940	0.010504	-0.001353	0.065861	0.007212
Laos	0.002320	-0.003560	0.003156	0.002005	0.015596	0.009523	-0.002645	0.053825	0.006762
Myanmar	0.001543	-0.002352	0.002162	0.002275	0.009395	0.008813	-0.002585	0.041468	0.007636
Vietnam	0.002657	-0.003699	0.003607	0.002148	0.020878	0.009682	-0.002117	0.062901	0.006089
North Korea	0.000409	-0.000771	0.000536	0.001047	0.000285	0.003101	-0.000473	0.009251	0.003561
South Korea	0.001096	-0.001929	0.001545	0.000096	0.007307	0.004241	-0.002528	0.025167	0.002527
Mongolia	0.000009	-0.000020	0.000010	0.000179	-0.000410	0.000244	0.000498	-0.001166	0.000743
India	0.002661	-0.003617	0.004402	-0.002182	0.029564	0.006935	-0.005887	0.062852	0.002425
Bangladesh	0.003057	0.001612	0.007974	-0.005758	0.052532	0.004960	-0.007537	0.070351	0.001505
Bhutan	0.000012	-0.000024	0.000010	0.000396	-0.000825	0.000352	0.001388	-0.002902	0.001244
Nepal	0.000031	-0.000071	0.000042	0.000476	-0.001229	0.000985	0.000999	-0.002955	0.002969
Pakistan	0.002036	-0.001316	0.005203	-0.004026	0.037424	0.002639	-0.003496	0.054240	-0.000362
Afghanistan	0.000003	-0.000005	0.000002	0.000088	-0.000179	0.000074	0.000313	-0.000635	0.000262
Tajikistan	0.000002	-0.000005	0.000002	0.000075	-0.000154	0.000066	0.000263	-0.000540	0.000232
Kyrgyzstan	-0.000000	0.000000	0.000000	-0.000000	0.000000	0.000000	-0.000000	0.000000	0.000000
Turkmenistan	0.000196	-0.000361	0.000242	0.001214	-0.001087	0.002255	0.001186	0.002555	0.003888
Iran	0.000094	-0.000187	0.000110	0.000919	-0.001540	0.001535	0.001303	-0.001209	0.003396
Syria	0.001096	-0.002094	0.001486	0.000847	0.003894	0.005123	-0.001885	0.021130	0.004271
Armenia	0.000007	-0.000014	0.000006	0.000219	-0.000461	0.000200	0.000750	-0.001590	0.000697
Sweden	0.000001	-0.000002	0.000001	0.000023	-0.000050	0.000026	0.000074	-0.000163	0.000087
Belarus	0.000011	-0.000021	0.000012	0.000161	-0.000316	0.000226	0.000386	-0.000737	0.000622
Ukraine	0.000048	-0.000097	0.000057	0.000514	-0.000935	0.000829	0.000918	-0.001373	0.001972
Poland	0.000013	-0.000027	0.000016	0.000200	-0.000382	0.000290	0.000478	-0.000867	0.000791
Austria	0.000011	-0.000022	0.000010	0.000239	-0.000512	0.000255	0.000706	-0.001532	0.000794
Hungary	0.000068	-0.000135	0.000079	0.000630	-0.001061	0.000988	0.001045	-0.001205	0.002145
Moldova	0.000051	-0.000105	0.000060	0.000570	-0.001067	0.000879	0.001039	-0.001667	0.002077
Romania	0.000087	-0.000173	0.000102	0.000846	-0.001387	0.001347	0.001307	-0.001251	0.002919

Continued on next page

Table S2.1 (continued)

Country	a_0(low)	a_1(low)	a_2(low)	a_0(moderate)	a_1(moderate)	a_2(moderate)	a_0(high)	a_1(high)	a_2(high)
Lithuania	0.000007	-0.000014	0.000008	0.000104	-0.000193	0.000148	0.000254	-0.000446	0.000406
Latvia	0.000004	-0.000007	0.000005	0.000059	-0.000112	0.000087	0.000153	-0.000276	0.000248
Estonia	0.000000	-0.000000	0.000000	0.000004	-0.000008	0.000003	0.000014	-0.000028	0.000011
Germany	0.000008	-0.000017	0.000009	0.000147	-0.000298	0.000196	0.000392	-0.000787	0.000571
Bulgaria	0.000139	-0.000270	0.000159	0.001158	-0.001660	0.001789	0.001622	-0.000537	0.003500
Greece	0.000294	-0.000563	0.000340	0.001662	-0.001764	0.002835	0.001539	0.003019	0.004442
Turkey	0.000067	-0.000136	0.000079	0.000729	-0.001348	0.001235	0.001125	-0.001613	0.002923
Albania	0.000000	0.000000	0.000000	0.000000	0.000000	0.000000	0.000000	0.000000	0.000000
Croatia	0.000159	-0.000307	0.000195	0.000989	-0.001158	0.001757	0.001142	0.000909	0.003065
Switzerland	0.000004	-0.000009	0.000004	0.000117	-0.000246	0.000111	0.000386	-0.000815	0.000372
Luxembourg	0.000000	0.000000	0.000000	0.000000	0.000000	0.000000	0.000000	0.000000	0.000000
Belgium	0.000002	-0.000004	0.000002	0.000060	-0.000128	0.000067	0.000205	-0.000440	0.000236
Netherlands	0.000003	-0.000006	0.000004	0.000068	-0.000134	0.000094	0.000207	-0.000398	0.000298
Portugal	0.000176	-0.000335	0.000229	0.001067	-0.001103	0.002136	0.001026	0.001846	0.003768
Spain	0.000123	-0.000242	0.000138	0.001169	-0.001888	0.001803	0.001666	-0.001324	0.003791
Ireland	0.000001	-0.000001	0.000001	0.000014	-0.000027	0.000015	0.000041	-0.000079	0.000045
New Caledonia	0.000000	0.000000	0.000000	0.000000	0.000000	0.000000	0.000000	0.000000	0.000000
Solomon Is.	0.000000	0.000000	0.000000	0.000000	0.000000	0.000000	0.000000	0.000000	0.000000
New Zealand	0.000002	-0.000004	0.000002	0.000056	-0.000127	0.000063	0.000195	-0.000442	0.000221
Australia	0.000028	-0.000053	0.000049	0.000253	-0.000213	0.000816	0.000245	0.000738	0.002048
Sri Lanka	0.004993	-0.006660	0.008688	-0.006514	0.066422	0.013468	-0.018312	0.157846	-0.000021
China	0.000806	-0.001467	0.001027	0.001526	0.001792	0.004875	-0.001179	0.017634	0.004611
Taiwan	0.000000	0.000000	0.000000	0.000000	0.000000	0.000000	0.000000	0.000000	0.000000
Italy	0.000072	-0.000145	0.000078	0.000809	-0.001498	0.001159	0.001412	-0.002192	0.002689
Denmark	0.000002	-0.000004	0.000003	0.000031	-0.000058	0.000054	0.000086	-0.000148	0.000157
United Kingdom	0.000002	-0.000004	0.000002	0.000043	-0.000084	0.000049	0.000130	-0.000252	0.000155
Iceland	0.000000	0.000000	0.000000	0.000000	0.000000	0.000000	0.000000	0.000000	0.000000
Azerbaijan	0.000096	-0.000185	0.000118	0.000840	-0.001199	0.001454	0.001205	-0.000465	0.003060
Georgia	0.000023	-0.000049	0.000027	0.000379	-0.000820	0.000571	0.000902	-0.001984	0.001643
Philippines	0.004028	-0.004856	0.007192	-0.006678	0.064311	0.010852	-0.016453	0.147638	-0.000799
Malaysia	0.003283	-0.005732	0.004356	0.004263	0.013783	0.018723	-0.010509	0.089776	0.013484
Brunei	0.002570	-0.004459	0.003136	0.007699	0.002706	0.017552	-0.001794	0.061654	0.016913
Slovenia	0.000090	-0.000176	0.000105	0.000784	-0.001238	0.001266	0.001164	-0.000905	0.002637
Finland	0.000001	-0.000002	0.000001	0.000026	-0.000052	0.000028	0.000076	-0.000158	0.000088
Slovakia	0.000028	-0.000056	0.000031	0.000351	-0.000685	0.000503	0.000746	-0.001368	0.001274
Czechia	0.000010	-0.000022	0.000011	0.000204	-0.000428	0.000242	0.000566	-0.001193	0.000721
Eritrea	0.001021	-0.001709	0.001430	0.002198	0.004995	0.007298	-0.000230	0.028703	0.008930
Japan	0.000868	-0.001561	0.001118	0.001274	0.003035	0.004735	-0.001496	0.020111	0.003993
Paraguay	0.002228	-0.003745	0.004091	-0.002237	0.022303	0.008640	-0.007327	0.056037	0.006358
Yemen	0.000836	-0.001417	0.001189	0.002119	0.003535	0.006773	-0.000383	0.024902	0.008059
Saudi Arabia	0.002201	-0.003941	0.003240	-0.000607	0.015090	0.006382	-0.003224	0.040767	0.004113
Antarctica	0.000000	0.000000	0.000000	0.000000	0.000000	0.000000	0.000000	0.000000	0.000000
N. Cyprus	0.000000	0.000000	0.000000	0.000000	0.000000	0.000000	0.000000	0.000000	0.000000
Cyprus	0.000000	0.000000	0.000000	0.000000	0.000000	0.000000	0.000000	0.000000	0.000000
Morocco	0.000193	-0.000363	0.000242	0.001325	-0.001308	0.002533	0.001170	0.002964	0.004461
Egypt	0.002032	-0.003982	0.002518	0.001006	0.005464	0.006660	-0.002829	0.029245	0.004851
Libya	0.000803	-0.001535	0.000980	0.001943	0.000180	0.004836	0.000213	0.013901	0.005341
Ethiopia	0.000032	-0.000069	0.000031	0.000984	-0.002151	0.000991	0.003330	-0.007342	0.003433
Djibouti	0.005398	-0.004782	0.009447	-0.001647	0.062225	0.008555	-0.004249	0.111036	0.002335
Somaliland	0.002127	-0.003767	0.002895	0.002423	0.010211	0.011898	-0.004920	0.055553	0.009661
Uganda	0.000118	-0.000230	0.000188	0.000739	-0.000571	0.003169	-0.000838	0.005740	0.007676
Rwanda	0.000000	0.000000	0.000000	0.000000	0.000000	0.000000	0.000000	0.000000	0.000000
Bosnia and Herz.	0.000139	-0.000268	0.000165	0.001020	-0.001344	0.001726	0.001241	0.000369	0.003203
North Macedonia	0.000051	-0.000105	0.000058	0.000618	-0.001246	0.000978	0.001119	-0.002122	0.002455
Serbia	0.000085	-0.000172	0.000101	0.000795	-0.001355	0.001314	0.001143	-0.001126	0.002803
Montenegro	0.000000	0.000000	0.000000	0.000000	0.000000	0.000000	0.000000	0.000000	0.000000
Kosovo	0.000064	-0.000131	0.000073	0.000699	-0.001342	0.001117	0.001144	-0.001881	0.002646
Trinidad and Tobago	0.000000	0.000000	0.000000	0.000000	0.000000	0.000000	0.000000	0.000000	0.000000
S. Sudan	0.001775	-0.003061	0.002574	0.001405	0.012469	0.011468	-0.007659	0.063244	0.009191

S2.2 Agricultural damage functions

TABLE S2.2: Cereal/Grains sectoral output (yield) shock per country (average of maize and soy from Li et al. (2025)[4]). These values correspond to the RCP8.5 scenario for four 20-year periods in the 21st century, showing percentage changes in yield relative to global mean temperature rise. Column headers denote the mean global temperature (°C) within each period. While yield changes are case-specific, the general trend indicates decreasing yields. In some countries, yields initially increase at lower temperatures and begin to decline at higher temperatures. In certain cases (e.g., Indonesia), yield changes remain positive across all temperature levels, albeit at varying rates.

Country	**0.45°**	**1.53°**	**2.87°**	**4.36°**	**Country**	**0.45°**	**1.53°**	**2.87°**	**4.36°**
Afghanistan	-1.97	-4.389	-12.336	-26.817	Angola	-0.708	-3.135	-9.670	-20.992
Albania	-0.909	-4.246	-12.216	-26.450	Argentina	2.256	2.829	0.675	-4.639
Armenia	-2.224	-5.897	-14.885	-30.850	Australia	1.349	0.387	-4.594	-14.075
Austria	2.444	1.608	-3.141	-13.719	Azerbaijan	0.890	-1.604	-8.749	-22.095
Burundi	2.263	1.747	-2.454	-10.618	Belgium	2.006	1.859	-1.580	-9.293
Benin	5.518	5.465	2.088	-4.861	Burkina Faso	2.425	1.393	-3.702	-14.258
Bangladesh	-0.271	-1.652	-6.453	-15.417	Bulgaria	-0.966	-3.436	-10.095	-23.249
Bosnia and Herzegovina	1.891	0.131	-5.822	-18.174	Belarus	5.507	5.085	0.335	-9.697
Belize	3.582	2.174	-2.910	-12.332	Bolivia	0.886	-2.791	-11.308	-26.285
Brazil	1.900	2.224	-1.091	-9.336	Bhutan	-1.326	-2.362	-7.019	-16.016
Botswana	5.902	4.214	-2.075	-14.868	Central African Republic	1.754	1.129	-3.282	-12.022
Canada	-1.581	-6.428	-16.761	-32.703	Switzerland	3.387	2.594	-2.319	-12.498
Chile	2.733	2.478	-1.452	-9.446	China	1.066	-1.086	-8.077	-20.925
Ivory Coast	4.296	3.224	-1.440	-9.820	Cameroon	2.824	1.862	-2.623	-11.329
Congo (Dem. Rep.)	1.668	0.439	-4.555	-13.956	Congo (Rep.)	2.647	1.365	-3.193	-11.424
Colombia	6.436	4.885	-0.711	-10.684	Costa Rica	2.315	0.266	-5.181	-14.449
Czech Republic	4.563	3.971	-0.420	-10.462	Germany	4.850	4.868	1.212	-7.247
Djibouti	7.821	6.934	2.215	-6.531	Denmark	1.099	1.173	-1.836	-8.158
Algeria	0.589	-2.937	-11.179	-25.214	Ecuador	-1.641	-0.866	-2.577	-7.184
Egypt	-2.365	-4.380	-10.107	-20.593	Eritrea	8.258	7.926	3.810	-4.867
Spain	6.107	5.033	-0.604	-11.759	Estonia	3.549	1.849	-4.545	-15.965
Ethiopia	2.647	2.543	-1.027	-8.652	Finland	3.932	2.563	-3.976	-15.896
France	5.973	5.831	1.719	-7.362	Gabon	4.953	4.337	0.754	-6.170
Georgia	-1.283	-5.534	-14.658	-30.728	Ghana	4.885	4.194	-0.023	-8.304
Guinea	3.295	1.697	-3.687	-12.498	Equatorial Guinea	6.968	6.928	4.147	-1.689
Greece	-1.661	-4.623	-11.870	-24.913	Guatemala	-1.102	-2.696	-8.153	-18.734
Guyana	-1.832	-5.567	-13.424	-25.771	Honduras	-1.353	-4.152	-11.106	-22.784
Croatia	0.620	-1.378	-7.517	-20.099	Hungary	1.979	0.248	-5.651	-17.845
Indonesia	5.191	6.674	5.663	2.337	India	3.140	2.554	-2.000	-11.242
Iran	0.569	-2.859	-11.329	-26.330	Iraq	5.081	2.090	-5.811	-20.552
Israel	1.767	-0.481	-6.310	-17.364	Italy	0.353	-2.048	-8.860	-21.864
Jordan	0.394	-2.736	-9.701	-22.215	Japan	0.239	-1.090	-5.906	-15.543
Kazakhstan	-1.141	-4.717	-14.533	-33.139	Kenya	0.428	0.848	-1.933	-7.973
Kyrgyzstan	1.181	-0.076	-6.943	-21.050	Cambodia	2.597	2.423	-0.531	-6.999
South Korea	3.217	1.281	-4.632	-15.015	Kosovo	-1.146	-4.043	-11.560	-25.749
Laos	4.230	4.127	0.786	-6.283	Lebanon	1.224	-2.048	-9.047	-21.549

Continued on next page

Table S2.2 (continued)

Country	0.45°	1.53°	2.87°	4.36°	Country	0.45°	1.53°	2.87°	4.36°
Liberia	2.960	1.233	-3.579	-11.115	Sri Lanka	0.194	0.690	-1.450	-6.117
Lesotho	8.154	7.261	2.031	-8.793	Lithuania	4.622	4.030	-0.582	-9.608
Luxembourg	4.544	4.377	0.735	-7.400	Latvia	3.937	2.557	-3.367	-14.313
Morocco	6.445	5.086	-0.267	-10.535	Moldova	4.759	3.560	-1.913	-13.383
Madagascar	-0.207	-1.784	-6.523	-14.982	Mexico	2.938	1.356	-4.054	-13.969
Macedonia	-0.984	-3.083	-9.633	-22.555	Mali	1.698	0.724	-4.536	-15.462
Myanmar	0.245	-0.712	-4.965	-13.132	Montenegro	0.630	-1.899	-8.892	-22.129
Mongolia	2.353	0.955	-5.919	-20.241	Mozambique	3.996	3.248	-1.601	-11.423
Malawi	3.677	2.763	-2.201	-11.922	Malaysia	1.675	1.411	-1.696	-7.385
Namibia	-0.623	-3.603	-11.142	-23.886	Niger	3.410	2.902	-1.379	-11.044
Nigeria	4.397	3.984	-0.039	-8.134	Nicaragua	-1.197	-4.292	-11.063	-21.987
Netherlands	2.549	2.341	-1.029	-8.426	Nepal	-1.770	-4.026	-10.553	-22.254
Pakistan	-5.925	-9.286	-17.330	-31.763	Panama	4.764	4.204	0.647	-5.883
Peru	-0.979	-2.021	-7.222	-16.733	Philippines	4.046	3.783	0.907	-4.685
Poland	4.250	3.626	-0.958	-10.594	North Korea	1.875	-0.840	-8.137	-20.945
Portugal	6.783	6.138	1.234	-8.303	Paraguay	-1.908	-3.164	-8.208	-18.482
Romania	1.406	-0.566	-6.770	-19.252	Russia	1.097	-1.486	-9.582	-25.105
Rwanda	-0.274	-1.511	-6.540	-15.693	Sudan	6.556	7.183	4.318	-2.762
South Sudan	3.810	4.464	1.813	-4.393	Sierra Leone	3.876	2.650	-1.875	-9.366
El Salvador	2.176	0.405	-5.170	-15.551	Somalia	1.178	0.899	-2.761	-10.512
Serbia	2.819	1.608	-3.791	-15.454	Suriname	-1.201	-2.894	-7.713	-15.385
Slovakia	2.194	0.170	-6.199	-18.754	Slovenia	2.029	1.044	-3.893	-14.999
Swaziland	2.809	1.788	-2.748	-12.157	Syria	-1.427	-5.429	-13.649	-28.236
Chad	0.977	0.084	-4.576	-14.337	Togo	4.047	3.493	-0.336	-7.701
Thailand	3.485	3.042	-0.349	-7.292	Tajikistan	-3.308	-7.139	-17.042	-34.822
Turkmenistan	3.073	1.214	-5.359	-17.998	East Timor	6.732	7.312	5.464	1.174
Turkey	-1.001	-4.583	-12.425	-27.006	Taiwan	1.768	1.572	-1.680	-7.054
Tanzania	0.996	0.231	-4.209	-12.452	Uganda	0.143	0.223	-3.153	-9.906
Ukraine	3.987	2.874	-2.526	-13.564	Uruguay	2.578	2.939	0.341	-5.488
USA	-2.027	-5.718	-14.208	-28.432	Uzbekistan	-1.538	-4.226	-12.049	-26.784
Venezuela	5.322	3.578	-2.181	-12.286	Vietnam	2.175	2.755	0.225	-5.725
South Africa	6.917	6.086	1.173	-9.086	Zambia	4.010	3.227	-1.657	-11.925
Zimbabwe	8.332	7.608	2.646	-8.050	Andorra	7.722	8.535	5.392	-2.839
Gaza	-0.378	-2.375	-7.770	-18.026	Hong Kong S.A.R.	0.399	0.330	-2.708	-8.729
Siachen Glacier	-4.649	-1.610	-2.969	-10.306	Liechtenstein	3.083	1.869	-3.536	-14.481
Macau S.A.R.	2.530	2.351	-0.872	-6.976	Monaco	5.524	6.126	3.087	-4.676
San Marino	0.890	-3.520	-12.677	-28.721					

TABLE S2.3: Paddy rice output (yield) shock per country from Li et al. (2025)[4]. Values correspond to the RCP8.5 scenario for four 20-year periods, with columns indicating the mean global temperature (°C) in each period. As in the cereal/grains case, yield changes are case-specific. In some instances, a large positive yield change (e.g., in Switzerland) does not imply a strong economic response, since baseline rice yields are very low in these regions. GTAP-INT 2 accounts for this by incorporating baseline yield information.

Country	0.45°	1.53°	2.87°	4.36°	Country	0.45°	1.53°	2.87°	4.36°
Afghanistan	4.425	2.109	-0.289	-0.254	Angola	-2.470	-4.983	-8.527	-11.795
Albania	1.436	0.050	-1.647	-2.299	Argentina	2.338	0.117	-3.772	-7.970
Armenia	1.358	-0.011	-1.010	0.032	Australia	-0.748	-2.915	-6.270	-9.229
Austria	6.883	12.943	19.932	29.766	Azerbaijan	5.399	1.120	-3.830	-8.031
Burundi	2.739	1.254	-1.376	-3.711	Benin	2.206	-3.103	-10.360	-18.504

Continued on next page

Table S2.3 (continued)

Country	0.45°	1.53°	2.87°	4.36°	Country	0.45°	1.53°	2.87°	4.36°
Burkina Faso	0.195	-5.693	-13.409	-21.528	Bangladesh	-2.665	-7.975	-14.540	-21.614
Bulgaria	-2.521	-4.065	-5.885	-6.612	Belarus	4.959	2.759	0.122	-1.396
Belize	1.811	-3.327	-10.273	-17.384	Bolivia	-5.692	-11.013	-17.066	-22.114
Brazil	5.162	0.852	-5.022	-10.870	Brunei	-1.174	-4.620	-9.764	-15.290
Bhutan	-4.473	-7.393	-11.366	-15.140	Botswana	2.202	-3.973	-11.111	-17.557
Central African Republic	-0.099	-3.216	-8.239	-13.567	Switzerland	5.461	10.143	15.598	23.471
Chile	-0.541	0.642	1.279	2.510	China	-0.921	-3.633	-7.087	-9.778
Ivory Coast	0.913	-3.957	-10.285	-16.796	Cameroon	-0.980	-4.113	-8.633	-13.378
Congo (DR)	-0.787	-3.397	-7.485	-11.674	Congo (Rep.)	-2.286	-5.876	-10.696	-15.780
Colombia	2.476	-0.723	-5.273	-9.495	Costa Rica	5.150	0.496	-5.810	-12.286
Cuba	5.700	1.015	-5.704	-12.854	Djibouti	-2.111	-9.723	-19.380	-28.953
Dominican Republic	-0.079	-2.510	-6.287	-9.997	Algeria	-1.590	-4.909	-9.108	-12.655
Ecuador	4.937	2.550	-1.233	-4.921	Egypt	-1.169	-6.116	-12.265	-18.817
Eritrea	2.420	-3.879	-12.005	-20.299	Spain	2.378	0.980	-1.112	-2.125
Ethiopia	3.252	0.577	-3.258	-6.877	France	2.007	1.154	-0.360	-0.953
Gabon	-0.124	-3.997	-9.410	-15.293	Georgia	0.921	2.003	3.509	7.151
Ghana	1.496	-3.565	-10.500	-17.972	Guinea	-1.981	-5.816	-11.046	-16.091
Gambia	0.412	-4.743	-11.618	-18.759	Guinea Bissau	1.046	-3.645	-10.132	-16.815
Equatorial Guinea	2.959	-0.590	-5.606	-11.077	Greece	-4.112	-6.242	-8.830	-10.544
Guatemala	1.064	-2.685	-7.761	-12.576	Guyana	-3.290	-7.447	-13.167	-19.007
Honduras	-1.241	-4.492	-8.767	-12.557	Haiti	3.975	0.297	-4.847	-10.036
Hungary	0.617	-2.209	-5.591	-8.350	Indonesia	11.460	6.972	0.495	-6.453
India	0.098	-5.946	-13.435	-21.327	Iran	7.458	1.638	-5.230	-11.378
Iraq	-7.135	-19.656	-33.579	-47.378	Italy	1.876	0.085	-2.346	-3.998
Jamaica	9.548	5.793	0.222	-5.765	Japan	1.176	-0.070	-1.895	-3.201
Kazakhstan	1.600	-1.921	-5.649	-7.762	Kenya	2.465	-0.391	-4.877	-9.708
Kyrgyzstan	3.568	6.813	11.371	19.189	Cambodia	1.307	-3.317	-9.683	-16.550
South Korea	-2.195	-3.639	-5.540	-6.836	Kosovo	0.777	-0.722	-2.496	-3.092
Laos	3.850	-1.161	-7.788	-14.405	Liberia	-1.260	-5.003	-9.875	-14.968
Sri Lanka	1.421	-2.097	-7.486	-13.327	Lesotho	3.003	1.965	0.811	1.044
Morocco	-0.673	-1.516	-2.874	-3.183	Moldova	5.885	1.799	-2.935	-7.072
Madagascar	-2.206	-4.559	-8.252	-12.205	Mexico	1.619	-2.986	-9.493	-15.966
Macedonia	-2.335	-3.712	-5.329	-5.733	Mali	2.972	-4.216	-13.243	-22.259
Myanmar	0.293	-4.584	-10.732	-17.131	Mongolia	3.420	5.449	8.442	14.383
Mozambique	0.009	-4.393	-10.328	-16.355	Mauritania	-5.978	-13.007	-22.000	-31.109
Malawi	3.562	0.067	-4.701	-9.233	Malaysia	-1.383	-4.503	-9.300	-14.472
Namibia	-8.021	-7.906	-7.934	-6.429	Niger	-1.441	-7.801	-16.153	-25.104
Nigeria	-0.414	-4.429	-10.288	-16.721	Nicaragua	-2.494	-6.526	-11.691	-16.677
Nepal	-2.243	-5.541	-9.662	-13.261	Pakistan	-4.153	-11.161	-19.510	-27.524
Panama	-1.105	-4.253	-9.128	-14.311	Peru	5.023	5.309	5.065	5.575
Philippines	-1.894	-4.813	-9.448	-14.566	Papua New Guinea	4.897	1.428	-3.825	-9.618
Poland	3.428	2.041	0.184	-0.699	North Korea	-0.227	-0.249	-0.168	1.325
Portugal	2.786	1.749	-0.392	-2.021	Paraguay	-0.207	-4.417	-9.887	-15.119
Romania	1.567	-1.868	-5.792	-9.101	Russia	3.061	3.600	4.780	8.595
Rwanda	0.865	-0.128	-2.055	-3.580	Sudan	3.258	-3.229	-11.818	-20.847
South Sudan	1.687	-2.626	-9.155	-16.140	Senegal	-2.193	-8.212	-16.006	-23.880
Sierra Leone	-1.288	-5.390	-11.018	-16.993	El Salvador	3.001	-1.373	-7.053	-12.595
Somalia	0.411	-3.798	-9.649	-16.262	Serbia	1.766	-0.071	-2.227	-3.282
Suriname	-5.086	-8.826	-14.320	-19.982	Slovakia	0.428	-0.665	-2.037	-2.312
Swaziland	0.921	-2.458	-6.763	-10.924	Syria	-7.223	-13.375	-19.855	-25.914
Chad	-2.601	-6.480	-12.224	-18.738	Togo	1.531	-3.177	-9.686	-16.807
Thailand	2.116	-3.191	-10.026	-17.092	Tajikistan	0.831	1.830	3.553	8.093
Turkmenistan	-0.668	-6.943	-14.684	-21.657	East Timor	5.974	2.781	-2.087	-7.585
Trinidad & Tobago	-0.652	-3.785	-8.714	-14.155	Tunisia	-0.831	-4.450	-8.949	-13.006
Turkey	-1.644	-3.191	-5.045	-6.110	Taiwan	0.715	-0.770	-3.593	-6.545
Tanzania	-0.764	-3.282	-7.218	-11.060	Uganda	0.292	-2.022	-6.079	-10.235
Ukraine	3.953	0.880	-2.528	-4.984	Uruguay	2.952	1.212	-2.149	-5.843

Continued on next page

Table S2.3 (continued)

Country	0.45°	1.53°	2.87°	4.36°	Country	0.45°	1.53°	2.87°	4.36°
USA	-0.503	-5.120	-10.865	-16.294	Uzbekistan	0.893	-1.892	-5.034	-6.518
Venezuela	1.535	-4.627	-12.279	-19.378	Vietnam	5.181	-0.017	-7.033	-14.383
South Africa	3.777	0.303	-3.854	-7.299	Zambia	-0.272	-3.172	-7.158	-10.731
Zimbabwe	2.612	-2.380	-8.493	-14.290	Andorra	4.395	5.691	6.937	9.816
Hong Kong S.A.R.	2.540	-0.967	-5.855	-10.867	Siachen Glacier	-1.680	4.201	11.979	23.129
Macau S.A.R.	1.687	-1.799	-6.661	-11.634	Monaco	7.535	4.910	1.235	-2.150
San Marino	-4.698	-3.244	-1.741	1.489	French Guiana	-0.419	-4.180	-9.584	-14.960

TABLE S2.4: Wheat output (yield) shock per country from Li et al. (2025)[4]. Values correspond to the RCP8.5 scenario for four 20-year periods, with columns indicating the mean global temperature (°C) in each period. Wheat yields exhibit an optimal temperature at which yield levels peak, followed by a decline as temperatures continue to rise. In some cases, this "optimum" is already exceeded at lower temperature increases, resulting in consistently negative yield changes, while in others, yields initially increase before declining at higher temperatures.

Country	0.45°	1.53°	2.87°	4.36°	Country	0.45°	1.53°	2.87°	4.36°
Afghanistan	0.329	-3.850	-9.681	-16.021	Angola	-3.804	-8.112	-14.297	-21.704
Albania	-0.503	-3.495	-7.686	-12.558	United Arab Emirates	-2.708	-10.300	-20.284	-31.149
Argentina	1.642	0.067	-3.124	-7.426	Armenia	-1.521	-3.030	-5.287	-7.690
Australia	2.226	-0.468	-5.034	-10.404	Austria	4.584	1.889	-2.118	-7.259
Azerbaijan	1.072	-2.307	-6.874	-12.288	Burundi	0.807	-2.348	-7.576	-13.888
Belgium	1.309	-0.188	-3.033	-6.721	Benin	4.890	-0.631	-8.630	-18.920
Burkina Faso	-0.618	-5.944	-13.629	-24.053	Bangladesh	-2.781	-7.688	-14.122	-22.465
Bulgaria	-3.693	-6.818	-10.911	-16.020	Bosnia and Herzegovina	1.220	-1.762	-5.815	-10.843
Belarus	7.233	3.987	-0.618	-5.855	Belize	3.991	-2.303	-10.486	-19.759
Bolivia	-3.135	-8.617	-15.641	-23.634	Brazil	3.472	-0.261	-5.528	-11.916
Bhutan	-2.512	-4.880	-8.557	-13.208	Botswana	8.302	1.349	-7.321	-17.565
Central African Republic	-0.665	-5.009	-11.955	-20.576	Canada	0.615	-1.647	-4.765	-8.108
Switzerland	6.206	3.765	-0.202	-4.833	Chile	1.860	-0.559	-3.864	-7.636
China	-0.535	-3.366	-7.603	-12.663	Cameroon	1.423	-3.233	-10.049	-18.802
Congo (DR)	-0.619	-4.723	-10.961	-18.680	Congo (Rep.)	-1.943	-6.662	-12.985	-20.712
Colombia	7.540	2.953	-3.546	-10.783	Czech Republic	5.455	2.992	-0.819	-5.710
Germany	5.505	3.389	-0.317	-4.895	Denmark	-1.327	-1.712	-3.381	-5.526
Algeria	0.293	-4.428	-10.632	-17.647	Ecuador	2.486	-0.605	-5.299	-10.797
Egypt	-5.074	-9.209	-14.640	-21.131	Eritrea	13.658	7.696	-0.771	-11.153
Spain	4.540	0.781	-4.809	-10.893	Estonia	3.705	1.351	-2.228	-6.043
Ethiopia	1.356	-1.672	-6.549	-12.676	Finland	2.640	0.913	-2.027	-4.969
France	5.173	2.671	-1.551	-6.560	Gabon	5.548	0.564	-6.169	-14.116
United Kingdom	-0.848	-1.305	-3.052	-5.402	Georgia	-1.430	-3.515	-6.458	-9.875
Equatorial Guinea	7.397	2.373	-4.401	-12.421	Greece	-4.807	-7.561	-11.348	-15.767
Guatemala	-2.196	-6.963	-13.460	-21.009	Guyana	-7.270	-12.056	-18.183	-24.773
Honduras	-4.013	-9.073	-15.725	-23.135	Croatia	-0.610	-3.683	-7.867	-13.163
Hungary	0.602	-2.556	-6.954	-12.423	India	1.198	-4.553	-12.283	-21.738
Ireland	-1.539	-1.439	-2.713	-4.526	Iran	2.459	-2.760	-9.185	-16.528
Iraq	6.811	-1.256	-10.397	-20.943	Israel	0.349	-3.981	-9.188	-15.532
Italy	2.478	-0.979	-5.887	-11.806	Jordan	-2.149	-6.830	-12.355	-18.916
Japan	0.025	-0.340	-1.493	-3.047	Kazakhstan	-3.800	-8.384	-14.201	-20.979
Kenya	-1.548	-4.640	-9.672	-16.032	Kyrgyzstan	2.357	0.767	-2.136	-5.371
Cambodia	3.533	-1.774	-8.901	-17.329	South Korea	3.553	1.755	-1.406	-5.163
Kosovo	-1.505	-4.041	-7.631	-11.927	Kuwait	5.445	-3.155	-13.343	-24.830
Laos	1.269	-3.129	-9.434	-16.802	Lebanon	-0.777	-4.555	-9.096	-14.575

Continued on next page

Table S2.4 (continued)

Country	0.45°	1.53°	2.87°	4.36°	Country	0.45°	1.53°	2.87°	4.36°
Libya	7.784	2.753	-3.872	-11.592	Lesotho	12.448	8.245	2.565	-3.796
Lithuania	4.999	2.568	-1.267	-5.560	Luxembourg	4.705	2.618	-1.022	-5.532
Latvia	4.915	2.581	-1.079	-5.133	Morocco	9.018	2.680	-5.007	-13.220
Moldova	6.997	2.345	-3.626	-10.835	Madagascar	-4.837	-8.679	-14.119	-20.698
Mexico	0.990	-4.350	-11.290	-19.374	Macedonia	-3.617	-6.163	-9.732	-13.898
Mali	-2.009	-9.034	-18.296	-29.552	Myanmar	-3.335	-7.752	-13.740	-20.918
Montenegro	-0.497	-2.699	-5.968	-9.820	Mongolia	4.970	5.243	4.850	4.356
Mozambique	5.455	-0.269	-8.205	-17.449	Mauritania	-7.225	-14.303	-23.623	-34.156
Malawi	3.422	-1.212	-7.883	-15.483	Malaysia	1.614	-2.471	-8.620	-15.986
Namibia	-2.409	-7.705	-14.864	-22.972	Niger	1.028	-3.729	-10.557	-20.427
Nigeria	5.643	0.974	-6.098	-16.139	Nicaragua	-5.126	-10.546	-17.319	-24.726
Netherlands	0.862	-0.258	-2.724	-5.995	Norway	-0.627	-0.839	-2.141	-3.732
Nepal	-2.116	-6.580	-12.851	-20.689	New Zealand	-0.071	-0.747	-2.506	-4.915
Oman	16.906	7.626	-4.217	-17.400	Pakistan	-8.910	-14.917	-22.490	-31.627
Peru	15.511	12.573	7.750	1.711	Poland	4.887	2.460	-1.420	-6.212
North Korea	3.742	2.495	0.056	-2.861	Portugal	9.559	5.264	-1.389	-8.466
Paraguay	-3.030	-6.975	-12.523	-19.322	Romania	0.204	-3.720	-8.774	-14.996
Russia	0.710	-3.021	-7.822	-13.338	Rwanda	-4.570	-7.292	-11.811	-17.400
Saudi Arabia	23.799	12.347	-1.693	-17.138	Sudan	13.142	6.126	-3.787	-16.072
South Sudan	5.035	0.446	-6.932	-16.235	Senegal	-2.094	-9.318	-18.323	-28.433
El Salvador	-5.648	-10.603	-17.139	-24.662	Somalia	-1.195	-5.527	-11.422	-19.134
Serbia	2.439	-1.180	-6.011	-11.973	Slovakia	1.234	-1.339	-5.154	-9.971
Slovenia	2.360	-0.364	-4.193	-9.113	Sweden	1.162	0.220	-1.977	-4.533
Swaziland	2.231	-2.030	-7.670	-14.534	Syria	-5.139	-9.289	-14.175	-20.015
Chad	-3.085	-7.933	-14.963	-24.506	Togo	8.571	2.660	-5.891	-15.832
Thailand	1.956	-2.970	-9.602	-17.493	Tajikistan	-5.262	-8.213	-12.564	-17.643
Turkmenistan	-2.361	-7.792	-15.146	-23.648	Tunisia	-3.893	-7.602	-12.701	-18.929
Turkey	-3.336	-6.015	-9.375	-13.378	Tanzania	1.614	-1.561	-6.813	-13.158
Uganda	-1.287	-4.055	-9.311	-15.736	Ukraine	6.774	2.634	-2.778	-9.248
Uruguay	1.952	0.067	-3.895	-9.056	USA	-1.443	-5.001	-9.456	-14.423
Uzbekistan	-4.438	-8.744	-14.617	-21.510	Venezuela	6.291	-1.603	-11.375	-21.756
Vietnam	15.601	10.606	3.497	-4.489	West Bank	-3.394	-7.305	-12.114	-18.007
Yemen	-16.702	-19.819	-24.602	-30.190	South Africa	11.974	6.857	0.285	-7.114
Zambia	5.636	-0.392	-8.455	-18.352	Zimbabwe	10.420	3.865	-4.624	-14.839
Andorra	12.439	9.202	4.022	-1.644	Gaza	-2.342	-6.414	-11.431	-17.649
Hong Kong S.A.R.	-0.157	-4.125	-9.770	-16.292	Siachen Glacier	-8.928	-5.350	-1.493	3.090
Liechtenstein	3.813	1.781	-1.579	-5.582	Macau S.A.R.	0.835	-2.907	-8.355	-14.527
Monaco	9.012	5.301	-0.335	-7.020	San Marino	0.909	-2.284	-6.821	-12.296

S2.3 Mortality rate damage functions

TABLE S2.5: Linear coefficients for the mortality changes (shocks to regional population and labor availability), in percentage change. Based on Bressler et al. (2021), no-income-adaptation scenario.

Region	Intercept	Slope	Region	Intercept	Slope
Afghanistan	-0.33	4.39	Ghana	-0.20	4.33
Albania	-0.14	2.05	Greece	-0.20	1.27
Algeria	-0.35	2.79	Guatemala	-0.09	2.48
Angola	-0.44	2.42	Guinea	-0.34	4.82
Argentina	-0.22	1.36	Guinea-Bissau	-0.21	3.98

Continued on next page

Table S2.5 (continued)

Region	Intercept	Slope	Region	Intercept	Slope
Armenia	-0.24	2.24	Hungary	-0.03	1.08
Australia	-0.24	0.28	Iceland	-0.01	-0.89
Austria	0.04	0.01	India	-0.19	4.17
Azerbaijan	-0.08	2.07	Indonesia	-0.15	2.59
Bahamas	0.01	1.01	Iran	-0.06	2.36
Bangladesh	-0.19	3.46	Iraq	-0.12	4.68
Belarus	-0.08	0.92	Ireland	-0.04	-0.51
Belgium	0.01	0.00	Israel	0.07	0.95
Belize	-0.04	2.61	Italy	0.02	0.75
Benin	-0.23	4.59	Japan	0.04	0.81
Bhutan	-0.17	1.57	Jordan	0.04	2.66
Bolivia	-0.88	1.91	Kazakhstan	-0.10	1.65
Bosnia and Herzegovina	0.02	1.40	Kenya	0.09	2.81
Botswana	-0.25	1.77	Laos	-0.25	3.44
Brazil	-0.22	1.72	Latvia	-0.09	0.74
Brunei	-0.16	0.44	Lebanon	0.11	1.06
Bulgaria	-0.13	1.36	Libya	-0.25	1.91
Burkina Faso	-0.14	5.71	Lithuania	-0.10	0.67
Burundi	-0.10	3.85	Luxembourg	0.04	-0.52
Cambodia	-0.14	4.18	Madagascar	-0.50	4.28
Cameroon	-0.31	3.76	Malawi	-0.31	4.67
Canada	-0.39	0.61	Malaysia	-0.15	1.55
Cape Verde	-0.20	2.45	Mali	-0.24	6.27
Central African Rep.	-0.30	5.16	Mauritania	-0.33	4.96
Chad	-0.28	5.72	Mexico	-0.06	1.15
Chile	-0.31	0.75	Moldova	-0.13	2.58
China	-0.24	2.37	Mongolia	-0.05	1.71
Colombia	-0.30	1.41	Morocco	-0.15	2.80
Comoros	-0.15	4.60	Mozambique	-0.19	4.61
Congo (Rep. of)	-0.31	2.97	Myanmar	-0.24	4.36
Costa Rica	-0.13	1.35	Namibia	-0.33	2.38
Côte d'Ivoire	-0.26	4.28	Nepal	-0.19	4.65
Croatia	0.04	1.13	Netherlands	0.01	-0.25
Cyprus	0.07	1.42	New Zealand	-0.04	0.07
Czech Republic	0.00	0.30	Nicaragua	-0.12	3.60
Denmark	0.02	-0.16	Niger	-0.37	6.88
Djibouti	-0.26	5.05	Nigeria	-0.28	4.23
Ecuador	-0.37	1.52	Norway	-0.14	-0.32
Egypt	-0.12	3.09	Oman	-0.19	1.72
El Salvador	-0.08	2.11	Pakistan	-0.29	4.75
Ethiopia	-0.15	3.16	Panama	-0.19	0.92
Finland	-0.24	0.06	Paraguay	-0.45	3.10
France	0.05	0.22	Peru	-0.37	0.96
Gabon	-0.21	1.66	Philippines	-0.02	2.98
Gambia	-0.17	4.14	Poland	-0.11	0.66
Georgia	-0.17	2.12	Portugal	0.05	0.75
Germany	0.00	0.03	Qatar	0.08	0.19

S2.4 Country-specific temperature change

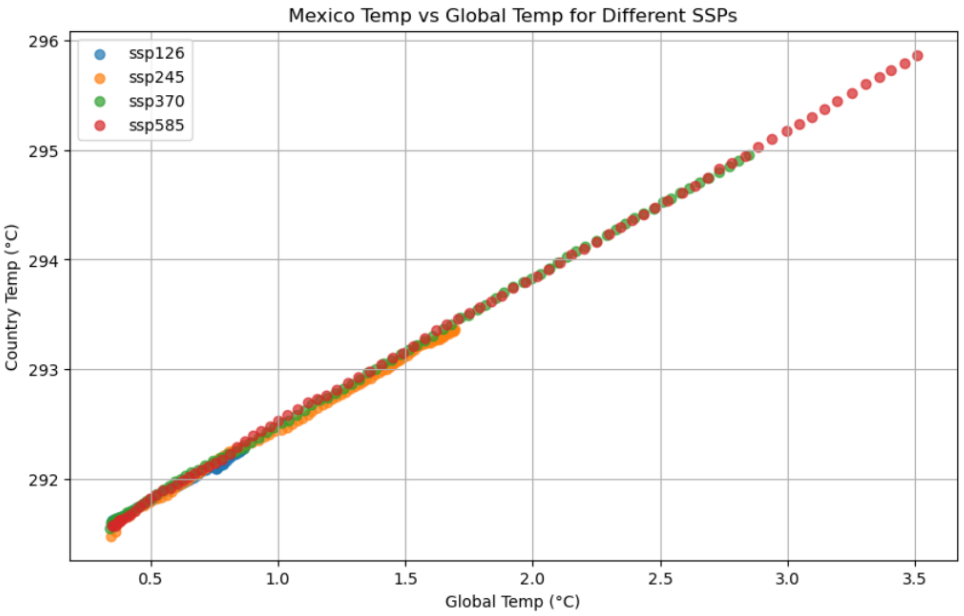

FIGURE S2.4: Example of linear dependency of the regional temperature on global mean temperature, under 4 temperature pathways (Mexico).

The calculation of regional temperatures is done using the same climate dataset as for labor productivity. Defining the countries by the population-weighted grid sum, we observe that country-level temperatures exhibit a consistent linear relationship with global mean temperatures, irrespective of the emission scenario (Figure S3). If regions assessed in the analysis are an aggregate of more countries, the corresponding coefficient is chosen to be an average of the coefficients of the countries it captures.

TABLE S2.6: Country-specific temperature linear coefficients derived from regression analysis. Values represent the rate of warming relative to the global average temperature increase.

Country	Value	Country	Value	Country	Value
Afghanistan	1.60	Ghana	0.84	Nigeria	0.80
Algeria	1.26	Greece	1.43	Norway	1.19
Angola	1.00	Guatemala	1.28	Oman	1.21
Argentina	1.23	Guinea	1.04	Pakistan	1.35
Armenia	1.45	Guinea-Bissau	0.96	Panama	0.93
Australia	1.06	Hungary	1.47	Paraguay	1.64
Austria	1.39	Iceland	0.80	Peru	1.24
Azerbaijan	1.30	India	1.18	Philippines	0.90
Bangladesh	1.14	Indonesia	0.93	Poland	1.34
Belarus	1.42	Iran	1.48	Portugal	1.40
Belgium	0.96	Iraq	1.56	Romania	1.48
Benin	0.75	Ireland	0.74	Russia	1.59
Bolivia	1.47	Israel	1.19	Saudi Arabia	1.40
Botswana	1.47	Italy	1.35	Senegal	1.03
Brazil	1.13	Japan	1.19	Serbia	1.53
Brunei	0.98	Jordan	1.41	Sierra Leone	0.94
Bulgaria	1.48	Kazakhstan	1.54	Slovakia	1.41
Burkina Faso	0.76	Kenya	0.99	Slovenia	1.50
Cambodia	0.94	Laos	1.10	South Africa	1.30
Cameroon	0.81	Latvia	1.36	South Korea	1.32
Canada	1.70	Liberia	0.88	Spain	1.38
Central African Rep.	0.59	Libya	1.20	Sri Lanka	0.95
Chad	0.78	Lithuania	1.35	Sudan	1.10
Chile	1.11	Madagascar	0.90	Sweden	1.30
China	1.36	Malawi	0.88	Switzerland	1.23
Colombia	1.16	Malaysia	0.96	Tanzania	0.90
Congo	0.92	Mali	0.91	Thailand	0.94
Costa Rica	0.82	Mauritania	1.12	Tunisia	1.24
Côte d'Ivoire	0.99	Mexico	1.35	Turkey	1.38
Croatia	1.50	Moldova	1.54	Uganda	0.78
Cuba	0.84	Mongolia	1.66	Ukraine	1.49
Czechia	1.34	Morocco	1.36	United Arab Emirates	1.32
Denmark	1.06	Mozambique	0.96	United Kingdom	0.92
Djibouti	1.12	Myanmar	1.11	United States of America	1.45
Ecuador	1.11	Namibia	1.34	Uruguay	1.02
Egypt	1.23	Nepal	1.26	Uzbekistan	1.50
Eritrea	1.18	Netherlands	1.01	Venezuela	1.29
Estonia	1.36	New Zealand	1.00	Vietnam	1.00
Ethiopia	1.13	Nicaragua	1.05	Yemen	1.16
Finland	1.51	Niger	0.97	Zambia	0.96
France	1.20	North Macedonia	1.52	Zimbabwe	1.12
Gabon	0.91				
Georgia	1.38				
Germany	1.20				

S2.5 Modified temperature pathways

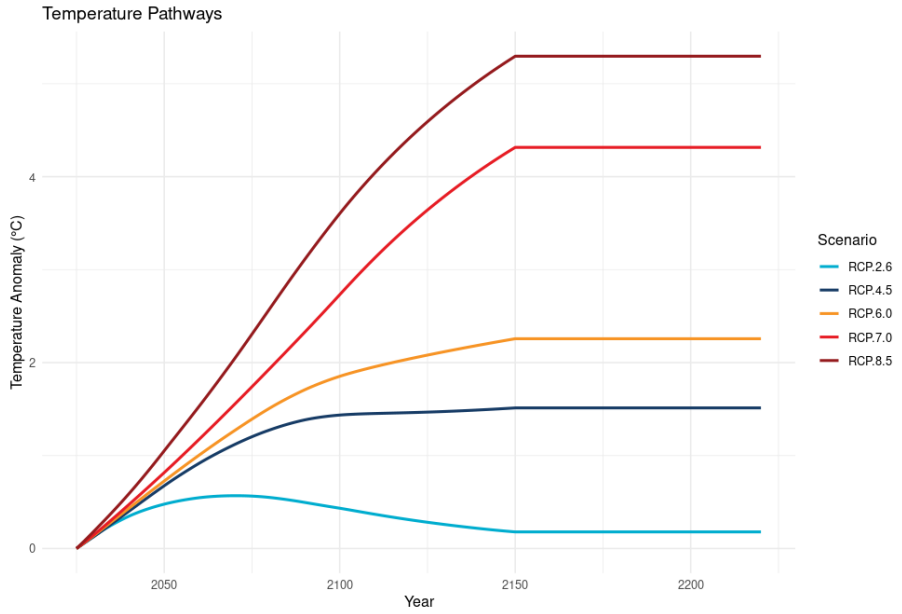

FIGURE S2.5: Pathways (RCPs) used in the analyses. Note that the temperatures are adjusted so that they remain constant after the year 2150.

S2.6 Region aggregation and baseline values

TABLE S2.7: Region aggregation and the corresponding baseline population and GDP. The rightmost column is the list of sectors/commodities included in this analysis.

Regions	Population (million)	GDP (million)	Sectors
Australia	24.606	1327042.5	Paddy rice
Rest of Oceania	16.519	263357.75	Wheat
China and Hong Kong	1393.787	12651701.312	Other Grains and Crops
Japan	126.786	4930838	Livestock and Meat Products
Republic of Korea	51.466	1623898.875	Forestry
Rest of East Asia	52.722	670066.309	Fishing
Indonesia	264.646	1015616.562	Mining and Extraction
Malaysia	31.105	319113.156	Processed Food
Thailand	69.21	456355.875	Textiles, Clothing and Leather
Viet Nam	94.597	223780.234	Wood products
India	1338.659	2651476.25	Paper products, publishing
Rest of South and SE	642.975	1561576.709	Petroleum, Chemical and Pharma
Canada	36.54	1649267.375	Rubber and plastic products
United States of America	325.147	19479580	Mineral products nec
Costa Rica	4.95	60516.098	Ferrous metals and Metal produ
Rest of North and Central America	168.503	1396768.126	Computer, electronic and optic
Argentina	44.045	643625.438	Electrical equipment
Brazil	207.834	2063513	Machinery, Motor and Equipment
Rest of South America	168.112	1306014.88	Manufactures nec

Continued on next page

Table S2.7 (continued)

Regions	Population (million)	GDP (million)	Sectors
Caribbean	42.388	377635.383	Electricity
Austria	8.798	417260.938	Gas and Water
Belgium	11.375	502761.688	Construction
Croatia	4.125	56212.895	Trade
Czechia	10.594	218626.969	Accommodation, Food and servic
Denmark	5.765	332118.812	Transport and Warehousing
Finland	5.538	256968.094	Communication
France	68.517	2640248	Financial, Insurance Real est
Germany	82.657	3690815.75	Public Administration and defe
Ireland	4.807	335431.125	Education
Italy	60.537	1961790.75	Other services
Netherlands	17.131	833867.688	
Portugal	10.3	221355.781	
Spain	46.593	1312528.875	
Slovakia	5.439	95393.047	
Slovenia	2.066	48588.93	
Sweden	10.058	541014.5	
United Kingdom of Great Britai	66.059	2698969.5	
Switzerland	8.452	704477.25	
Rest of EU25	93.513	1347639.025	
Rest of EFTA	5.661	429714.236	
Russian Federation	144.497	1574200.5	
Ukraine	44.831	112090.469	
Rest of Eastern Europe	22.942	121594.828	
Rest of Europe	8.371	74168.125	
Rest of Former Soviet Union	71.263	283005.188	
Iran (Islamic Republic of)	80.674	486629.656	
Saudi Arabia	33.099	688587.938	
T rkiye	81.102	858994.188	
United Arab Emirates	9.487	385607.125	
Rest of Western Asia	141.682	1156911.349	
Rest of North Africa	191.98	625742.352	
Ghana	29.121	60405.359	
Rest of Western Africa	366.603	572412.535	
Gabon	2.065	14929.512	
South-Central Africa	137.408	142738.324	
Ethiopia	106.4	81770.305	
Rest of Eastern Africa	344.951	419522.709	
South Africa	57	381449.312	
Rest of Southern African Custo	7.824	35693.257	
Rest of World	0.003	101.224	

S2.7 Simulation results

TABLE S2.8: GDP losses under RCP2.6 scenario, in percentages. The year 2200 stands for long term damages.

Regions	2035	2050	2075	2100	2200
Australia	0.130128	0.050121	-0.111317	-0.129478	0.07927
Rest of Oceania	0.060973	-0.064229	-0.327291	-0.383978	-0.082187
China and Hong Kong	-0.238831	-0.817001	-1.358253	-1.2191	-0.362984
Japan	-0.093173	-0.344533	-0.740949	-0.814291	-0.331428
Republic of Korea	-0.084645	-0.376425	-0.749011	-0.748321	-0.245169
Rest of East Asia	0.008064	-0.221436	-0.518957	-0.505579	-0.092958
Indonesia	0.105196	-0.633437	-1.79445	-1.540317	-0.15855
Malaysia	-0.456463	-1.300121	-2.061541	-1.810515	-0.588091
Thailand	-0.406776	-1.098892	-1.79173	-1.643378	-0.599392
Viet Nam	-0.929714	-2.18727	-3.005548	-2.352756	-0.838777
India	-1.030472	-2.779821	-3.932769	-3.176921	-1.005207
Rest of South and SE	-0.687837	-1.990842	-3.020746	-2.575297	-0.808651
Canada	0.202265	0.090658	-0.098171	-0.101142	0.162224
United States of America	0.046756	-0.088532	-0.310057	-0.329415	-0.03692
Costa Rica	-0.424774	-1.232487	-1.991277	-1.780055	-0.606218
Rest of North and Central America	-0.086453	-0.388888	-0.83944	-0.888914	-0.288914
Argentina	-0.055963	-0.3637	-0.666024	-0.600489	-0.130012
Brazil	-0.245664	-0.764921	-1.202855	-1.047301	-0.322406
Rest of South America	-0.06175	-0.512763	-0.963475	-0.835799	-0.101672
Caribbean	-0.578227	-1.818579	-3.119231	-2.943562	-1.010297
Austria	0.117796	0.188393	0.069434	-0.088354	-0.058167
Belgium	0.155198	0.232438	0.089051	-0.091214	-0.038821
Croatia	-0.145042	-0.367909	-0.640493	-0.642245	-0.285585
Czechia	0.135314	0.201696	0.056075	-0.108454	-0.049437
Denmark	0.12796	0.165966	0.053023	-0.063133	-0.012211
Finland	0.297385	0.421981	0.350394	0.22061	0.223503
France	0.050228	0.045349	-0.099685	-0.204627	-0.106527
Germany	0.115973	0.16085	0.049089	-0.071133	-0.025079
Ireland	0.213543	0.279882	0.14787	0.00689	0.049969
Italy	-0.035214	-0.14709	-0.374975	-0.463987	-0.221892
Netherlands	0.154919	0.268819	0.131683	-0.068784	-0.022655
Portugal	-0.092706	-0.260861	-0.51507	-0.567066	-0.274405
Spain	-0.120841	-0.294257	-0.527648	-0.558289	-0.284809
Slovakia	0.115338	0.149285	-0.00576	-0.15359	-0.040865
Slovenia	-0.027295	-0.136299	-0.370282	-0.45336	-0.209598
Sweden	0.256531	0.350276	0.233602	0.081964	0.122951
United Kingdom of Great Britain	0.130719	0.19184	0.118861	0.016938	0.022805
Switzerland	0.115138	0.163951	0.030861	-0.110454	-0.052349
Rest of EU25	0.068651	0.02714	-0.163789	-0.255916	-0.077582
Rest of EFTA	0.232454	0.343933	0.287905	0.1674	0.142186
Russian Federation	-0.023985	-0.239433	-0.531739	-0.551573	-0.16299
Ukraine	0.071799	-0.008185	-0.331813	-0.314592	-0.103716
Rest of Eastern Europe	0.061124	-0.001142	-0.171074	-0.191901	-0.054796
Rest of Europe	-0.164147	-0.456173	-0.791403	-0.786066	-0.334758
Rest of Former Soviet Union	-0.223514	-0.751008	-1.241632	-1.146353	-0.396001
Iran (Islamic Republic of)	-0.213977	-0.785334	-1.467332	-1.420846	-0.511958
Saudi Arabia	-0.341658	-1.177063	-1.914889	-1.67753	-0.505122
T rkiye	0.025602	-0.162436	-0.516034	-0.599502	-0.17255
United Arab Emirates	-0.378064	-1.32055	-2.242674	-2.078113	-0.650759
Rest of Western Asia	-0.46421	-1.253596	-1.861382	-1.603515	-0.583244
Rest of North Africa	-0.381237	-1.092293	-1.69773	-1.494174	-0.513868
Ghana	-1.102165	-2.968094	-4.18978	-3.366263	-0.983486
Rest of Western Africa	-0.680226	-1.80243	-2.556515	-2.063035	-0.63662
Gabon	-0.093654	-0.690758	-1.539985	-1.55711	-0.40102
South-Central Africa	-0.545402	-1.574251	-2.379317	-2.010037	-0.581212
Ethiopia	-0.277366	-0.930148	-1.566524	-1.371543	-0.504481
Rest of Eastern Africa	-0.778868	-2.032426	-2.855461	-2.35135	-0.835184
South Africa	-0.226174	-0.571578	-0.884334	-0.800576	-0.326639
Rest of Southern African Customs	-0.221382	-0.718858	-1.194502	-1.110248	-0.360039
Rest of World	0.164104	0.270538	0.210567	0.063517	0.03051

TABLE S2.9: GDP losses under RCP6.0 scenario, in percentages. The year 2200 stands for long term damages.

Regions	2035	2050	2075	2100	2200
Australia	0.17636	0.107663	-0.253575	-0.588117	-0.86477
Rest of Oceania	0.107306	0.014985	-0.575246	-1.148511	-1.584961
China and Hong Kong	-0.204406	-1.060542	-2.785055	-3.948008	-4.624374
Japan	-0.034087	-0.292422	-1.184518	-2.012759	-2.708961
Republic of Korea	-0.022609	-0.371277	-1.351495	-2.135379	-2.668335
Rest of East Asia	0.034843	-0.259507	-1.081151	-1.734691	-2.170989
Indonesia	0.090452	-1.471078	-5.707966	-8.628512	-10.300979
Malaysia	-0.470342	-1.807706	-4.612278	-6.52655	-7.574222
Thailand	-0.421669	-1.523896	-3.845028	-5.488034	-6.553163
Viet Nam	-1.005036	-3.303372	-7.18613	-9.270152	-10.140116
India	-1.133362	-4.043792	-8.729971	-11.267004	-12.315344
Rest of South and SE	-0.726136	-2.753948	-6.443733	-8.699571	-9.796544
Canada	0.277018	0.179468	-0.267249	-0.658991	-0.948942
United States of America	0.077874	-0.064011	-0.604051	-1.091426	-1.461804
Costa Rica	-0.431044	-1.644166	-4.226271	-6.015812	-6.989703
Rest of North and Central America	-0.068121	-0.439785	-1.529628	-2.501411	-3.305902
Argentina	-0.047764	-0.477216	-1.37808	-2.008934	-2.390586
Brazil	-0.234553	-1.033214	-2.56034	-3.577126	-4.178636
Rest of South America	-0.053738	-0.749886	-2.251352	-3.277507	-3.869451
Caribbean	-0.587792	-2.366745	-6.123313	-8.759188	-10.331062
Austria	0.201431	0.465021	0.563064	0.391414	0.062842
Belgium	0.218407	0.496307	0.571138	0.337965	-0.075097
Croatia	-0.100007	-0.373979	-1.129963	-1.753677	-2.22148
Czechia	0.19044	0.425809	0.444554	0.204034	-0.200546
Denmark	0.236217	0.434076	0.468882	0.313328	0.078643
Finland	0.387262	0.692578	0.832831	0.721042	0.484846
France	0.139307	0.265098	0.175964	-0.062068	-0.367852
Germany	0.180836	0.369483	0.393889	0.226706	-0.032742
Ireland	0.272253	0.518362	0.563354	0.395605	0.156417
Italy	0.002934	-0.060655	-0.443845	-0.8891	-1.370871
Netherlands	0.187414	0.510764	0.626373	0.390896	-0.047317
Portugal	-0.062049	-0.223746	-0.766696	-1.291353	-1.755869
Spain	-0.075777	-0.250502	-0.773784	-1.24577	-1.634127
Slovakia	0.141633	0.299471	0.234525	-0.048531	-0.501004
Slovenia	0.035412	-0.008563	-0.390574	-0.820316	-1.229892
Sweden	0.389805	0.702137	0.809769	0.643202	0.344803
United Kingdom of Great Britain	0.190089	0.390404	0.476332	0.385822	0.222629
Switzerland	0.199046	0.42604	0.458859	0.267944	-0.026111
Rest of EU25	0.101305	0.128716	-0.147253	-0.514085	-0.905461
Rest of EFTA	0.307155	0.591265	0.759363	0.695157	0.518924
Russian Federation	1.51e-4	-0.246795	-0.905252	-1.44751	-1.870971
Ukraine	0.115153	-0.145948	-1.180506	-1.911283	-2.398219
Rest of Eastern Europe	0.099865	0.035778	-0.369783	-0.717842	-0.968055
Rest of Europe	-0.139019	-0.502801	-1.335415	-1.979501	-2.452325
Rest of Former Soviet Union	-0.200523	-0.898286	-2.283014	-3.22953	-3.787421
Iran (Islamic Republic of)	-0.197727	-0.994382	-2.879324	-4.286174	-5.20887
Saudi Arabia	-0.346004	-1.586563	-4.002686	-5.558054	-6.350416
T rkiye	0.074433	-0.103167	-0.911765	-1.724793	-2.451968
United Arab Emirates	-0.389129	-1.749587	-4.440723	-6.284422	-7.410482
Rest of Western Asia	-0.473246	-1.679159	-3.813253	-5.107441	-5.750106
Rest of North Africa	-0.374807	-1.45404	-3.487419	-4.795292	-5.510638
Ghana	-1.183384	-4.300028	-9.344478	-12.073581	-13.215443
Rest of Western Africa	-0.716389	-2.622757	-5.811518	-7.603127	-8.413212
Gabon	-0.07962	-0.852109	-3.044414	-4.865241	-6.131485
South-Central Africa	-0.54966	-2.209597	-5.231336	-7.088574	-8.050492
Ethiopia	-0.234651	-1.235269	-3.290822	-4.56421	-5.207519
Rest of Eastern Africa	-0.815003	-2.795206	-6.041238	-7.860405	-8.633321
South Africa	-0.213322	-0.729177	-1.713672	-2.361564	-2.751826
Rest of Southern African Customs	-0.222887	-0.943894	-2.353798	-3.34631	-4.015117
Rest of World	0.20453	0.497749	0.721732	0.660848	0.447278

Regions	2035	2050	2075	2100	2200
Australia	0.191215	0.133456	-0.249327	-0.729499	-1.507924
Rest of Oceania	0.118462	0.02637	-0.643906	-1.527152	-2.89518
China and Hong Kong	-0.23426	-1.14642	-3.19526	-5.11725	-7.486984
Japan	-0.023339	-0.283416	-1.285381	-2.517674	-4.518648
Republic of Korea	-0.014914	-0.373383	-1.507308	-2.748499	-4.478437
Rest of East Asia	0.032901	-0.279508	-1.235627	-2.277276	-3.734055
Indonesia	0.053781	-1.751916	-6.952725	-11.959463	-18.242042
Malaysia	-0.515118	-1.975185	-5.455538	-8.879006	-13.14732
Thailand	-0.458659	-1.660226	-4.481753	-7.24182	-10.923896
Viet Nam	-1.103624	-3.623786	-8.489042	-12.42183	-16.444872
India	-1.263045	-4.428204	-10.174458	-14.700007	-19.22394
Rest of South and SE	-0.800968	-2.99734	-7.473393	-11.370285	-15.737496
Canada	0.298651	0.220163	-0.252115	-0.822821	-1.68705
United States of America	0.08232	-0.060749	-0.668713	-1.413583	-2.562609
Costa Rica	-0.467449	-1.786629	-4.933474	-8.030752	-11.904429
Rest of North and Central America	-0.072221	-0.468481	-1.708435	-3.156038	-5.485906
Argentina	-0.059101	-0.517852	-1.569685	-2.585429	-3.890652
Brazil	-0.257945	-1.112297	-2.949593	-4.678758	-6.87092
Rest of South America	-0.074056	-0.827	-2.623999	-4.333494	-6.458894
Caribbean	-0.637859	-2.564267	-7.007892	-11.193543	-16.406
Austria	0.235282	0.550335	0.782294	0.696635	0.09294
Belgium	0.246573	0.568791	0.778553	0.619881	-0.189133
Croatia	-0.095411	-0.376181	-1.261728	-2.277871	-3.794879
Czechia	0.214981	0.486223	0.617878	0.431504	-0.351572
Denmark	0.280987	0.527655	0.671201	0.571684	0.115954
Finland	0.423561	0.780778	1.049502	1.027056	0.608194
France	0.173458	0.342352	0.333682	0.092481	-0.57774
Germany	0.206802	0.431396	0.5514	0.432891	-0.072415
Ireland	0.300732	0.580483	0.739172	0.647552	0.21841
Italy	0.012312	-0.039664	-0.424122	-1.01103	-2.193325
Netherlands	0.209071	0.570961	0.82402	0.678764	-0.147866
Portugal	-0.057242	-0.218697	-0.812484	-1.574658	-2.88371
Spain	-0.066926	-0.237483	-0.810883	-1.509773	-2.642615
Slovakia	0.155448	0.335082	0.347203	0.075567	-0.831308
Slovenia	0.054405	0.029346	-0.343827	-0.905995	-1.948638
Sweden	0.444874	0.82632	1.086477	1.015877	0.472032
United Kingdom of Great Britain	0.21602	0.451138	0.630414	0.607234	0.317582
Switzerland	0.234868	0.508851	0.657249	0.529061	-0.034558
Rest of EU25	0.113617	0.15215	-0.104868	-0.574379	-1.542662
Rest of EFTA	0.343094	0.673683	0.962428	1.001453	0.726443
Russian Federation	7.05e-4	-0.255736	-0.975312	-1.742038	-2.894838
Ukraine	0.127888	-0.185228	-1.393648	-2.591261	-4.185557
Rest of Eastern Europe	0.111303	0.043375	-0.398294	-0.933007	-1.733817
Rest of Europe	-0.143363	-0.522236	-1.453672	-2.404668	-3.77151
Rest of Former Soviet Union	-0.214223	-0.952937	-2.55097	-4.037648	-5.893134
Iran (Islamic Republic of)	-0.210664	-1.074452	-3.264965	-5.428483	-8.309929
Saudi Arabia	-0.384241	-1.725914	-4.61192	-7.207342	-10.217515
T rkiye	0.082408	-0.097552	-1.015978	-2.258488	-4.413348
United Arab Emirates	-0.431125	-1.894626	-5.061142	-7.968538	-11.621348
Rest of Western Asia	-0.513501	-1.812242	-4.378376	-6.581052	-9.049495
Rest of North Africa	-0.407839	-1.566929	-3.99962	-6.185013	-8.782251
Ghana	-1.316738	-4.690005	-10.888803	-15.785179	-20.682608
Rest of Western Africa	-0.794631	-2.859299	-6.80515	-10.080439	-13.55877
Gabon	-0.092404	-0.93116	-3.468176	-6.263929	-10.362277
South-Central Africa	-0.607258	-2.393725	-6.08679	-9.344262	-13.086134
Ethiopia	-0.24693	-1.331214	-3.753788	-5.928016	-8.402225
Rest of Eastern Africa	-0.889127	-3.027289	-6.981265	-10.226036	-13.594401
South Africa	-0.225717	-0.77643	-1.934732	-2.987697	-4.304325
Rest of Southern African Customs	-0.24611	-1.017358	-2.678373	-4.256419	-6.375521
Rest of World	0.225522	0.556919	0.909098	0.962739	0.617076

TABLE S2.10: GDP losses under RCP7.0 scenario, in percentages. The year 2200 stands for long term damages.

Regions	2035	2050	2075	2100	2200
Australia	0.239608	0.233197	-0.147347	-0.854342	-3.629088
Rest of Oceania	0.146292	0.07811	-0.772129	-2.466681	-8.408184
China and Hong Kong	-0.257764	-1.281741	-3.985685	-7.67432	-17.079488
Japan	0.01531	-0.217691	-1.431801	-3.606287	-11.429032
Republic of Korea	0.024161	-0.329709	-1.773677	-4.144934	-11.394086
Rest of East Asia	0.043463	-0.28569	-1.517697	-3.487015	-9.659593
Indonesia	0.013566	-2.222627	-9.493389	-19.983737	-49.134731
Malaysia	-0.551257	-2.243243	-7.176294	-14.817158	-37.173573
Thailand	-0.488407	-1.868439	-5.722519	-11.327509	-27.105441
Viet Nam	-1.200387	-4.17386	-11.017391	-19.585808	-36.944685
India	-1.400764	-5.084441	-12.955235	-22.138364	-39.667869
Rest of South and SE	-0.868194	-3.383151	-9.461004	-17.32395	-35.443164
Canada	0.370523	0.363046	-0.099903	-0.950863	-4.119549
United States of America	0.101962	-0.02298	-0.759658	-2.07875	-6.809641
Costa Rica	-0.49536	-2.002746	-6.343159	-12.891811	-32.170524
Rest of North and Central America	-0.066074	-0.480864	-2.019072	-4.512376	-13.463812
Argentina	-0.062809	-0.564725	-1.917238	-3.776248	-8.966743
Brazil	-0.262755	-1.215497	-3.661627	-7.071699	-16.384382
Rest of South America	-0.081643	-0.929386	-3.317887	-6.646302	-15.392906
Caribbean	-0.678129	-2.855745	-8.704536	-16.524823	-36.470878
Austria	0.303321	0.75637	1.314238	1.630677	0.048462
Belgium	0.296994	0.744788	1.263734	1.480549	-0.936614
Croatia	-0.067186	-0.342528	-1.486131	-3.507131	-10.317038
Czechia	0.258767	0.636022	1.02768	1.159321	-0.981886
Denmark	0.38293	0.76486	1.194456	1.411242	0.20783
Finland	0.49961	0.994646	1.581801	1.954229	0.880199
France	0.253803	0.546707	0.76851	0.698271	-1.349506
Germany	0.258223	0.582477	0.932113	1.086091	-0.295665
Ireland	0.34991	0.731937	1.135573	1.395636	0.488315
Italy	0.03774	0.034072	-0.325758	-1.1304	-5.182142
Netherlands	0.241118	0.71772	1.267106	1.519366	-0.802669
Portugal	-0.038856	-0.176764	-0.85827	-2.116878	-7.200929
Spain	-0.035853	-0.175435	-0.82314	-1.986015	-6.402795
Slovakia	0.176878	0.430072	0.617826	0.526832	-2.026894
Slovenia	0.10293	0.144859	-0.173315	-0.907367	-4.458021
Sweden	0.570753	1.141178	1.803667	2.200747	0.865333
United Kingdom of Great Britain	0.267121	0.597212	0.996729	1.257713	0.516535
Switzerland	0.309352	0.715487	1.151001	1.359736	-0.113431
Rest of EU25	0.138999	0.227957	0.02272	-0.571133	-3.945642
Rest of EFTA	0.418255	0.87766	1.462902	1.907817	1.350141
Russian Federation	0.014275	-0.236383	-1.057023	-2.188822	-5.885201
Ukraine	0.158669	-0.220222	-1.76539	-3.91942	-9.927942
Rest of Eastern Europe	0.136914	0.084778	-0.421574	-1.317091	-4.620674
Rest of Europe	-0.134636	-0.520638	-1.621871	-3.138213	-7.835567
Rest of Former Soviet Union	-0.209577	-1.003406	-3.016342	-5.626202	-12.41561
Iran (Islamic Republic of)	-0.209934	-1.16976	-3.968754	-7.783407	-18.275953
Saudi Arabia	-0.413938	-1.932983	-5.772021	-10.79967	-23.145214
T rkiye	0.109851	-0.04568	-1.201889	-3.569323	-13.274371
United Arab Emirates	-0.46273	-2.09964	-6.204502	-11.483782	-24.914434
Rest of Western Asia	-0.543063	-2.011912	-5.433923	-9.735413	-19.55265
Rest of North Africa	-0.424498	-1.725772	-4.945729	-9.15072	-19.392169
Ghana	-1.439426	-5.339555	-13.820932	-23.822131	-42.87977
Rest of Western Africa	-0.861591	-3.250662	-8.713926	-15.643516	-30.483004
Gabon	-0.09537	-1.016351	-4.273712	-9.360377	-27.865436
South-Central Africa	-0.640253	-2.670316	-7.702682	-14.434462	-30.295447
Ethiopia	-0.230785	-1.446702	-4.618626	-8.735846	-18.390729
Rest of Eastern Africa	-0.952784	-3.397992	-8.773155	-15.35516	-29.200253
South Africa	-0.225597	-0.832244	-2.31926	-4.248888	-9.289206
Rest of Southern African Customs	-0.260983	-1.114534	-3.264861	-6.152423	-14.097969
Rest of World	0.253947	0.684849	1.305581	1.727043	0.642439

TABLE S2.11: GDP losses under RCP8.5 scenario, in percentages. The year 2200 stands for long term damages.

Regions	2035	2050	2075	2100	2200
Australia	0.289413	0.291964	-0.238962	-1.324871	-4.836169
Rest of Oceania	0.186053	0.068314	-1.329215	-4.20652	-12.129063
China and Hong Kong	-0.343689	-1.714615	-5.607702	-11.079439	-22.570385
Japan	0.051602	-0.257019	-2.103492	-5.620333	-15.906815
Republic of Korea	0.045093	-0.439723	-2.645481	-6.452976	-15.998115
Rest of East Asia	0.040287	-0.409221	-2.257597	-5.386615	-13.426889
Indonesia	-0.153173	-3.540425	-14.395726	-30.831832	-71.366149
Malaysia	-0.710373	-3.076666	-10.700851	-23.284265	-57.644699
Thailand	-0.616655	-2.518418	-8.214053	-16.829448	-37.387899
Viet Nam	-1.543182	-5.659031	-15.497235	-27.781788	-48.177731
India	-1.829748	-6.751874	-17.701507	-30.346004	-49.754775
Rest of South and SE	-1.12062	-4.484935	-13.191345	-24.687445	-46.514219
Canada	0.439447	0.445931	-0.20621	-1.520063	-5.51376
United States of America	0.119072	-0.047978	-1.166193	-3.307568	-9.542185
Costa Rica	-0.618659	-2.682628	-9.243378	-19.812313	-47.845574
Rest of North and Central America	-0.074665	-0.619465	-2.849103	-6.743479	-18.435508
Argentina	-0.094033	-0.751525	-2.668906	-5.449372	-11.912235
Brazil	-0.333666	-1.600371	-5.136629	-10.294737	-22.145382
Rest of South America	-0.147397	-1.299166	-4.756141	-9.750363	-20.621793
Caribbean	-0.842612	-3.733539	-12.050204	-23.540325	-47.935886
Austria	0.422859	1.062405	1.866074	2.170124	-0.112858
Belgium	0.40186	1.031875	1.78261	1.898395	-1.651854
Croatia	-0.05324	-0.434356	-2.233123	-5.606007	-15.161239
Czechia	0.349612	0.874895	1.456656	1.510343	-1.493308
Denmark	0.528798	1.070863	1.685803	1.88099	0.209309
Finland	0.624518	1.299386	2.128862	2.522043	0.899738
France	0.368182	0.791261	1.114006	0.883501	-1.875991
Germany	0.351065	0.807471	1.315962	1.420589	-0.523156
Ireland	0.449763	0.97973	1.574853	1.853191	0.649441
Italy	0.076427	0.098224	-0.41154	-1.732871	-7.093104
Netherlands	0.320872	0.982834	1.781631	1.972717	-1.430794
Portugal	-0.016778	-0.182018	-1.190086	-3.244561	-10.005267
Spain	-0.001379	-0.167043	-1.12257	-3.002789	-8.783076
Slovakia	0.229457	0.58401	0.878612	0.644682	-2.845059
Slovenia	0.171468	0.256147	-0.194518	-1.397206	-5.974692
Sweden	0.749458	1.545651	2.495727	2.922739	1.003914
United Kingdom of Great Britain	0.356635	0.817266	1.384643	1.651782	0.531787
Switzerland	0.430183	1.00508	1.638696	1.816077	-0.240168
Rest of EU25	0.186219	0.3147	0.015448	-1.005553	-5.497675
Rest of EFTA	0.535854	1.167876	2.006709	2.552285	1.652568
Russian Federation	0.022159	-0.28535	-1.3728	-2.971975	-7.389493
Ukraine	0.203977	-0.430669	-2.626289	-5.800392	-12.95056
Rest of Eastern Europe	0.182121	0.090747	-0.665747	-2.136014	-6.436012
Rest of Europe	-0.140932	-0.622094	-2.113175	-4.303469	-10.026076
Rest of Former Soviet Union	-0.249119	-1.261175	-4.04966	-7.802637	-15.841792
Iran (Islamic Republic of)	-0.24946	-1.534298	-5.464054	-11.041648	-23.761477
Saudi Arabia	-0.53877	-2.559506	-8.024711	-15.428967	-30.516607
T rkiye	0.140515	-0.089515	-1.972119	-6.128723	-20.514498
United Arab Emirates	-0.599988	-2.738802	-8.445274	-16.008065	-32.141867
Rest of Western Asia	-0.675869	-2.617665	-7.433748	-13.617778	-25.239107
Rest of North Africa	-0.53186	-2.259	-6.820161	-12.931613	-25.236149
Ghana	-1.888196	-7.101928	-18.957204	-32.775991	-54.02953
Rest of Western Africa	-1.12403	-4.357531	-12.201494	-22.246961	-40.076931
Gabon	-0.135183	-1.369301	-6.127085	-14.288848	-42.868566
South-Central Africa	-0.835183	-3.5728	-10.879202	-20.91165	-40.460233
Ethiopia	-0.265608	-1.92012	-6.435505	-12.406205	-23.577676
Rest of Eastern Africa	-1.199491	-4.439925	-12.025181	-21.406537	-37.501319
South Africa	-0.263276	-1.060548	-3.128441	-5.928682	-12.105828
Rest of Southern African Customs	-0.335679	-1.450375	-4.467086	-8.675019	-18.418032
Rest of World	0.334798	0.930809	1.780926	2.16581	0.283655

Bibliography

[1] Nicholas J. Leach, Stuart Jenkins, Zebedee Nicholls, Christopher J. Smith, John Lynch, Michelle Cain, Tristram Walsh, Bill Wu, Junichi Tsutsui, and Myles R. Allen. FaIRv2.0.0: a generalized impulse response model for climate uncertainty and future scenario exploration. *Geoscientific Model Development*, 14(5):3007–3036, May 2021. ISSN 1991-959X. doi: 10.5194/gmd-14-3007-2021. Publisher: Copernicus GmbH.

[2] M Brockmeier. A graphical exposition of the gtap model. 2001.

[3] Thomas W Hertel. *Global Trade Analysis: Modeling and Applications*. Cambridge University Press, 1997.

[4] Christine Li, James Camac, Andrew Robinson, and Tom Kompas. Predicting changes in agricultural yields under climate change scenarios and their implications for global food security. *Scientific Reports*, 15(1):2858, 2025.

[5] Valérie Masson-Delmotte, Panmao Zhai, Anna Pirani, Sarah L Connors, Clotilde Péan, Sophie Berger, Nada Caud, Y Chen, L Goldfarb, MI Gomis, et al. Climate change 2021: the physical science basis. *Contribution of working group I to the sixth assessment report of the intergovernmental panel on climate change*, 2(1):2391, 2021.

[6] Sergey K Gulev, Peter W Thorne, Jinho Ahn, Frank J Dentener, Catia M Domingues, Sebastian Gerland, Daoyi Gong, Darrell S Kaufman, Hyacinth C Nnamchi, Johannes Quaas, et al. Changing state of the climate system. 2021.

[7] Howard Kunreuther, Shreekant Gupta, Valentina Bosetti, Roger Cooke, Varun Dutt, Minh Ha-Duong, Hermann Held, Juan Llanes-Regueiro, Anthony Patt, Ekundayo Shittu, et al. Integrated risk and uncertainty assessment of climate change

response policies. In *Climate Change 2014: Mitigation of Climate Change: Working Group III Contribution to the Fifth Assessment Report of the Intergovernmental Panel on Climate Change*, pages 151–206. Cambridge University Press, 2014.

[8] James Risbey, Milind Kandlikar, and Anand Patwardhan. Assessing integrated assessments. *Climatic Change*, 34(3):369–395, 1996.

[9] Karen Fisher-Vanden and John Weyant. The evolution of integrated assessment: Developing the next generation of use-inspired integrated assessment tools. *Annual Review of Resource Economics*, 12(1):471–487, 2020.

[10] O. Geoffroy, D. Saint-Martin, D. J. L. Olivié, A. Voldoire, G. Bellon, and S. Tytéca. Transient Climate Response in a Two-Layer Energy-Balance Model. Part I: Analytical Solution and Parameter Calibration Using CMIP5 AOGCM Experiments. *Journal of Climate*, 26(6):1841–1857, March 2013. ISSN 0894-8755, 1520-0442. doi: 10.1175/JCLI-D-12-00195.1. Publisher: American Meteorological Society Section: Journal of Climate.

[11] Raphael Calel and David A Stainforth. On the physics of three integrated assessment models. *Bulletin of the American Meteorological Society*, 98(6):1199–1216, 2017.

[12] John Weyant. Some contributions of integrated assessment models of global climate change. *Review of Environmental Economics and Policy*, 2017.

[13] Kenneth Strzepek, Michael Jacobsen, Brent Boehlert, and James Neumann. Toward evaluating the effect of climate change on investments in the water resources sector: insights from the forecast and analysis of hydrological indicators in developing countries. *Environmental Research Letters*, 8(4):044014, 2013.

[14] Brian C O'Neill, Elmar Kriegler, Keywan Riahi, Kristie L Ebi, Stephane Hallegatte, Timothy R Carter, Ritu Mathur, and Detlef P Van Vuuren. A new scenario framework for climate change research: the concept of shared socioeconomic pathways. *Climatic change*, 122:387–400, 2014.

[15] Delavane B Diaz. Estimating global damages from sea level rise with the coastal impact and adaptation model (ciam). *Climatic Change*, 137(1):143–156, 2016.

[16] Gunnar Luderer, Marian Leimbach, Nico Bauer, Elmar Kriegler, Lavinia Baumstark, Christoph Bertram, Anastasis Giannousakis, Jerome Hilaire, David Klein, Antoine Levesque, et al. Description of the remind model (version 1.6). 2015.

[17] David Anthoff and Richard SJ Tol. The climate framework for uncertainty, negotiation and distribution (fund): Technical description, version 3.6. *FUND Doc*, 2014.

[18] Chris W Hope. The social cost of co2 from the page09 model. Technical report, Economics Discussion Papers, 2011.

[19] William Nordhaus. Estimates of the social cost of carbon: concepts and results from the dice-2013r model and alternative approaches. *Journal of the Association of Environmental and Resource Economists*, 1(1/2):273–312, 2014.

[20] Robert D Atkinson and Darrene Hackler. Economic doctrines and approaches to climate change policy. *The İnformation Technology & Innovation Foundation*, 2010.

[21] Rajendra K Pachauri, Myles R Allen, Vicente R Barros, John Broome, Wolfgang Cramer, Renate Christ, John A Church, Leon Clarke, Qin Dahe, Purnamita Dasgupta, et al. *Climate change 2014: synthesis report. Contribution of Working Groups I, II and III to the fifth assessment report of the Intergovernmental Panel on Climate Change*. Ipcc, 2014.

[22] Mark New, Diana Reckien, David Viner, Carolina Adler, So-Min Cheong, Cecilia Conde, Andrew Constable, Erin Coughlan de Perez, Annamaria Lammel, Reinhard Mechler, et al. Decision-making options for managing risk. In *Climate Change 2022: Impacts, Adaptation and Vulnerability: Contribution of Working Group II to the Sixth Assessment Report of the Intergovernmental Panel on Climate Change*, pages 2539–2654. Cambridge University Press, 2022.

[23] John Von Neumann and Oskar Morgenstern. Theory of games and economic behavior: 60th anniversary commemorative edition. In *Theory of games and economic behavior*. Princeton university press, 2007.

[24] Leonard J Savage. *The foundations of statistics*. Courier Corporation, 1972.

[25] Nicholas Stern. Stern review: The economics of climate change. 2006.

[26] William Nordhaus. *A question of balance: Weighing the options on global warming policies*. Yale University Press, 2008.

[27] William Nordhaus. *The climate casino: Risk, uncertainty, and economics for a warming world*. Yale University Press, 2013.

[28] Martin C Hänsel, Moritz A Drupp, Daniel JA Johansson, Frikk Nesje, Christian Azar, Mark C Freeman, Ben Groom, and Thomas Sterner. Climate economics support for the un climate targets. *Nature Climate Change*, 10(8):781–789, 2020.

[29] Martin L Weitzman. Additive damages, fat-tailed climate dynamics, and uncertain discounting. *Economics*, 3(1):20090039, 2009.

[30] Robert S Pindyck. Climate change policy: what do the models tell us? *Journal of Economic Literature*, 51(3):860–872, 2013.

[31] Frank Ackerman and Elizabeth A Stanton. Climate risks and carbon prices: Revising the social cost of carbon. *Economics*, 6(1):20120010, 2012.

[32] Robert S Pindyck. The climate policy dilemma. *Review of Environmental Economics and Policy*, 2013.

[33] B. O'Neill, M. van Aalst, Z. Zaiton Ibrahim, L. Berrang Ford, S. Bhadwal, H. Buhaug, D. Diaz, K. Frieler, M. Garschagen, A. Magnan, G. Midgley, A. Mirzabaev, A. Thomas, and R. Warren. Key risks across sectors and regions. In H.-O. Pörtner, D.C. Roberts, M. Tignor, E.S. Poloczanska, K. Mintenbeck, A. Alegría, M. Craig, S. Langsdorf, S. Löschke, V. Möller, A. Okem, and B. Rama, editors, *Climate Change 2022: Impacts, Adaptation, and Vulnerability. Contribution of Working Group II to the Sixth Assessment Report of the Intergovernmental Panel on Climate Change*, pages 2411–2538. Cambridge University Press, Cambridge, UK and New York, NY, USA, 2022. doi: 10.1017/9781009325844.025.

[34] Christopher B Field and Vicente R Barros. *Climate change 2014–Impacts, adaptation and vulnerability: Regional aspects*. Cambridge University Press, 2014.

[35] Elmar Kriegler and Thomas Bruckner. Sensitivity analysis of emissions corridors for the 21st century. *Climatic change*, 66(3):345–387, 2004.

[36] Abraham Charnes and William W Cooper. Chance-constrained programming. *Management science*, 6(1):73–79, 1959.

[37] Hermann Held, Elmar Kriegler, Kai Lessmann, and Ottmar Edenhofer. Efficient climate policies under technology and climate uncertainty. *Energy Economics*, 31: S50–S61, 2009.

[38] Leon Clarke, Kejun Jiang, Keigo Akimoto, Mustafa Babiker, Geoffrey Blanford, Karen Fisher-Vanden, J-C Hourcade, Volker Krey, Elmar Kriegler, Andreas Löschel, et al. Assessing transformation pathways. 2014.

[39] Anthony Patt. Extreme outcomes: the strategic treatment of low probability events in scientific assessment. *Risk, Decision and Policy*, 4(1):1–15, 1999.

[40] Terrence Iverson and Charles Perrings. Precaution and proportionality in the management of global environmental change. *Global Environmental Change*, 22(1):161–177, 2012.

[41] Felix Otto and Hermann Held. Targets in international climate policy (mis) understanding two degrees? Technical report, WiSo-HH Working Paper Series, 2022.

[42] Matthias GW Schmidt, Alexander Lorenz, Hermann Held, and Elmar Kriegler. Climate targets under uncertainty: challenges and remedies: A letter. *Climatic change*, 104:783–791, 2011.

[43] Roger A Blau. Stochastic programming and decision analysis: an apparent dilemma. *Management Science*, 21(3):271–276, 1974.

[44] Irving H Lavalle. On information-augmented chance-constrained programs. *Operations research letters*, 4(5):225–230, 1986.

[45] Hermann Held. Cost risk analysis: Dynamically consistent decision-making under climate targets. *Environmental and Resource Economics*, 72(1):247–261, 2019.

[46] Elnaz Roshan, Mohammad M. Khabbazan, and Hermann Held. Cost-risk trade-off of mitigation and solar geoengineering: Considering regional disparities under probabilistic climate sensitivity. *Environmental and Resource Economics*, 72:263–279, 2019.

[47] Elnaz Roshan, Mohammad M Khabbazan, and Hermann Held. A scheme for jointly trading off costs and risks of solar radiation management and mitigation under long-tailed climate sensitivity probability density distributions. *Environmental Modeling & Assessment*, 26:823–836, 2021.

[48] Delf Neubersch. *Value of information under climate targets: An application of cost-risk analysis*. PhD thesis, Universität Hamburg Hamburg, 2014.

[49] Robert Roth, Delf Neubersch, and Hermann Held. Evaluating delayed climate policy by cost-risk analysis. Technical report, WiSo-HH Working Paper Series, 2020.

[50] Kaj-Ivar van der Wijst, Andries F Hof, and Detlef P van Vuuren. On the optimality of 2° c targets and a decomposition of uncertainty. *Nature communications*, 12(1): 2575, 2021.

[51] Michael Sureth, Matthias Kalkuhl, Ottmar Edenhofer, and Johan Rockström. A welfare economic approach to planetary boundaries. *Jahrbücher für Nationalökonomie und Statistik*, 243(5):477–542, 2023.

[52] Hermann Held. Towards a completed cost risk analysis of the climate problem: Dealing with consolidated impacts and updated targets. *Available at SSRN 4701971*, 2024.

[53] Myles R. Allen, David J. Frame, Chris Huntingford, Chris D. Jones, Jason A. Lowe, Malte Meinshausen, and Nicolai Meinshausen. Warming caused by cumulative carbon emissions towards the trillionth tonne. *Nature*, 458(7242):1163–1166, 2009. Publisher: Nature Publishing Group.

[54] H. Damon Matthews, Nathan P. Gillett, Peter A. Stott, and Kirsten Zickfeld. The proportionality of global warming to cumulative carbon emissions. *Nature*, 459 (7248):829–832, June 2009. ISSN 1476-4687. doi: 10.1038/nature08047. Number: 7248 Publisher: Nature Publishing Group.

[55] Malte Meinshausen, Nicolai Meinshausen, William Hare, Sarah C. B. Raper, Katja Frieler, Reto Knutti, David J. Frame, and Myles R. Allen. Greenhouse-gas emission targets for limiting global warming to 2 °C. *Nature*, 458(7242):1158–1162, April 2009. ISSN 1476-4687. doi: 10.1038/nature08017. Number: 7242 Publisher: Nature Publishing Group.

[56] Kirsten Zickfeld, Michael Eby, H. Damon Matthews, and Andrew J. Weaver. Setting cumulative emissions targets to reduce the risk of dangerous climate change. *Proceedings of the National Academy of Sciences*, 106(38):16129–16134, September 2009. doi: 10.1073/pnas.0805800106. Publisher: Proceedings of the National Academy of Sciences.

[57] T. F. Stocker, D. Qin, G.-K. Plattner, M. Tignor, S. K. Allen, J. Doschung, A. Nauels, Y. Xia, V. Bex, and P. M. Midgley, editors. *Summary for policymakers*, pages 3–29. Cambridge University Press, Cambridge, UK, 2013. doi: 10.1017/CBO9781107415324.004.

[58] V. Masson-Delmotte, P. Zhai, A. Pirani, S. L. Connors, C. Péan, S. Berger, N. Caud, Y. Chen, L. Goldfarb, M. I. Gomis, M. Huang, K. Leitzell, E. Lonnoy, J. B. R. Matthews, T. K. Maycock, T. Waterfield, O. Yelekçi, R. Yu, and B. Zhou, editors. *Summary for policymakers*, pages 3–32. Cambridge University Press, 2021. doi: 10.1017/9781009157896.001.

[59] Nathan P. Gillett, Vivek K. Arora, Damon Matthews, and Myles R. Allen. Constraining the Ratio of Global Warming to Cumulative CO2 Emissions Using CMIP5 Simulations. *Journal of Climate*, 26(18):6844–6858, September 2013. ISSN 0894-8755, 1520-0442. doi: 10.1175/JCLI-D-12-00476.1. Publisher: American Meteorological Society Section: Journal of Climate.

[60] Katarzyna B Tokarska, Nathan P Gillett, Andrew J Weaver, Vivek K Arora, and Michael Eby. The climate response to five trillion tonnes of carbon. *Nature climate change*, 6(9):851–855, 2016.

[61] T Herrington and K Zickfeld. Path independence of climate and carbon cycle response over a broad range of cumulative carbon emissions. *Earth System Dynamics*, 5(2):409–422, 2014.

[62] Richard Millar, Myles Allen, Joeri Rogelj, and Pierre Friedlingstein. The cumulative carbon budget and its implications. *Oxford Review of Economic Policy*, 32(2):323–342, January 2016. ISSN 0266-903X. doi: 10.1093/oxrep/grw009.

[63] M. R. Raupach. The exponential eigenmodes of the carbon-climate system, and their implications for ratios of responses to forcings. *Earth System Dynamics*, 4(1): 31–49, 2013. doi: 10.5194/esd-4-31-2013.

[64] Andrew H MacDougall and Pierre Friedlingstein. The origin and limits of the near proportionality between climate warming and cumulative co2 emissions. *Journal of Climate*, 28(10):4217–4230, 2015.

[65] Martin Leduc, H. Damon Matthews, and Ramón de Elía. Quantifying the Limits of a Linear Temperature Response to Cumulative CO2 Emissions. *Journal*

of Climate, 28(24):9955–9968, December 2015. ISSN 0894-8755, 1520-0442. doi: 10.1175/JCLI-D-14-00500.1. Publisher: American Meteorological Society Section: Journal of Climate.

[66] Zebedee Nicholls. Reduced Complexity Model Intercomparison Project (RCMIP). pages EGU21–3707, April 2021. doi: 10.5194/egusphere-egu21-3707. Conference Name: EGU General Assembly Conference Abstracts ADS Bibcode: 2021EGUGA..23.3707N.

[67] Simon Dietz and Frank Venmans. Cumulative carbon emissions and economic policy: In search of general principles. *Journal of Environmental Economics and Management*, 96:108–129, July 2019. ISSN 0095-0696. doi: 10.1016/j.jeem.2019.04.003.

[68] Simon Dietz, Frederick van der Ploeg, Armon Rezai, and Frank Venmans. Are Economists Getting Climate Dynamics Right and Does It Matter? *Journal of the Association of Environmental and Resource Economists*, 8(5):895–921, September 2021. ISSN 2333-5955. doi: 10.1086/713977. Publisher: The University of Chicago Press.

[69] William Nordhaus. Evolution of modeling of the economics of global warming: changes in the dice model, 1992–2017. *Climatic change*, 148(4):623–640, 2018.

[70] Gerhard Petschel-Held, Hans-Joachim Schellnhuber, Thomas Bruckner, Ferenc L Toth, and Klaus Hasselmann. The tolerable windows approach: theoretical and methodological foundations. *Climatic Change*, 41:303–331, 1999.

[71] Chris Hope. Critical issues for the calculation of the social cost of co 2: why the estimates from page09 are higher than those from page2002. *Climatic Change*, 117: 531–543, 2013.

[72] Delf Neubersch, Hermann Held, and Alexander Otto. Operationalizing climate targets under learning: An application of cost-risk analysis. *Climatic change*, 126: 305–318, 2014.

[73] Hermann Held. Cost Risk Analysis: Dynamically Consistent Decision-Making under Climate Targets. *Environmental and Resource Economics*, 72(1):247–261, January 2019. ISSN 1573-1502. doi: 10.1007/s10640-018-0288-y.

[74] Matthias Kalkuhl and Leonie Wenz. The impact of climate conditions on economic production. evidence from a global panel of regions. *Journal of Environmental Economics and Management*, 103:102360, 2020.

[75] Richard SJ Tol. A meta-analysis of the total economic impact of climate change. *Energy Policy*, 185:113922, 2024.

[76] Maximilian Kotz, Anders Levermann, and Leonie Wenz. The economic commitment of climate change. *Nature*, 628(8008):551–557, 2024.

[77] Tamma A Carleton and Solomon M Hsiang. Social and economic impacts of climate. *Science*, 353(6304):aad9837, 2016.

[78] Adrien Bilal and Diego R Känzig. The macroeconomic impact of climate change: Global vs. local temperature. Technical report, National Bureau of Economic Research, 2024.

[79] Peter H Howard and Thomas Sterner. Few and not so far between: a meta-analysis of climate damage estimates. *Environmental and Resource Economics*, 68(1):197–225, 2017.

[80] Roberto Roson and Marina Sartori. Estimation of climate change damage functions for 140 regions in the gtap 9 database. *Journal of Global Economic Analysis*, 1(2): 78–115, 2016.

[81] Tom Kompas, Van Ha Pham, and Tuong Nhu Che. The Effects of Climate Change on GDP by Country and the Global Economic Gains From Complying With the Paris Climate Accord. *Earth's Future*, 6(8):1153–1173, August 2018. ISSN 2328-4277, 2328-4277. doi: 10.1029/2018EF000922.

[82] Shouro Dasgupta, Nicole van Maanen, Simon N Gosling, Franziska Piontek, Christian Otto, and Carl-Friedrich Schleussner. Effects of climate change on combined labour productivity and supply: an empirical, multi-model study. *The Lancet Planetary Health*, 5(7):e455–e465, 2021.

[83] Mengzhen Zhao, Jason Kai Wei Lee, Tord Kjellstrom, and Wenjia Cai. Assessment of the economic impact of heat-related labor productivity loss: a systematic review. *Climatic Change*, 167(1):22, 2021.

[84] R. Daniel Bressler, Frances C. Moore, Kevin Rennert, and David Anthoff. Estimates of country level temperature-related mortality damage functions. *Scientific Reports*, 11(1):20282, October 2021. ISSN 2045-2322. doi: 10.1038/s41598-021-99156-5.

[85] Franziska Piontek, Laurent Drouet, Johannes Emmerling, Tom Kompas, Aurélie Méjean, Christian Otto, James Rising, Bjoern Soergel, Nicolas Taconet, and Massimo Tavoni. Integrated perspective on translating biophysical to economic impacts of climate change. *Nature Climate Change*, 11(7):563–572, July 2021. ISSN 1758-678X, 1758-6798. doi: 10.1038/s41558-021-01065-y.

[86] Marshall Burke, Solomon M Hsiang, and Edward Miguel. Global non-linear effect of temperature on economic production. *Nature*, 527(7577):235–239, 2015.

[87] KR Pearson, Brian R Parmenter, Alan A Powell, Peter J Wilcoxen, and PB Dixon. *Notes and problems in applied general equilibrium economics*. Elsevier, 2014.

[88] Sebastian Döll. Climate change impacts in computable general equilibrium models: An overview. 2009.

[89] Francesco Bosello, Fabio Eboli, and Roberta Pierfederici. Assessing the Economic Impacts of Climate Change - An Updated CGE Point of View. *SSRN Electronic Journal*, 2012. ISSN 1556-5068. doi: 10.2139/ssrn.2004966.

[90] Kazeem Alasinrin Babatunde, Rawshan Ara Begum, and Fathin Faizah Said. Application of computable general equilibrium (cge) to climate change mitigation policy: A systematic review. *Renewable and Sustainable Energy Reviews*, 78:61–71, 2017. ISSN 1364-0321. doi: https://doi.org/10.1016/j.rser.2017.04.064.

[91] Matthew Cantele, Payal Bal, Tom Kompas, Michalis Hadjikakou, and Brendan Wintle. Equilibrium Modeling for Environmental Science: Exploring the Nexus of Economic Systems and Environmental Change. *Earth's Future*, 9(9):e2020EF001923, September 2021. ISSN 2328-4277, 2328-4277. doi: 10.1029/2020EF001923.

[92] Roberto Roson and Dominique Van der Mensbrugghe. Climate change and economic growth: impacts and interactions. *International Journal of Sustainable Economy*, 4 (3):270–285, 2012.

[93] Rob Dellink, Elisa Lanzi, and Jean Chateau. The sectoral and regional economic consequences of climate change to 2060. *Environmental and resource economics*, 72: 309–363, 2019.

[94] Warwick J McKibbin, Adele C Morris, Peter J Wilcoxen, and Weifeng Liu. The role of border carbon adjustments in a us carbon tax. *Climate Change Economics*, 9(01):1840011, 2018.

[95] Shiro Takeda and Toshi H Arimura. A computable general equilibrium analysis of environmental tax reform in japan with a forward-looking dynamic model. *Sustainability science*, 16(2):503–521, 2021.

[96] Pham Van Ha and Tom Kompas. Solving intertemporal cge models in parallel using a singly bordered block diagonal ordering technique. *Economic Modelling*, 52:3–12, 2016.

[97] Pham Van Ha, Tom Kompas, Hoa Thi Minh Nguyen, and Chu Hoang Long. Building a better trade model to determine local effects: A regional and intertemporal gtap model. *Economic Modelling*, 67:102–113, 2017.

[98] Angel Aguiar, Badri Narayanan, and Robert McDougall. An overview of the gtap 9 data base. *Journal of Global Economic Analysis*, 1(1):181–208, 2016.

[99] Pham Van Ha, Tom Kompas, and Matthew Cantele. GTAP_INT 2.0 - A forward looking CGE model for climate change and trade policy analysis. Manuscript, Centre of Excellence for Biosecurity Risk Analysis, University of Melbourne, 2025.

[100] Ottmar Edenhofer, Nico Bauer, and Elmar Kriegler. The impact of technological change on climate protection and welfare: Insights from the model MIND. *Ecological Economics*, 54(2):277–292, August 2005. ISSN 0921-8009. doi: 10.1016/j.ecolecon.2004.12.030.

[101] Alexander Lorenz, Matthias GW Schmidt, Elmar Kriegler, and Hermann Held. Anticipating climate threshold damages. *Environmental Modeling & Assessment*, 17:163–175, 2012.

[102] Chris Smith, Donald P Cummins, Hege-Beate Fredriksen, Zebedee Nicholls, Malte Meinshausen, Myles Allen, Stuart Jenkins, Nicholas Leach, Camilla Mathison, and Antti-Ilari Partanen. fair-calibrate v1. 4.1: calibration, constraining, and validation

of the fair simple climate model for reliable future climate projections. *Geoscientific Model Development*, 17(23):8569–8592, 2024.

[103] Francesco Bosello and Roberto Roson. Estimating a climate change damage function through general equilibrium modeling. *Department of Economics, University Ca'Foscari of Venice Research Paper*, (08-07), 2007.

[104] Francesco Bosello, Fabio Eboli, and Roberta Pierfederici. Assessing the economic impacts of climate change. *FEEM (Fondazione Eni Enrico Mattei), Review of Environment, Energy and Economics (Re3)*, 2012.

[105] Bård Lahn. A history of the global carbon budget. *WIREs Climate Change*, 11(3):e636, 2020. ISSN 1757-7799. doi: 10.1002/wcc.636. _eprint: https://onlinelibrary.wiley.com/doi/pdf/10.1002/wcc.636.

[106] Joeri Rogelj, Drew Shindell, Kejun Jiang, Solomone Fifita, Piers Forster, Veronika Ginzburg, Collins Handa, Haroon Kheshgi, Shigeki Kobayashi, Elmar Kriegler, et al. Mitigation pathways compatible with 1.5 c in the context of sustainable development. In *Global warming of 1.5 C*, pages 93–174. Intergovernmental Panel on Climate Change, 2018.

[107] H Damon Matthews and Andrew J Weaver. Committed climate warming. *Nature Geoscience*, 3(3):142–143, 2010.

[108] Andrew H MacDougall, Thomas L Frölicher, Chris D Jones, Joeri Rogelj, H Damon Matthews, Kirsten Zickfeld, Vivek K Arora, Noah J Barrett, Victor Brovkin, Friedrich A Burger, et al. Is there warming in the pipeline? a multi-model analysis of the zero emissions commitment from co 2. *Biogeosciences*, 17(11):2987–3016, 2020.

[109] Katharine L Ricke and Ken Caldeira. Maximum warming occurs about one decade after a carbon dioxide emission. *Environmental Research Letters*, 9(12):124002, 2014.

[110] ZRJ Nicholls, Robert Gieseke, J Lewis, A Nauels, and Malte Meinshausen. Implications of non-linearities between cumulative co2 emissions and co2-induced warming for assessing the remaining carbon budget. *Environmental Research Letters*, 15(7): 074017, 2020.

[111] Andrew H MacDougall. The oceanic origin of path-independent carbon budgets. *Scientific Reports*, 7(1):10373, 2017.

[112] P. Forster, T. Storelvmo, K. Armour, W. Collins, J.-L. Dufresne, D. Frame, D.J. Lunt, T. Mauritsen, M.D. Palmer, M. Watanabe, M. Wild, and H. Zhang. The earth's energy budget, climate feedbacks, and climate sensitivity supplementary material. In V. Masson-Delmotte, P. Zhai, A. Pirani, S. L. Connors, C. Péan, S. Berger, N. Caud, Y. Chen, L. Goldfarb, M. I. Gomis, M. Huang, K. Leitzell, E. Lonnoy, J. B. R. Matthews, T. K. Maycock, T. Waterfield, O. Yelekçi, R. Yu, and B. Zhou, editors, *Climate Change 2021: The Physical Science Basis. Contribution of Working Group I to the Sixth Assessment Report of the Intergovernmental Panel on Climate Change*, book section 7. Cambridge University Press, Cambridge, UK and New York, NY, USA, 2021.

[113] Richard J. Millar, Zebedee R. Nicholls, Pierre Friedlingstein, and Myles R. Allen. A modified impulse-response representation of the global near-surface air temperature and atmospheric concentration response to carbon dioxide emissions. *Atmospheric Chemistry and Physics*, 17(11):7213–7228, June 2017. ISSN 1680-7316. doi: 10.5194/acp-17-7213-2017. Publisher: Copernicus GmbH.

[114] Tomohiro Hajima, Michio Watanabe, Akitomo Yamamoto, Hiroaki Tatebe, Maki A Noguchi, Manabu Abe, Rumi Ohgaito, Akinori Ito, Dai Yamazaki, Hideki Okajima, et al. Development of the miroc-es2l earth system model and the evaluation of biogeochemical processes and feedbacks. *Geoscientific Model Development*, 13(5): 2197–2244, 2020.

[115] Tongwen Wu, Yixiong Lu, Yongjie Fang, Xiaoge Xin, Laurent Li, Weiping Li, Weihua Jie, Jie Zhang, Yiming Liu, Li Zhang, et al. The beijing climate center climate system model (bcc-csm): The main progress from cmip5 to cmip6. *Geoscientific Model Development*, 12(4):1573–1600, 2019.

[116] Wolfgang A Müller, Johann H Jungclaus, Thorsten Mauritsen, Johanna Baehr, Matthias Bittner, R Budich, Felix Bunzel, Monika Esch, Rohit Ghosh, Helmut Haak, et al. A higher-resolution version of the max planck institute earth system model (mpi-esm1. 2-hr). *Journal of Advances in Modeling Earth Systems*, 10(7): 1383–1413, 2018.

[117] Roland Séférian, Pierre Nabat, Martine Michou, David Saint-Martin, Aurore Voldoire, Jeanne Colin, Bertrand Decharme, Christine Delire, Sarah Berthet, Matthieu Chevallier, et al. Evaluation of cnrm earth system model, cnrm-esm2-1: Role of earth system processes in present-day and future climate. *Journal of Advances in Modeling Earth Systems*, 11(12):4182–4227, 2019.

[118] Tilo Ziehn, Matthew A Chamberlain, Rachel M Law, Andrew Lenton, Roger W Bodman, Martin Dix, Lauren Stevens, Ying-Ping Wang, and Jhan Srbinovsky. The australian earth system model: Access-esm1. 5. *Journal of Southern Hemisphere Earth Systems Science*, 70(1):193–214, 2020.

[119] Chris Hope. The marginal impact of co2 from page2002: an integrated assessment model incorporating the ipcc's five reasons for concern. *Integrated Assessment Journal*, 6(1), 2006.

[120] Fortunat Joos, Raphael Roth, Jan S Fuglestvedt, Glen P Peters, Ian G Enting, Werner Von Bloh, Victor Brovkin, Eleanor J Burke, Michael Eby, Neil R Edwards, et al. Carbon dioxide and climate impulse response functions for the computation of greenhouse gas metrics: a multi-model analysis. *Atmospheric Chemistry and Physics*, 13(5):2793–2825, 2013.

[121] Mohammad M Khabbazan and Hermann Held. On the future role of the most parsimonious climate module in integrated assessment. *Earth System Dynamics*, 10 (1):135–155, 2019.

[122] Keith P Shine, Jan S Fuglestvedt, Kinfe Hailemariam, and Nicola Stuber. Alternatives to the global warming potential for comparing climate impacts of emissions of greenhouse gases. *Climatic change*, 68(3):281–302, 2005.

[123] Malte Meinshausen, Sarah CB Raper, and Tom ML Wigley. Emulating coupled atmosphere-ocean and carbon cycle models with a simpler model, magicc6–part 1: Model description and calibration. *Atmospheric Chemistry and Physics*, 11(4): 1417–1456, 2011.

[124] John Kennedy, Blair Trewin, Richard Betts, Peter Thorne, Piers Foster, Peter Siegmund, Markus Ziese, Sulagna Mishra, Stefan Uhlenbrook, Jorge Alvar-Beltran, et al. State of the climate 2024. update for cop29. 2024.

[125] William J Ripple, Christopher Wolf, Jillian W Gregg, Johan Rockström, Michael E Mann, Naomi Oreskes, Timothy M Lenton, Stefan Rahmstorf, Thomas M Newsome, Chi Xu, et al. The 2024 state of the climate report: Perilous times on planet earth. *BioScience*, page biae087, 2024.

[126] Paris Agreement. Paris agreement. In *report of the conference of the parties to the United Nations framework convention on climate change (21st session, 2015: Paris). Retrived December*, volume 4, page 2. HeinOnline, 2015.

[127] International Energy Agency (IEA). Co2 emissions in 2023, 2024. URL https://www.iea.org/reports/co2-emissions-in-2023. Licence: CC BY 4.0.

[128] Christopher W Callahan and Justin S Mankin. National attribution of historical climate damages. *Climatic Change*, 172(3):40, 2022.

[129] Matthew A Borg, Jianjun Xiang, Olga Anikeeva, Dino Pisaniello, Alana Hansen, Kerstin Zander, Keith Dear, Malcolm R Sim, and Peng Bi. Occupational heat stress and economic burden: A review of global evidence. *Environmental research*, 195: 110781, 2021.

[130] UNDRR Cred. Human cost of disasters. an overview of the last 20 years: 2000–2019. *CRED, UNDRR, Geneva*, 609, 2020.

[131] Lucie Adélaïde, Olivier Chanel, and Mathilde Pascal. Health effects from heat waves in france: an economic evaluation. *The European Journal of Health Economics*, pages 1–13, 2022.

[132] National Emergency Management Agency National Bureau of Statistics and United Nations Development Programme. Nigeria impact of flood, recovery and mitigation assessment report 2022-2023, final report, 2023. Final Report.

[133] Peter H. Howard and Thomas Sterner. Few and Not So Far Between: A Meta-analysis of Climate Damage Estimates. *Environmental and Resource Economics*, 68(1):197–225, September 2017. ISSN 0924-6460, 1573-1502. doi: 10.1007/s10640-017-0166-z.

[134] Matthew E Kahn, Kamiar Mohaddes, Ryan NC Ng, M Hashem Pesaran, Mehdi Raissi, and Jui-Chung Yang. Long-term macroeconomic effects of climate change: A cross-country analysis. *Energy Economics*, 104:105624, 2021.

[135] Felix Pretis, Moritz Schwarz, Kevin Tang, Karsten Haustein, and Myles R Allen. Uncertain impacts on economic growth when stabilizing global temperatures at 1.5 c or 2 c warming. *Philosophical Transactions of the Royal Society A: Mathematical, Physical and Engineering Sciences*, 376(2119):20160460, 2018.

[136] Alexandros Nikas, Haris Doukas, and Andreas Papandreou. A detailed overview and consistent classification of climate-economy models. *Understanding risks and uncertainties in energy and climate policy: Multidisciplinary methods and tools for a low carbon society*, pages 1–54, 2019.

[137] Tommaso Ciarli and Maria Savona. Modelling the evolution of economic structure and climate change: a review. *Ecological economics*, 158:51–64, 2019.

[138] Erwin L Corong, Thomas W Hertel, Robert McDougall, Marinos E Tsigas, and Dominique Van Der Mensbrugghe. The standard gtap model, version 7. *Journal of Global Economic Analysis*, 2(1):1–119, 2017.

[139] Phuong Thao Nguyen. Simulating the environmental and economic effects of a carbon tax in vietnam: a static computable general equilibrium analysis. *Management of Environmental Quality: An International Journal*, 34(6):1647–1667, 2023.

[140] Nina Knittel, Martin W. Jury, Birgit Bednar-Friedl, Gabriel Bachner, and Andrea K. Steiner. A global analysis of heat-related labour productivity losses under climate change—implications for Germany's foreign trade. *Climatic Change*, 160(2): 251–269, May 2020. ISSN 0165-0009, 1573-1480. doi: 10.1007/s10584-020-02661-1.

[141] Elena Ianchovichina and Terrie L Walmsley. *Dynamic modeling and applications for global economic analysis*. Cambridge University Press, 2012.

[142] Kangxin An, Shihui Zhang, Jiaxin Zhou, and Can Wang. How can computable general equilibrium models serve low-carbon policy? a systematic review. *Environmental Research Letters*, 18(3):033002, 2023.

[143] Mustafa Babiker, Angelo Gurgel, Sergey Paltsev, and John Reilly. Forward-looking versus recursive-dynamic modeling in climate policy analysis: A comparison. *Economic Modelling*, 26(6):1341–1354, 2009.

[144] Tom Kompas and Pham Van Ha. The 'curse of dimensionality'resolved: The effects of climate change and trade barriers in large dimensional modelling. *Economic Modelling*, 80:103–110, 2019.

[145] Tord Kjellstrom, Ingvar Holmer, and Bruno Lemke. Workplace heat stress, health and productivity–an increasing challenge for low and middle-income countries during climate change. *Global health action*, 2(1):2047, 2009.

[146] Organisation for Economic Co-operation and Development (OECD). *Towards Greener and More Inclusive Societies in Southeast Asia*. Development Centre Studies. OECD Publishing, Paris, 2024. doi: 10.1787/294ce081-en. URL https://doi.org/10.1787/294ce081-en.

[147] Thorsten Mauritsen, Jürgen Bader, Tobias Becker, Jörg Behrens, Matthias Bittner, Renate Brokopf, Victor Brovkin, Martin Claussen, Traute Crueger, Monika Esch, et al. Developments in the mpi-m earth system model version 1.2 (mpi-esm1. 2) and its response to increasing co2. *Journal of Advances in Modeling Earth Systems*, 11(4):998–1038, 2019.

[148] Karl-Hermann Wieners, Marco Giorgetta, Johann Jungclaus, Christian Reick, Monika Esch, Matthias Bittner, Veronika Gayler, Helmuth Haak, Philipp de Vrese, Thomas Raddatz, Thorsten Mauritsen, Jin-Song von Storch, Jörg Behrens, Victor Brovkin, Martin Claussen, Traute Crueger, Irina Fast, Stephanie Fiedler, Stefan Hagemann, Cathy Hohenegger, Thomas Jahns, Silvia Kloster, Stefan Kinne, Gitta Lasslop, Luis Kornblueh, Jochem Marotzke, Daniela Matei, Katharina Meraner, Uwe Mikolajewicz, Kameswarrao Modali, Wolfgang Müller, Julia Nabel, Dirk Notz, Karsten Peters-von Gehlen, Robert Pincus, Holger Pohlmann, Julia Pongratz, Sebastian Rast, Hauke Schmidt, Reiner Schnur, Uwe Schulzweida, Katharina Six, Bjorn Stevens, Aiko Voigt, and Erich Roeckner. Mpi-m mpi-esm1.2-lr model output prepared for cmip6 scenariomip. Earth System Grid Federation, 2019. URL https://doi.org/10.22033/ESGF/CMIP6.793. Version YYYYMMDD.

[149] Center for International Earth Science Information Network CIESIN Columbia University. Gridded population of the world, version 4 (gpwv4): Population count, revision 11, 2018. URL https://doi.org/10.7927/H4JW8BX5. Accessed: 20 07 2024.

[150] Tord Kjellstrom, R Sari Kovats, Simon J Lloyd, Tom Holt, and Richard SJ Tol. The direct impact of climate change on regional labor productivity. *Archives of environmental & occupational health*, 64(4):217–227, 2009.

[151] Gholamheidar Teimori, Mohammad Reza Monazzam, Parvin Nassiri, Farideh Golbabaei, Somayeh Farhang Dehghan, Mohammad Javad Ghannadzadeh, and Mehdi Asghari. Applicability of the model presented by australian bureau of meteorology to determine wbgt in outdoor workplaces: A case study. *Urban Climate*, 32:100609, 2020.

[152] Peter Bröde, Dusan Fiala, Bruno Lemke, and Tord Kjellstrom. Estimated work ability in warm outdoor environments depends on the chosen heat stress assessment metric. *International journal of biometeorology*, 62:331–345, 2018.

[153] International Labour Organization. Working on a warmer planet: the impact of heat stress on labour productivity and decent work, 2019.

[154] Antonio Gasparrini, Yuming Guo, Francesco Sera, Ana Maria Vicedo-Cabrera, Veronika Huber, Shilu Tong, Micheline de Sousa Zanotti Stagliorio Coelho, Paulo Hilario Nascimento Saldiva, Eric Lavigne, Patricia Matus Correa, et al. Projections of temperature-related excess mortality under climate change scenarios. *The Lancet Planetary Health*, 1(9):e360–e367, 2017.

[155] Antonio Gasparrini, Yuming Guo, Masahiro Hashizume, Eric Lavigne, Antonella Zanobetti, Joel Schwartz, Aurelio Tobias, Shilu Tong, Joacim Rocklöv, Bertil Forsberg, et al. Mortality risk attributable to high and low ambient temperature: a multicountry observational study. *The lancet*, 386(9991):369–375, 2015.

[156] Angel Aguiar, Maksym Chepeliev, Erwin Corong, and Dominique Van Der Mensbrugghe. The global trade analysis project (gtap) data base: Version 11. *Journal of Global Economic Analysis*, 7(2), 2022.

[157] Mark Lynas, Benjamin Z Houlton, and Simon Perry. Greater than 99% consensus on human caused climate change in the peer-reviewed scientific literature. *Environmental Research Letters*, 16(11):114005, 2021.

[158] IPCC. Summary for policymakers, 2023.

[159] Alexandre K Magnan, Hans-Otto Pörtner, Virginie KE Duvat, Matthias Garschagen, Valeria A Guinder, Zinta Zommers, Ove Hoegh-Guldberg, and Jean-Pierre Gattuso. Estimating the global risk of anthropogenic climate change. *Nature Climate Change*, 11(10):879–885, 2021.

[160] J. Rogelj, D. Shindell, K. Jiang, S. Fifita, P. Forster, V. Ginzburg, C. Handa, H. Kheshgi, S. Kobayashi, E. Kriegler, L. Mundaca, R. Séférian, and M.V. Vilariño. Mitigation pathways compatible with 1.5°c in the context of sustainable development. In V. Masson-Delmotte, P. Zhai, H.-O. Pörtner, D. Roberts, J. Skea, P.R. Shukla, A. Pirani, W. Moufouma-Okia, C. Péan, R. Pidcock, S. Connors, J.B.R. Matthews, Y. Chen, X. Zhou, M.I. Gomis, E. Lonnoy, T. Maycock, M. Tignor, and T. Waterfield, editors, *Global Warming of 1.5°C. An IPCC Special Report on the impacts of global warming of 1.5°C above pre-industrial levels and related global greenhouse gas emission pathways, in the context of strengthening the global response to the threat of climate change, sustainable development, and efforts to eradicate poverty*, pages 93–174. Cambridge University Press, Cambridge, UK and New York, NY, USA, 2018. doi: 10.1017/9781009157940.004.

[161] William D Nordhaus. Optimal greenhouse-gas reductions and tax policy in the" dice" model. *The American Economic Review*, 83(2):313–317, 1993.

[162] W Nordhaus. Managing the global commons: The economics of climate change, 1994.

[163] Daniel Bodansky. The copenhagen climate change conference: a postmortem. *American Journal of International Law*, 104(2):230–240, 2010.

[164] Carlo C Jaeger and Julia Jaeger. Three views of two degrees. *Regional Environmental Change*, 11:15–26, 2011.

[165] David I Armstrong McKay, Arie Staal, Jesse F Abrams, Ricarda Winkelmann, Boris Sakschewski, Sina Loriani, Ingo Fetzer, Sarah E Cornell, Johan Rockström, and Timothy M Lenton. Exceeding 1.5 c global warming could trigger multiple climate tipping points. *Science*, 377(6611):eabn7950, 2022.

[166] Ravi Jagannathan. Use of sample information in stochastic recourse and chance-constrained programming models. *Management science*, 31(1):96–108, 1985.

[167] Cancún Agreements. Framework convention on climate change: Report of the conference of the parties on its sixteenth session, held in cancún from 29 november to 10 december 2010. Technical report, FCCC/CP/2010/7/Add. 1, 2010.

[168] Ottmar Edenhofer, Nico Bauer, and Elmar Kriegler. The impact of technological change on climate protection and welfare: Insights from the model mind. *Ecological economics*, 54(2-3):277–292, 2005.

[169] Nicholas J Leach, Stuart Jenkins, Zebedee Nicholls, Christopher J Smith, John Lynch, Michelle Cain, Tristram Walsh, Bill Wu, Junichi Tsutsui, and Myles R Allen. Fairv2. 0.0: a generalized impulse response model for climate uncertainty and future scenario exploration. *Geoscientific Model Development*, 14(5):3007–3036, 2021.

[170] R. J. Millar, Z. R. Nicholls, P. Friedlingstein, and M. R. Allen. A modified impulse-response representation of the global near-surface air temperature and atmospheric concentration response to carbon dioxide emissions. *Atmospheric Chemistry and Physics*, 17(11):7213–7228, 2017. doi: 10.5194/acp-17-7213-2017.

[171] F. Joos, R. Roth, J. S. Fuglestvedt, G. P. Peters, I. G. Enting, W. von Bloh, V. Brovkin, E. J. Burke, M. Eby, N. R. Edwards, T. Friedrich, T. L. Frölicher, P. R. Halloran, P. B. Holden, C. Jones, T. Kleinen, F. T. Mackenzie, K. Matsumoto, M. Meinshausen, G.-K. Plattner, A. Reisinger, J. Segschneider, G. Shaffer, M. Steinacher, K. Strassmann, K. Tanaka, A. Timmermann, and A. J. Weaver. Carbon dioxide and climate impulse response functions for the computation of greenhouse gas metrics: a multi-model analysis. *Atmospheric Chemistry and Physics*, 13 (5):2793–2825, 2013. doi: 10.5194/acp-13-2793-2013.

[172] Olivier Geoffroy, David Saint-Martin, Dirk JL Olivié, Aurore Voldoire, Gilles Bellon, and Sophie Tytéca. Transient climate response in a two-layer energy-balance model. part i: Analytical solution and parameter calibration using cmip5 aogcm experiments. *Journal of climate*, 26(6):1841–1857, 2013.

[173] Femke JMM Nijsse, Peter M Cox, and Mark S Williamson. Emergent constraints on transient climate response (tcr) and equilibrium climate sensitivity (ecs) from historical warming in cmip5 and cmip6 models. *Earth System Dynamics*, 11(3): 737–750, 2020.

[174] Tom ML Wigley and Sarah CB Raper. Interpretation of high projections for global-mean warming. *Science*, 293(5529):451–454, 2001.

[175] P.A. Arias, N. Bellouin, E. Coppola, R.G. Jones, G. Krinner, J. Marotzke, V. Naik, M.D. Palmer, G.-K. Plattner, J. Rogelj, M. Rojas, J. Sillmann, T. Storelvmo, P.W. Thorne, B. Trewin, K. Achuta Rao, B. Adhikary, R.P. Allan, K. Armour, G. Bala, R. Barimalala, S. Berger, J.G. Canadell, C. Cassou, A. Cherchi, W. Collins, W.D. Collins, S.L. Connors, S. Corti, F. Cruz, F.J. Dentener, C. Dereczynski, A. Di Luca, A. Diongue Niang, F.J. Doblas-Reyes, A. Dosio, H. Douville, F. Engelbrecht, V. Eyring, E. Fischer, P. Forster, B. Fox-Kemper, J.S. Fuglestvedt, J.C. Fyfe, N.P. Gillett, L. Goldfarb, I. Gorodetskaya, J.M. Gutierrez, R. Hamdi, E. Hawkins, H.T. Hewitt, P. Hope, A.S. Islam, C. Jones, D.S. Kaufman, R.E. Kopp, Y. Kosaka, J. Kossin, S. Krakovska, J.-Y. Lee, J. Li, T. Mauritsen, T.K. Maycock, M. Meinshausen, S.-K. Min, P.M.S. Monteiro, T. Ngo-Duc, F. Otto, I. Pinto, A. Pirani, K. Raghavan, R. Ranasinghe, A.C. Ruane, L. Ruiz, J.-B. Sallée, B.H. Samset, S. Sathyendranath, S.I. Seneviratne, A.A. Sörensson, S. Szopa, I. Takayabu, A.-M. Tréguier, B. van den Hurk, R. Vautard, K. von Schuckmann, S. Zaehle, X. Zhang, and K. Zickfeld. *Technical Summary*, page 33144. Cambridge University Press, Cambridge, United Kingdom and New York, NY, USA, 2021. doi: 10.1017/9781009157896.002.

[176] Franziska Piontek, Laurent Drouet, Johannes Emmerling, Tom Kompas, Aurélie Méjean, Christian Otto, James Rising, Bjoern Soergel, Nicolas Taconet, and Massimo Tavoni. Integrated perspective on translating biophysical to economic impacts of climate change. *Nature Climate Change*, 11(7):563–572, 2021.

[177] Vito Avakumović, Van Ha Pham, Eduardo Alastrué de Asenjo, Christine Li, and Tom Kompas. Climate change impacts in a forward-looking economy: New labor productivity assessment, agriculture, and health in gtap-int 2.0.0. In preparation, 2024.

[178] R Daniel Bressler, Frances C Moore, Kevin Rennert, and David Anthoff. Estimates of country level temperature-related mortality damage functions. *Scientific reports*, 11(1):20282, 2021.

[179] Vito Avakumović. Carbon budget concept and its deviation through the pulse response lens. *Earth System Dynamics*, 15(2):387–404, 2024.

[180] J. S. Kikstra, Z. R. Nicholls, C. J. Smith, J. Lewis, R. D. Lamboll, E. Byers, and K. Riahi. The ipcc sixth assessment report wgiii climate assessment of mitigation pathways: from emissions to global temperatures. *Geoscientific Model Development*, 15(24):9075–9109, 2022. doi: 10.5194/gmd-15-9075-2022.

[181] J. Ramirez-Villegas, A. J. Challinor, P. K. Thornton, and A. Jarvis. Implications of regional improvement in global climate models for agricultural impact research. *Environmental Research Letters*, 8(2):024018, 2013. doi: 10.1088/1748-9326/8/2/024018.

[182] James E. Neumann et al. Climate damage functions for estimating the economic impacts of climate change in the united states. *Review of Environmental Economics and Policy*, 2020. doi: 10.1093/reep/rez021.

[183] Francesco Bosello and Roberto Roson. Estimating a Climate Change Damage Function through General Equilibrium Modeling. *SSRN Electronic Journal*, 2007. ISSN 1556-5068. doi: 10.2139/ssrn.1000839.

[184] Malte Meinshausen, Sarah C. B. Raper, and Tom M. L. Wigley. Emulating coupled atmosphere-ocean and carbon cycle models with a simpler model, magicc6–part 1: Model description and calibration. *Atmospheric Chemistry and Physics*, 11(4):1417–1456, 2011. doi: 10.5194/acp-11-1417-2011.

[185] J. W. Harrison and K. R. Pearson. Computing solutions for large general equilibrium models using gempack. Technical report, Centre of Policy Studies, Monash University, 1996. Technical Paper No. G-116.

[186] Howard Howe. Development of the extended linear expenditure system from simple saving assumptions. *European Economic Review*, 6(3):305–310, 1975.

[187] Pham Van Ha, Tom Kompas, and Matthew Cantele. The next generation of forward looking cge model in trade policy analysis. Manuscript, 2025.

[188] Angel Aguiar, Maksym Chepeliev, Erwin L. Corong, Robert A. McDougall, and Dominique van der Mensbrugghe. The Global Trade Analysis Project (GTAP) data base: Version 11. *Journal of Global Economic Analysis*, 7(2):1–110, March 2023. doi: 10.21642/JGEA.070201AF.